MICROCOPY RESOLUTION TEST CHART

NATIONAL BUREAU OF STANDARDS-1963-A

/2

UNIVERSITY OF LOWELL
Lowell, Massachusetts   01854

STUDIES OF THE DEVELOPMENT OF CYCLONES

OVER SOUTHERN CHINA COASTAL AREAS AND ADJACENT SEAS

by

Wen Tang

Department of Earth Science

DTIC
ELECTE
JAN 2 3 1985
S
B

November 1984
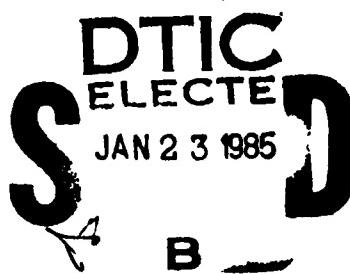
84   12   21   150

TABLE OF CONTENTS

LIST OF FIGURES

LIST OF FIGURES (Cont'd)

LIST OF FIGURES (Cont'd)

Page

LIST OF TABLES

x

STUDIES OF THE DEVELOPMENT OF CYCLONES
OVER SOUTHERN CHINA COASTAL AREAS AND ADJACENT SEAS

Abstract

The present study is an investigation of the development of cyclones in the southern part of China and coastal areas and the adjacent sea in the spring. . number of meteorological factors contribute to the genesis and development of low pressure systems in this area, This investigation is an effort to find the most important of these factors under given conditions, and to study the mechanism of the development.

When the Southwest monsoon season starts in April, warm moist air begins its invasion from the Indian Ocean northward into South China. Storms usually develop as the warm moist air encounters the cold, dry air mass from the north. The topography has also played a great role in the cyclone development. China has a high plateau to its west and complex terrain to the south which complicates the circulation. Our study stresses the thermo-hydrodynamics of cyclonic circulations that lead to the development. Our study may be divided into three parts: a) synoptic, b) analytical and theoretical, and c) numerical.

A number of cyclogenetic cases have been selected; maps at different levels for each case have been analyzed. Based on the equations of our theoretical model, each term in the equations were measured from the maps and tabulated. These data are analyzed statistically and interpreted. It shows that the most important contribution factors are the baroclinic and the condensational heating effects.

An analytical and theoretical model is developed in order to determine
how the presence of the Tibetan Plateau and other factors affect the
cyclogenesis. Solution under linearized conditions is obtained. The
500 mb trough position is in general agreement with observations.

A two-level numerical model of GCM developed by Oregon State
University was used to model the cyclone development under normal climatic
conditions in the region. The integration was done numerically for a
period of one year. Then another simulation for cases without any
mountains in the region was run for a whole season to see whether the
Tibetan Plateau and mountains in south China make a difference in the
development of cyclones in Spring. Indeed we have found a great deal of
difference. Mainly, the coastal development has been moved far to the
west, where the desert is presently located.

I. Introduction

The development of synoptic systems is largely controlled by geographic factors, such as terrain, land and sea distributions, their surface conditions, and latitudinal location. China is situated in the southeast region of the huge Eurasian continent, a large portion is in the east part of the Tsinghai-Tibetan Plateau and the Altai Mountain Ranges. To its east, there lies a long coastal line with warm ocean currents coming from the south, driven by the Pacific anticyclone. The persisting winter and summer monsoons are affected mainly by these geographic factors. The cold wave in the winter and Mei-Yu in the summer are the meteorological products of the large and synoptic circulations interacting with mesoscale conditions. The cyclogensis problem in the area is thus unique in this respect.

Because of the presence of the Tsinghai-Tibetan and Mongolian Plateaus and Mountain Ranges east of them, there are favorable regions for cyclogenesis in China. One is Inner Mongolia and the Northeast Provinces in the North; the other is in southern China between the Yangtze River and the Nan-Ling Mountains (a southern mountain range, near the southern coast). In general, the frequency of cyclogenesis is higher in the coastal region than far inland. Cyclogenesis in the south usually takes place in the springtime. During one ten-year period (1921-1931) in Southern China, there were 74 cases of cyclogenesis in the Spring (Liu, 1980). For the coastal area and the adjacent seas, the geographic and temporal distributions of cyclogenesis between 1967 and 1976 are shown in Figs. 1, 2a and 2b (Liu, 1980). The isopleth in Fig. 1 represents the number of cyclones that formed within a radius of 2.5° latitude. It is seen that region III has the highest rate of cyclogenesis.

1

Chung et al. (1976) have also studied the frequency of cyclogenesis for the entire east Asiatic continent and have found similar results in the general region, except further inland (Fig. 3), especially in the northern region, where some cyclones originate farther to the west, then die down and regenerate after they pass over the mountains. Those at the southeast of Tibet are more or less a permanent type once formed.

Figure 4a, b, and c are the Mean 700 mb charts for January, April, and June. It can be seen that a southwest - northeast oriented trough meanders between 95°E and 105°E along 25°N latitude. The trough intensifies as the season changes from winter to summer. Without seeing the surface map, one can imagine that the southern part of China and the Yangtze River region are favorable for cyclogenesis and development. Indeed, one Chinese aphorism describes the climate over Kweichow Province and the adjacent area as "without three consecutive clear days and without three miles of flat land."

In view of the results from the reported synoptic and statistical studies, as well as other evidence, the topography appears to play an important role in cyclogenesis. This study investigates the basic physics involved in the cyclogenesis problem in southern China, its coastal region, and adjacent seas, by considering the Tibetan Plateau effect and also other additional meteorological variables. In order to proceed we started to reanalyze a number of weather maps to suit our purpose of investigation, paying special attention to synoptic and smaller scales. We studied the basic contributions of various physical and meteorological variables. A linearized analytical model is developed to study the various effects attributed to the presence of the Tibetan Plateau and finally, a numerical two-level GCM model was incorporated in this study which included such

parameters as radiation, moisture and convection. This model was developed by Oregon State University and has been demonstrated to successfully simulate many features of the observed climate. We have the opportunity to utilize it to analyze the generation of absolute vorticity and detailed general results for both cases with the Tibetan Plateau and without it. All these studies are reported in Chapter I, II and III below.

CHAPTER I

THE SYNOPTIC STUDY

1. General characteristics of cyclones, in Southern China and coastal regions.

Although the continental polar air mass in Asia is somewhat modified during early and middle spring, anticyclones over north or northeast Asia continue to have great intensity. Except for some migrating cyclones moving in from the west, anticyclones over northern China often have a surface pressure of approximately 1040 mb at their centers, with ridges extending southeastward toward the East China Sea and the south of Japan. At the same time the Pacific High begins to intensify, gradually invading northward into the southern part of China. A quasi-stationary low pressure system centers just southeast of the Tsinghai-Tibetan Plateau, and a trough extends northeastward from the low. A quasi-stationary front often builds along this trough. This trough usually has an inverted V-shape, with pressure ascendent pointing northeastward, different from what is often observed in the extra-tropical cyclonic trough extending southwestward with pressure ascendent pointing in the same southwest direction. At first, a wave or a closed low pressure center may develop on the stationary front. The magnitude of the surface pressure at the center is not really low, about 1008 mb on the average. Some surface and 500 mb charts representing the typical conditions can be seen in Figs. 5a, b, c, to 13a, b, c.

The surface low usually does not deepen rapidly; the rate of deepening is about -2 mb per day. The synoptic situation in general is that when a migrating anticyclone in northern China moves southeastward to sea it produces a return flow with easterly components to bring the modified moist maritime air mass toward mainland China. When this easterly flow

4

encounters the southwesterly flow from the south in southern China, it forms either a shear line or a quasi-stationary front. If the south-westerly flow is very strong and moist, precipitation usually takes place along the front and/or behind the front in a large area in the cold air. As the low pressure area deepens and is intensified by favorable conditions, heavy precipitation may result which may lead to local flood problems in various locations.

Cyclogenesis in this area is usually associated with the presence of the jet stream in the vicinity. The presence of the jet stream implies a higher temperature gradient with warm air to its south. At this latitude moisture is indeed rather high. At the left side of the exit region of the jet stream, the upward motion is strong, and precipitation occurs there.

In the winter the major jet stream is situated in lower latitudes. In spring the jet stream gradually weakens and migrates northward. As it encounters the Tibetan Plateau, it may split into two branches. The southern branch will acquire more cyclonic vorticity. The zone of maximum wind inclines more strongly to the north as altitude increases; therefore, the lower level jet stream will be situated south of the upper air jet stream by a few degrees of latitude. Cyclonic vorticity can then be created in the lower troposphere and vortices can thus be developed at 850 mb. It is for this reason that, on the surface map, there may be only an inverted V-shaped trough in southern China, but on the 850 mb chart, there can be a closed cyclonic center.

The Tibetan Plateau may contribute greatly to cyclogenesis on its lee. On the other hand the mountain terrain yields a frictional effect to reduce the intensity of growth. Thus the cyclogenesis taking place far inland is rather sluggish and very weak. As it moves eastward to the coastal region

5

and finally over the water's surface, cyclones develop more rapidly. With the support of the baroclinic effect cyclones will deepen further.

The above discussion of the general characteristics of cyclogenesis in the area is very descriptive and observational in nature. We shall proceed to consider also the quantitative study, with measurements and calculations on analyzed charts based on theoretical equations.

2.   Theoretical basis and equations:

In order to determine the degree of growth of a cyclone, we use the rate of change of relative vorticity of a closed low pressure system as a fundamental factor of development. The calculation of the vorticity is based on a simplified two-level model (1000 mb - 500 mb). The basic equations utilized are the quasi-geostrophic vorticity equation and the hydrostatic-thermodynamic energy equation which may be written, respectively, as

$$\frac{\partial}{\partial t} \nabla^2 \psi = -\vec{V} \cdot \nabla (\nabla^2 \psi + f) + f \frac{\partial \omega}{\partial p} +$$
$$+ \left(\frac{\partial \omega}{\partial y} \frac{\partial u}{\partial p} - \frac{\partial \omega}{\partial x} \frac{\partial v}{\partial p} \right)$$

(1.1)

and

$$\frac{\partial}{\partial t} \frac{\partial \psi}{\partial p} = -\vec{V} \cdot \nabla \left(\frac{\partial \psi}{\partial p} \right) - \frac{\sigma}{p} \omega - \frac{1}{f_o} \frac{R}{p} \frac{\dot{q}}{c_p}$$

(1.2)

where

ψ = Stream function = $\frac{gZ}{f_o}$

ω = Vertical velocity in pressure coordinates

(u,v) = Velocity components along the x - and y - axis directions

σ = Stability factor

$\dot{q}$ = Rate of nonadiabatic heating

6

and the remaining variables and parameters have their usual meaning.

The vorticity equation used here is somewhat different from ones often used, in which the tilting term is usually neglected for synoptic problems and linear models since typically it is assumed to have a relatively small magnitude. However, this term may become important since precipitation may be essential for development of vorticity in cyclogenesis problems. Thus the vertical velocity contributions should be included for investigation especially over sloping terrain. Experiments and actual synoptic analysis have proven this correct (Pichler, 1973; Pichler and Steinacker, 1975; Steinacker, 1976). For the same reason non-adiabatic heating is also included in the energy equation. The non-adiabatic heating term is used here mainly for describing the latent heat release effect. As pointed out by various studies in China (Chen et al., 1978) precipitation usually precedes cyclogenesis. So, although the study of cyclogenesis in China is similar to that in other parts of the world, it may be different in this respect.

The vorticity equation is applied to the 1000 mb level, and the energy equation can be converted into the thickness equation in the 100 mb - 500 mb layer. In both equations there are terms containing ω and its derivatives. The solution of the vertical velocity should, in principle, be sought from the Omega equation.

For our synoptic study here we have made assumptions and taken an approach similar to those made by an earlier joint effort, the "Lee-cy" program conducted by NATO, CNR, and ITAV group (CENFAM, 1963), studying lee cyclogenesis south of the Alps and in the Genoa area. The vertical velocity is divided into 2 basic groups. One is due to the baroclinic effect and the other is due solely to the orographic effect. If we let ω' and ω'' represent these

7

quantities respectively, then the total vertical velocity, ω, at the middle of the layer, is

$$\omega = \omega' + \omega''$$

where ω' and ω" are assumed to be as follows:

$$\omega' = \omega'_{500} \, Sin \frac{\pi}{2} \left(\frac{1000 - p}{1000 - 500} \right)$$

and   (1.3)

$$\omega'' = \left(\frac{p}{1000} \right)^4 \omega''_{1000}$$

Since the size of the cyclone in discussion has a scale of somewhat less than 1000 km, the β effect can be neglected. By substituting Eq. (1.3) into Eq. (1.1) and letting $\psi = \frac{gZ}{f_o}$ and $H = Z_{500} - Z_{1000}$ = thickness in Eq. (1.2) yields, respectively,

$$\frac{\partial}{\partial t} \nabla^2 \psi = - \vec{V} \cdot \nabla (\nabla^2 \psi) + c_1 \omega' + c_2 \omega''$$
$$+ \left(\frac{\partial \omega}{\partial y} \frac{\partial u}{\partial p} - \frac{\partial \omega}{\partial x} \frac{\partial v}{\partial p} \right)$$ (1.4)

and

$$\left(\frac{\partial}{\partial t} + \vec{V}_3 \cdot \nabla \right) H = S_1 \omega' + S_2 \omega'' + \overline{W}$$ (1.5)

where

$$c_1 = - \frac{\sqrt{2}}{2} \frac{2 f_o}{\Delta p}$$

$$c_2 = - \frac{2 f_o}{\Delta p} \left[1 - \left(\frac{3}{4} \right)^4 \right]$$

$$S_1 = \frac{\sqrt{2}}{2} \frac{\Delta p}{g} \sigma$$

8

$$S_2 = \left(\frac{3}{4}\right)^4 \frac{\Delta p}{g} \sigma \qquad (1.6)$$

$\Delta p \quad = \quad 500 \text{ mb}$

$\vec{V}_3 \quad = \quad$ geostrophic wind vector at 750 mb level

$\overline{W} \quad = \quad$ non-adiabectic heating essentially due to latent heat release.

But the ω'' attributed to orography can also be divided into the vertical velocities ω''_s, caused by the slope effect, and ω''_f, caused by friction by the terrain, since

$$\omega''_s (x,y) = - \rho_o g \, \vec{V}_4 \cdot \nabla h (x,y) \; .$$

and

$$\omega''_f (x,y) = - \rho_o g \, \frac{D}{\left(\frac{3}{2}\pi + 2\alpha_o\right)} \left(\frac{g}{f} \, \nabla^2 Z(x,y) \right) \; .$$

where

$h(x,y) \quad = \quad$ the contour of the terrain

$Z(x,y) \quad = \quad$ the contour height of the 1000 mb surface

$\vec{V}_4 \qquad = \quad$ geostrophic wind vector at 1000 mb surface $\qquad (1.7)$

$2\alpha_o \qquad = \quad \frac{\pi}{6}$

$D \qquad = \quad$ Depth of the Ekman layer (Panofsky, 1956)

For a two-level model for the 1000-500 mb layer, the vertical velocities ω' and ω'' at the middle of the layer are

$$\omega' = \frac{\sqrt{2}}{2} \, \omega'_{500}(x,y) \; ,$$

$$\omega'' = \left(\frac{3}{4}\right)^4 \omega''_{1000}(x,y) \; . \qquad (1.8)$$

9

Substituting Eqs. (1.7) and (1.8) into Eqs. (1.4) and (1.5) and eliminating ω'_{500}, we obtain the vorticity equation. The rate of change of relative vorticity at 1000 mb is then seen to be equal to

$$\frac{d\zeta}{dt} = \alpha\left(\frac{\partial}{\partial t} + \vec{V}_3\cdot\nabla\right)H + \beta\omega''_s + \beta\omega''_f$$
$$- \left(\frac{\partial\omega}{\partial y}\frac{\partial u}{\partial p} - \frac{\partial\omega}{\partial x}\frac{\partial v}{\partial p}\right) \tag{1.9}$$

Where $\quad \alpha = c_1/s_1 \quad, \quad \beta = c_2 - s_2\alpha$

ζ = relative vorticity at 1000 mb.

$\alpha\dfrac{\partial H}{\partial t}$ = contribution of the vorticity growth due to thickness tendency.

$\alpha\vec{V}_3\cdot\nabla H$ = contribution of the vorticity growth due to thickness advection.

$\beta\omega''_s$ = contribution of the vorticity growth due to slope effect of terrain.

$\beta\omega''_f$ = contribution of the vorticity growth due to friction effect.

$\dfrac{\partial\omega}{\partial y}\dfrac{\partial u}{\partial p} - \dfrac{\partial\omega}{\partial x}\dfrac{\partial v}{\partial p}$ = contribution of the vorticity growth due to tilting effect.

$-\alpha\overline{W}$ = contribution of the vorticity growth due to latent heat release.

The non-adiabatic heating contribution is the most difficult term to handle because of its complexity. Not only does it contain various kinds of transfer process but also it is difficult to fit complicated condensation heating calculations into a simple model of cyclone development to be solved basically by graphical methods. Even with radiosonde data, the

10

non-adiabatic heating or cooling effect cannot be satisfactorily simulated. But the precipitation prior to or during the formation of a cyclone system in the spring has been reported as a very important factor in cyclogenesis in the area. The release of latent heat should be an important contributor, as compared to other non-adiabatic effects. The sensible heat supply from the earth or water surface in springtime should be relatively small. As for the radiative heating aspect, one cannot expect a large change in the relatively short period of a few days. Except for the condensational heating, all other contributing heating or cooling (e.g. evaporation) factors are neglected here.

In order to incorporate the important latent heat release effect we have tried to modify an empirical approach developed by Li (1982) and originally by Charney et al. (1964).

The quantity $\overline{W}$ may be written explicitly as

$$\overline{W} = \frac{R \, \Delta P}{\rho \, g} \, Q \tag{1.10}$$

where Q is the condensational heating in the concerned layer. This function Q is parameterized in the following fashion

$$Q = -\eta(p) \int_{P_{top}}^{P_{base}} \omega \frac{dq}{dp} \, dp \simeq -\eta(p) \, \overline{\omega} \, q_s \tag{1.11}$$

where q_s is the specific humidity, $\eta(p)$ is the Vertical distribution function of the condensational heating function, P_{base} and P_{top} are the pressures at the cloud base and top respectively, and $\overline{\omega}$ is the average vertical pressure velocity in the cloud layer. For the two-level (750 mb - 250 mb) model, $\overline{\omega}$ is taken as the ω at 500 mb. In this model we are

11

interested in the 1000-500 mb layer where $\bar{\omega}$ should be taken to be the value
at 750 mb.

Adapting the approach of parametenzation used by Li (1982) for cumulus
convective heating at 500 mb and 1000 mb in Yangtze River area, we assume

$$H_2 - \frac{R\eta_2 q_s}{2 P_2 S_2} = 0.55$$

$$H_4 = \frac{R\eta_4 q_s}{2 P_4 S_2} = 0.46 \qquad (1.12)$$

where subscripts 2 and 4 denote the level referred to, S_2 is the average
stability factor ($S_2 = 2 \times 10^{-4}$ e.g.s unit), and R and P are the gas
constants for dry air and pressure respectively. With the above formula,
$\eta_2 q_s$ and $\eta_4 q_s$ are solved. Taking $\eta_3 q_s$ for the 750 mb value as the mean of
$\eta_2 q_s$ and $\eta_4 q_s$ we have

$$\eta_3(p) q_s = 5.15 \times 10^{-5} \quad \frac{cm \; sec^2 \; {}^\circ K}{gm} \qquad (1.13)$$

Since the q_s used in the earlier cumulus convective study is believed to be
too high for our purpose, only 50% of the q_s above is used in our case.

Now let us go back to consider the evaluation of $\bar{\omega}$ at the 750 mb
level. Since the vertical motion in convection is a combination of three
factors - the slope effect, the friction effect, and the baroclinic effect,
then the resultant $\bar{\omega}$ should be approximately,

$$\bar{\omega} = \frac{1}{2} \omega'_{500} + \left(\frac{3}{4}\right)^4 \omega''_{1000} \qquad (1.14)$$

12

the nonadiabatic heating term $-\alpha\overline{W}$ due to latent heat release becomes:

$$\overline{W} = \left(-\frac{R}{2\Delta p}\frac{\Delta p}{g}z_3 q_s\right)\omega'_{500} + \left[-\left(\frac{3}{4}\right)^4\frac{R\Delta p}{g}z_3 q_s\right]\cdot$$

$$\cdot \omega''_{1000} \simeq \delta S_1 \cdot \omega'_{500} - \delta S_2 \cdot \omega''_{1000} \qquad (1.15)$$

where $\delta S_1 = -\frac{1}{2}\frac{R\Delta p}{p g}z_3 q$ and $\delta S_2 \simeq 0.6\,\delta S_1$. When there is no condensation, $\delta S_1 = \delta S_2 = 0$, implying $\overline{W}=0$. Substituting Eq. (1.15) into Eq. (1.5) yields

$$\left(\frac{\partial}{\partial t} + \vec{V}_3\cdot\nabla\right)H = \left(S_1 - \delta S_1\right)\omega'_{500} - \left(S_2 - \delta S_2\right)\omega''_{1000} \quad (1.16)$$

As in Eq. (1.9), we use Eqs. (1.4) and Eq.(1.16) to eliminate ω'_{500} and obtain

$$\frac{d\zeta}{dt} = \alpha'\left(\frac{\partial}{\partial t} + \vec{V}_3\cdot\nabla\right)H + \beta\omega''_s + \beta'\omega''_f +$$

$$+ \left(\frac{\partial\omega}{\partial y}\frac{\partial u}{\partial p} - \frac{\partial\omega}{\partial x}\frac{\partial v}{\partial p}\right), \qquad (1.17)$$

where

$$\alpha' = \frac{C_1}{S_1 - \delta S_1}$$

$$\beta' = C_2 - \left(S_2 - \delta S_2\right)\alpha' . \qquad (1.18)$$

13

It can be seen that the condensational heating term $-\alpha\overline{W}$ has been split and is implicitly involved in the first three terms on the right hand side of Eq. (1.17). However $\alpha\overline{W}$ can also be determined through the following manipulation.

Subtracting Eq. (1.17) from Eq. (1.9) yields

$$(\alpha - \alpha')\frac{dH}{dt} + (\beta - \beta')\omega''_{1000} - \alpha\overline{w} = 0$$

where

$$\alpha = \frac{C_1}{S_1}$$

$$\alpha' = \frac{C_1}{S_1 - \delta S_1}$$

after substituting Eqs. (1.18) and (1.20) into Eq. 1.19) and rearranging, we have

$$-\alpha\overline{w} = \frac{C_1\,\delta S_1}{S_1(S_1 - \delta S_1)}\left[\left(\frac{\partial}{\partial t} + \vec{V}_3 \cdot \nabla\right)H - \left(S_2 - S_1\frac{\delta S_2}{\delta S_1}\right)\omega''_{1000}\right] \qquad (1.21)$$

where $\delta S_2/\delta S_1 \cong 0.60$. Quantities on the right hand side of Eq. (1.21) can either be known constants or already determined variables.

3. The evaluation procedure and solutions.

Since the topographical effect is one of the important factors to be examined, the contour map of the surface elevation in the eastern part of

14

China is useful and is shown in Fig. 1.1. The contours are not labeled in even intervals; rather the intervals decrease rapidly as they approach the coast. The relief map is not smoothed. Since the region of investigation is closer to the coast than to the Plateau, the slope is rather small. Quantities to be measured from the analyzed weather maps and chart are on a two degree by two degree mesh grid around the center of cyclone in question. Based on readings and measurement on the maps, the following terms are calculated as shown in Eq. (1.9).

a. $\alpha\frac{\partial H}{\partial t}$ the local rate of change of thickness between the 1000 mb and 500 mb surfaces is calculated by the central difference formula with a time interval of 24 hrs. Therefore the thickness radings used in the calculation are determined 12 hrs. before and after the time point in consideration. Then multiply $\frac{\Delta H}{\Delta t}$ by the coefficient α to yield the desired value.

b. $\alpha\vec{V}_3 \cdot \nabla H$ Here $\vec{V}_3$ represents the wind vector at the 750 mb surface. The subscript 3 will be dropped from all velocity vectors and their components in this section. The wind vectors are taken directly from 850 mb and 500 mb and are interpolated to give appropriate values on grid points. The directions for $\vec{V}$ are interpolated in a linear fashion. The magnitude is determined by following the thermal wind formula between levels. Thus the wind vector was determined. As for the vector ∇H, the magnitude $|\nabla H|$ is also determined by grid values of H along X- and Y-axis directions. Since

15

$\alpha^{1}\vec{V}.\nabla H$ can be obtained for each case. An example of interpolations of the wind vector on the 750 mb surface illustrated below (Fig. 1.2).

Assume that V_{500} and V_{850} represent the wind vectors on 500 mb and 850 mb respectively. Ther thermal wind between $\vec{V}_{500}$ and $\vec{V}_{850}$ is represented by $\vec{V}_{th}$ which is equal to $\vec{V}_{500}-\vec{V}_{850}$. These vectors are drawn to scale. The 750 mb wind direction is determined as

$$\theta_{750} \simeq \theta_{850} + \left(\frac{100}{350}\right)\left(\theta_{500} - \theta_{850}\right)$$

where θ is the reading of the direction from the map. The magnitude of $\vec{V}$ is determined by measuring the length of the vector $\vec{V}$ in the drawing and converting this to speed, and finally breaking it into components u and v. With these and $\frac{\Delta H}{\Delta X}$ and $\frac{\Delta H}{\Delta Y}$ the quantity $\vec{V}.\nabla H$ can be determined.

c. $\beta\omega_s$ - As seen in Eq. (1.7) this term is the component of the vertical motion due to the forcing of the terrain. The wind $\vec{V}$ is taken from the surface chart for speed and from the 1000 mb map for direction, using a cross-countour angle of 20°. However, near the center of a low, winds tend to be fairly calm and so the averaging of the $\vec{V}$ on grids around the center are used to determine the quantities u and v. ∇h is calculated by finding the elevations of the terrain at each of the grid points and dividing by the distance between two adjacent points in the X- or the Y- axis direction, with grid spacing 2d.

d. $\beta\omega_f$ - This term is due to the Ekman pumping effect, which appears in Eq. (1.9). Since, near the point in question, it is directly proportional to the relative vorticity of $\nabla^2 Z$ on the 1000 mb surface, $\nabla^2 Z$ is also calculated by using the conventional finite difference formula of the Laplacian, i.e. $\left[\sum_{i=1}^{4} Z_i - 4Z_o\right]/d^2$, where Z_i is the contour height at

16

any grid point close to the center, where $Z = Z_0$, and d is the size of the grid mesh.

e. $\dfrac{\partial \omega}{\partial y} \dfrac{\partial u}{\partial p} - \dfrac{\partial \omega}{\partial x} \dfrac{\partial v}{\partial p}$ - The computation involved in this tilting term is more complicated because of the product of differentials of orthogonal directions. Since this term is evaluated at the 1000 mb level, the vertical differential part will be computed by using the forward difference formula where pressures are converted to height. The ω''_{1000} is the resultant of the slope and friction contributions. Over flat terrain and ocean, only the frictional effect part is present.

f. $-\alpha \overline{W}$ - The non-adiabatic heating here includes only the condensational heating. Contributions other than this are omitted as explained earlier. The calculation of $\alpha \overline{W}$ is based on the total time rate change of thickness and the vertical velocity at the 100 mb surface level value and is a very tedious process. Although Eq. (1.17) can be used to calculate the time rate change of vorticity without using $-\alpha \overline{W}$, for statistical analysis, individual change due to the $-\alpha W$ term is needed. The coefficients $c_1 \delta s_1 / [s_1(S_1 - \delta S_1)]$ and $(S_2 - S_1 \dfrac{\delta S_2}{\delta S_1})$ can be evaluated with constants given earlier.

g. $\dfrac{d\zeta}{dt}$ - The vorticity was calculated by direct measurement of the Laplacian of Z from the 1000 mb map by finite difference methods. The time rate of change of vorticity is obtained by using the central difference method for vorticity 12 hrs. before and 12 hrs. after the time in question. The measurements were made following the center of the low pressure system.

4. Computational Results and Discussion.

Of the 25 sprintime cases studied, 18 were used in the statistical analysis. The seven cases not included were omitted due to the large discrepancies between direct measurements of $\dfrac{d\zeta}{dt}$ and values of $\dfrac{d\zeta}{dt}$

17

obtained by evaluating the terms in the vorticity equation. Such

discrepancies may have arisen in part due to poor or unavailable data on

the weather charts used (e.g. over coastal water surface). The tabulated

data for each of the 18 cases are shown in Table 1.

Table 1. Data calculated for each term in the vorticity equation
shown in Eq. (1.9) for each of the 18 cases.

OBS	ID	Y	X_1	X_2	X_3	X_4	X_5	X_6
1	1	9.490	0.675	2.850	-0.00567	-0.625	0.0074	3.1300
2	2	2.780	1.890	3.060	0.00000	-0.739	-3.4000	4.3700
3	3	3.820	2.030	2.130	-0.00488	-0.588	4.3200	3.6800
4	4	10.200	0.900	4.000	2.32000	-0.465	-0.9760	4.2700
5	5	-2.550	0.900	-4.690	0.20100	-0.556	-2.8900	0.0321
6	6	1.500	-1.350	3.500	0.00444	-0.482	-0.8690	1.9200
7	7	1.160	0.000	2.690	0.11800	-0.465	-0.8040	2.3800
8	8	6.940	0.450	2.810	0.00000	-0.396	-1.5100	2.8800
9	9	12.000	0.900	6.190	0.00000	-0.649	-0.6820	6.2300
10	10	5.090	2.030	1.250	0.04610	-0.786	0.5150	2.9200
11	11	-25.200	-3.150	-5.030	-0.03130	-0.542	-0.6260	0.0522
12	12	15.400	2.030	0.880	0.35200	-0.626	0.4710	2.5600
13	13	3.240	3.010	1.580	0.04460	-0.336	-1.1000	4.0300
14	14	9.490	1.350	1.140	0.59400	-0.373	1.1900	2.1700
15	15	-4.770	2.840	-3.450	0.00000	-0.565	-2.4100	0.0511
16	16	0.347	0.900	1.490	0.00000	-0.259	-2.5600	2.1000
17	17	6.710	5.130	-0.847	-0.39400	-0.419	1.0400	3.8000
18	18	3.820	2.300	-0.467	0.00000	-0.572	-1.8900	2.4600

where

$$Y = \frac{d\zeta}{dt}$$

$$X_1 = \alpha' \frac{\partial H}{\partial t}$$

$$X_2 = \alpha' \vec{V}_{750} \cdot \nabla H$$

$$X_3 = \beta \omega'_s$$

$$X_4 = \beta \omega''_f$$

$$X_5 = \frac{\partial \omega}{\partial y} \frac{\partial u}{\partial p} - \frac{\partial \omega}{\partial x} \frac{\partial v}{\partial p}$$

$$X_6 = -\alpha \vec{W}$$

18

The mean values of the terms together with their standard deviation in the vorticity equation above are calculated and given in Table 2 below.

Table 2.   Mean values and standard deviations of all variables in the vorticity equations

SAS VARIABLE	MEAN (10^{-10} c.g.s)	STD DEV (10^{-10} c.g.s.)
Y	3.303722	8.756093
X_1	1.268611	1.768421
X_2	1.060333	2.989902
X_3	0.180238	0.568234
X_4	-0.524611	0.138272
X_5	-0.676309	1.814343
X_6	2.724189	1.617610

It is clearly shown the X_1, X_2, X_3 and X_6 concur to an increase in Y, while X_4 and X_5 affect Y differently. This is physically reasonable in all cases except X_5. All variables except X_6 are characterized by very large values of standard deviation as a consequence of very large fluctuations. This fluctuation may be common to cases of very weak cyclogenesis of a small scale depression which develop over land but which mature rather rapidly once out to sea.

A linear multiple regression analysis is also made. The regression equation is a polynomial of the form below.

$$Y = b_0 + b_1 x_1 + b_2 x_2 + b_3 x_3 + b_4 x_4 + b_5 x_5 + b_6 x_6$$

The multiple correction coefficient r was calculated stepwise by first including only the X, term, then by including both the X, and X_2 terms, then, the X_1, X_2 and X_3 term, etc. The basic formula used for the calculation is

$$r = \left[1 - \Sigma(Y_i - Y_i')^2 \Big/ \Sigma(Y_i - \bar{Y})^2 \right]^{1/2}$$

19

In the expression for r,

Y_i = the value of   measured directly for a given case

Y_i' = $b_0 + b_1 X_{1i} + b_2 X_{2i} + \cdots\cdots$, the estimated value of

$\overline{Y}$ = the average of the directly measured value of

An importance indicator was also calculated . The computed correlation coefficients for varying numbers of terms used in the vorticity equation is listed in Table 3.

Table 3. Multiple correlation coefficients, r.

VARIABLES	CORRELATION COEFFICIENTS	INCREASEMENT
X_1	0.518	0.518
X_1, X_2	0.855	0.337
X_1, X_2, X_3	0.871	0.016
X_1, X_2, X_3, X_4	0.873	0.002
X_1, X_2, X_3, X_4, X_5	0.875	0.002
X_1, X_2, X_3, X_4, X_5, X_6	0.889	0.012

From Table 3, one can see that the largest increases of r occur with the inclusion of X_1 and X_2, the term X_6 is also seen to be quite significant.

Another calculation of an index of "importance" is also made, based on the formula below:

$$I = \left| \frac{100 \, b_i \overline{X}_i}{\overline{Y'}} \right| \qquad \left(i = 1, 2, \cdots\cdots 6 \right)$$

where

I = importance value

b_i = the regression coefficient associated with a given X_i

and

Y' = the average of the estimated value of $\frac{d\zeta}{dt}$.

20

The results are shown in Table 4.

Table 4. Index of importance

TERM	I
X_1	108.43
X_2	88.00
X_3	6.26
X_4	77.66
X_5	8.36
X_6	157.69

The relative importance of each individual term from the index of importance point of view is given in Table 4 and yields a similar conclusion to that obtained from Table 3. That is, the three most important terms are the X_1, X_2, and X_6, corresponding to the thickness tendency, thickness advection and condensational heating effects.

The first two terms also represent the baroclinic and advection of thermal vorticity effects respectively. This conclusion from the statistical analysis performed in the study appears in agreement with the evidence from observation and synoptic analysis.

However, one must be aware of some important basic principles of statistics. First, the scatter of the data set should be examined. Because data obtained may be missing in a certain range, a point in a Scatter diagram may become so-called "Out lier" which will affect the statistical result significantly. A large amount of additional observation and measurement may have to be included in the study so that the values of Y versus X_i ($i = 1....6$) on each Scatter diagram can have a sound least-square analysis.

For the multiple correlation coefficient computation the regression coefficients b_i are not necessarily unique, depending how the variables X_i

21

are introduced stepwise in the calculations. For example, the first variable was selected into the model because it has the largest correlation with Y. The second variable was selected into the model because it has the next largest correlation coefficient with Y of the remaining independent variables In some cases if two independent variables have similar high correlation with Y and at the same time there is also high correlation between these variables, then after one of the variables has been selected with the model, the other one may become irrelevant in the explaining the variance in Y, and hence becomes an "unimportant variable." Even worse, the sign of the second variable may change from positive to negative or vise versa. Therefore, variation between X and Y are not clear.

The regression coefficients may change, even with the same set of data, depending on how they are calculated. Although the total effect remains the same, the effect of each individual variable is not independent of the other variables. Since there is a correlation between variables, the order in which the variables are introduced into the calculation of importance makes a difference in the resulting correlation coefficients. The laborious effort needed to pursue this question will not be continued in this investigation until further cases are studied.

Combining this synoptic and meso-scale study of the cyclone development with the analytical and numerical approaches of Parts II and III will lead more to thorough understanding of the cyclogenesis problem in Southern Chinese coastal areas and seas.

CHAPTER II

The Theoretical Study

1. Earlier work and the present task

In Chapter I we have used composite and statistical studies to investigate the relative importance o arious meteorological factors contributing to vorticity generation near centers of cyclones formed and developed in eastern and southern China, the coastal area, and adjacent seas for some selected cases. These studies are basically of synoptic and smaller scale in nature and cannot account for how the massive Tsinghai-Tibetan Plateau affects cyclogenesis in the aforementioned area. In this chapter, we develop a two-level model with an analytical approach. Studies of the influence of topography on large scale circulation began three decades ago (Steward, 1948; Charney and Eliassen, 1949; Elliott and Smith, 1949; Bolin, 1950). Since then, the orographic influence has been brought to the attention of meteorologists. The recent ALPEX program especially has aroused a great deal of interest in the cyclogenesis problem in the lee of Alps and over the Gulf of Genoa area. Many sophisticated numerical models have been utilized relating to the simulation of the terrain related cyclogenesis a problem which will be discussed briefly in Chapter III. Theoretical models concerning cyclogenesis and the effect of large terrain on circulation in regional scales with analytical approach are also numerous (e.g. Buzzi and Tibaldi, 1977; Edelmann, 1972; Smith, 1984). The emphasis of each model is different.

In this study we utilized a 2-level model by including tilting and condensational effects under simple assumptions. This is a simple model.

23

but it may be all that is needed for the study of cyclogenesis in this region, if the computed results at the 500 mb level are reasonable when compared to what actually happens in the atmosphere. For example, will a trough originating in the lee of the Tibetan Plateau have about the same location as the actual 500 mb trough most often responsible for cyclones that develop in the coastal area? Yes, the theoretical position of the 500 mb trough for the steady state solution is at 112°E, 22° east of the center of the Tibetan Plateau. This compares well with reality; the actual troughs on the 500 mb charts, that correspond to the locality of most frequent cyclogenesis, do occur in approximately the same place. In the next section we shall show the equations used in this theoretical model.

2. Basic equation

The vorticity equation and the hydrostatic and thermodynamic energy equations may be written as, respectively,

$$\frac{\partial}{\partial t}\nabla^2\psi^* + \vec{V}^* \cdot \nabla(\nabla^2\psi^* + f) \simeq f_o \frac{\partial \omega^*}{\partial p} + \frac{\partial}{\partial p}\left(-\frac{\partial \psi^*}{\partial y}\right)\frac{\partial \omega^*}{\partial y} \tag{2.1}$$
$$-\frac{\partial}{\partial p}\left(\frac{\partial \psi^*}{\partial x}\right)\frac{\partial \omega^*}{\partial x} ,$$

and

$$\frac{\partial}{\partial t}\frac{\partial \psi^*}{\partial p} + \vec{V}^* \cdot \nabla\left(\frac{\partial \psi^*}{\partial p}\right) = -\frac{\sigma}{f_o}\omega^* - \frac{R}{p}Q , \tag{2.2}$$

where stream function ψ^*, velocity vector $\vec{V}^*$, and vertical velocity ω^* are assumed

24

$$\psi^* = -U(p)\, y + \psi(x,y,t)$$

$$\vec{V}_{\wedge}^* = \vec{k} \times \nabla \psi_{\wedge}^* \qquad \left(U^* = -\frac{\partial \psi^*}{\partial y} \right) \qquad (2.3)$$

$$\omega^* = \omega(x,y,p)$$

The quantities ψ and ω without asterisks (*) represent perturbations. The non-adiabatic heating term Q is $\dot{q}/C_p$ where q is the rate of change of heat energy per unit mass. The rest of the notations have their usual meanings. We apply equations to a two-level model at 500 mb level under a steady state assumption. The perturbation equation for Figs. (2.1) and (2.2) become

$$U\frac{\partial}{\partial x}\nabla^2\psi + \beta\frac{\partial \psi}{\partial x} \simeq f_0\frac{\partial \omega}{\partial p} + \frac{\partial U}{\partial p}\frac{\partial \omega}{\partial y}, \qquad (2.4)$$

$$U\frac{\partial}{\partial x}\frac{\partial \psi}{\partial p} - \frac{\partial U}{\partial p}\frac{\partial \psi}{\partial x} = -\frac{\sigma\omega}{f_0} - \frac{R}{f_0 P_2}\zeta(P_2)\bar{\omega}q_s. \qquad (2.5)$$

Apply the above equations (2.4) and (2.5) to 500 mb surface and assume that

$$\omega_1 \simeq \frac{1}{2}\omega_2$$

$$\omega_3 \simeq \frac{1}{2}(\omega_2 + \omega_4)$$

$$v_2 = \frac{1}{2}(v_1 + v_3) = v$$

and

$$Q = -n(P)\,\bar{\omega}q_s.$$

then Eqs. (2.4) and (2.5) become,

$$U \nabla^2 v + \beta v = \frac{f_0}{\Delta p} \omega_4(x,y) + \frac{\Delta U}{\Delta p} \frac{\partial \omega_2}{\partial y} \tag{2.6}$$

$$U \frac{\partial v}{\partial p} + \frac{\partial U}{\partial p} v = -\frac{\sigma}{f_0} \omega_2 - \frac{R \eta(P_2) q_s}{2 f_0 P_2} \omega_2 \tag{2.7}$$

$$= -\left(\frac{\sigma}{f_0} + \frac{R \eta q_s}{2 f_0 P_2}\right) \omega_2 \ .$$

where ω_4 = pressure vertical velocity at 1000 mb surface

U = mean zonal geostrophic wind velocity at 500 mb surface

$\eta(P)$ = moisture distribution function (e.g. $\eta(P_2)$) is moisture distribution function at 500 mb, i.e. level 2

q_s = specific humidity

The parameterization of non-adiabatic heating, which is assumed to be due solely to condensation by convective process, is adapted from earlier work by Charney and Eliassen (1964) and Li (1982). As can be seen from a number of analyses of cyclogenesis in southern China, Chinese scientists believe that the convective condensation heating is the most important factor for development. This simple parameterization may be considered obsolete for its simplicity, yet the general physical basis remains sound and the simple form is suitable for the present linearized two-level model.

Based on many map analyses for the cyclogenesis studies, they have also believed that the advective effect is in general very weak and even negligible in comparison to the convective condensation heating. The basis for neglecting the advection of thickness (the first term on the left hand side of Eq. (2.7)) may be that for the cyclones generated in this area, the pressure or contour gradient initially is very weak, or that the size of the closed isobars of a Low pressure is rather small, in the neighborhood of 500-1000 km. Therefore, the neglect of the small thickness advection

26

effect may be justified. However, for extratropical cyclogenesis, the baroclinic effect may still be the most important contributing factor in growth. In the present study we set forth from this point of view by neglecting $U\frac{\partial v}{\partial p}$ in the first term but retain $-v\frac{\partial U}{\partial p}$ in the second term of Eq. (2.7), because the thermal wind effect is essential for growth in a baroclinic model. It follows from Eq. (2.7) that

$$\omega \equiv \omega_2 = \frac{-v\;\frac{\Delta U}{\Delta p}}{\left(\frac{\sigma}{f_0} + \frac{R\,?\,\theta_s}{2\,f_0\,p_2}\right)} = -\frac{1}{\gamma}\left(\frac{\Delta U}{\Delta p}\right)v \qquad (2.8)$$

where $\Delta U > 0$ and $\Delta p > 0$

The vertical velocity at 1000 mb surface $\omega_4(x,y)$ in Eq. (2.6) serves as the boundary condition of ω at the lower boundary. Since we are seeking the influence of the Tibetan Plateau, this term is the most important term we have to consider. When flow encounters a mountain barrier, two important effects result: one is that the air will be forced to go upward and/or around the mountain by the sloping mountain surface. The other is that the flow will experience friction and drag produced by the presence of the mountain surface. For simplicity we neglect the friction influence. Then the ω_4 may be simply written as

$$\omega_4 = -U_4 \rho_4\; g \frac{\partial}{\partial x} H(x,y) \qquad (2.9)$$

where $H(x,y)$ is the terrain profile. In our case $H(x,y)$ should be terrain profile of the Tibetan Plateau. An idealistic profile for Tibetan Plateau, $H(x,y)$ may be assumed as

$$H(x,y) = \frac{H_0}{2\tan^{-1}\frac{\alpha}{a}}\left[\tan^{-1}\frac{(x+d)}{a} - \tan^{-1}\frac{(x-d)}{a}\right] \cdot$$

$$\cdot \exp\left[-\alpha^2 y\right], \tag{2.10}$$

where H_0 = the height of the peak of the Tibetan Plateau

h,k = the distance between the peak of the Plateau and the origin of

the horizontal coordinates (x=y=o at 0°N and 0°E)

d = the half width of the plateau

a = the scale factor of the plateau in the x-axis direction

α = slope factor in the y-axis direction

The schematic profile of H in the X-Z cross-section may be seen in

Fig. (2.1) and the profile in y-axis direction is simply a Guassian curve.

The center of Tibetan Plateau is assumed to be taken at 32°N, 90°E.

With the given $H(x,y)$, ω_4 can be obtained rather easily and written as

$$\omega_4(x,y) = -\frac{U_4\,\rho_4\,g\,H_0\,a}{2\,\tan^{-1}\frac{d}{a}}\cdot\left[\frac{1}{a^2+\left(x-(h-d)\right)^2} - \right.$$

$$\left. - \frac{1}{a^2+\left(x-(h+d)\right)^2}\right]\cdot\exp\left[-\alpha^2(y-k)^2\right]. \tag{2.11}$$

Substituting Eqs. (2.8) and (2.11) into Eq. (2.6) yields

$$\nabla^2 v + \frac{\beta}{U}v = \frac{1}{\gamma U}\left(\frac{\Delta U}{\Delta p}\right)^2\frac{\partial v}{\partial p} + \frac{f_0 U_4}{2U\Delta p}\left(-\rho_4 g\right)\frac{H_0 a}{2\tan^{-1}\frac{d}{a}}\cdot$$

$$\left[\frac{1}{a^2 + x-(h-d)} - \frac{1}{a^2 + x-(h+d)}\right]\cdot \tag{2.12}$$

$$\cdot \exp\left[-\alpha^2(y-k)^2\right].$$

This equation can be simplified by assuming that

28

$$v(x,y) = \sum_{n=1}^{n=\infty} \tilde{v}(y) \sin \frac{n\pi}{L} x \qquad (2.13)$$

Substituting (2.13) into (2.12) and multiplying each side by $\frac{2}{L} \sin \frac{n\pi}{L} x$, and then integrating with respect to x from x=0 to L, yields

$$\tilde{v}_n''(y) + \left[\frac{\beta}{U} - \left(\frac{n\pi}{L}\right)^2 \right] \tilde{v}_n(y)$$

$$= A \tilde{v}_n'(y) + i C \exp\left[-\alpha^2 y^2\right], \qquad (2.14)$$

where L = the length of half of the latitudinal circle at 45°N, and

$$A = \frac{1}{\gamma U} \left(\frac{\Delta U}{\Delta p} \right)^2 \qquad (2.15)$$

$$C = \frac{H_0}{\left(\tan^{-1} \frac{d}{a}\right) L} \int_0^L \left[\frac{1}{a^2 + [x - (\hbar - d)]^2} - \frac{1}{a^2 + [x - (\hbar + d)]^2} \right] \sin \frac{n\pi}{L} x \, dx$$

Now apply the transformation to (2.15) by using

$$\tilde{v}_n = \hat{v}_n(y) \exp\left[\frac{A}{2} y \right] \qquad (2.16)$$

to eliminate $\tilde{v}_n'$ term in Eq. (2.14). We have

$$\hat{v}_n'' + \left[\frac{\beta}{U} - \left(\frac{n\pi}{L}\right)^2 - \frac{A}{4} \right] \hat{v}_n = C \exp\left[\frac{A}{2} y - \alpha^2 (y - \hbar)^2 \right] \qquad (2.17)$$

or $\qquad \hat{v}_n'' + N^2 \hat{v}_n = S(y) \qquad (2.18)$

29

where (2.19)

$$N^2 = \frac{\beta}{U} - \frac{A^2}{4} - \left(\frac{n\pi}{L}\right)^2$$

$$S(y) = C \exp\left[-\frac{A}{2}y - \alpha^2(y-h)^2\right]$$

Eq. (2.18) has the form of the well-known non-homogeneous simple harmonic equations with force function $S(y)$ if N^2 is positive. Solutions with appropriate boundary conditions can be obtained easily, in a straight forward manner.

3. The solution

The wave number n in the x-axis direction in N^2 of (2.19) varies from 1 to ∞.

For $n < n_c$, the critical wave number, $N^2 > 0$ (i.e. $\left(\frac{n\pi}{L}\right)^2 > \frac{\beta}{U} - \frac{A^2}{4}$) and for $n > n_c$, $N^2 < 0$. Therefore the property of the solution depends upon the critical number n_c in general.

For $n < n_c$ we have a periodic solution. The particular solution is

$$\frac{1}{N} \int_{y_1}^{y} \sin N(y-\xi) S(\xi) d\xi$$

The total solution for $\hat{v}_n(y)$, is

$$\hat{v}_n(y) = A_n \cos Ny + B_n \sin Ny + \frac{1}{N} \int_{y_1}^{y} \sin N(y-\xi) S(\xi) d\xi \quad (2.20)$$

For $n > n_c$, we have exponential solution. The total solution is

30

$$\hat{v}_{n2}(y) = C_n \exp(Ny) + D_n \exp(-Ny) +$$
$$+ \frac{1}{N} \int_{\eta_1}^{y} \sinh N(y - \xi) S(\xi) d\xi \qquad (2.21)$$

The final solution for $v(x,y)$ can then simply be written as

$$V = \sum_{n=1}^{n=n_c} \hat{v}_{n1}(y) \cdot \exp \frac{A}{2} y \cdot \sin \frac{n\pi}{L} x +$$
$$\sum_{n=n_c+1}^{n=\infty} \hat{v}_{n2}(y) \exp \frac{A}{2} y \cdot \sin \frac{n\pi}{L} x \qquad (2.22)$$

In order to obtain the exact solution of $\hat{v}_{n1}$ and $\hat{v}_{n2}$ we need two appropriate lateral boundary conditions. A set of simplest conditions is

$$v = 0 \qquad \text{at } y=0 \text{ and } y=L$$

This implies that

$$\hat{v}_{n1} = \hat{v}_{n2} = 0 \qquad \text{at } y=0 \text{ and } y=\ell. \qquad (2.23)$$

Applying the first boundary condition at y=0, to Eq. (2.20), the coefficients, A_n and B_n are

$$A_n = 0 \text{ and } B_n = - \frac{1}{N \sin N\ell} \int_0^\ell \sin N(\ell - \xi) S(\xi) d\xi, \qquad (2.24)$$

when applying it to Eq. (2.21), we have C_n and D_n as

$$C_n = - \frac{\int_0^\ell \sinh N(\ell - \xi) S(\xi) d\xi}{2N \sinh N\ell} \qquad , D_n = -C_n. \qquad (2.25)$$

Substituting Eqs. (2.24) and (2.25) into (2.20) and (2.21), and then

31

finally into Eq. (2.22) we have the perturbation velocity, v, in the meridional direction as

$$v(x,y) = \sum_{n=1}^{n=n_c} \left\{ \frac{1}{N} \exp\left(\frac{A}{2}y\right) \left[\frac{\sin Ny}{\sin N\ell} \int_0^\ell \sin N(\ell-\xi) S(\xi) d\xi + \right. \right.$$
$$\left. \left. + \int_0^y \sin N(y-\xi) S'(\xi) d\xi \right] \sin \frac{n\pi}{L} x \right\} +$$
$$+ \sum_{n=n_c+1}^{n=\infty} \left\{ \frac{1}{N} \exp\left(\frac{A}{2}y\right) \left[- \frac{\sinh Ny}{\sinh N\ell} \int_0^\ell \sinh N(\ell-\xi) S(\xi) d\xi + \right. \right.$$
$$\left. \left. + \int_0^y \sinh N(y-\xi) S(\xi) d\xi \right] \sin \frac{n\pi}{L} x \right\} . \quad (2.26)$$

The corresponding stream function can be obtained by integration of $v = \frac{\partial \psi}{\partial x}$ to yield

$$\psi(x,y) = \int v(x,y) dx + f(y) \quad (2.27)$$

The arbitrary function $f(y)$ is to be determined by an appropriate condition along the x-axis direction such that $\psi=0$ at $x=0$.

The final perturbation solution for stream functions $\psi(x,y)$ is

$$\psi(x,y) = \sum_{n=1}^{n=n_c} \left\{ \frac{\exp\left(\frac{A}{2}y\right)}{N \frac{n\pi}{L}} \frac{1}{\sin N\ell} \left[\int_0^y \sin N\ell \sin N(y-\xi) - \right. \right.$$
$$\left. \left. - \int_0^\ell \sin Ny \sin N(\ell-\xi) \right] S(\xi) d\xi \cdot \left(1 - \cos \frac{n\pi}{L} x \right) \right\} +$$
$$+ \sum_{n=n_c+1}^{n=\infty} \left\{ \frac{\exp\left(\frac{A}{2}y\right)}{N \frac{n\pi}{L}} \frac{1}{\sinh N\ell} \left[\int_0^y \sinh N\ell \sinh N(y-\xi) - \right. \right.$$
$$\left. \left. - \int_0^\ell \sinh Ny \sinh N(\ell-\xi) \right] S(\xi) d\xi \cdot \left(1 - \cos \frac{n\pi}{L} x \right) \right\} \quad (2.28)$$

The total solution of the stream function ψ^* can be obtained by substituting (2.28) into the next equation

$$\psi^*(x,y) = -Uy + \psi(x,y) \quad (2.29)$$

32

By just taking the Laplacian of Eq. (2.29), one obtains the vertical component of the relative vorticity, ζ, which is shown in Eq. (2.30).

$$
\begin{aligned}
\zeta = \sum_{n=1}^{n_c} &\left\{ \left[\!\!\left[Q \exp(A\eta/2) \left[\int_0^\eta \sin N\ell \, \sin N(\eta-\xi) - \right.\right.\right.\right. \\
& \left. - \int_0^\ell \sin N\eta \, \sin N(\ell-\xi) \right] S(\xi)\,d\xi \Big] \cos\frac{n\pi}{L}x + \\
& + \left[\!\!\left[\frac{\frac{A^2}{4}-N^2}{M} \exp(A\eta/2) \left[\int_0^\eta \sin N\ell \, \sin N(\eta-\xi) - \right.\right.\right. \\
& \left. - \int_0^\ell \sin N\eta \, \sin N(\ell-\xi) \right] S(\xi)\,d\xi + \\
& + \frac{AN}{M} \exp(A\eta/2) \left[\int_0^\eta \sin N\ell \, \cos N(\ell-\xi) - \right. \\
& \left. - \int_0^\ell \cos N\eta \, \sin N(\ell-\xi) \right] S(\xi)\,d\xi + \\
& + \frac{1}{M} \exp(A\eta/2) \left[\frac{A}{2} \sin N\ell \, \sin N(\eta-\xi) + \right. \\
& \left.\left. + N \sin N\ell \, \cos N(\ell-\xi) \right] S(\xi) \right]\!\!\Big] \left(1-\cos\frac{n\pi}{L}x\right) \right\} + \\
+ \sum_{n=n_c+1}^{n=\infty} &\left\{ \left[\!\!\left[R \exp(A\eta/2) \left[\int_0^\eta \sinh N\ell \, \sinh N(\eta-\xi) - \right.\right.\right.\right. \\
& \left. - \int_0^\ell \sinh N\eta \, \sinh N(\ell-\xi) \right] S(\xi)\,d\xi \right]\!\!\Big] \cos\frac{n\pi}{L}x + \\
& + \left[\!\!\left[\frac{\frac{A^2}{4}+N^2}{M} \exp(A\eta/2) \left[\int_0^\eta \sinh N\ell \, \sinh N(\eta-\xi) - \right.\right.\right. \\
& \left. - \int_0^\ell \sinh N\eta \, \sinh N(\ell-\xi) \right] S(\xi)\,d\xi + \\
& + \frac{AN}{M} \exp(A\eta/2) \left[\int_0^\eta \sinh N\ell \, \cosh N(\eta-\xi) - \right. \\
& \left. - \int_0^\ell \cosh N\eta \, \sinh N(\eta-\xi) \right] S(\xi)\,d\xi + \\
& + \frac{1}{M} \exp(A\eta/2) \left[\frac{A}{2} \sinh N\ell \, \sinh N(\eta-\xi) + \right. \\
& \left.\left. + N \sinh N\ell \, \cosh N(\eta-\xi) \right] S(\xi) \right]\!\!\Big] \left(1-\cos\frac{n\pi}{L}x\right) \right\}.
\end{aligned}
$$

(2.30)

33

where

$$Q = \frac{\frac{n\pi}{L}}{N \sin N\ell}$$

$$R = \frac{\frac{n\pi}{L}}{N \sinh N\ell}$$

$$M = N \frac{n\pi}{L} \sinh N\ell$$

$$N = \left[\frac{\beta}{U} - \frac{A^2}{4} - \left(\frac{n\pi}{L}\right)^2 \right]^{\frac{1}{2}}$$

$$A = \frac{1}{\gamma} \left(\frac{\Delta U}{\Delta p}\right)^2$$

The contour pattern of the relief H(x,y) assumed for the Tibetan Plateau is shown in Fig. 2.2. The slopes of the east and west sides of the barrier are steeper, as in the actual Plateau. With H(x,y) and the vertical velocity, ω_4(x,y), produced by the terrain as shown in Eq. (2.11), the forcing term is then determined. The component due to $v\frac{\partial H}{\partial y}$ is assumed to be of higher order in nature and is not included. Based on these assumptions the numerical solutions of the perturbations meridional velocity component, the total stream function and the relative vorticity are computed and are shown in the next section.

4. Results and Discussion

The numerical solutions for v, ψ^*, and ζ are evaluated based on the following parameters in c.g.s. units:

$f_0 = 2\Omega \sin 32° = 0.77 \times 10^{-4}$ $\qquad \ell = 6.6 \times 10^8$

$g = 980$ $\qquad \alpha = 1.37 \times 10^{-8}$

$\zeta_4 = .001$ $\qquad L = 1.7 \times 10^4$

$U_4 = 400$ $\qquad n_{max} = 36$

$U_2 = 2000$ $\qquad n_c = 5$

$\beta = 2\Omega\cos 32°/R = 1.9 \times 10^{-13}$ $\qquad A = 1.28 \times 10^{-9}$

$\Delta P = 0.5 \times 10^6$ $\qquad \sigma = 2.4 \times 10^{-4}$

$H_0 = 5.6 \times 10^5$ $\qquad Rn_2 q_s/2P_2 = 1.6 \times 10^{-4}$

$a = 1 \times 10^7$

$d = 10^8$

In order to see how much the tilting term affects the solutions, we have computed the exponential part of the solutions for $n > n_c$ for two cases: including the tilting effect, so that $A \neq 0$, and not including it, so that $A = 0$. The results yield no significant difference in v, ψ^*, and ζ (Figs. 2.3, 2.4 and 2.5) for the two cases. This appears to justify the assumption that the tilting effect has little influence on the synoptic scale circulation for the general case or for the case based on this model. The computations for the complete solution including parts of both wave and the exponential solutions are based on this conclusion. The total wave number included in this computation is 36 and $n_c = 5$. The solutions for v, ψ^* and ζ in the region near the Tibetan Plateau are shown in Figs. (2.6, 2.7 and 2.8) respectively. From each of these calculations one can locate the position of 500 mb trough at approximately 2300 km (or at the corresponding meridional distance of 20° latitude at 30°N) east of the

35

center of the Plateau. As mentioned earlier, the theoretical position is close to the actual mean 500 mb trough position, which corresponds to the genesis of surface cyclones near the coastal region and/or East China Sea (see Fig. 1), where cyclogenesis is most frequent.

The position relationship between the surface low pressure center and the corresponding 500 mb trough in the region for each case can be seen from the following three sets of actual weather maps shown in Figs. (2.9) to (2.11) as well as Figs. 5 to 14. These maps do support the theoretical finding. The positive relative vorticity center is developed in the lee at a distance of 2300 km from the peak of the Tibetan Plateau. This is similar to the solution with friction case in the lee of a circular mountain obtained by Buzzi and Tibaldi (1977). The intensity of the cyclonic vorticity is, however, only $0.09 \times 10^{-4} \sec^{-1}$, and is one order of magnitude smaller than the Coriolis parameter of $0.77 \times 10^{-4} \sec^{-1}$ at 32°N, the same latitude where the vorticity center is. The relatively small magnitude of relative vorticity is believed attributable to the linear approach of the simple model.

The inclusion of the wave solution part in y in addition to the exponential part does not really change the solution near the Plateau much, except near the lateral boundaries. The difference, which may be diminished by including some dissipation effect, is not large. Since we are interested in cyclogenesis of the synoptic scale or even smaller and are specifically concerned with the mean trough position in the neighborhood of the barrier, we consider that this linear model serves our purpose. This model considers the non-adiabatic heating effect but in a very simple way, in that it is assumed to be directly proportional to the vertical velocity at 500 mb. Its influence to growth of a cyclone may only slightly

36

change the intensity and shorten the wave length slightly.

The total stream function on 500 mb surface for the entire globe of the earth is shown in Fig. 2.12. It can be seen that the next trough away from the Tibetan Plateau is approximately 9400 km away from the peak center, corresponding to 85° longitude at 30°N, so that the major trough is at about 175°E. This major trough is believed responsible for the development of the permanent Aleutian Low in the Aleutian Island and Alaska region.

This theoretical result appears to be in good agreement with observations and to indicate that coastal cyclogenesis and cyclone development are affected mainly by the Tibetan Plateau.

The two-level linear model developed in this study is based on a number of simple assumptions on baroclinic, non-adiabatic heating and tilting effects. They can be improved and made more realistic. Since we have utilized a real sophisticated two-level numerical model, some development in this study based on linear approach without numerical calculation may not be worthy and will not be presented here. To see how the two-level numerical model works, we shall proceed to the next chapter.

CHAPTER III

THE NUMERICAL STUDY

I.   Introduction

In the earlier introduction and in Chapter I we have discussed
climatological and synoptic aspects of cyclogenesis in the eastern and
southern China region. The massive Tsinghai-Tibetan Plateau is to its West
and complex terrain, to its south. As seen from climatological data,
historical maps, and the synoptic analysis, cyclogenesis does take place in
the aforementioned area and is related to the topographic effect. The
results of a simple linear model as developed and discussed in Chapter II
have also shown that a trough at 110°E and a positive cyclonic relative
vorticity are generated in the lee of the Plateau. This upper air pattern
implies that a cyclone would be created at surface level. But the detailed
physical processes concerning the surface cyclone development are
incomplete. In order to include many other contributing factors in a model
to enable the growth to be realistic, a numerical model should be utilized.
Indeed various numerical models have been developed to study the orographic
influence on various scales of circulation induced by mountain terrain
(e.g. Bleck, 1977; Egger, 1972, 1974; Okamura, 1975; Trevisan, 1976; Mahrer
and Pielke, 1977; Murakami, 1979, 1980, 1981; Masuda, 1978; Tibaldi, 1979;
Tibaldi and Buzzi, 1982). Numerical simulations applied to study general
circulation that take into account Far East Plateaus and mountains are also
numerous (e.g. Holloway and Manabe, 1971; Manabe and Terpstra, 1974;
Smagorinsky, 1974; Hahn and Manabe, 1975; Kasahara, 1974; Kasahara,
Washington, and Sasamori, 1973; Kasahara, 1981; Gates, 1982, Kuo and Quan,

1982). Many of them are for typical winters and summers. Although there are more sophisticated models, the model we use here is perfectly adequate for simulating circulation and climate for springtime in the region discussed in this study, and in fact this is probably one of the best 2-level model that has been published.

In this study we investigate the problem of cyclogenesis in the region, using a method based on a two-level numerical model developed by investigators at Oregon State University. This model has a long history and has undergone a series of modifications and improvements, and is very sophisticated in its treatment of radiation, moisture and convection. Its successful simulated results, which are comparable with those of all other outstanding contemporary numerical models, have proven that this model is one of the most valuable models available at present (Potter and Gates, 1984). Furthermore, the model is relatively inexpensive to run. Although this model is primarily a general circulation model, it has been used successfully in climate simulation and it should present no problem for cyclogenesis studies in the lee of the largest scale mountain complex in the world. We are convinced that this OSU two-level model is the model best suited for this study. In fact, the results of this experiment are very satisfactory in many respects.

We take two approaches. First, with the output of model simulations under normal climatic conditions for a period of one year, we want to see whether cyclogenesis will take place or not in the general area. Then we analyze the development by considering each contributing factor in turn. Second, since orography is believed to be a major factor contributing to the development of cyclones in the southern China area East of the Tibetan Plateau, it is interesting to investigate what would happen if the huge

39

mountain complex were removed and whether cyclogenesis would still take place in this region. These are the ultimate goals of this numerical experiment.

II. The model

The complete description of the model would be a tremendous task and is impossible to give here on account of its huge volume of material. We shall only list the important differential equations and the vorticity equation developed and applied to this particular study. Complete documentation concerning the description of this 2-level model can be obtained from the original report (Ghan et al., 1982).

The vertical structure of this model is shown in Fig. (3.1). The principal variables involved at each level are marked accordingly. The σ-coordinate is defined as

$$\sigma = \frac{P-P_T}{\pi} \text{ and } \pi = P_s - P_T$$

where P is the pressure, P_T is the constant pressure at the top of the model, equal to 200 mb, and P_s is the surface pressure. The levels at which $\sigma = 0, \frac{1}{4}, \frac{1}{2}, 3/4$, and 1 are designated as levels 0,1,2,3,4, and respectively. In this figure the dependent variables $\vec{V}(u,v)$, T, π, q, ϕ, α, $\dot{p}$ and $\dot{\sigma}$ have their usual meanings the quantities $\vec{F}$ and $\dot{H}$ represent horizontal frictional force per unit mass and diabatic heating per unit mass respectively and $\dot{Q}$ represents the rate of moisture addition per unit mass. P is the precipitation rate, S is the snow mass, W the ground wetness, X_s surface albedo, T_s surface momentum flux, CL_1, CL_2, CL_3 and CL_4 represent the cloud type. The horizontal momentum equation at levels 1 and

40

3 are, respectively,

$$\frac{\partial}{\partial t}(\pi \vec{V_1}) + \nabla \cdot (\pi \vec{V_1}\vec{V_1}) + 2\pi \dot{\sigma_2}\vec{V_2} + \pi f \vec{k} \times \vec{V_1} +$$
$$+ \pi \nabla \phi_1 + \pi \sigma_1 \alpha_1 \nabla \pi = \pi \vec{F_1} \quad , \tag{3.1}$$

$$\frac{\partial}{\partial t}(\pi \vec{V_3}) + \nabla \cdot (\pi \vec{V_3}\vec{V_3}) - 2\pi \dot{\sigma_2}\vec{V_2} + \pi f \vec{k} \times \vec{V_3} +$$
$$+ \pi \nabla \phi_3 + \pi \sigma_3 \alpha_3 \nabla \pi = \pi \vec{F_3} \quad , \tag{3.2}$$

and the thermodynamic energy equations for levels 1 and 3 are, respectively,

$$\frac{\partial}{\partial t}(\pi T_1) + \nabla \cdot (\pi T_1 \vec{V_1}) + 2\left(\frac{p_1}{p_{oo}}\right)^\kappa \pi \dot{\sigma_2}\theta_2 - \tag{3.3}$$
$$- \frac{\pi \alpha_1 \sigma_1}{c_p}\left(\frac{\partial \pi}{\partial t} + \vec{V_1}\cdot \nabla \pi\right) = \pi \frac{\dot{H_1}}{c_p} \quad .$$

$$\frac{\partial}{\partial t}(\pi T_3) + \nabla \cdot (\pi T_3 \vec{V_3}) - 2\left(\frac{p_1}{p_{oo}}\right)^\kappa \pi \dot{\sigma_2}\theta_2 - \tag{3.4}$$
$$- \frac{\pi \alpha_3 \sigma_3}{c_p}\left(\frac{\partial \pi}{\partial t} + \vec{V_3}\cdot \nabla \pi\right) = \pi \frac{\dot{H_3}}{c_p} \quad ,$$

where $\vec{V_2} = \frac{1}{2}(\vec{V_1} + \vec{V_3})$ and $\theta_2 = (\theta_1 + \theta_3)$, and the remaining variables and parameters have their usual meaning. The mass continuity equation is

$$\frac{\partial}{\partial t}\pi + \nabla \cdot (\pi \vec{V}) + \frac{\partial}{\partial \sigma}(\pi \dot{\sigma}) = 0 \tag{3.5}$$

since the boundary conditions $\dot{\sigma} = 0$ at $\sigma = 0$ and 1, Eq. (2.5) reduced to the prognostic equation for the surface pressure, i.e.

$$\frac{\partial}{\partial t}\pi = -\frac{1}{2}\nabla \cdot \left[\pi(\vec{V_1} + \vec{V_3})\right]$$

and the diagnostic vertical velocity equation at level 2 becomes

$$\dot{\sigma_2} = \frac{1}{4\pi}\nabla \cdot \left[\pi(\vec{V_3} - \vec{V_1})\right] \tag{3.6}$$

41

The moisture continuity equations as at levels 1 and 3, are

$$\frac{\partial}{\partial t}\left(\pi q_1\right) + \nabla\cdot\left(\pi q_1 \vec{V_1}\right) + 2\pi \dot{\sigma_2} q_2 = \pi \dot{Q_1} \qquad (3.7)$$

and

$$\frac{\partial}{\partial t}\left(\pi q_3\right) + \nabla\cdot\left(\pi q_3 \vec{V_3}\right) - 2\pi \dot{\sigma_2} q_2 = \pi \dot{Q_3} \qquad (3.8)$$

The hydrostatic equation is

$$\frac{\partial}{\partial t}\phi + \pi\alpha = 0 \quad .$$

Integration of the hydrostatic equations yields the geopotential at levels 1 and 3 as

$$\phi_1 = \phi_s + c_p \frac{\theta_2}{2}\left[\left(\frac{p_3}{p_\infty}\right)^\kappa - \left(\frac{p_1}{p_\infty}\right)^\kappa\right] + \frac{\pi}{2}\left(\sigma_3 \alpha_3 + \sigma_1 \alpha_1\right) \qquad (3.9)$$

$$\phi_3 = \phi_s - c_p \frac{\theta_2}{2}\left[\left(\frac{p_3}{p_\infty}\right)^\kappa - \left(\frac{p_1}{p_\infty}\right)^\kappa\right] + \frac{\pi}{2}\left(\sigma_3 \alpha_3 + \sigma_1 \alpha_1\right) \qquad (3.10)$$

The treatment of all physical processes and parameterizations concerning conditions at the earth's surface, in the boundary layer, and in the troposphere, as well as the details of the numerical integration in this model, are described in the original documentation (Ghan et al., 1982).

For the analysis in this study we derived the vorticity equation based on the equations above in spherical coordinates in terms of various dynamic quantities similar to those appearing in previous chapters, so that a

composite study can be made.

The absolute vorticity equation may be written as follows

$$\frac{\partial}{\partial t} z = -\nabla \cdot (\vec{\overline{V}}\,\overline{z}) - \nabla \cdot (\vec{V}'z') + 2\,\dot{\sigma}_2\,z' -$$
$$- \vec{k} \cdot \left[\vec{V}' \times \nabla (2\,\dot{\sigma}_2) \right] + J(\pi, \overline{\sigma\alpha}) - \quad (3.11)$$
$$- \vec{k} \cdot \nabla \times \vec{\overline{F}}$$

where $Z = \dfrac{\partial v}{a\cos\phi\,\partial\lambda} - \dfrac{\partial u}{a\,\partial\phi} + \dfrac{\tan\phi\,u}{a}$ = vertical component of relative vorticity in spherical coordinates.

The term on the left hand side is the local rate of change of absolute vorticity. The first and second terms on the right hand side are respectively the import of vorticity and thermal vorticity through the boundary of unit area on the level 2 surface per unit time; the third term is the vertical vorticity advection by the vertical velocity at level Z; the fourth term is the tilting term; the fifth term is the solenoid term; and the last term is the Newtonian friction.

The finite difference expression of the vorticity equation, the parameterization, and the constants used are listed in the appendix. All terms mentioned above in the vorticity equations are calculated in addition to many basic meterological variables for both the WPTC and NTPC.

III. Results

A.   Result for the With Tibetan Plateau Case (WTPC)

The results presented here are the outcome of integrating the 2-level model for a one-year simulation time. The most exciting result is that cyclogenesis does take place in the month of April and the cyclone gradually deepens as it moves to East China Sea, as can be seen from the

43

sea-level pressure chart from Fig. (3.2), just as in the actual synoptic development shown in Figs. 5 to 14. The mean sea-level pressure distribution for April as well as for the Spring season in the area are also similar (see Figs. 3.3, 3.4, 3.5). The movement of the low pressure can also be traced from the computed time change of absolute vorticity at level 2 in Fig. (3.6). The interaction between upper levels and sea level leads to the cyclogenesis. The axis of maximum U component at level 3 shown in Fig. (3.7), with a magnitude of 24 m sec^{-1}, is quasi-stationary, situated approximately along the southern Chinese coast and South China Sea. This may be associated with the so-called "low level jet" often named by Chinese scientists. This lower level jet is highly correlated with rainstorms and development of low pressure systems. Fig. (3.8) shows the North-South components of wind velocity V_3 at level 3. The movement of the surface low closely correlates with the negative V, implying that the warm air invades from a southerly direction. The ridge of the warm temperature wave moves slowly eastward [Fig. (3.9)]. The precipitation rate as shown in Fig. 3.10 increases from nil to about 20 mm day^{-1} along the coast and to the east of Taiwan. Since this model is not a mesoscale model, one cannot be very critical of the magnitude. Since the vertical velocity is responsible for the rate of precipitation, we see by examining the vertical velocity, $\dot{\sigma}_2$ (Fig. 3.11) that the distribution of the high values of $\dot{\sigma}_2$ justifies the location of occurrence of the precipitation.

The absolute vorticity is shown in Fig. (3.12) with units "day^{-1}". If f is taken as the Coriolis acceleration at 30°N, $f_{30} = 0.72 \times 10^{-4}$ sec^{-1}. Then the vorticity of 1 day^{-1} corresponds to $0.16 f_{30}$.

When the absolute vorticity is 6 day^{-1}, the vorticity is approximately the planetary vorticity at that latitude. Therefore the relatively large

44

vorticity center moves from the top of the plateau on April 17 to the East

China Sea on April 20. The surface low pressure center is also located in

approximately the same vicinity. The vorticity center reaches a minimum at

approximately 30°N and 117°E on April 19 and intensifies again as it moves

over the water surface. This kind of transition also appears in the total

rate of change of absolute vorticity at the same level, that is, $\sigma = \frac{1}{2}$.

Figs. (3.13) and (3.14) show the import of vorticity and thermal

vorticity per unit time, respectively. The magnitude of the import

vorticity is much larger than that for thermal vorticity. Thus the

former contributes more to the local rate of increase vorticity for the

cyclone. The import term of the absolute vorticity $-\nabla \cdot \left(\vec{V} \, \overline{\overline{\zeta}} \right)$ is the sum of

$-\overline{\vec{V}} \cdot \nabla \overline{\overline{\zeta}} - \overline{\overline{\zeta}} \, \nabla \cdot \overline{\vec{V}}$. The first term of these two is the advection of

vorticity and the second term of these two is due to the divergence effect.

Unfortunately we did not separate them in the computation. However,

considering the circulation situation at both sea level and at level 2, the

deepening of 4 mb in the last stage (April 20) may be attributed to the

horizontal divergence term. The maximum thermal vorticity important for

the same day is only 2 day^{-1} and is somewhat out of phase from the center

of the maximum intensity and sea-level low center. Therefore, we believe

that the contribution for thermal vorticity import is relatively small.

The contribution due to the tilting effect is restricted to the foot of the

plateau (Fig. 3.15). As the low pressure system moves away the tilting

effect even contributes in the negative sense. The vertical vorticity

advection (Fig. 3.16) has some contribution to the growth to the absolute

vorticity. The positive center almost follows the movement of the

vorticity center at level 2. Fig. 3.1 shows the solenoid distribution.

The largest negative solenoid term is at the lee of the Plateau, and covers

more or less the entire region east of 105°E. It persists throughout all periods. The reason is as follows. At level 2, the temperature ascendant points southward and the ascendant of pressure difference between ground surface and the 200 mb points eastward (i.e. $\nabla\pi$). There $\nabla\pi \times \nabla(\overline{\sigma\alpha})$ would produce a negative vorticity east of the Plateau. The friction term contribution to the possible change of absolute vorticity is also very small.

b. Results for the No Tibetan Plateau Case (NTPC)

As seen from Fig. (3.18), the contour of the relief is set to zero elevation east of 60°E and south of 50°N in the Asian continent for this experiment and the surface condition is assumed to be the same as the plain area in the Eastern China. The simulation starts from the month of February. The boundary conditions for meteorological variables at the earth's surface will be determined from the model itself as integration time goes on.

The kinds of meteorological variables and parameters simulated in this NTPC are the same as those for the WTPC, so that one may use them for comparison. Indeed the most important and interesting thing to see is whether the cyclones that formerly developed in the area will remain to form in the same area and if not, how much the difference is.

The first thing to examine is the mean monthly sea level pressure chart for March (Fig. 3.19) and for April (Fig. 3.20). The low pressure system formerly situated in the southern Chinese coast is no longer in sight. The Tibetan High is also gone. Now almost the entire Asiatic continent is occupied by a huge low pressure system centered in the northwest of China where the deserts are now located. The average center pressure vary from 989 to 991 mb. Their intensity is very close to that of

46

the Aleutian Low in winter or those of typhoons in summer. The low pressure centers, formerly located at east of Japan, now have moved to center on the Japanese Islands, with center pressure of about 982 mb. A sequential sea-level pressure chart form 12z March 1 to 12z May 31 in every five-day interval is shown in Fig. (3.21).

In March, the average low pressure center is near the Takla Makan Basin in the Sinkiang Province of China and in Central Eurasia.

The cyclone track for March is in general from SW to NE along the northwest Chinese border line to Siberian and then down from NW to SE through Mongolia or the Northeast provinces of China to Japan. The high pressure system occasionally penetrates southward. The Pacific High may branch off in the India Region and split to yield a separate cell. The separated high then moves eastward and gradually dissipates as it moves out of the Chinese mainland. When April arrives, the huge low pressure system in the west takes a somewhat straighter eastward or southeastward path instead of the wavy path observed in March. The intensity decreases rapidly except in the far North. The separated High from the Pacific anticyclone appears to expand somewhat Northward. But the intensity is rather weak. In May the low pressure system moving eastward becomes more filled. The Chinese mainland has an essentially zonal flow at the surface.

The daily 12z sea level pressure maps from April 17 to April 20 are shown in Fig. (3.22). It can be seen that the huge cyclone moves almost straight eastward across China toward Japan with rather high intensity, in contrast to that of the WTPC in which the intensity is feeble during the formation stage in southern China. It is conceivable that the anticyclonic intensity for the NTPC is very weak and is not compatible with the situation of anticyclonic dominance in a large region in China in the WTPC.

47

The zonal and meridional wind speeds at level 3 (Fig. 3.23 and Fig. 3.24) have about the same magnitude as before in the WTPC. The zonal wind at level 1 at low latitudes for the NTPC (Fig. 3.25) is about the same as that of the WTPC. However, in the NTPC, at middle latitudes such as 45°N, easterlies from high latitudes move southward and take the place of the pure westerlies that are observed in the WTPC.

The easterlies at level 1 at this latitude imply the presence of an anticyclone over east Siberia at that level. This is the direct consequence of the movement of the huge and intense surface cyclonic system from Siberia toward Japan and of dynamic interaction by vertical circulation and divergence processes. For the meridional component at this level (Fig. 3.26) over the Asian continent, the centers of the maximum meridional wind are out of phase with those of the WTPC. They have longer wave length and smaller magnitude compared to those of the WTPC because of the barrier effect at lower levels.

As for the temperature at level 3 (Fig. 3.27), it is conceivable that the isotherms are more zonally oriented because the terrain is completely flat, in contrast to the cellular structure with warm and cold cores in the WTPC which exists because of the elevation and radiation effects. But the warm ridge remains aligned in the North-South direction toward Japan. This is true because the large scale land-sea distribution and the warm ocean current remain the same for the NTPC, not influenced much by the removal of the Tibetan Plateau.

The cold center over the Tibetan Plateau region is evidently attributed to the Plateau's higher elevation. However, a warm ridge still exists over the same location in NTPC. The reason may be the invasion of warm air from the east African Coast and from the southwest monsoon above

the Indian Ocean.

The temperature field at level 1 are also different for the two cases; isotherms are also nearly zonal over the Continent in the NTPC (Fig. 3.28), while warm and cold packets are found in the WTPC. The thermal ridges are located just off the coast for both the WTPC and the NTPC.

Fig. (3.29) shows the sigma vertical velocity at level 2. The center of upward and downward motion propagate eastward in the NTPC, while in the WTPC they are more or less stationary. The center of downward motion (positive sigma vertical velocity) is south of the dominating anticyclone over the region where the Tibetan Plateau used to be and the center of upward motion is east of it, because of southerly flow over Southern China.

The absolute vorticity pattern in this period at level 2 (Fig. 3.30) south of 45°N is similar to that of WTPC. For the WTPC, the pattern is in general agreement with the results of the theoretical study in Chapter II (Fig. 2.8) in which there are two positive relative vorticity centers on each side of the Plateau, which are more or less stationary as a direct consequence of the presence of the Tibetan Plateau. In the NTPC, the vorticity center at the southern part of China is stronger because it is already a well-developed cyclone and is moving with slightly higher speed. In both cases the axes of maximum and minimum vorticity tilt toward the Northwest.

Considering the total precipitation rate, the regions with high rate generally in the region near the East China Sea and south of Japan. Precipitation is associated with the huge cyclone in this area but here, the precipitation does not necessarily take place to the east-northeast of the associated cyclone. The high precipitation rate is believed to be

49

associated closely with southerly flow and with the warm ocean currents in the region, which are capable of yielding stronger evaporation and of producing higher moisture content in the air (Fig. 3.32). Relatively smaller rates are found for northern regions, as well as for the WTPC. The region of maximum atmospheric heating (Fig. 3.32) is strongly correlated with that of high precipitation rate because of the release of latent heat.

Now we come to the analysis of the rate of change of absolute vorticity (Fig. 3.33), which does show a high correlation between the rate change of vorticity and the vorticity field at the same level. Because the huge, strong cyclone moves through from the west in the NTPC, the positive rate of change of the absolute vorticity at level 2 is relatively higher and spreads over a larger area than in the WTPC. Among the terms contributing to this change of absolute vorticity, the import of the vorticity term remains to be a dominant term (Fig. 3.34), as in the WTPC case. The import of the thermal vorticity (Fig. 3.35) is even less important. The solenoid term (Fig. 3.36) and friction term (Fig. 3.37) contributions are all minimal.

IV. Conclusions and Discussions

These numerical experiments, based on the two level GCM model developed by OSU for the simulation of cyclogenesis and development in eastern and southern China and its adjacent waters in spring for both the WTPC and the NTPC with simulation periods of one year and three months, respectively, are considered successful. The simulation results for the WTPCindicate that the behavior of circulation and sea level pressure systems is similar to what happens in the mean actual situation. Indeed cyclogenesis does take place in this area in spring. That is, cyclones are

first generated in southwest China and/or southeast of the Tsinghai-Tibetan Plateau and then move eastward to the East China Sea and its general vicinity and then intensify.

One of our major goals is to investigate how important the role of the Tibetan Plateau is in cyclogenesis in the area in Spring. Thus we need to study the NTPC with a sophisticated numerical model. The most exciting result is that the cyclone track is mainly along the $50^\circ N$ latitude line starting from the west and stretching east to Japan. There is no indication of cyclogenesis in the southwest and south China in the NTPC, while there is cyclogenesis in the area in the WTPC (Fig. 3.39).

Only one cyclone passes through this region in the entire spring season, originating far to the west at about $75^\circ E$. This can also clearly be seen from Fig. (3.39). In a way this is in agreement with the findings obtained by Manabe and Terpstra (1974), in that the Mei-Yu system associated summer monsoon moves in July from the observed position to a position much farther north. Although the present study is only for the spring season, cyclogenesis in this period usually precedes the emergence of the Mei-Yu. The cyclone developed in the spring is a form of a small low pressure system similar to Mei-Yu. However, this spring cyclone is limited to somewhat lower latitudes and does not occur so persistently as the Mei-Yu.

Based on this study we can conclude that cyclogenesis in southern China and further development in the East China Sea and adjacent waters are mainly attributed to the presence of the Tibetan Plateau. Otherwise, no cyclones would form or develop in the region except for those developed far inland in which occasionally pass through this region.

51

We consider now the composite analysis of the absolute vorticity generation at level 2 in the 2-level model. The import of absolute vorticity is the major contributing factor to the local rate of change of absolute vorticity. This indicates that the horizontal divergence could be the most important factor in development. The import of thermal vorticity and the vertical advection of relative vorticity are relatively small. The rest of the terms, such as the tilting and friction effects, are very small. This is probably because the model used is originally for large scale general circulation studies; synoptical scale and definitely mesoscale phenomena may be not suitably simulated by this model. The solenoidal effect is also, in general, small except for one case in which it is large.

The OSU two-level model for GCM studies has served the simulation of the seasonal cyclogenesis in the lee of the Tibetan Plateau with success and has provided a definite answer to our quest.

SUMMARY

The study of cyclogenesis in southern China, over east Chinese coastal
areas and adjacent seas during springtime under this investigation utilized
three methods, namely synoptic, analytical, and numerical, and has produced
interesting results. By examining hundreds of surface and upper air maps,
and consulting a large amount of scientific literature concerning
cyclogenesis in this are, some unique characteristics are found and
reported.

During spring warm air starts to invade northward from the south and
typically encounters either the return flow from a modified continental
anticyclone, moving out of the Asian continent to the south of Japan, or an
easterly flow, from a weak anticylclone centered further to the north; and
they form an inverted V-shaped trough. At first, along this trough a
shear line or a quasi-stationary front is established. When a jet stream
is present in southern China, low level convergence of moist air generally
produces often intense precipitation over a large area. A small, weak low
pressure system then may develop when a 500 mb trough intensifies at about
100°E or in the general vicinity. The low is very weak with a central
pressure usually over 1000 mb, but it deepens as it moves out to sea.

Statistical analysis of the results of synoptic analysis of eighteen
cases in vorticity-generating terms, calculated by graphical methods, has
indicated that the most important contribution to the growth remains to be
the baroclinic effect; condensation is second. The scale considered here
is in general smaller than that of mature cyclones. The contribution by
terrain and tilting effects are small, especially when the low pressure
system is over the ocean. The terrain effect is thus minimal. However,

this does not mean that large scale terrain such as the Tibetan Plateau is not important. The baroclinic effect interacts with the horizontal divergence and convergence field which is indirectly influenced by the large scale topography. This can be seen by comparing the results of the numerical model for the case with the Tibetan Plateau included and the case where the Tibetan Plateau was not included.

The theoretical study is based upon a simple two-level linearized model which includes the non-adiabatic heating and tilting effects. The results show that the tilting effect is small, in agreement with the finding in synoptic analysis reported earlier here as well as elsewhere. The non-adiabatic heating parametrization used in the model, though crude, has produced a reasonable trough position of 500 mb level for cyclogenesis. Therefore, the theoretical two-level model has served our purpose well.

The numerical model has provided us many interesting results. The most exciting outcomes are first, that with Tibetan Plateau, cyclogenesis does take place in the southern part of China and these lows gradually develop and intensify as they move over coastal waters and out to sea. With No Tibetan Plateau (and flat terrain assumed) over the region east of 60°E and south of 50°N there is no cyclogenesis in the aforementioned area, only lows moving from the far west, passing through southern China and the coast. Without the plateau, cyclones generally take far northern routes. The most important vorticity generating factor contributing to cyclone development is the import of absolute vorticity which in turn derived from the divergence and advection effects.

All in all, this investigation has provided some interesting and valuable results to aid in further understanding of the fundamental problem of cyclogenesis in the southern Chinese coastal areas and the adjacent sea.

54

ACKNOWLEDGEMENTS

REFERENCES

Bleck, R., 1977. Numerical simulation of lee cyclogenesis in the Gulf of
    Genoa. Mon. Weather Rev., 105, 428-445.

Bolin, B., 1950. On the influence of the earth's orography on the general
    character of the Westerlies. Tellus, 2, 184-195.

Buzzi, A., and S. Tibaldi, 1977. Inertial and frictional effects on
    rotating and stratified flow over topography. Quart. J. Roy. Meteor.
    Soc., 103, 135-150.

CENFAM, 1963 - Research Report No. 3 on Project "Lee-Cy", Instituto di
    Fisica dell'Atomosfera, Roma.

Charney, J.G., and A. Eliassen, 1964. On the growth of the hurricane
    depression. J. Atmos. Sci., 21, 68-75.

Chen, C.B., Gee, C.C., and P.C. Chu, 1978. Numerical simulation of
    cyclogenesis with precipitation. Baoyu Wenji, 94-101, Jiling People's
    Publishers (In Chinese).

Chung, Y.S., Hage, K.D., and E.R. Reinelt, 1976. On lee cyclogenesis and
    air flow in the Canadian Rocky Mountains and the east Asian mountains.
    Mon. Weather Rev., 104, 879-891.

Edelman, W., 1972. An analytical solution for stationary barotropic flow
    crossing a meridional mountain barrier. Beitr. Phys. Atmos., 45,
    87-93.

Egger, J., 1972. Numerical experiments on the cyclogenesis in the Gulf of
    Genoa. Ibid, 45, 320-346.

_____, 1974. Numerical experiments on lee cyclogenesis. Mon.
    Weather Rev., 102, 847-860.

Gates, W.L., 1982. The effects of mountains on the atmospheric general
    circulation and climate. Climatic Research Institute Report, Oregon
    State University, Corvallis, Oregon, 97331.

Ghan, S.J., Lingras, J.W., Schlesinger, M.E., R.L. Mobley and W.L. Gates,
    1982. A documentation of the OSU two-level atmospheric general
    circulation model. Climate Research Institute Report No. 35, Oregon
    State University, Corvallis, Oregon, 97331.

Hahn, D.G., and S. Manabe, 1975. The role of the mountains in the south
    Asian monsoon. J. Atmos. Sci., 32, 1515-1541.

Kasahara, A., 1979. Influence of orography on the atmospheric general
    circulation. NCAR MS 0501-79-01, Boulder, Colordao.

_____, and W.M. Washington, 1971. General circulation experiments with a six layer NCAR model including orography, cloudiness, and surface temperature calculation. J. Atmos. Sci., 25, 657-701.

_____, and T. Sasamori, 1973. Simulation experiments with a 12-layer stratospheric global circulation model. Ibid, 30, 1229-1251.

Kuo, H.L., and Y.E. Qiam, 1982. Numerical simulation of the development of mean monsoon circulation in July. Mon. Weather Rev., 110, 1879-1897.

Li, K.C., Chen, J.J., Yang, K.C., Sung, C.S., Chen, C.C., Chou, M.Y., Hsu, Y.F., Yeh, T.C., and C.C. Chang, 1976. An annulus experimental simulation of the low vortex to the southeast of the Chinghai-Tibetan Plateau. Scientia Sinica, 19, 286-294.

Li, C.Y., 1982. On the mechanism of the genesis of cyclone over the Changjiang and Huaihe River Basin. Scientia Atmospherica Sinica, 6, 258-263 (In Chinese).

Liu, K.Y., 1980. Extrotropical cyclogenesis in the central region of China mainland and its influence on the weather conditions in Northern Taiwan. Nat. Sci. Comm. Monthly. ROC, 8, 171-183 (In Chinese).

Mahrer, Y., and R.A. Pielke, 1977. A numerical study of the airflow over irregular terrain. Beitr. Phys. Atmos., 50, 98-113.

Murakami, T., 1979. Winter monsoonal surges over East and Southeast Asia. J. Meteor. Soc. Japan, 57, 133-158.

_____, 1980. Orographic influence of the Tibetan Plateau on the Asiatic winter monsoon circulation, Part I. Largescale aspects. Ibid, 59, 40-65.

_____, 1981. Orographic influence of the Tibetan Plateau on the Asiatic winter monsoon circulation, Part III. Short period oscillation. Ibid, 59, 173-200.

_____, 1981. Orographic influence of the Tibetan Plateau on the Asiatic winter monsoon circulation, Part V. Long period oscillation. Ibid, 59, 201-219.

Panofsky, H., 1956. Introduction to dynamic meteorology. The Pennsylvania State University, University Park, Pennsylvania, 243 pp.

Pichler, H., 1973. Theorie einer Zyklogenese unter Berucksichtigung von Kondensation. Arch. Met. Geoph. Biok., Ser. A, 22, 1-19.

_____, and R. Steinacker, 1975. Zur Frageder Zyklogenese in den mittbern breiten unter Berucksichtigung von freiwerdender Kondensations warme. Ibid, Ser. A, 24, 117-129.

Potter, G.L. and W.L. Gates, 1984. A preliminary intercomparison of the seasonal response of two atmospheric climate models. Mon. Wea. Rev., 112, 909-917.

Okamura, Y., 1975. Numerical experiments of orographic effect on the large scale motion of the atmosphere. Papers in Meteorology and Geophysics, 27, 1-20.

Smagorinsky, J., 1974. Global atmospheric modelling and the numerical simulation on climate. Weather and Climate Modification, W.N. Hess (editor) 633-686. J. Wiley and Sons Inc., New York.

Smith, R.B., 1984. A theory of lee cyclogenesis. J. Atmos. Sci., 41, 1159-1168.

Steinaker, R., 1976. Zur Vorticity produktion bei zyklongenetishen Progzessen. Arch. Met. Geoph. Biokl., Ser. A., 25, 97-115.

Stewart, H.J., 1948. A theory of the effect of obstacles on the waves in the westerlies. J. Meteor., 5, 236.

Tibaldi, S., 1979. Lee cyclogenesis and its numerical simulation with special attention to the Alpine Region: A review. Geophys. Astrophys. Fluid Dyn., 13, 25-49.

_____, and A. Buzzi, 1982. Orographic influences on Mediterranean lee cyclogenesis and European blocking in a global numerical model. European Centre for Medium-Range Weather Forecasting, Tech. Rep. No. 29, Reading, England, 46 pp.

Trevisan, A., 1976. Numerical experiments on the influence of orography on cyclone formation with isentropic primitive equation model. J. Atmos. Sci., 33, 768-780.

The finite difference absolute vorticity equation in Chapter III corresponding to 3.11 and each individual term are listed below.

$$\frac{\partial \bar{\bar{z}}}{\partial t} = -\nabla\cdot(\bar{\vec{v}}\,\bar{z}) - \nabla\cdot(\vec{v}'z') + 2\dot{\sigma}z'' - \vec{k}\cdot\left[\vec{v}'' \times \nabla(2\dot{\sigma}_2)\right] +$$
$$- J(\pi, \overline{\sigma\alpha}) - \vec{k}\cdot\nabla\times\vec{\bar{F}} .$$

$$\nabla\cdot(\bar{\vec{v}}\,\bar{z}) = \frac{\partial(m\bar{u}\,\bar{z})}{m\,\partial x} + \frac{\partial(m\bar{v}\,\bar{z})}{m\,\partial y} .$$

$$\nabla\cdot(\vec{v}'z') = \frac{\partial(m u'z')}{m\,\partial x} + \frac{\partial(m v'z')}{m\,\partial y} .$$

$$\vec{k}\cdot\left[\vec{v}'' \times \nabla(2\dot{\sigma}_2)\right] = 2\left[\frac{m u''}{m}\frac{\partial\dot{\sigma}_2}{\partial y} - \frac{m v''}{m}\frac{\partial\dot{\sigma}_2}{\partial x}\right] .$$

$$J(\pi, \overline{\sigma\alpha}) = \frac{\partial\pi}{\partial x}\frac{\partial(\overline{\sigma\alpha})}{\partial y} - \frac{\partial\pi}{\partial y}\frac{\partial(\overline{\sigma\alpha})}{\partial x} .$$

$$\vec{k}\cdot\nabla\times\vec{\bar{F}} = \frac{\partial(mcv_1)}{m\,\partial x} - \frac{\partial(mcu_s)}{m\,\partial y}$$

$$\overline{(\quad)} = \frac{(\quad)_1 + (\quad)_3}{2} , \quad (\quad)'' = \frac{(\quad)_1 - (\quad)_3}{2}$$

$$z = \nabla\times\vec{V}\cdot\vec{k} = \frac{\partial(mv)}{\partial x} - \frac{\partial(mu)}{\partial y} + f$$

$$m = \Delta x = a\cos\phi\cdot\Delta\lambda , \quad n = \Delta y = a\,\Delta\phi$$

$$a = 6.375\times10^6 m, \quad \Delta\lambda = 5°, \quad \Delta\phi = 4°$$

$$C = \frac{10\,g\,\rho_4\,C_D}{\pi}\,MAX(|V'|, 2)$$

$$|V'| = \frac{1}{4\Delta x}\left[\left(|\vec{V_s}|_{i-\frac{1}{2}, j-\frac{1}{2}} + |\vec{V_s}|_{i+\frac{1}{2}, j-\frac{1}{2}}\right)\Delta x_{i-\frac{1}{2}} + \right.$$
$$\left. + \left(|\vec{V_s}|_{i-\frac{1}{2}, j+\frac{1}{2}} + |\vec{V_s}|_{i+\frac{1}{2}, j+\frac{1}{2}}\right)\Delta x_{j+\frac{1}{2}}\right]$$

$$\rho_4 = \frac{\pi + 200}{10\,R\,T_4}$$

$$C_D = \begin{cases} 0.002\left(1 + \frac{3\cdot\phi_0}{g\,5000}\right) & \text{over land} \\ Min\left[0.0025, 0.001\,(1. + 0.07|V'|)\right] & \text{over water} \end{cases}$$

$$\vec{V_s} = 0.7 \left(1.5 \vec{V_3} - 0.5 \vec{V_1} \right).$$

Finite differencing to the π grid.

$$\nabla \cdot (\vec{V} \bar{z}) = \frac{1}{4 \Delta x_j^2} \left[\left(\Delta x_{j+\frac{1}{2}} \bar{u}_{i+\frac{1}{2},j+\frac{1}{2}} + \Delta x_{j-\frac{1}{2}} \bar{u}_{i+\frac{1}{2},j-\frac{1}{2}} \right) \left(\bar{z}_{i+1,j} + \bar{z}_{i,j} \right) - \right.$$

$$- \left(\Delta x_{j+\frac{1}{2}} \bar{u}_{i-\frac{1}{2},j+\frac{1}{2}} + \Delta x_{j-\frac{1}{2}} \bar{u}_{i-\frac{1}{2},j-\frac{1}{2}} \right) \left(\bar{z}_{i,j} + \bar{z}_{i-1,j} \right) \right] +$$

$$- \frac{1}{4 \Delta x_j \Delta y} \left[\Delta x_{j+\frac{1}{2}} \left(\bar{v}_{i+\frac{1}{2},j+\frac{1}{2}} + \bar{v}_{i-\frac{1}{2},j+\frac{1}{2}} \right) \left(\bar{z}_{i,j+1} + \bar{z}_{i,j} \right) - \right.$$

$$\left. - \Delta x_{j-\frac{1}{2}} \left(v_{i+\frac{1}{2},j-\frac{1}{2}} + v_{i-\frac{1}{2},j-\frac{1}{2}} \right) \left(z_{i,j} + z_{i,j-1} \right) \right],$$

$$\nabla \cdot (\vec{V^*} \bar{z}^*) = \text{Same as above } u^*, v^*, z^*$$

$$\vec{k} \cdot \left[\vec{V} \times \nabla (2\dot{\sigma_2}) \right] = \frac{2}{4 \Delta x_i \Delta y} \left[\Delta x_{j+\frac{1}{2}} \left(u^*_{i+\frac{1}{2},j+\frac{1}{2}} + u^*_{i-\frac{1}{2},j+\frac{1}{2}} \right) \left(\dot{\sigma}_{2_{i,j+1}} - \dot{\sigma}_{2_{i,j}} \right) + \right.$$

$$\left. + \Delta x_{j-\frac{1}{2}} \left(u^*_{i+\frac{1}{2},j-\frac{1}{2}} + u^*_{i-\frac{1}{2},j-\frac{1}{2}} \right) \left(\dot{\sigma}_{2_{i,j}} - \dot{\sigma}_{2_{i,j-1}} \right) \right] -$$

$$- \frac{2}{4 \Delta x_j^2} \left[\left(\Delta x_{j+\frac{1}{2}} v^*_{i+\frac{1}{2},j+\frac{1}{2}} + \Delta x_{j-\frac{1}{2}} v^*_{i+\frac{1}{2},j-\frac{1}{2}} \right) \left(\dot{\sigma}_{2_{i+1,j}} - \dot{\sigma}_{2_{i,j}} \right) + \right.$$

$$\left. + \left(\Delta x_{j+\frac{1}{2}} v^*_{i-\frac{1}{2},j+\frac{1}{2}} + \Delta x_{j-\frac{1}{2}} v^*_{i-\frac{1}{2},j-\frac{1}{2}} \right) \left(\dot{\sigma}_{2_{i,j}} - \dot{\sigma}_{2_{i-1,j}} \right) \right].$$

$$J(\pi, \overline{\sigma \alpha}) = \frac{1}{4 \Delta x_j \Delta y} \left(\pi_{i+1,j} - \pi_{i-1,j} \right) \left(\overline{\sigma \alpha}_{i,j+1} - \overline{\sigma \alpha}_{i,j-1} \right) -$$

$$- \frac{1}{4 \Delta x_j \Delta y} \left(\pi_{i,j+1} - \pi_{i,j-1} \right) \left(\overline{\sigma \alpha}_{i+1,j} - \overline{\sigma \alpha}_{i-1,j} \right),$$

$$\dot{\sigma_2} = - \frac{1}{4 \pi_{i,j}} \left\{ \left[\left(\Delta x_{j+\frac{1}{2}} u^*_{i+\frac{1}{2},j+\frac{1}{2}} + \Delta x_{j-\frac{1}{2}} u^*_{i+\frac{1}{2},j-\frac{1}{2}} \right) \left(\pi_{i+1,j} + \pi_{i,j} \right) - \right. \right.$$

$$\left. - \left(\Delta x_{j+\frac{1}{2}} u^*_{i-\frac{1}{2},j+\frac{1}{2}} + \Delta x_{j-\frac{1}{2}} u^*_{i-\frac{1}{2},j-\frac{1}{2}} \right) \left(\pi_{i,j} + \pi_{i-1,j} \right) \right] \Big/ 2 \left(\Delta x_{j+\frac{1}{2}} - \Delta x_{j-\frac{1}{2}} \right) \Delta x_j$$

$$+ \frac{1}{4 \Delta x_j \Delta y} \left[\left(v^*_{i+\frac{1}{2},j+\frac{1}{2}} + v^*_{i-\frac{1}{2},j+\frac{1}{2}} \right) \left(\pi_{i,j+1} + \pi_{i,j} \right) \Delta x_{j+\frac{1}{2}} - \right.$$

$$\left. \left. - \left(v^*_{i+\frac{1}{2},j-\frac{1}{2}} + v^*_{i-\frac{1}{2},j-\frac{1}{2}} \right) \left(\pi_{i,j} + \pi_{i,j-1} \right) \Delta x_{j-\frac{1}{2}} \right] \right\}.$$

$$\vec{k} \cdot \nabla \times \vec{\vec{F}} = \frac{1}{4 \Delta x_i^2} \Big[\big(\Delta x_{j+\frac{1}{2}} \, \mathcal{V}_{s_{i+\frac{1}{2},j+\frac{1}{2}}} + \Delta x_{j-\frac{1}{2}} \, \mathcal{V}_{s_{i+\frac{1}{2},j-\frac{1}{2}}} \big) \big(C_{i+1,j} + C_{i,j} \big) -$$

$$- \big(\Delta x_{j+\frac{1}{2}} \, \mathcal{V}_{s_{i-\frac{1}{2},j+\frac{1}{2}}} + \Delta x_{j-\frac{1}{2}} \, \mathcal{V}_{s_{i-\frac{1}{2},j-\frac{1}{2}}} \big) \big(C_{i-1,j} + C_{i,j} \big) \Big] -$$

$$- \frac{1}{4 \Delta x_j \, \Delta y} \Big[\Delta x_{j+\frac{1}{2}} \big(u_{s_{i+\frac{1}{2},j+\frac{1}{2}}} + u_{s_{i-\frac{1}{2},j+\frac{1}{2}}} \big) \big(C_{i,j+1} + C_{i,j} \big) -$$

$$- \Delta x_{j-\frac{1}{2}} \big(u_{s_{i+\frac{1}{2},j-\frac{1}{2}}} + u_{s_{i-\frac{1}{2},j-\frac{1}{2}}} \big) \big(C_{i,j} + C_{i,j-1} \big) \Big] \, ,$$

$$z^* = \frac{1}{2 \Delta x_j^2} \Big[\Delta x_{j+\frac{1}{2}} \big(\mathcal{V}^*_{i+\frac{1}{2},j+\frac{1}{2}} - \mathcal{V}^*_{i-\frac{1}{2},j+\frac{1}{2}} \big) + \Delta x_{j-\frac{1}{2}} \big(\mathcal{V}^*_{i+\frac{1}{2},j-\frac{1}{2}} - \mathcal{V}^*_{i-\frac{1}{2},j-\frac{1}{2}} \big) \Big] -$$

$$- \frac{1}{2 \Delta x_j \, \Delta y} \Big[\Delta x_{j+\frac{1}{2}} \big(u^*_{i+\frac{1}{2},j+\frac{1}{2}} + u^*_{i-\frac{1}{2},j+\frac{1}{2}} \big) - \Delta x_{j-\frac{1}{2}} \big(u^*_{i+\frac{1}{2},j-\frac{1}{2}} + u^*_{i-\frac{1}{2},j-\frac{1}{2}} \big) \Big] \, ,$$

$$\vec{z} = \text{Same as above with } u^*, v^*$$

$$\vec{\vec{v}} = \frac{\vec{\vec{y}}_1 + \vec{\vec{v}}_3}{2}$$

$$\vec{v}^* = \frac{\vec{v}_1^* - \vec{v}_3^*}{2}$$
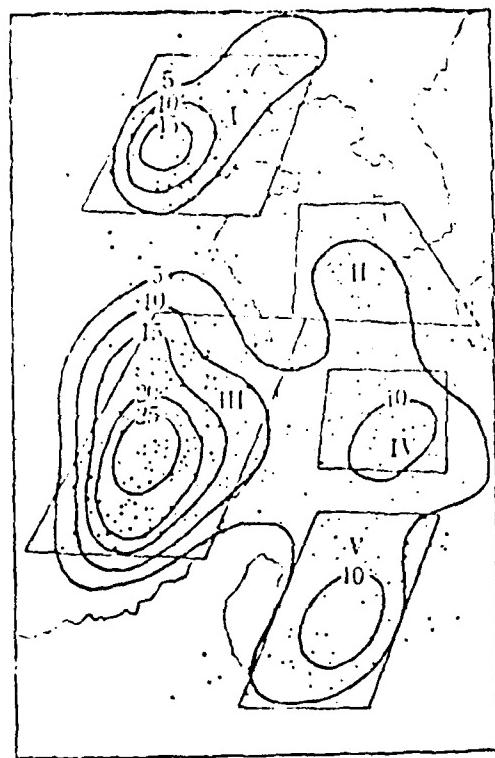
Fig. 1   Geographic distribution of numbers of cyclogenesis between one
ten year period from 1967-1976 (after Liu, 1980).
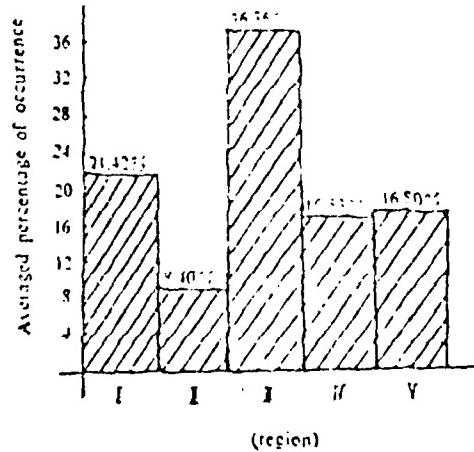
Fig. 2a.   The percentage of occurrence of
each region with total of 343
cases.
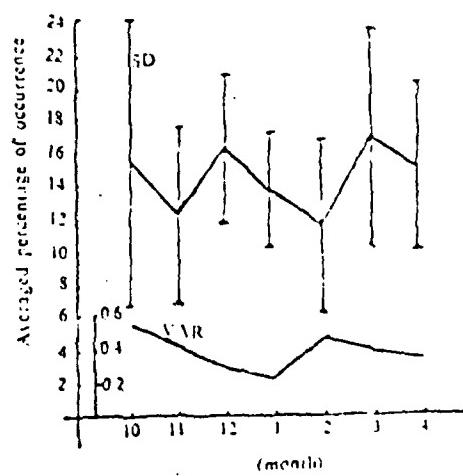
Fig. 2b.   Monthly averaged percentage of
cyclogenesis bases on data
shown in Fig. 1 (after Liu,
1980).
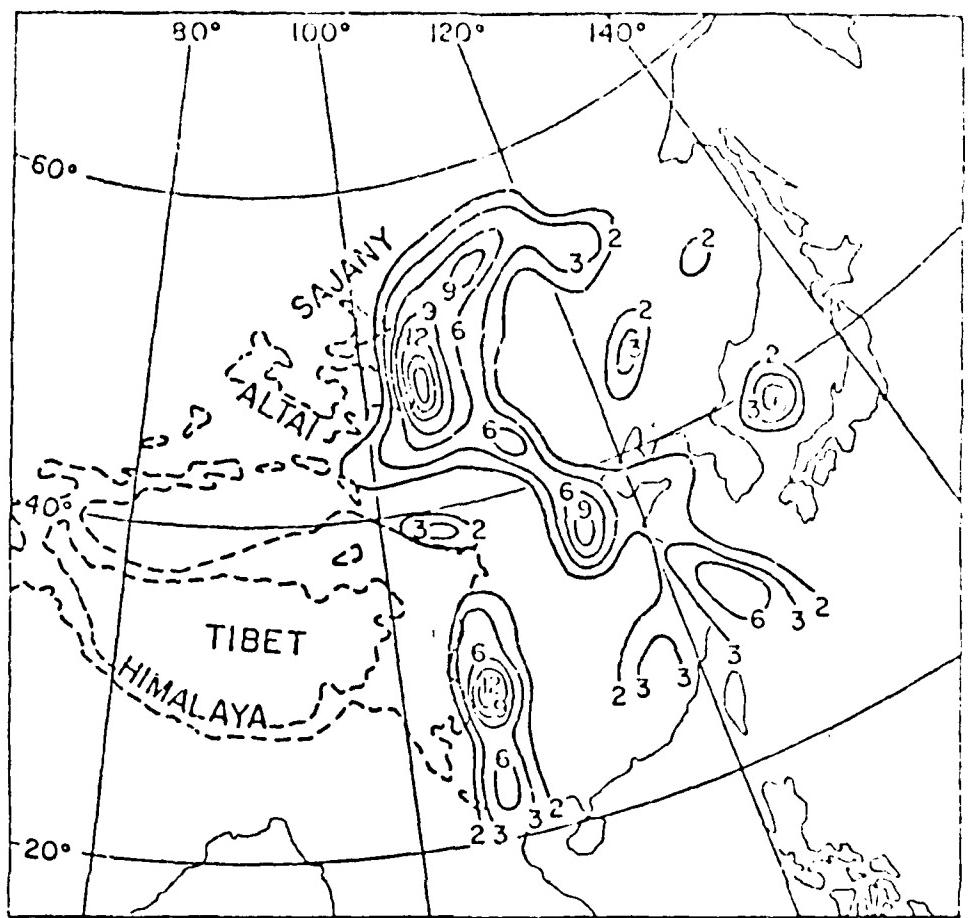
Fig. 3 Frequency distribution of cyclones generated in 2.5° quadrangle areas over East Asia during 1958 (Chung et. al., 1976).
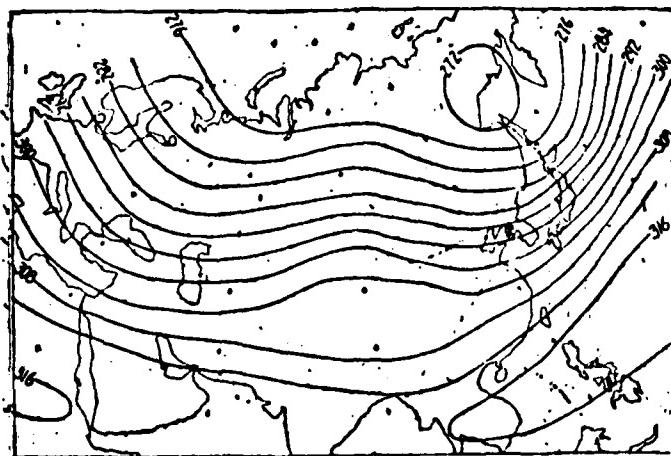
Fig. 4a. Historical mean January 700 mb chart (after Li , 1976).
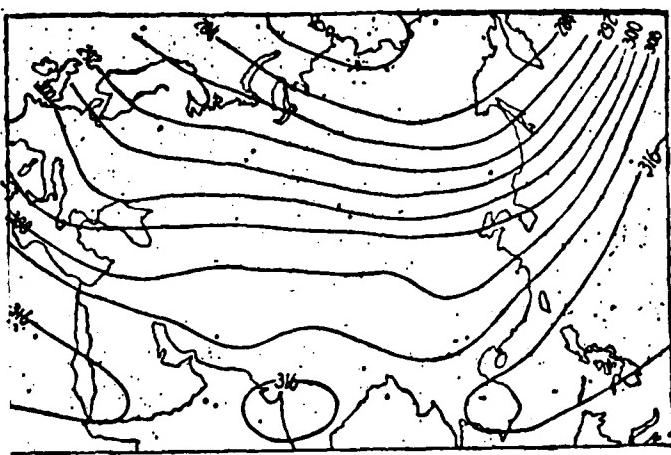
Fig. 4b. Historical mean April 700 mb chart (after Li , 1976).
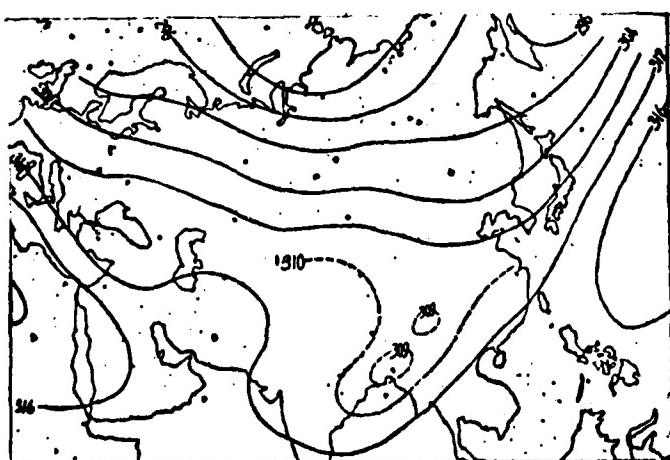
Fig. 4c. Historical mean June 700 mb chart (after Li , 1976).

1200 GMT

(b)

(a)
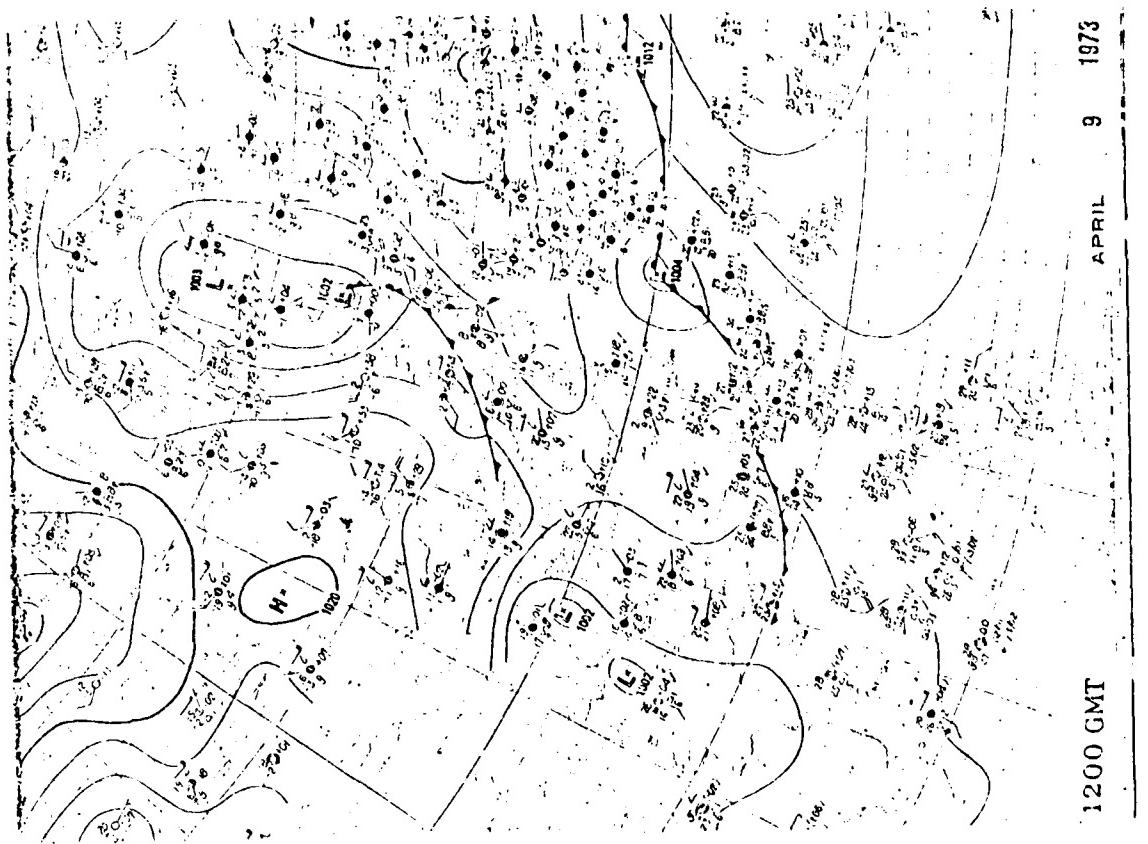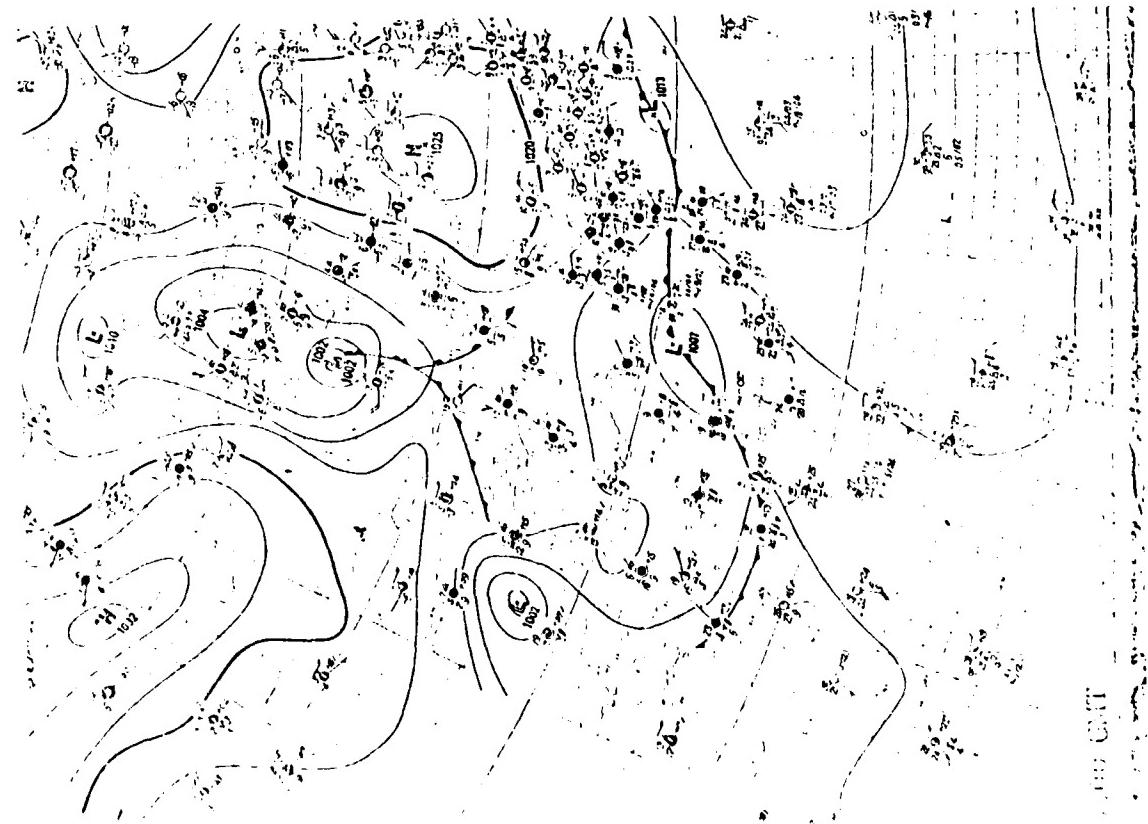
APRIL 9 1973

Fig. 5 Surface charts for (a) 06Z, and (b) 12Z and (c) 500 mb chart for 12Z, April 9, 1973.

68

APRIL 9 1973

(c)

1200 GMT

(b)

APRIL 10 1973

(a)
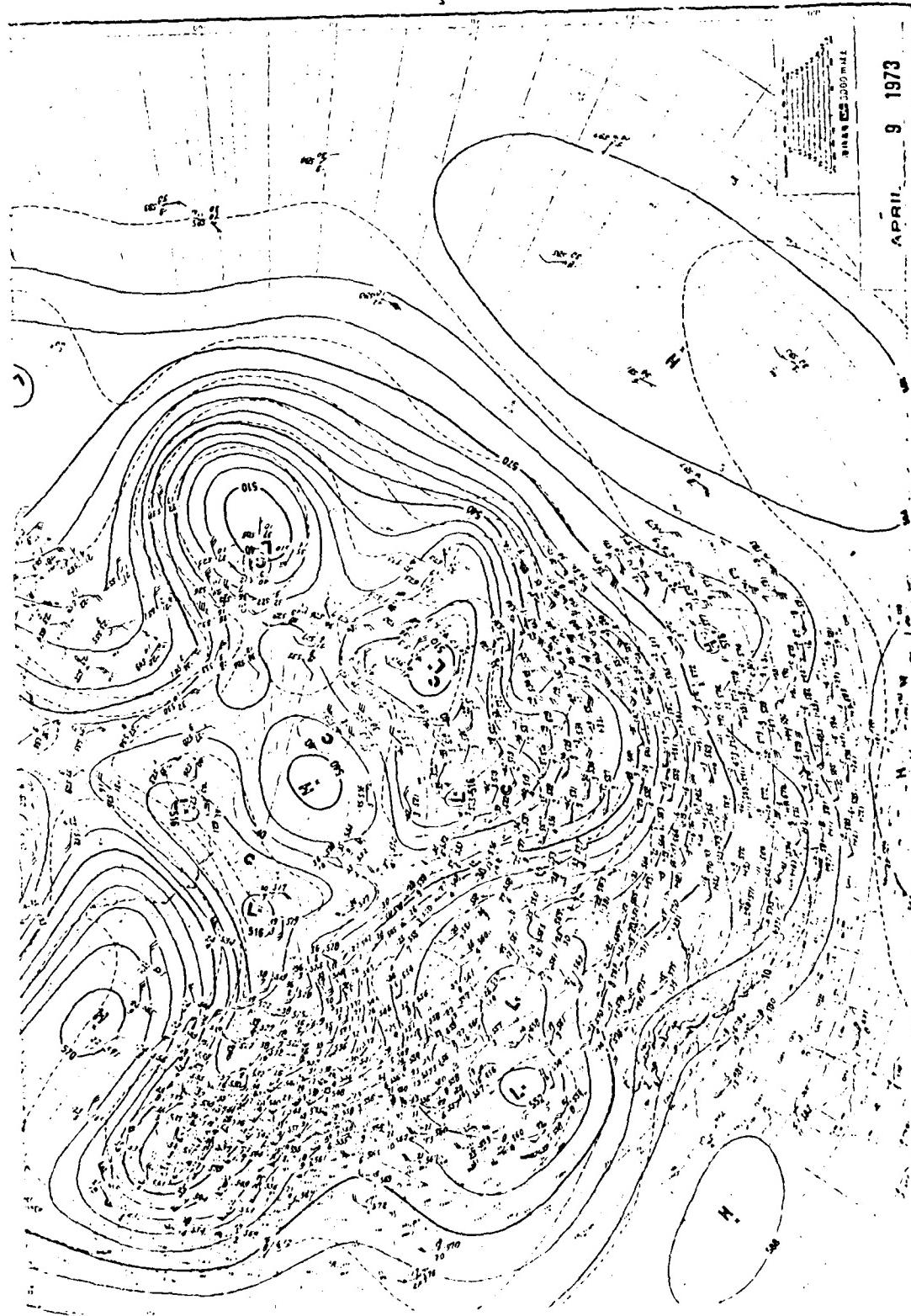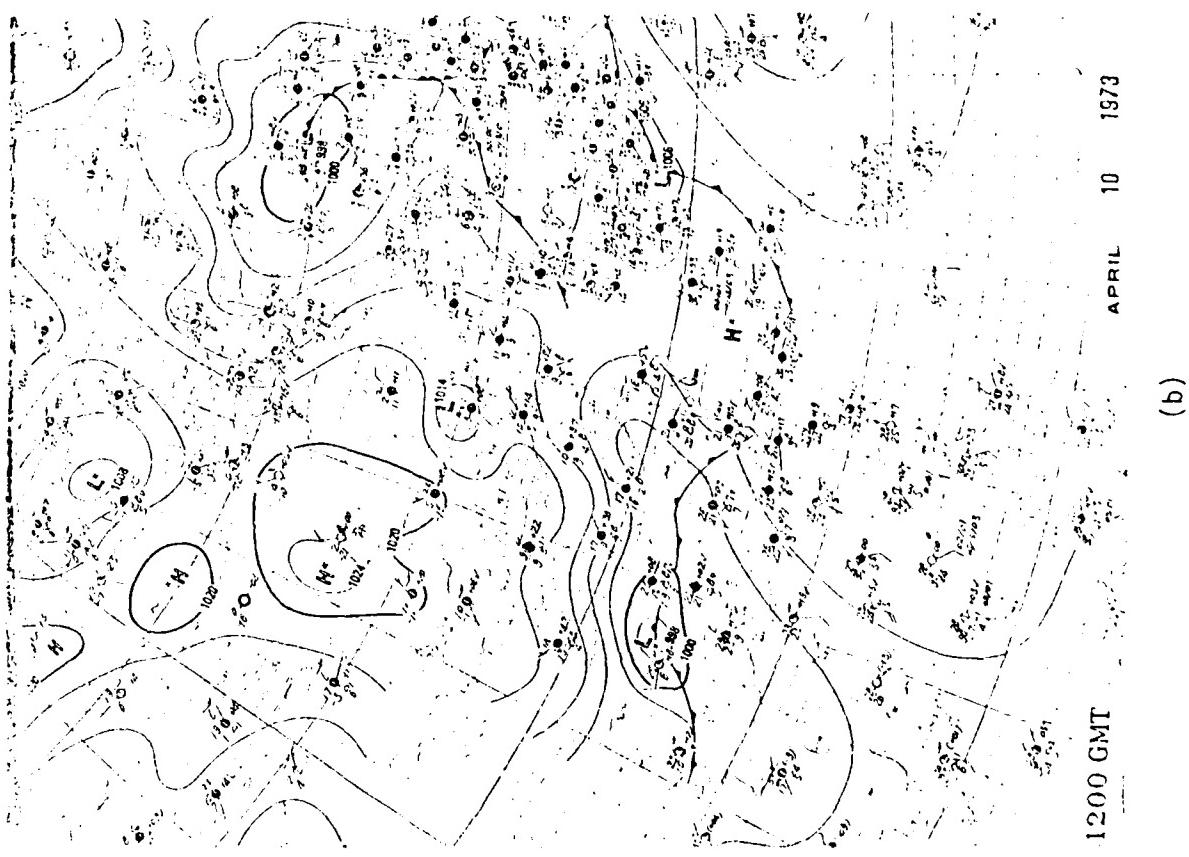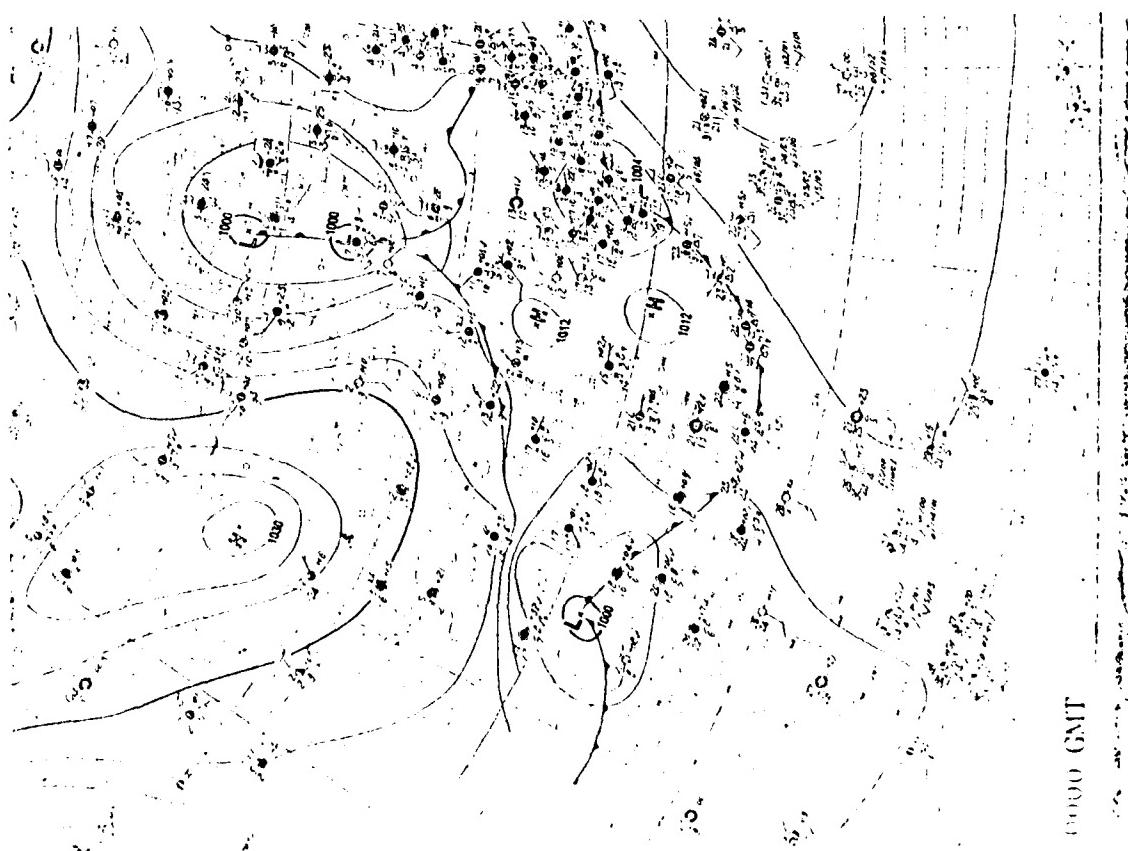
Fig. 6. As in Fig. 5, except for April 10, 1973.

70

APRIL 10 1973

(c)

71

1200 GMT   APRIL   11   1973
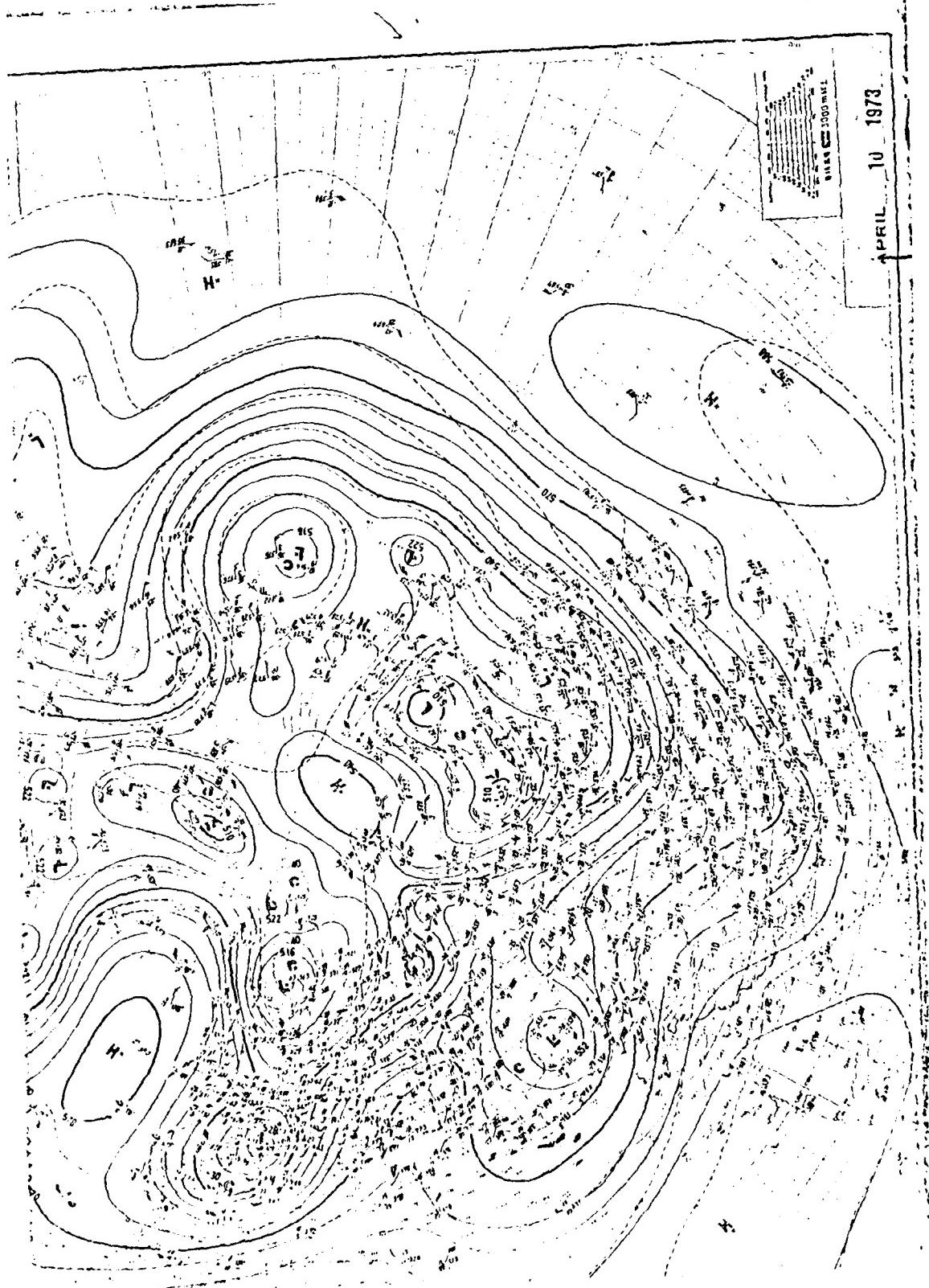
(b)
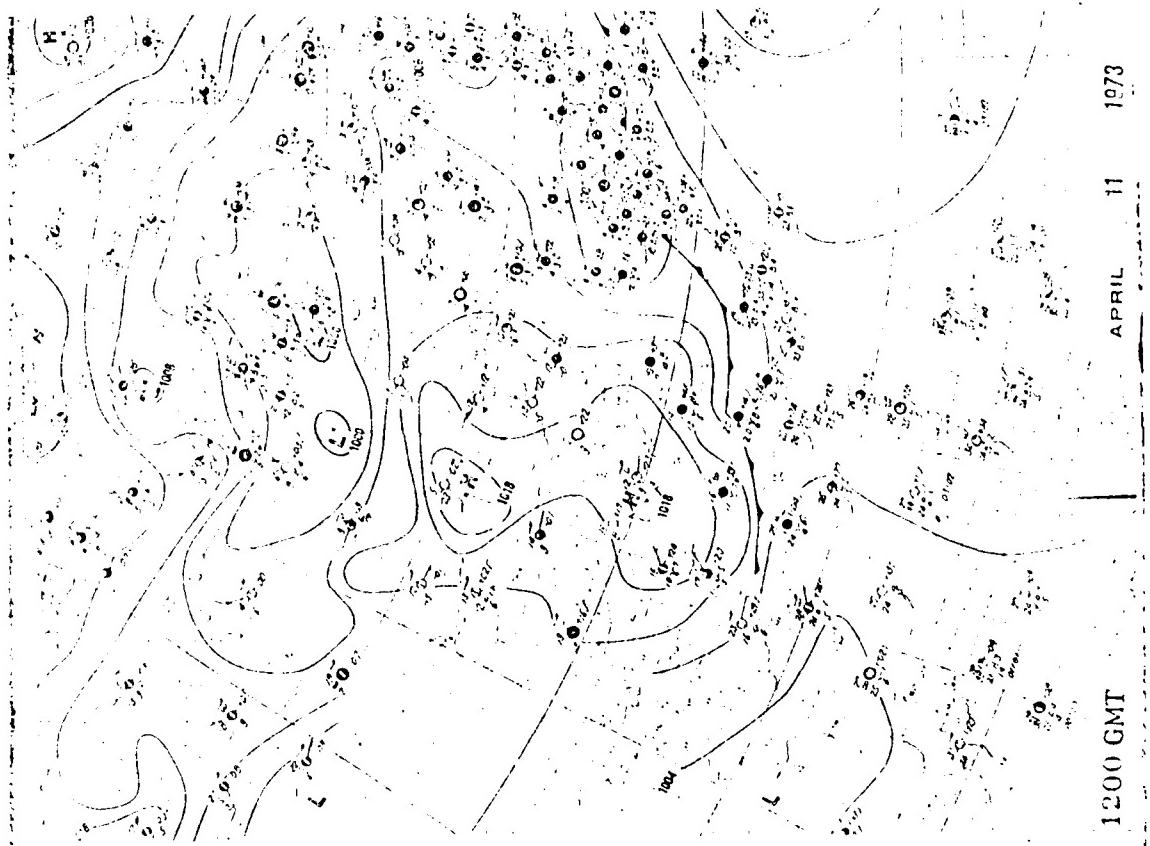
(a)
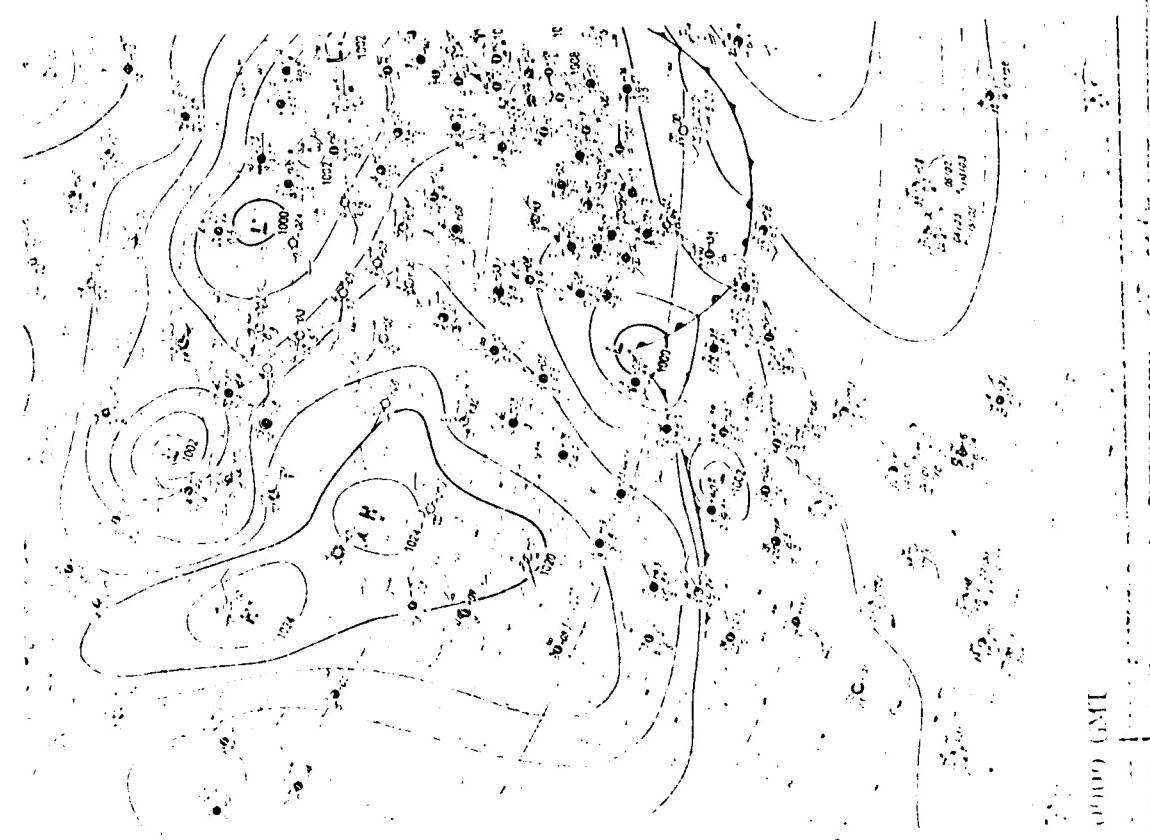
Fig. 7 As in Fig. 5, except for April 11, 1973.

72

APRIL 11 1973

(c)

73

(b)

(d)

APRIL 20 1974

Fig. 3 As in Fig. 5, except for April 20, 1973.

APRIL 20 1974

(c)

75

(b)

(a)
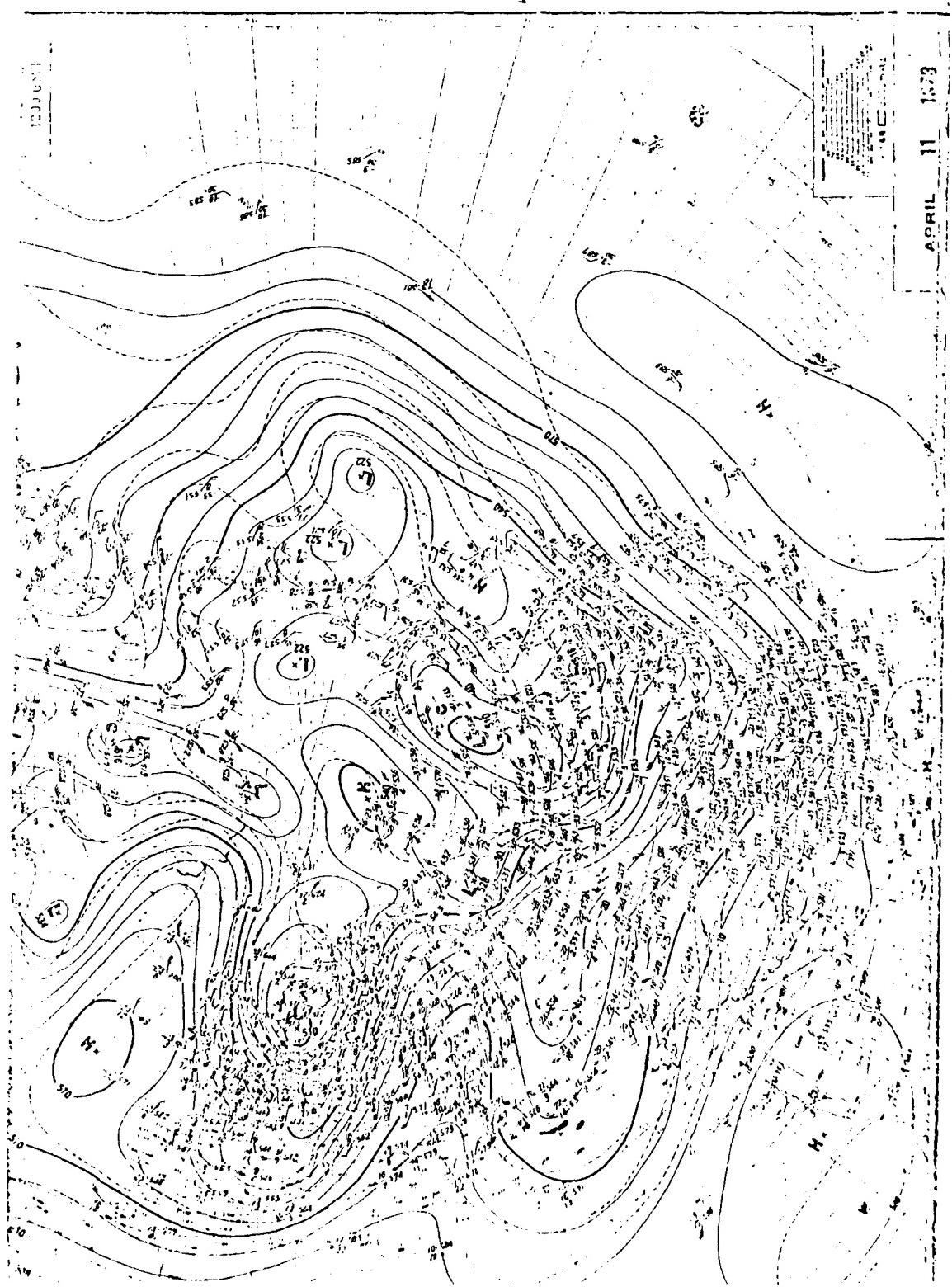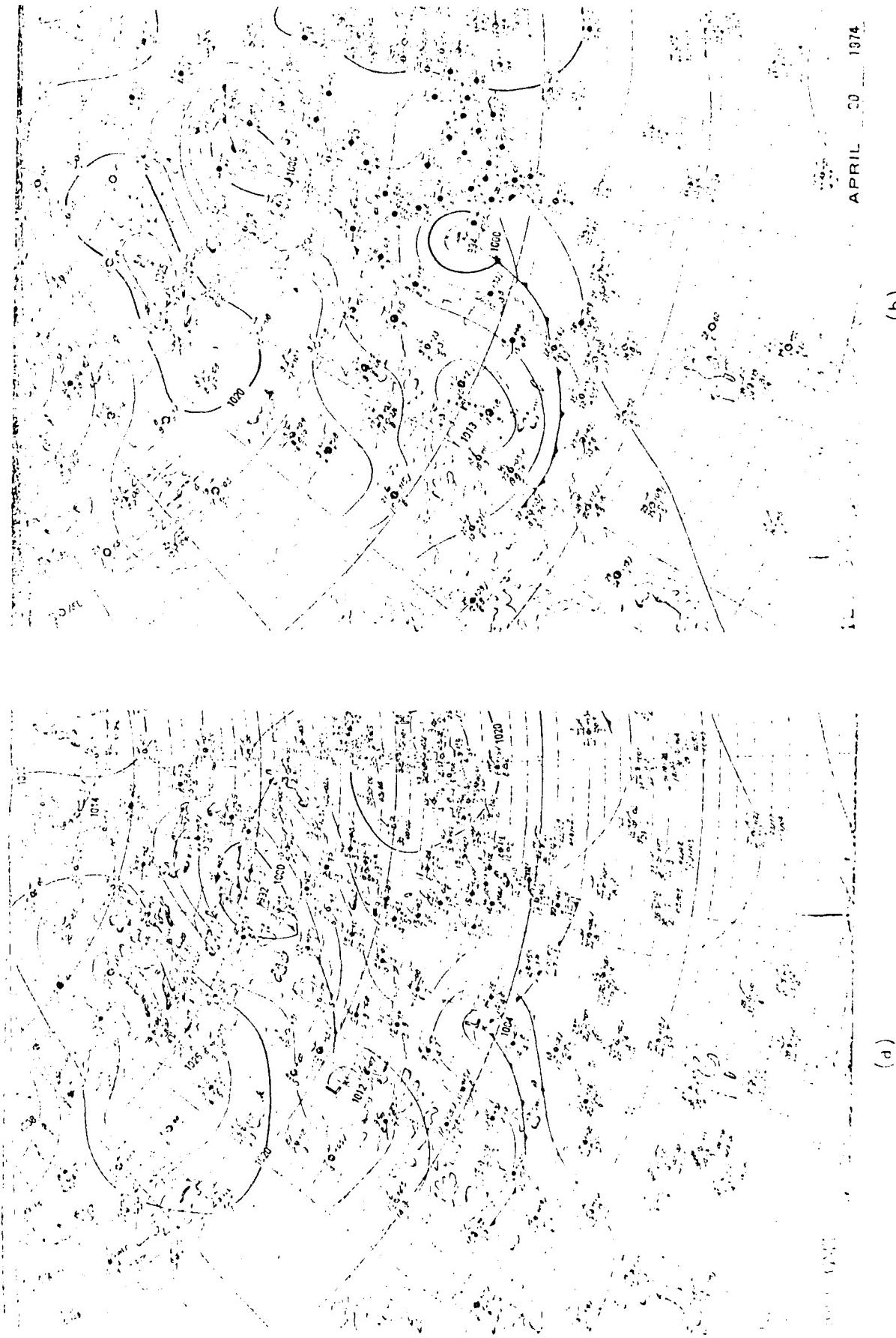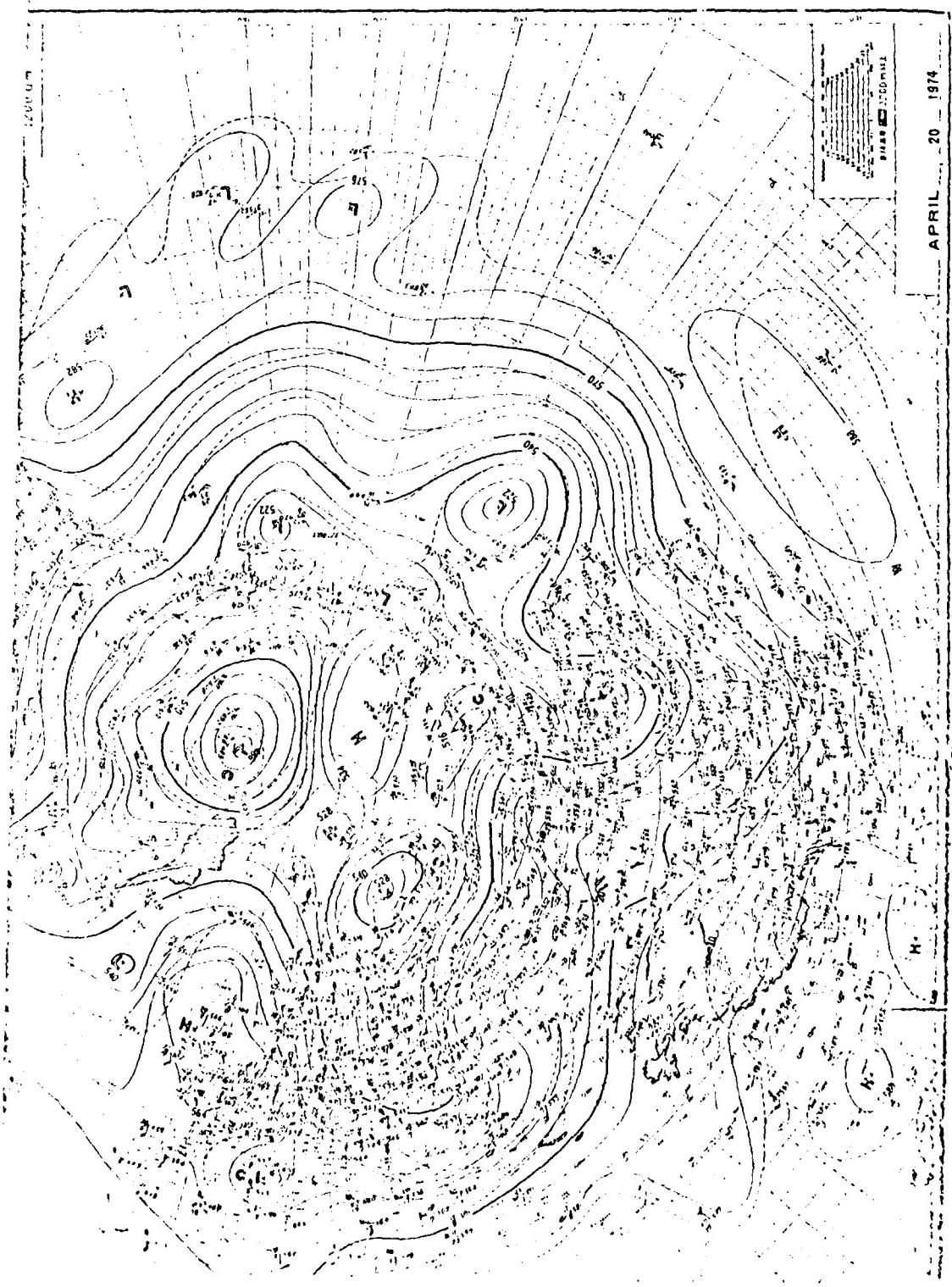
MARCH 19 1975

Fig. 9 As in Fig. 5, except for March 19, 1975.

76

MARCH 19 1975

(c)

77

1200 GMT

(b)

MARCH 29, 1977

(a)
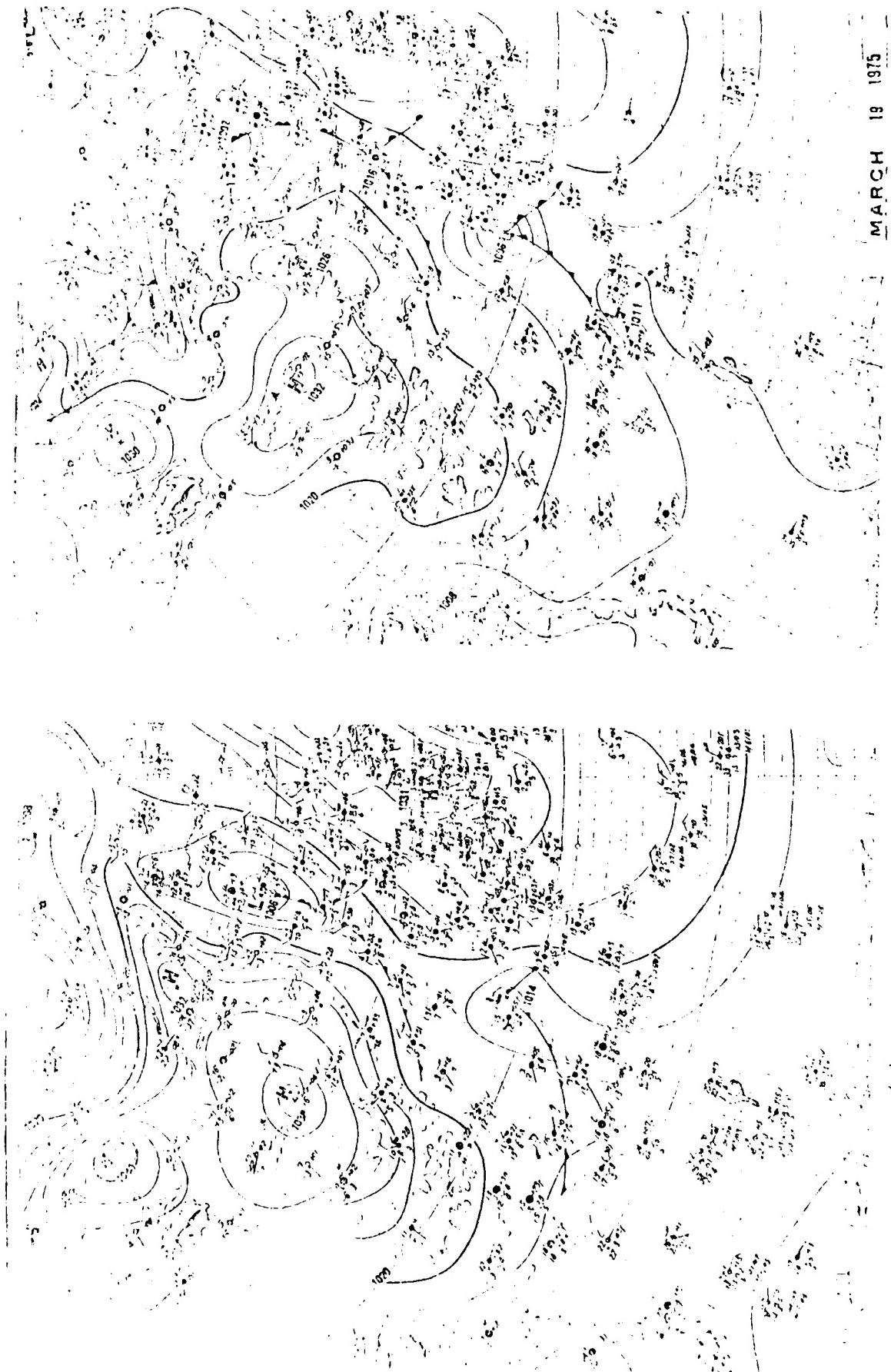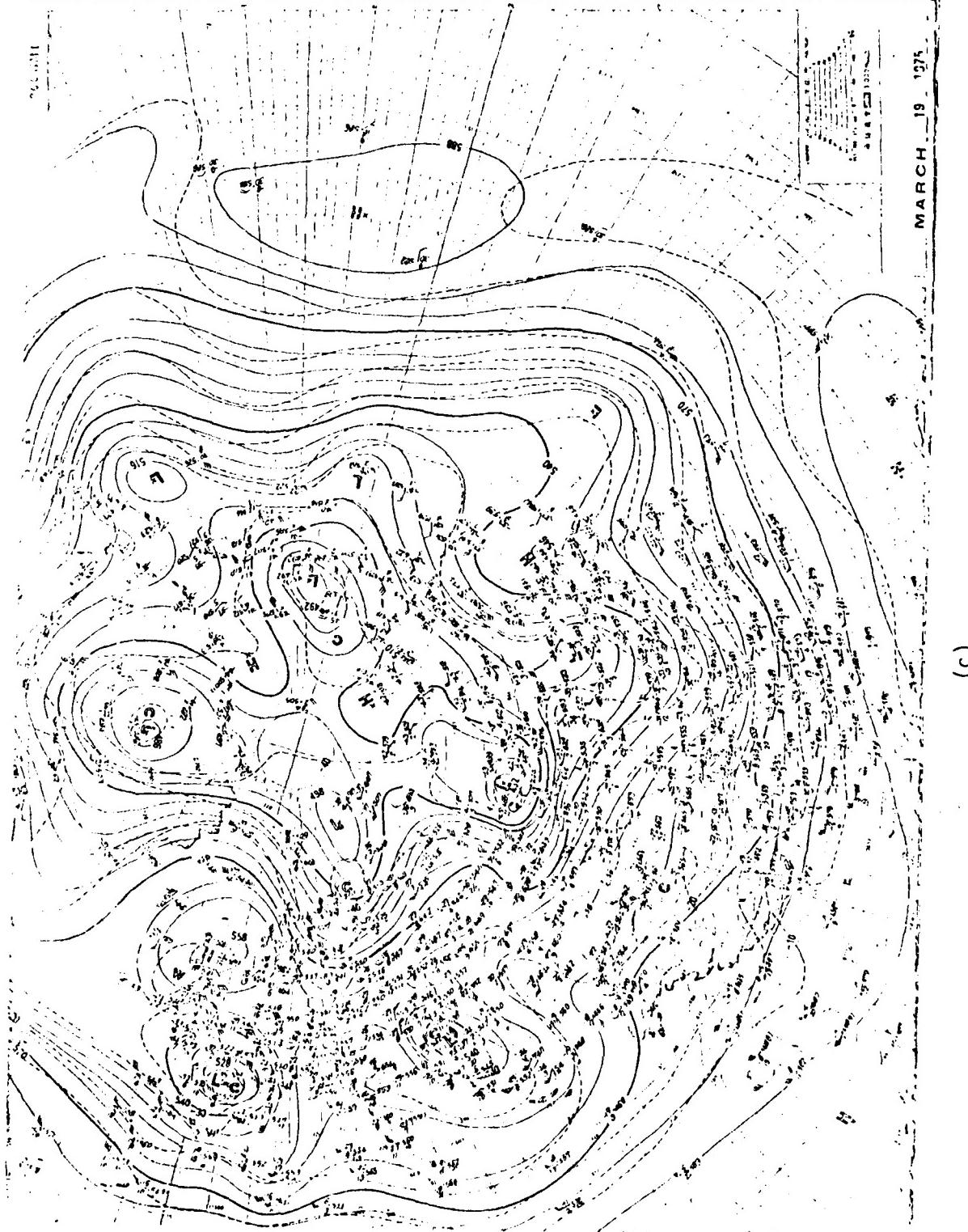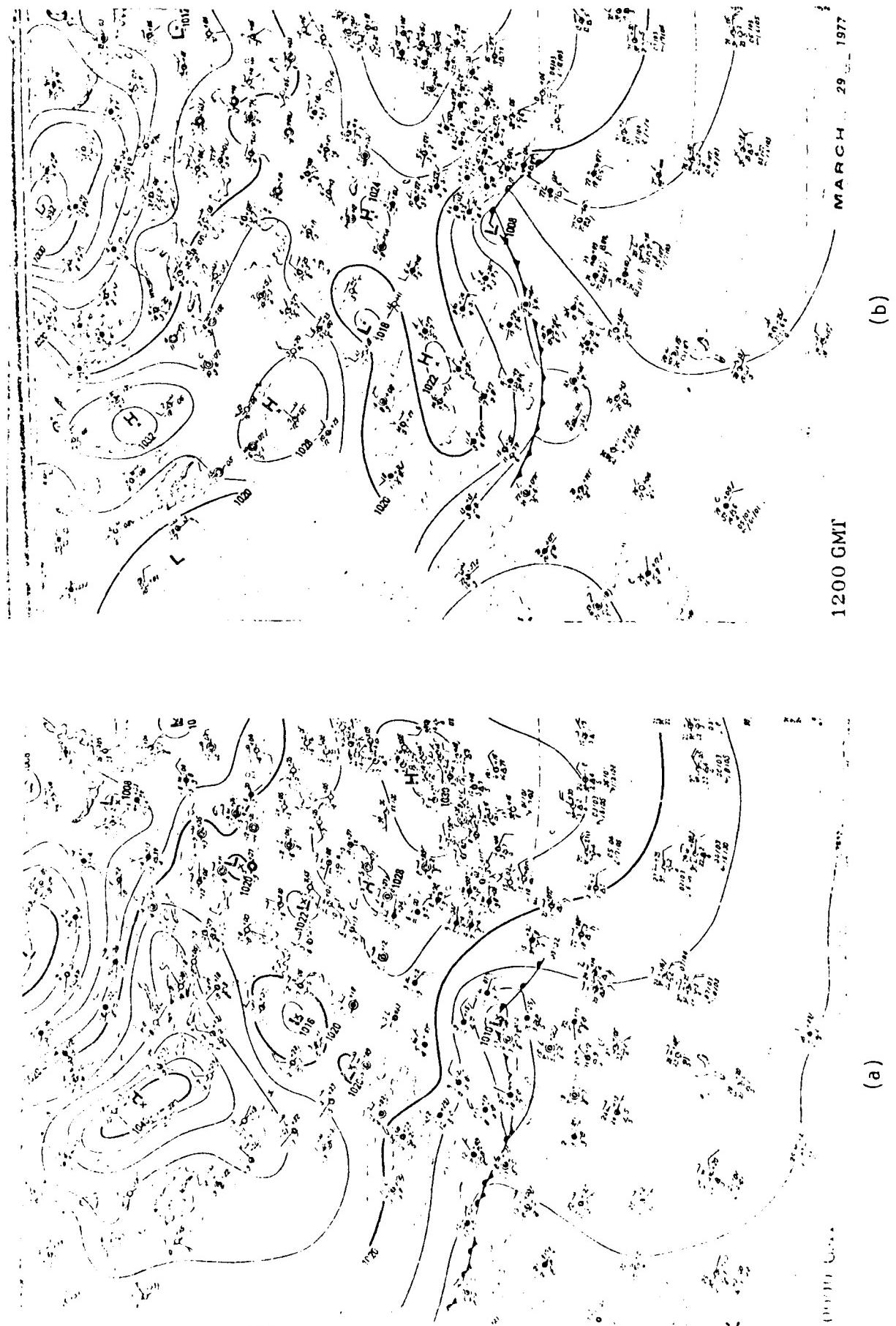
Fig. 10 As in Fig. 5, except for March 29, 1977.

78

MARCH. 20 1977

(c)

1200 GMT

APRIL 14 1977

(a)

(b)
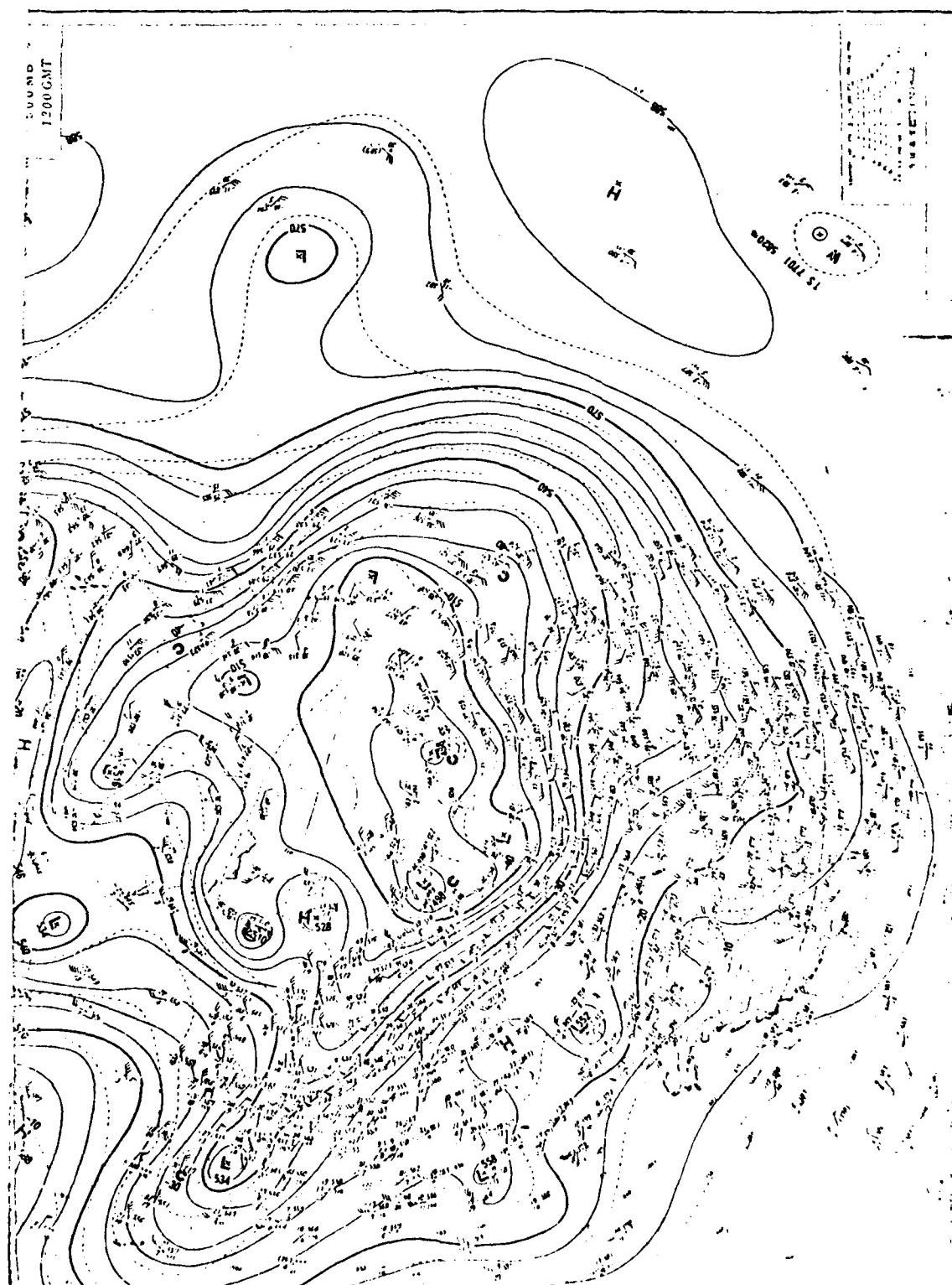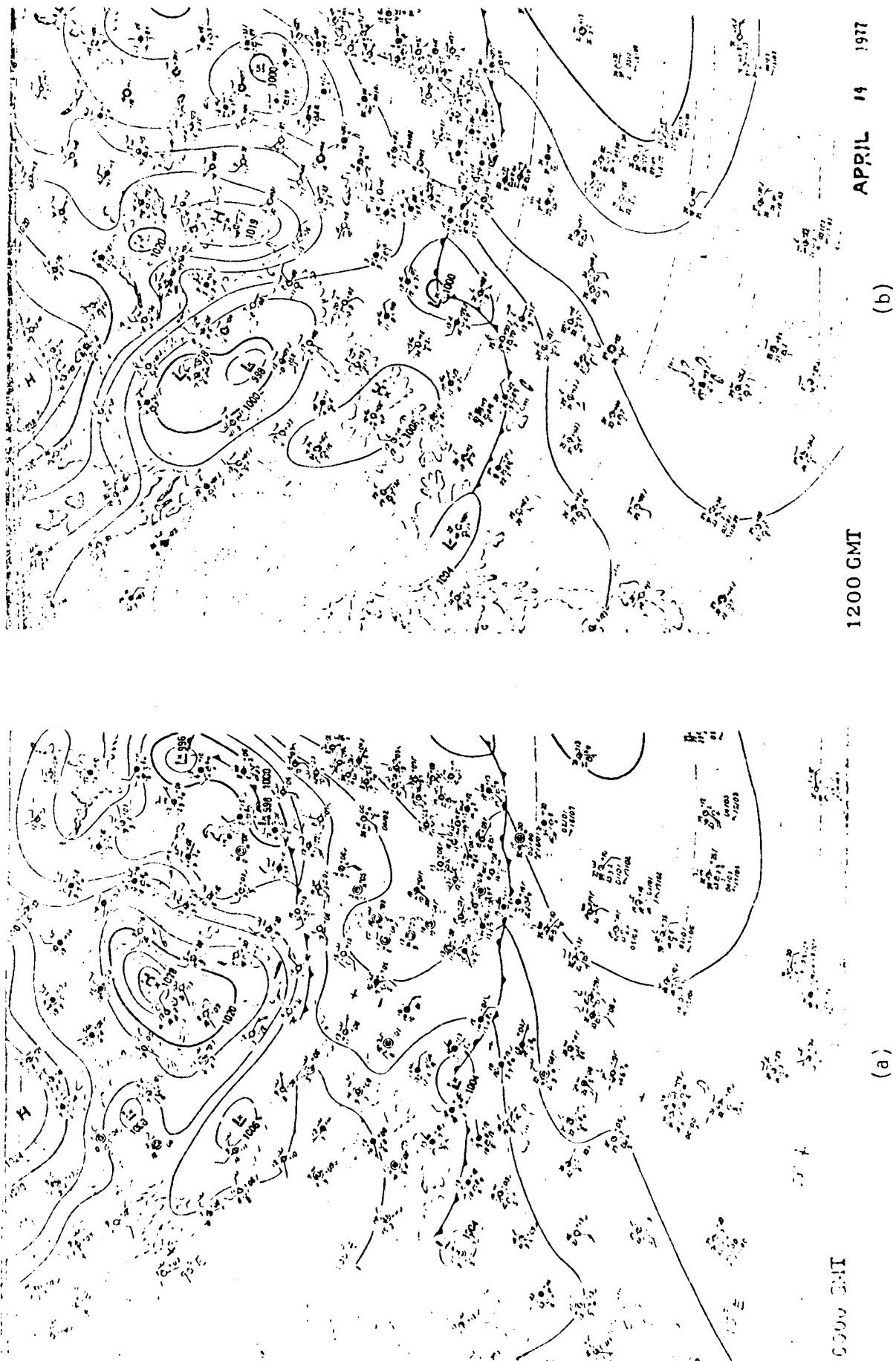
Fig. 11 As in Fig. 5, except for April 14, 1977.

(c)

1200 GMT

MARCH 20 1978

(b)
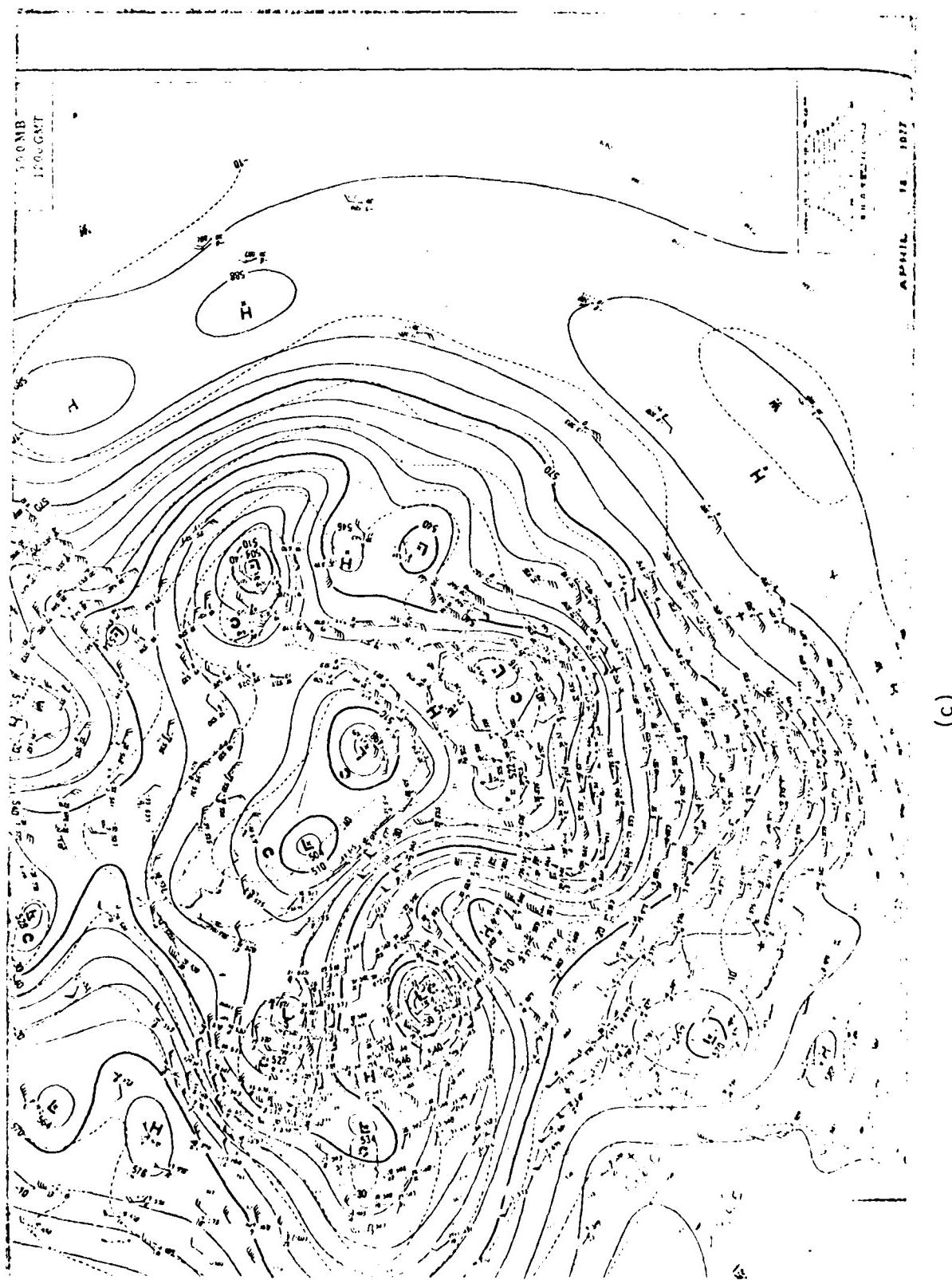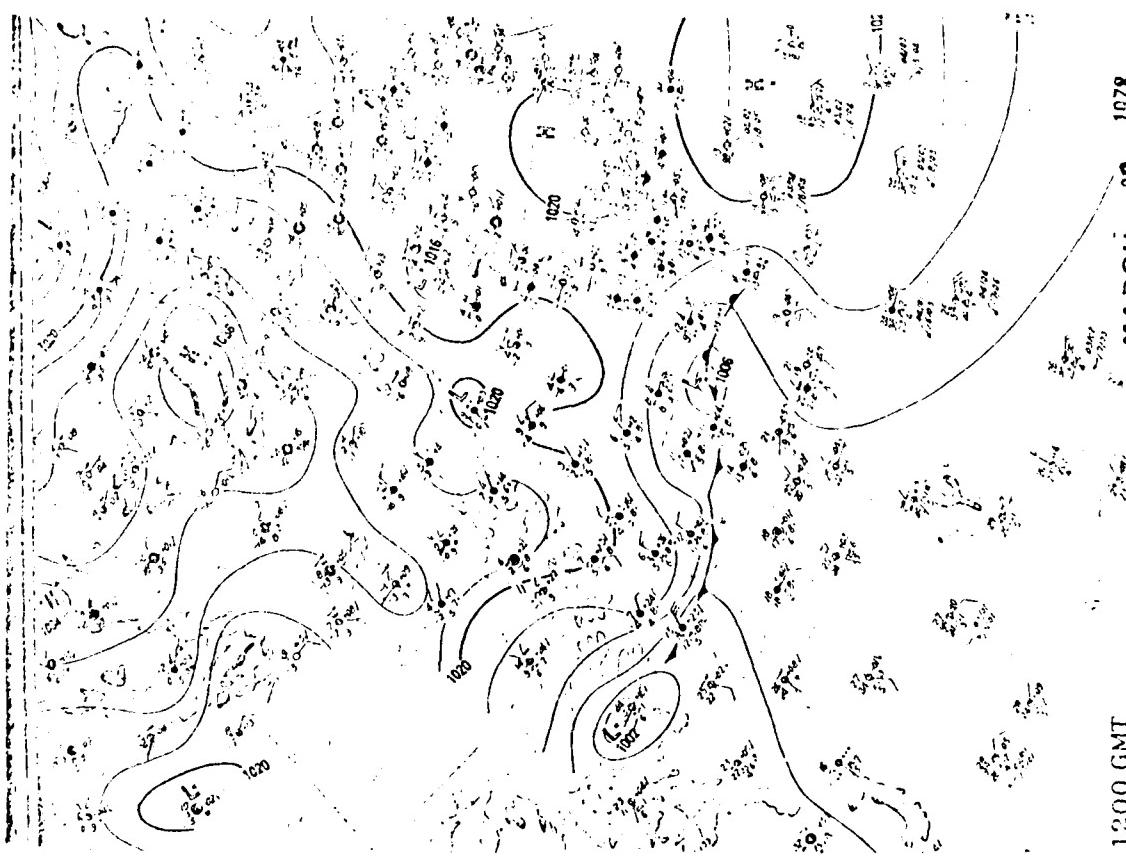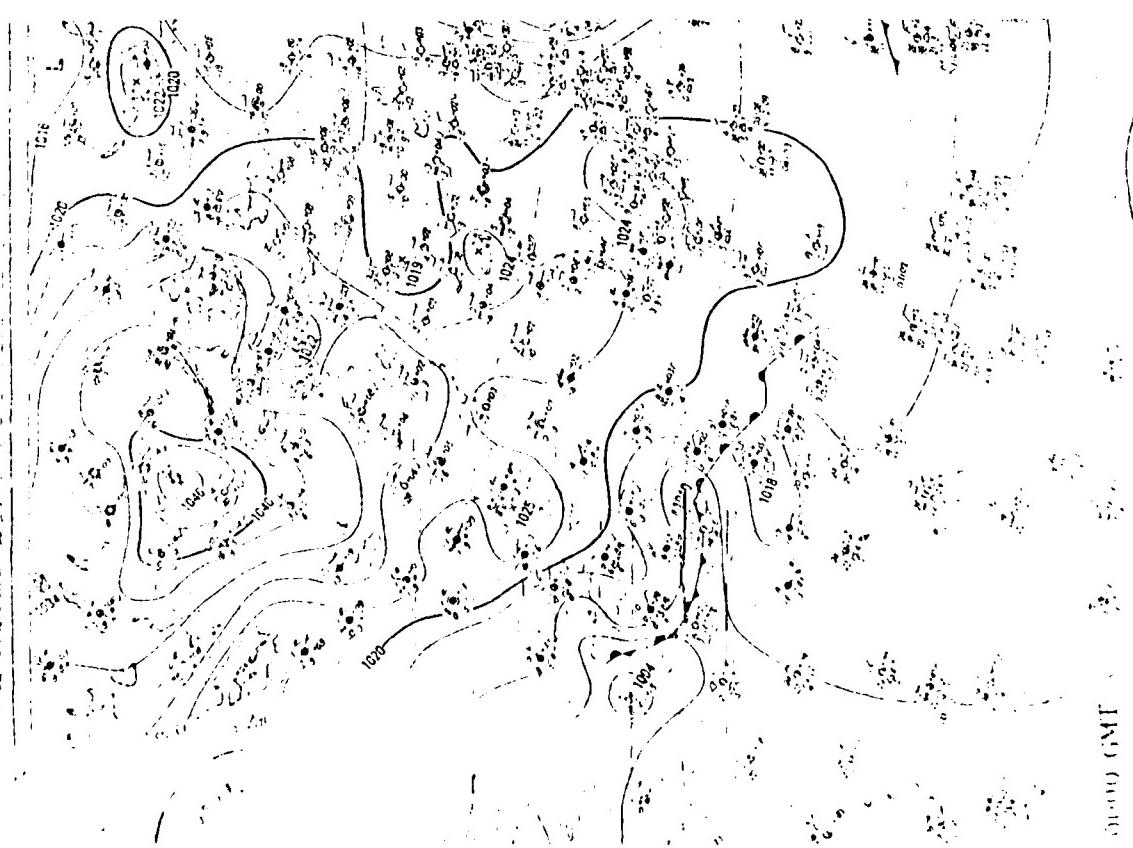
(a)

Fig. 12 As in Fig. 5, except for March 20, 1978.

82

(c)

1200 GMT

(b)

APRIL 6 1979

(a)
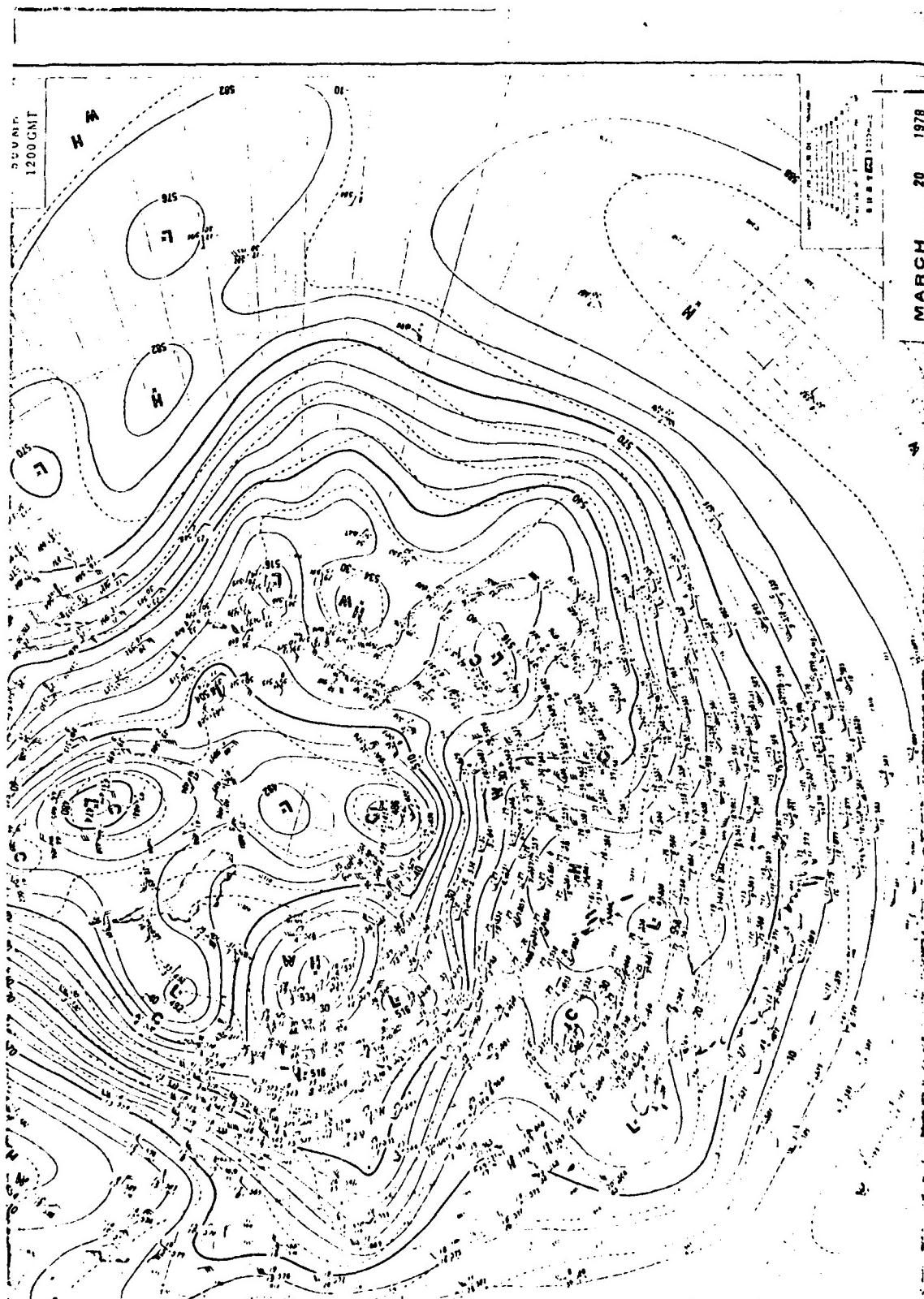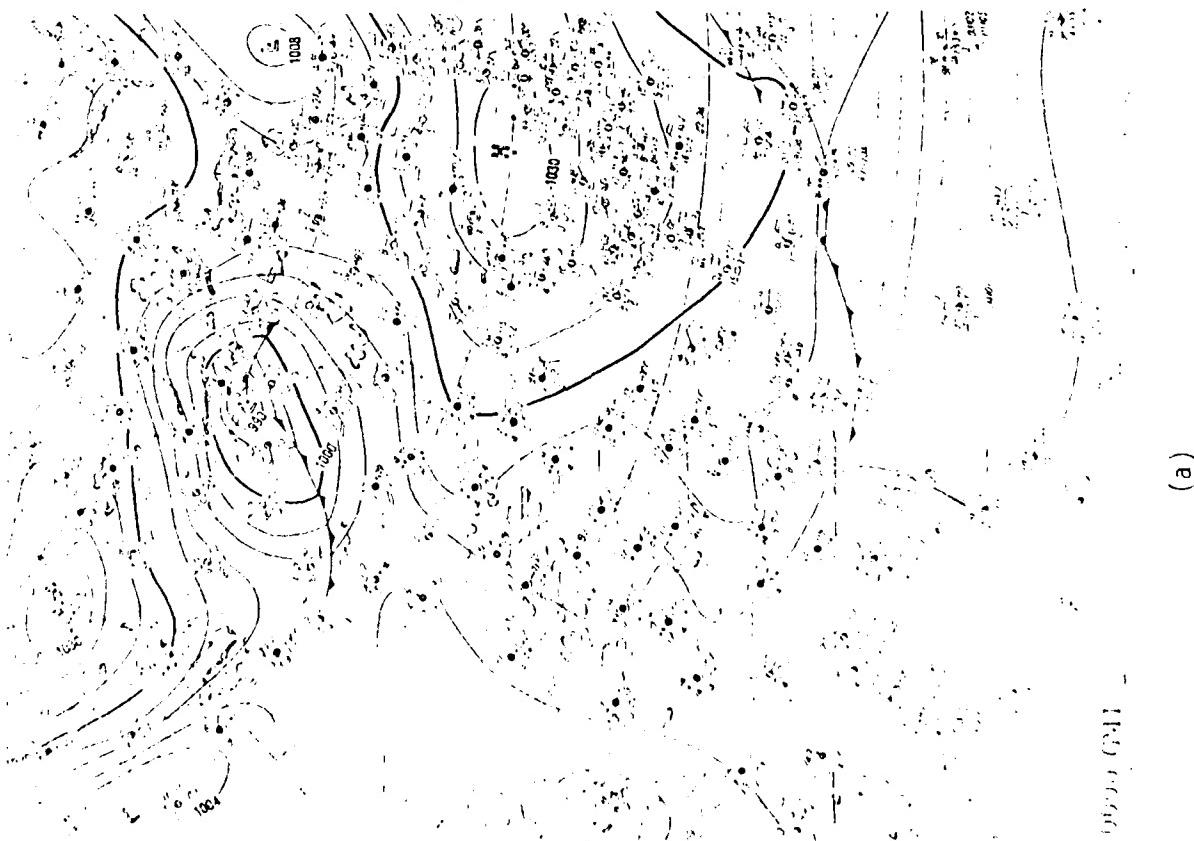
Fig. 13 As in Fig. 5, except for April 6, 1979.

APRIL 6 1979

(c)

85
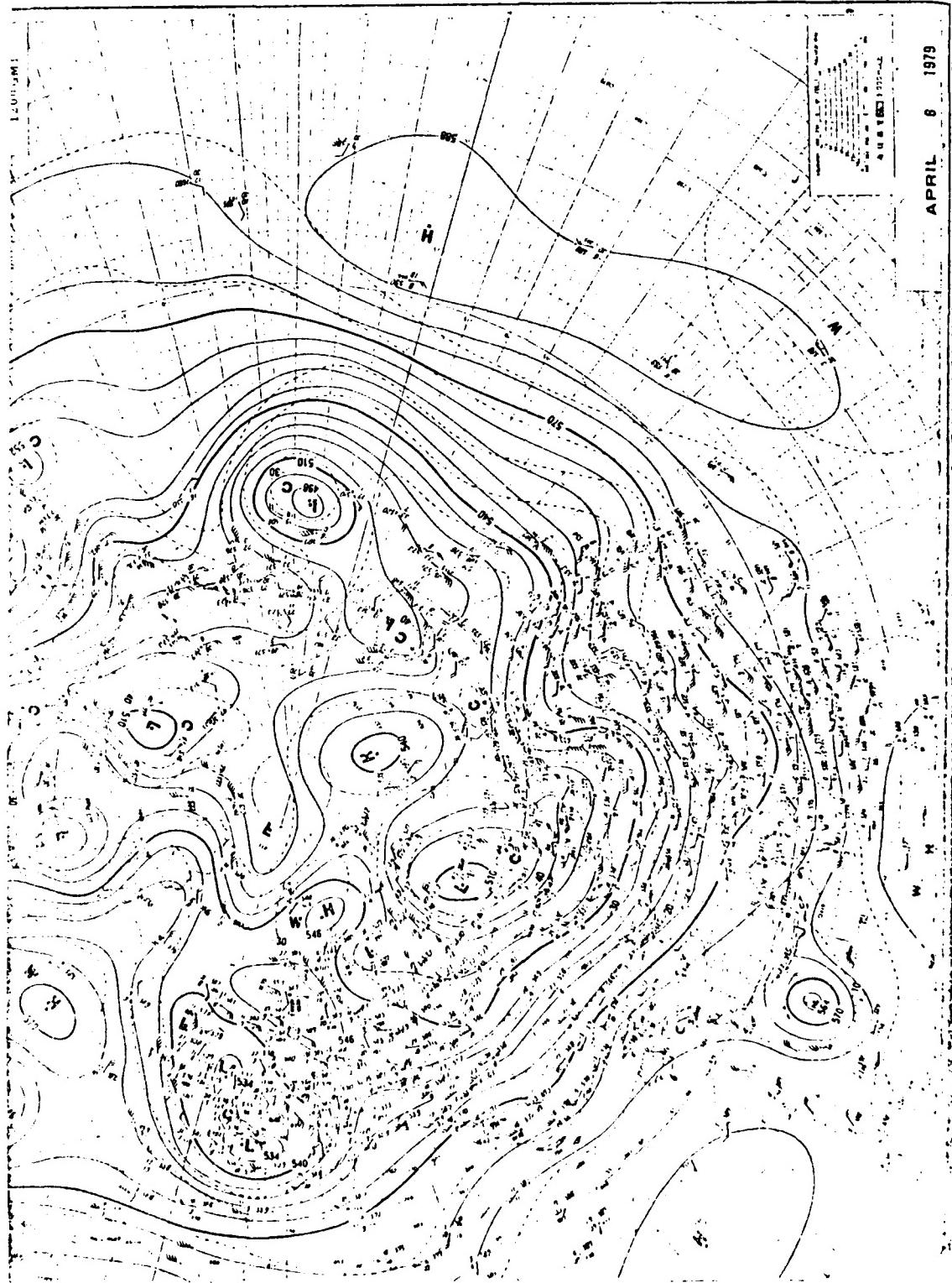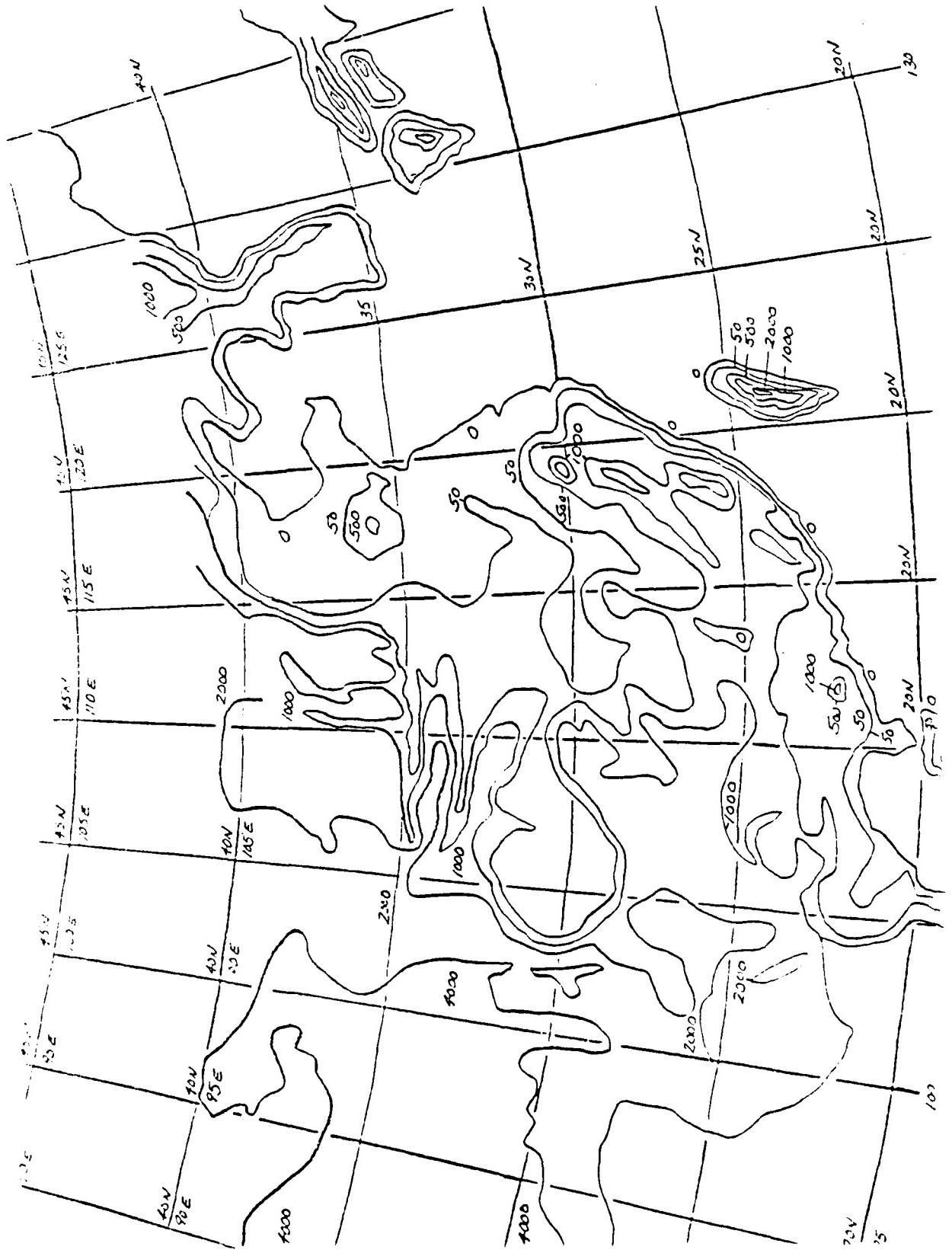
Fig. 1.1 Contour of surface elevation (unit m) of East Asia.
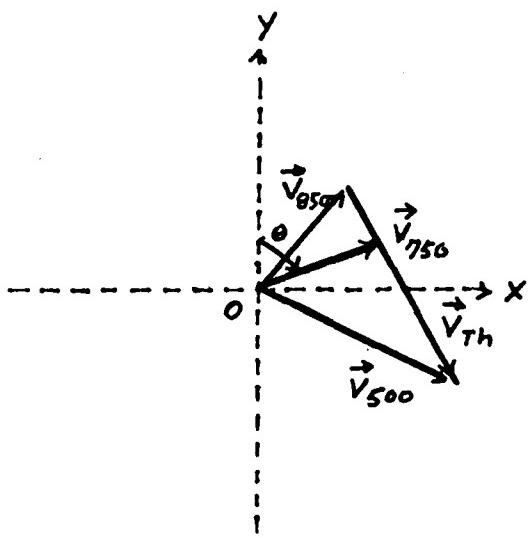
Fig. 1.2 Determination of the geostrophic Wind
Vector by a graphical method.
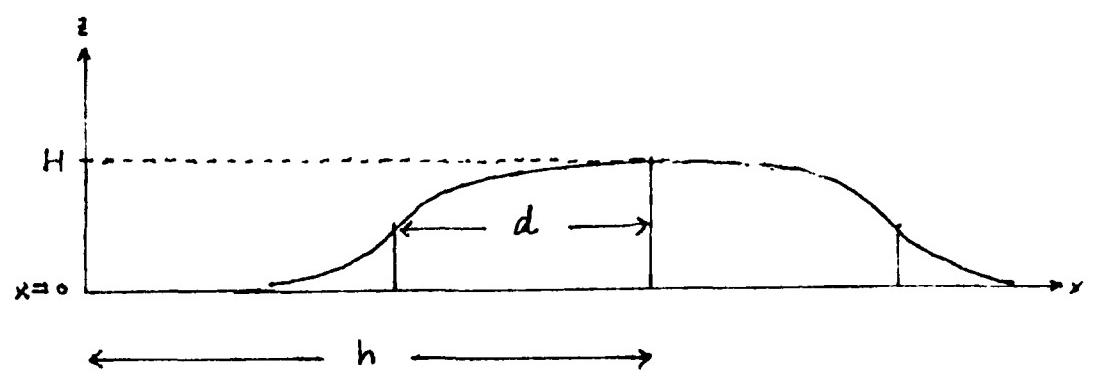
Fig. 2.1   The schematic profile of the X-Z cross-section of H(x,y) at y=0.

END
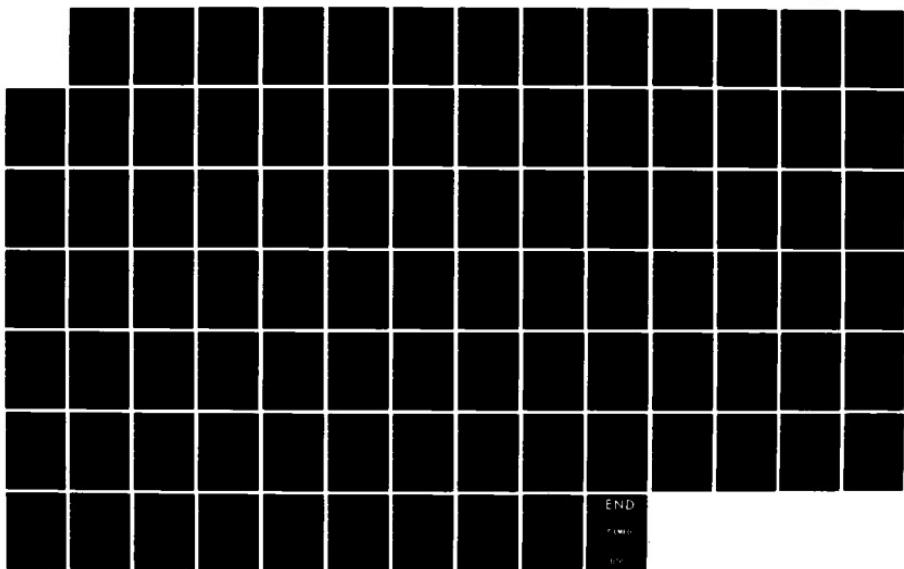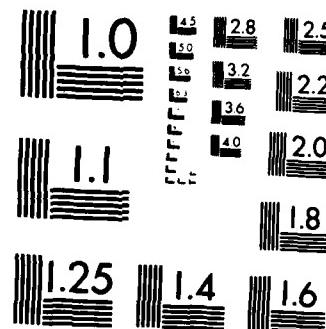
MICROCOPY RESOLUTION TEST CHART
NATIONAL BUREAU OF STANDARDS-1963-A
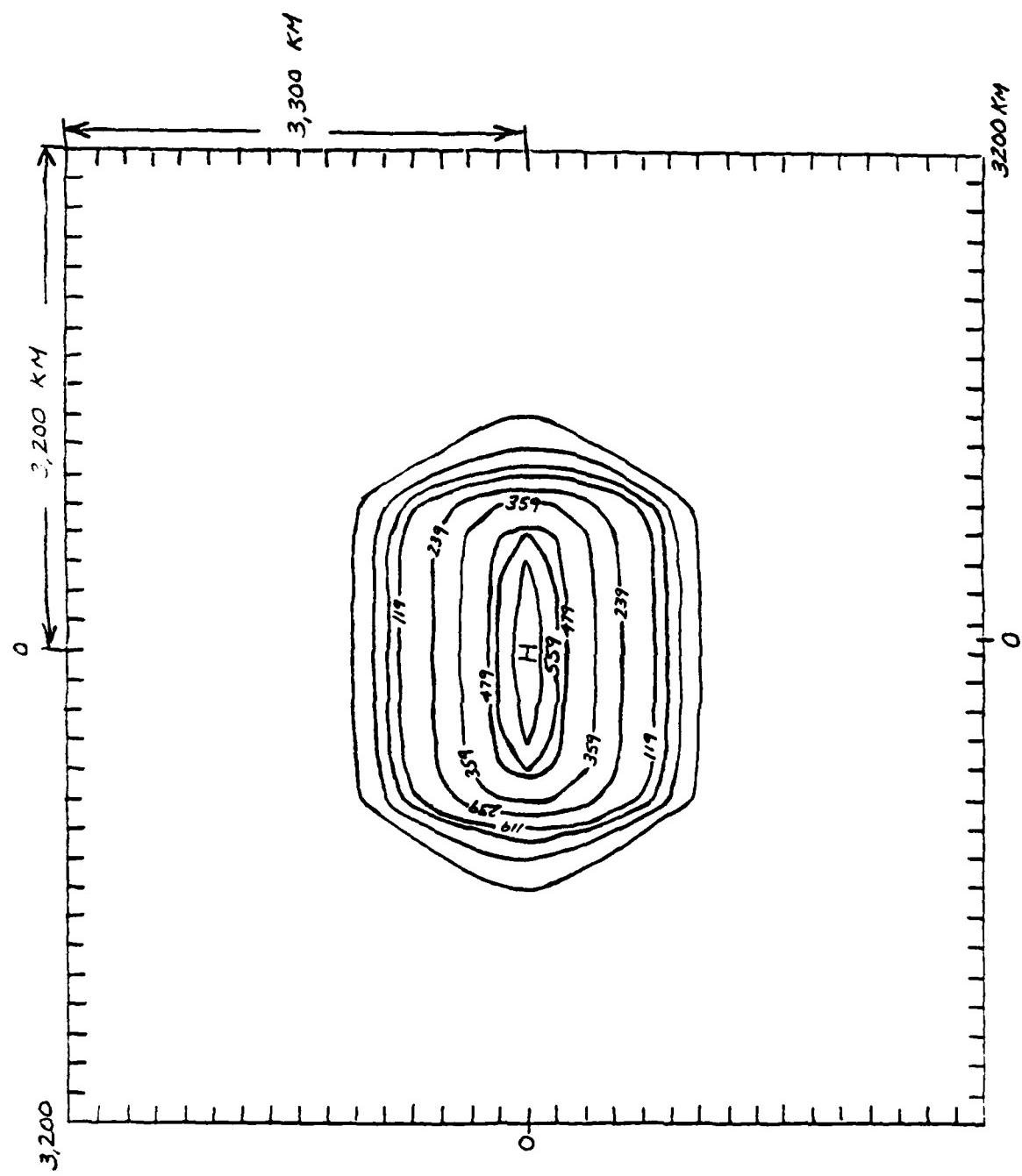
Fig. 2.2 The contour map of H(x,y) assumed for the Tibetan Plateau (unit 10m).

89
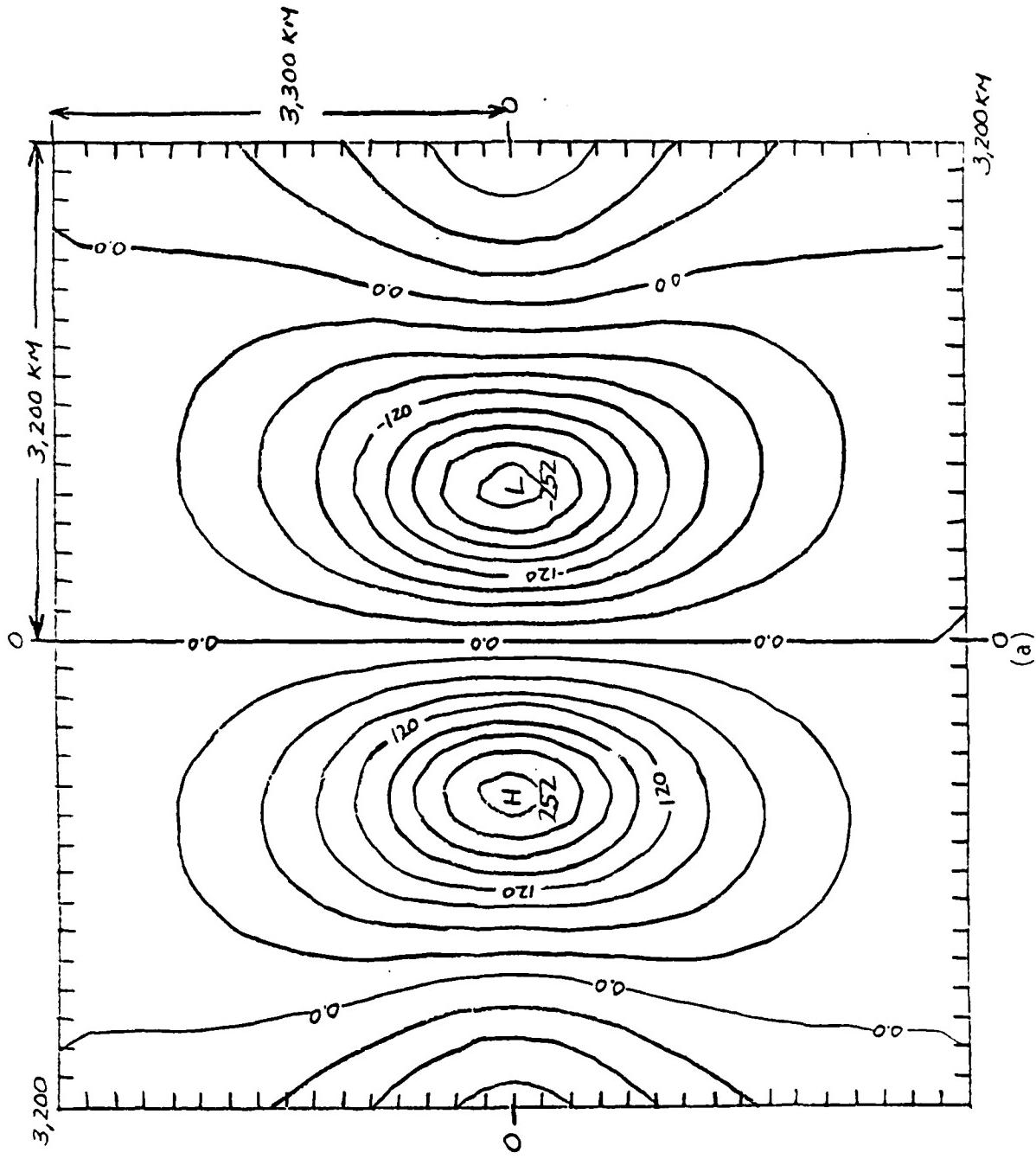
Fig. 2.3 v(cm sec^{-1}) field over the plateau and vicinity for (a) A=0 and (b) A=0 cases exponential part of the solution.

90
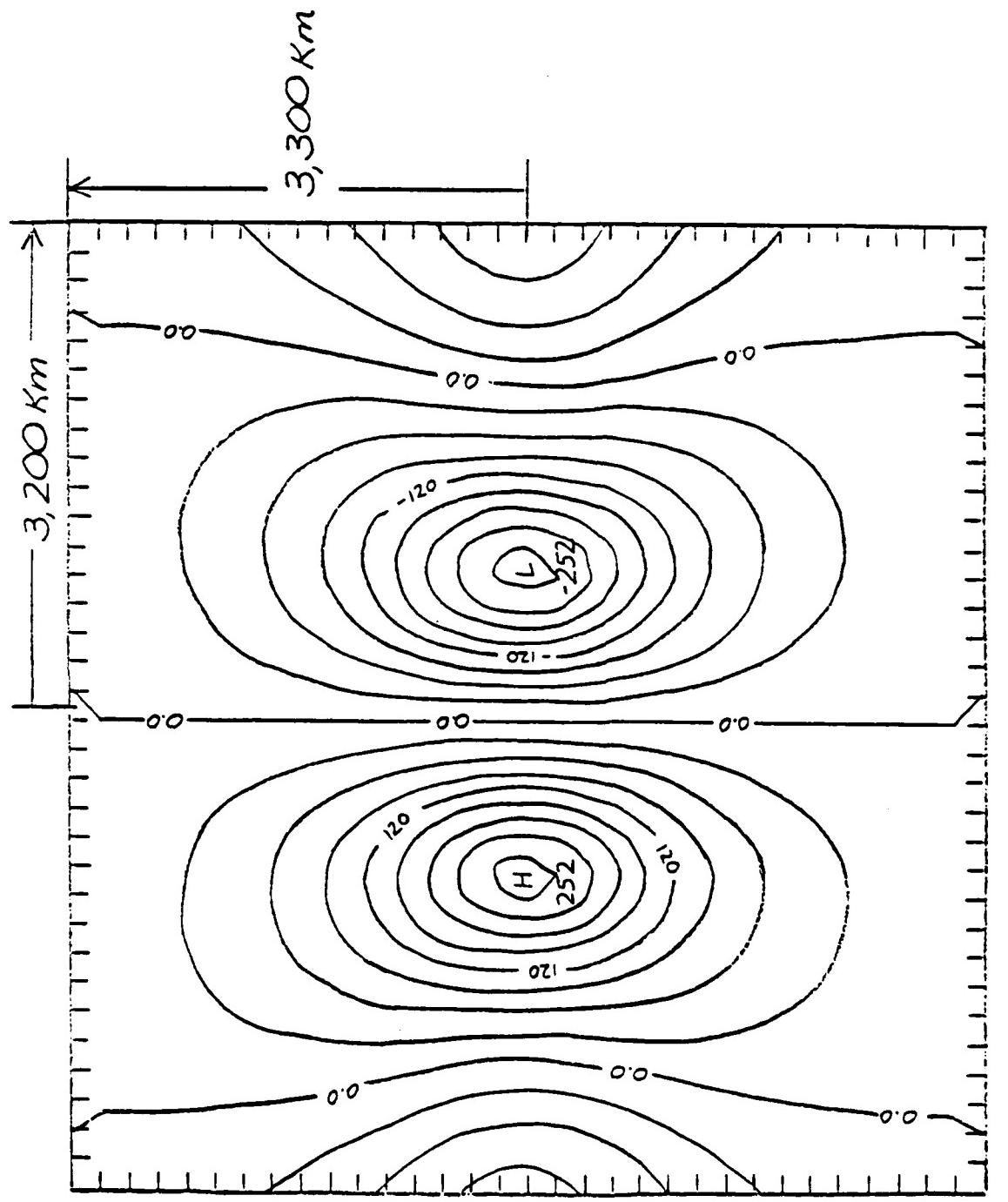
(b)
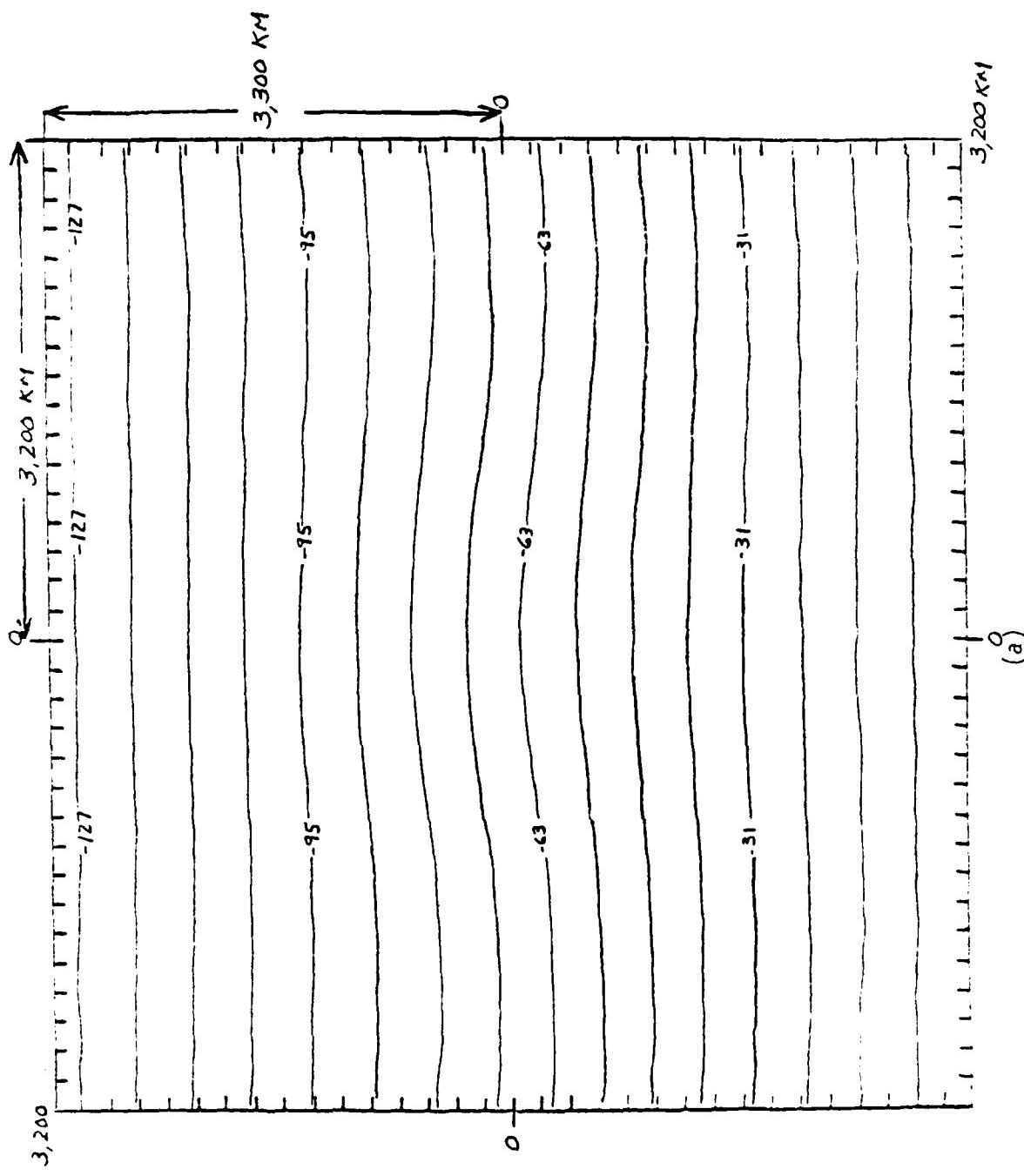
Fig. 2.4 $\psi^{*}(10^{10} \text{ cm}^{2} \text{ sec}^{-1})$ field with the same conditions as in Fig. 2.3.

(b)

93

(b)
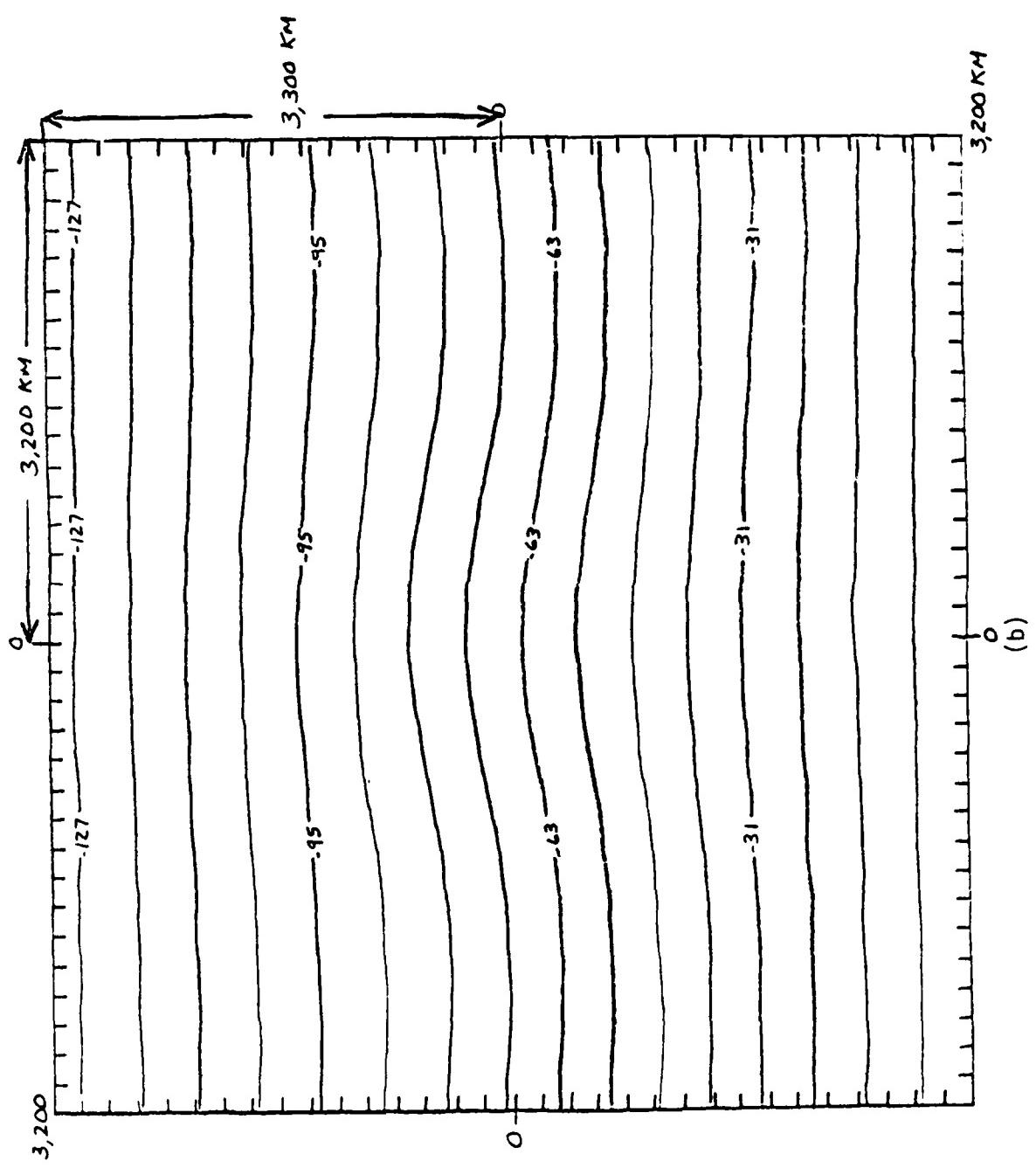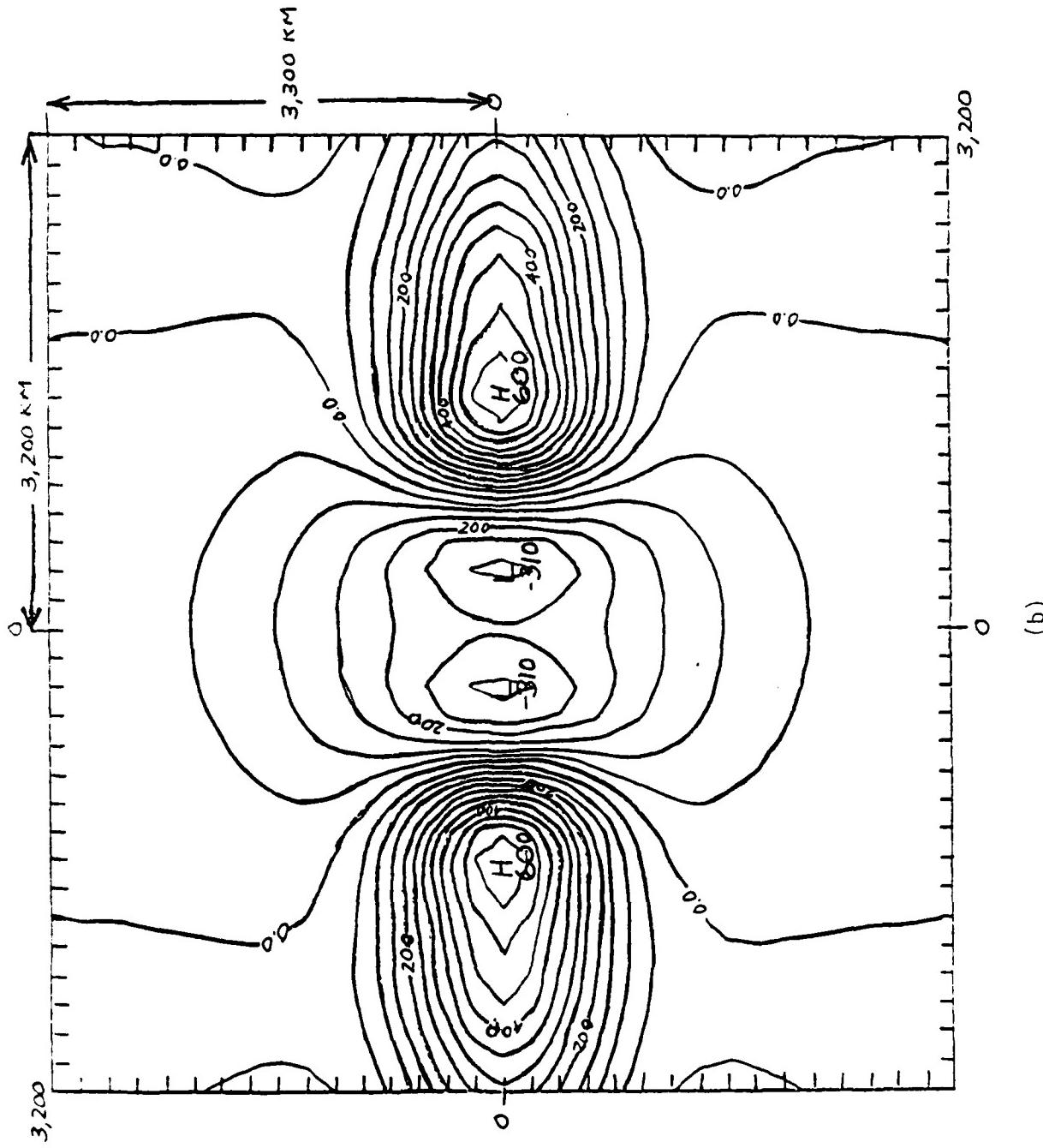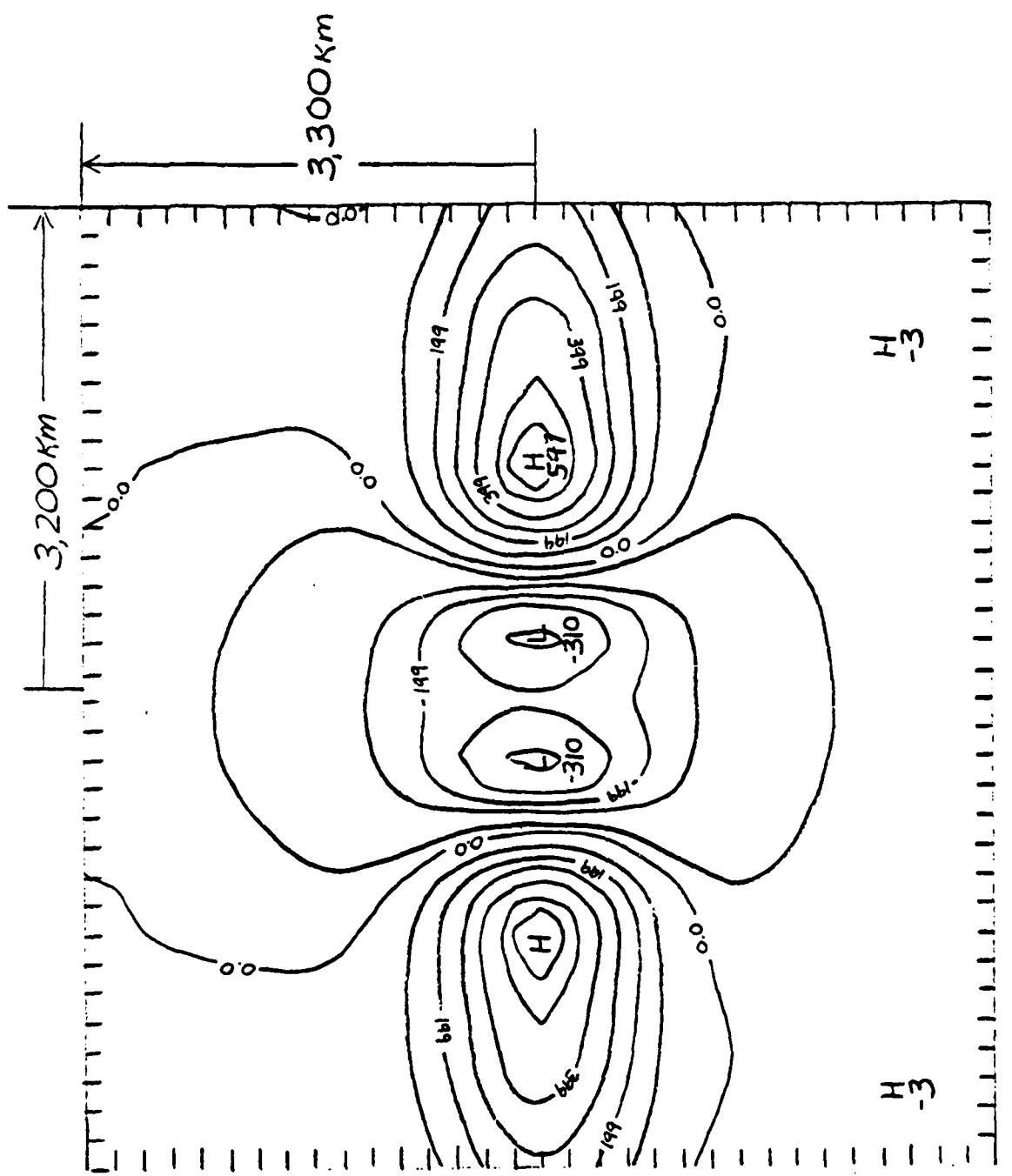
Fig. 2.5 $\zeta(10^{-8}\ sec^{-1})$ field with the same conditions as in Fig. 2.3.

(a)
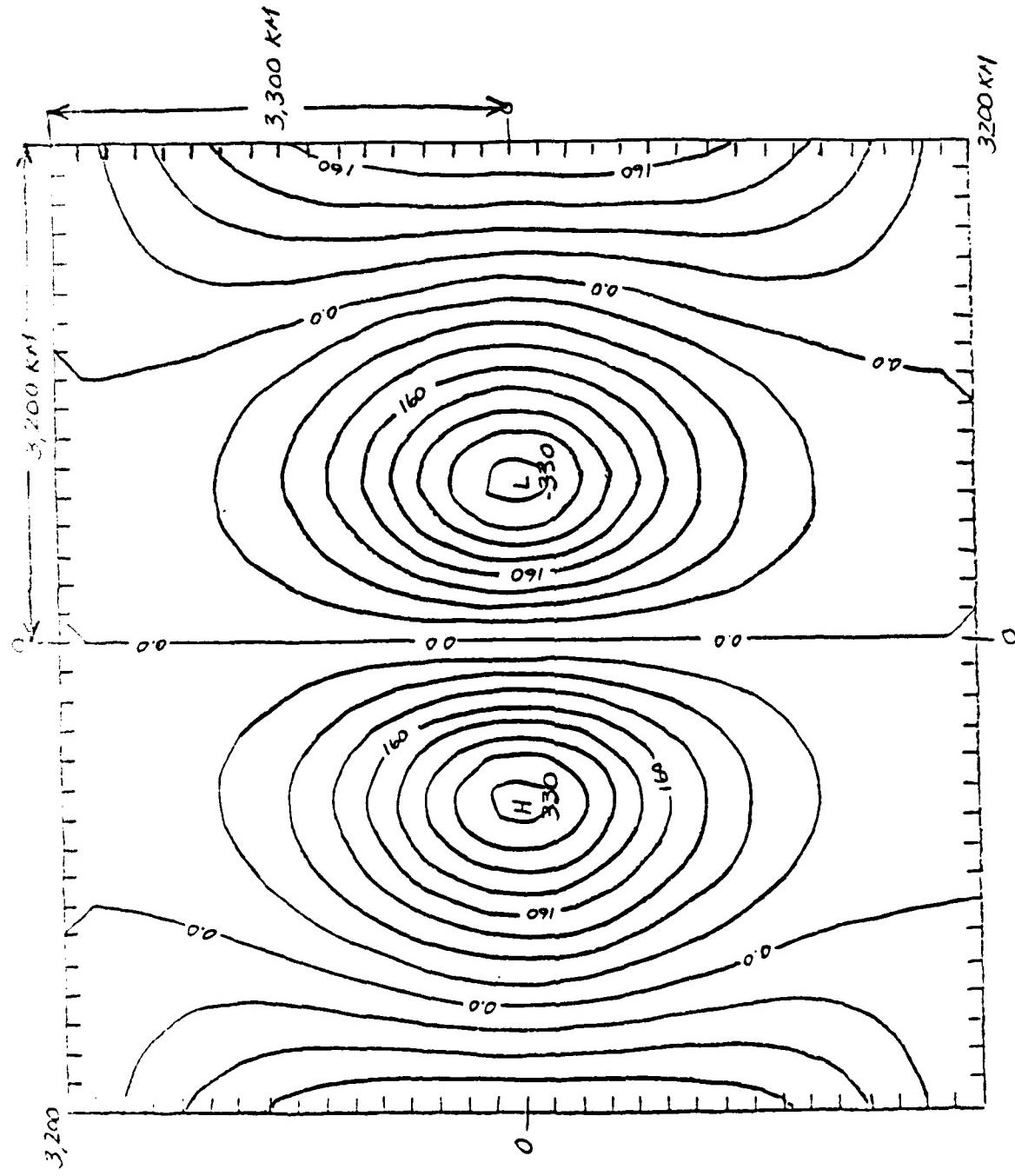
Fig. 2.6 Total solution of V for A=0 case.

96
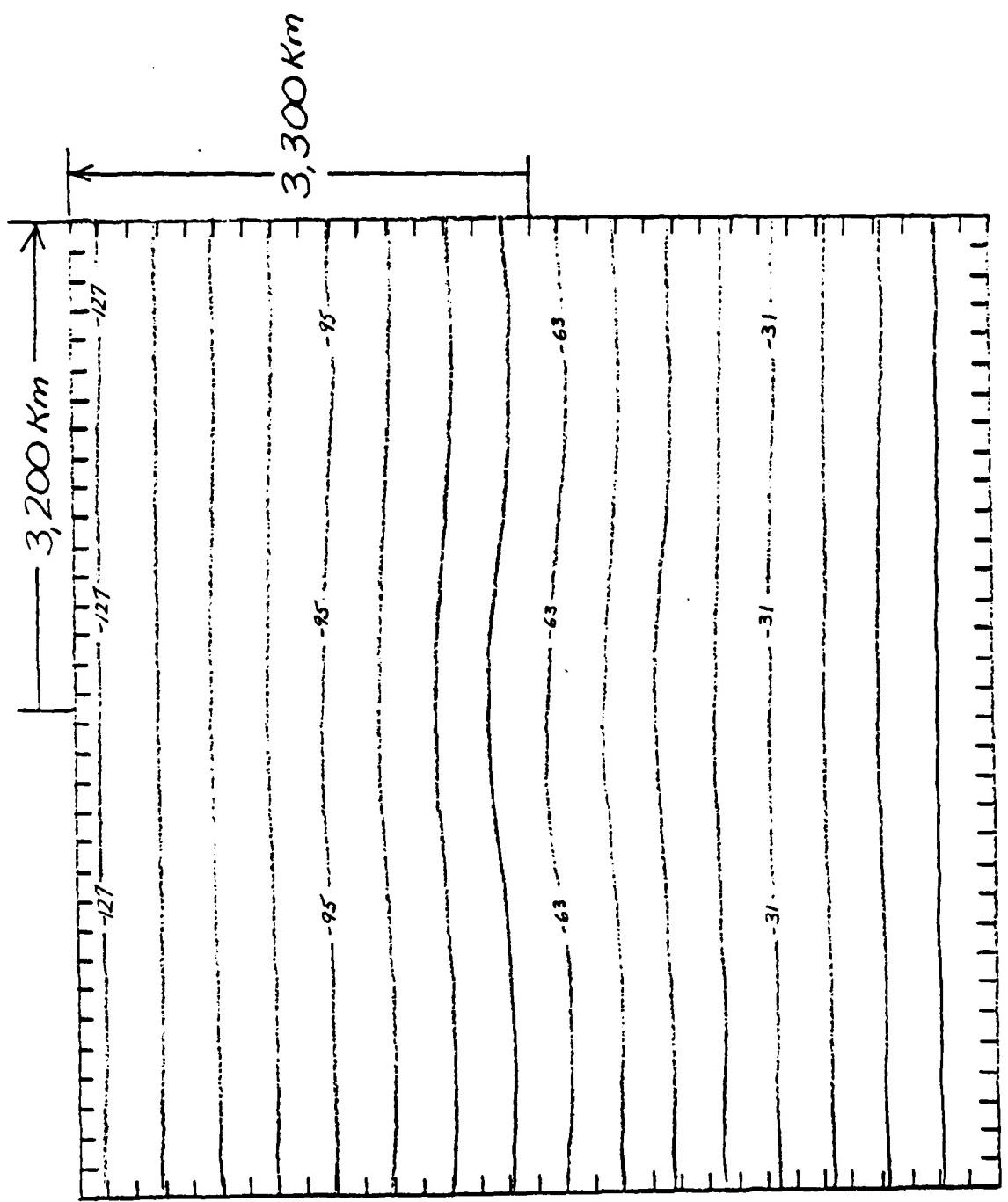
Fig. 2.7 Total solution of ψ for A = 0 case.

97
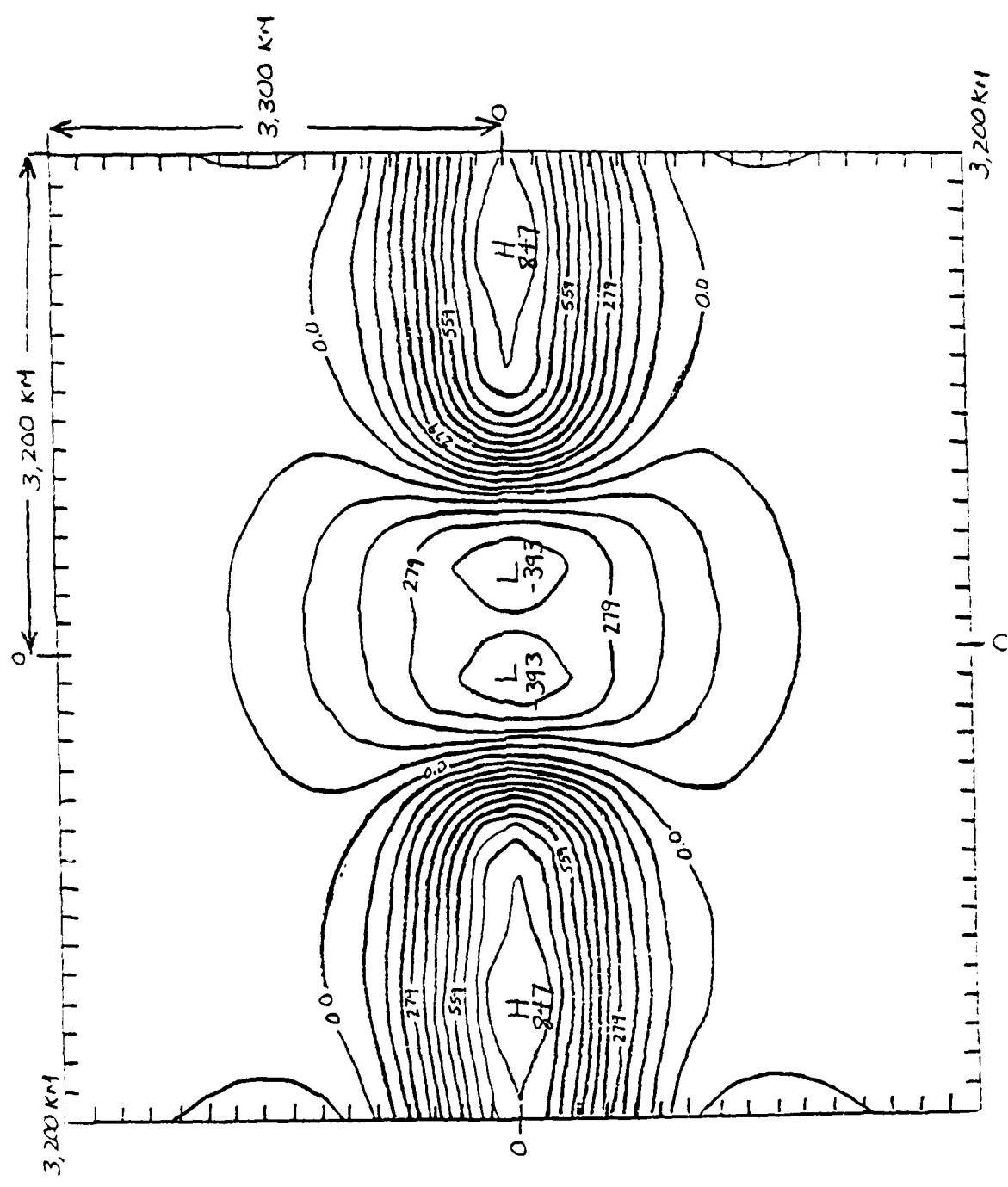
Fig. 2.3 Total solution of ζ for A = 0 case.
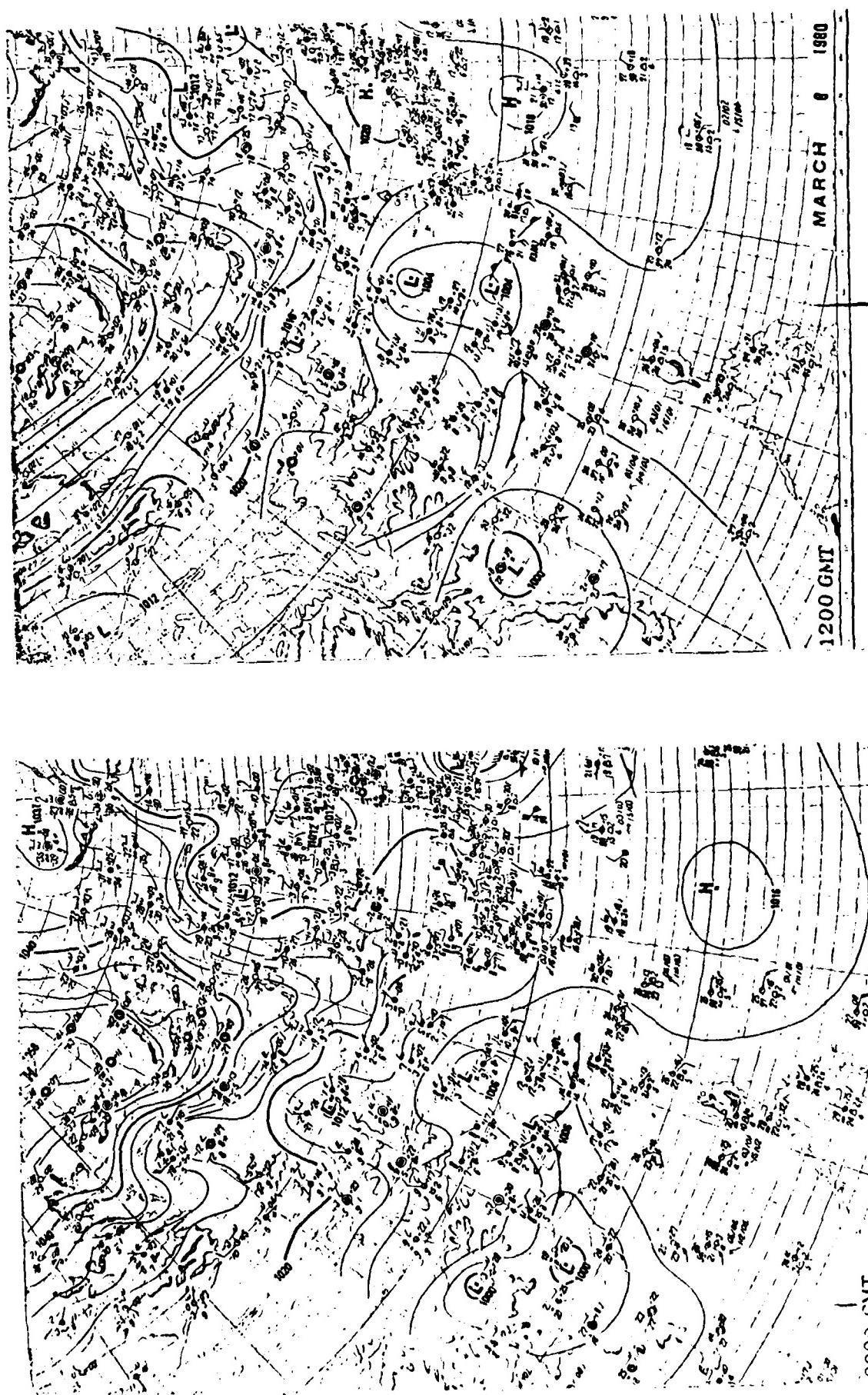
Fig. 2.9 Surface maps for (a) 00Z and (b) 12Z and (c) 500 mb for 12Z, March 8, 1980.

99

MARCH 8 1980

(c)

1200 GMT

MARCH 27, 1980

(b)

Fig. 5, except for March 27, 1980.

101

500 Mb
1200GMT

MARCH 24, 1990

(c)

102

1200 GMT

MARCH 22 1980

(b)

(a)
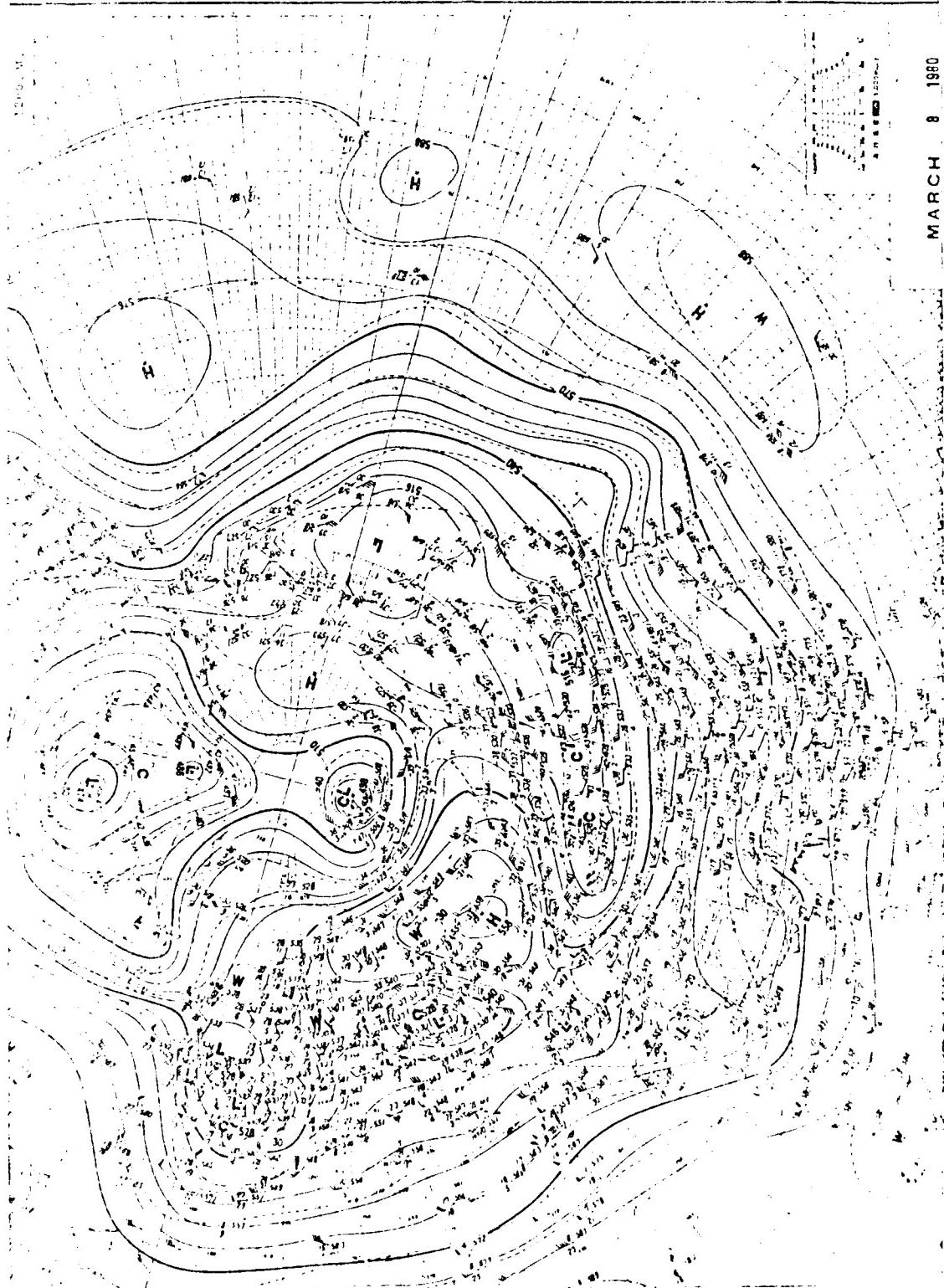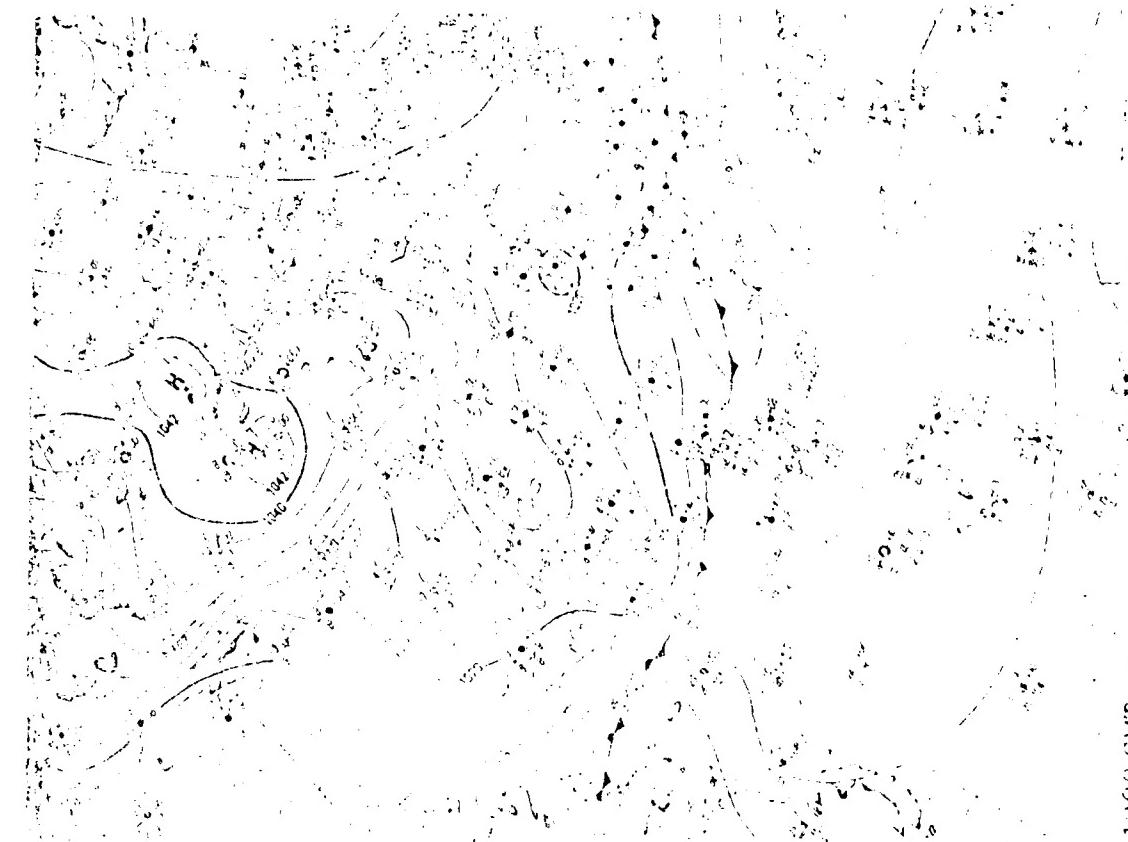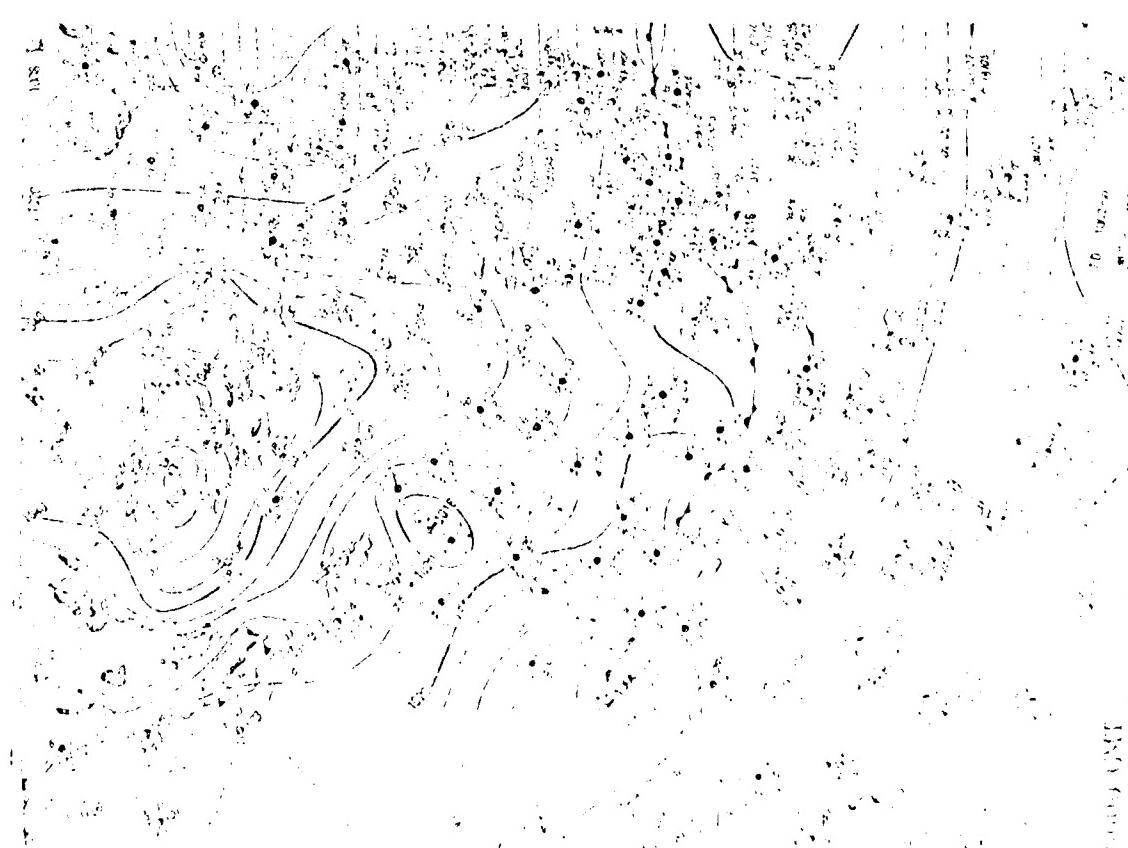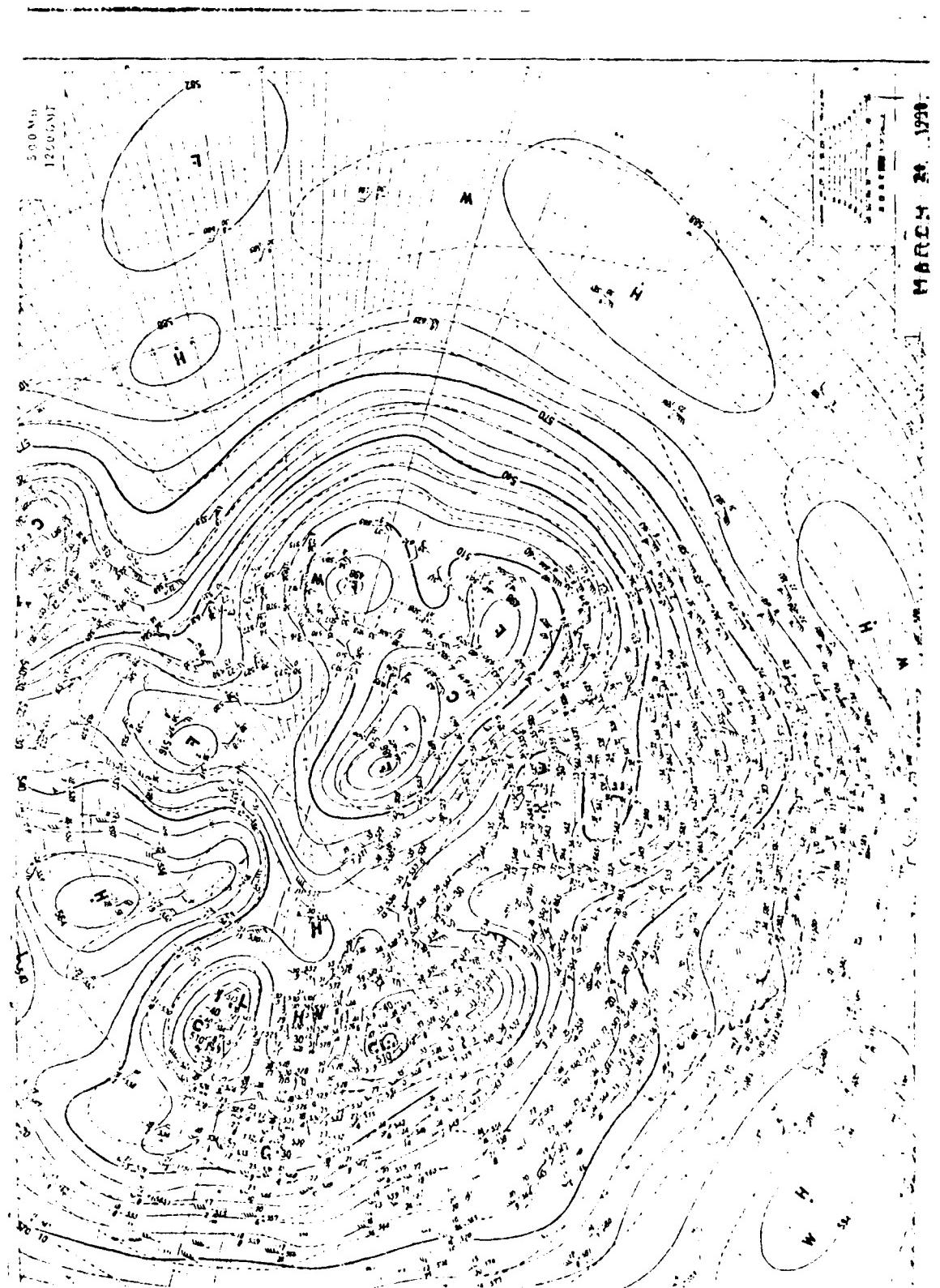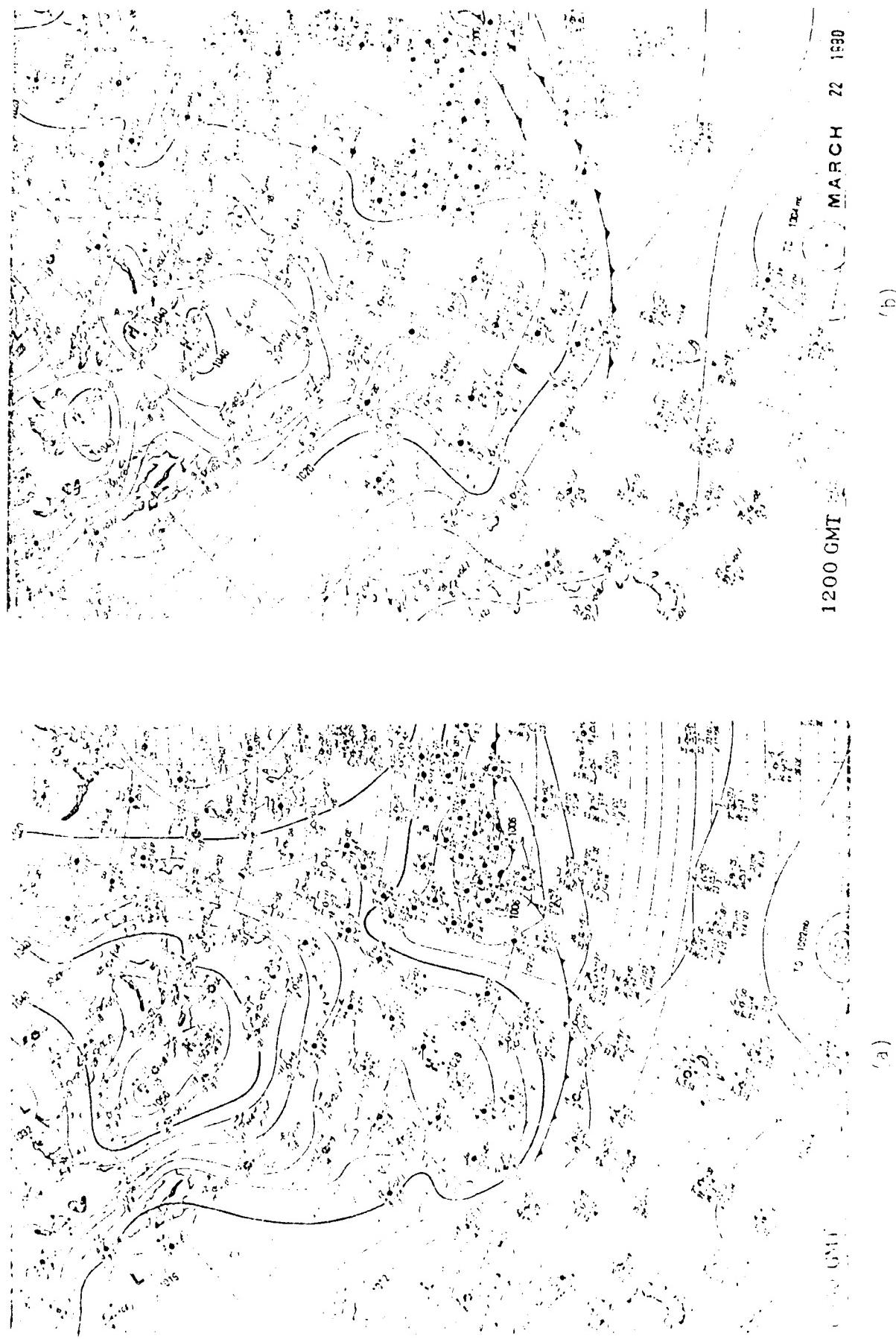
Fig. 2.11 As in Fig. 5, except for March 22, 1980.

MARCH 22 1990

1200 GMT

(c)

3,300 km

17,000 km

Fig. 2.22 Total positive of 1×10^{-8} sec^{-1}) in global scale.

105
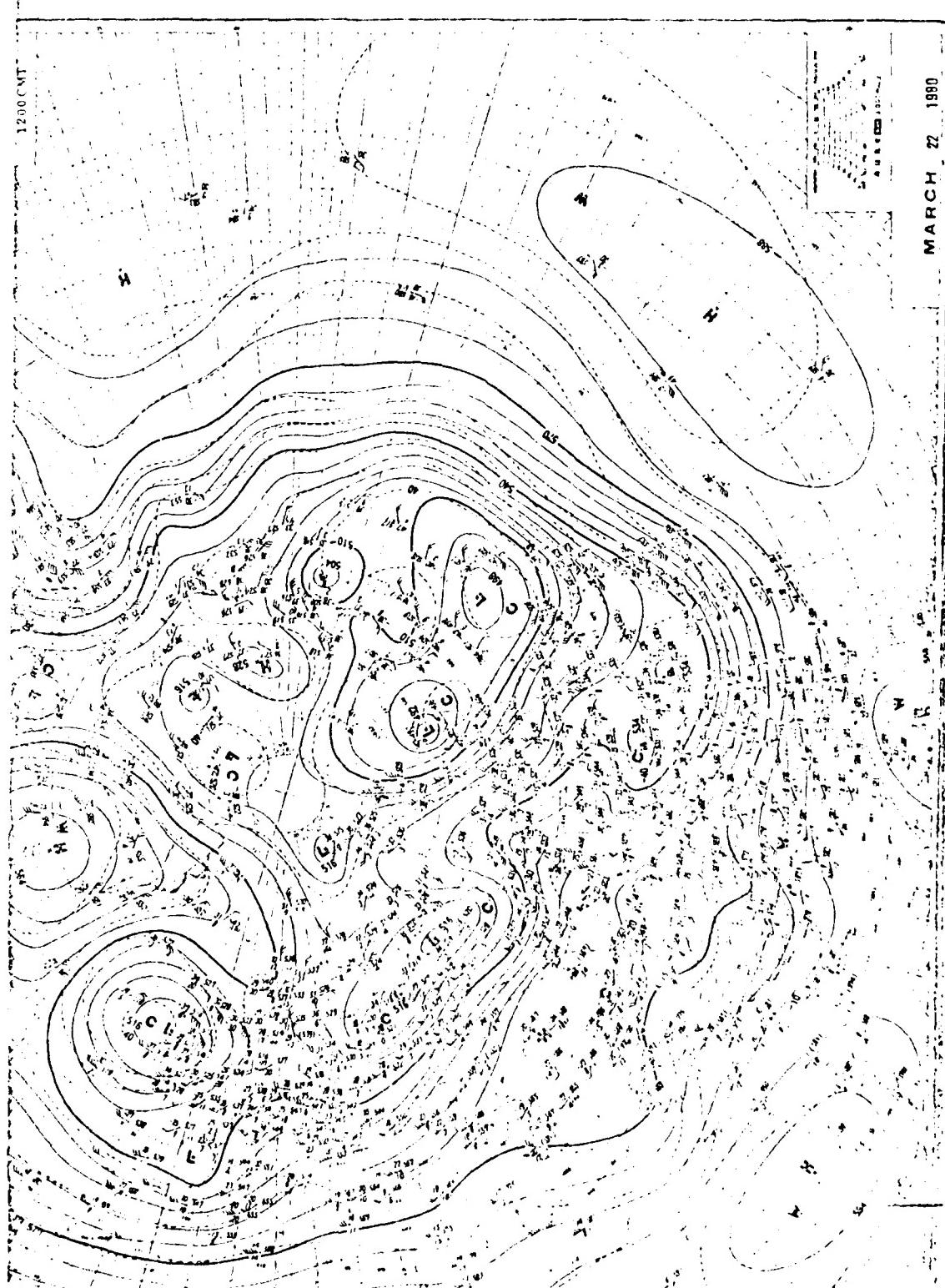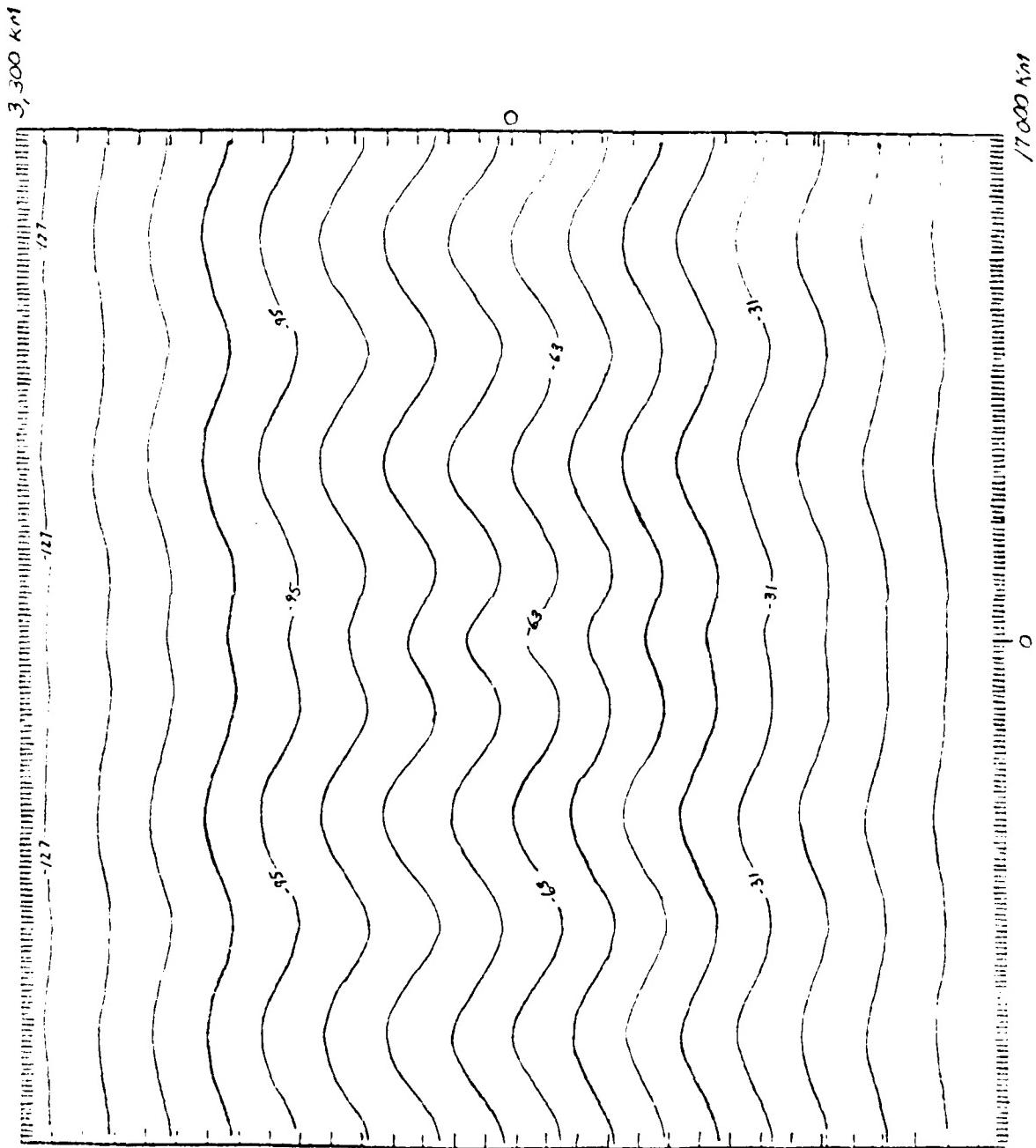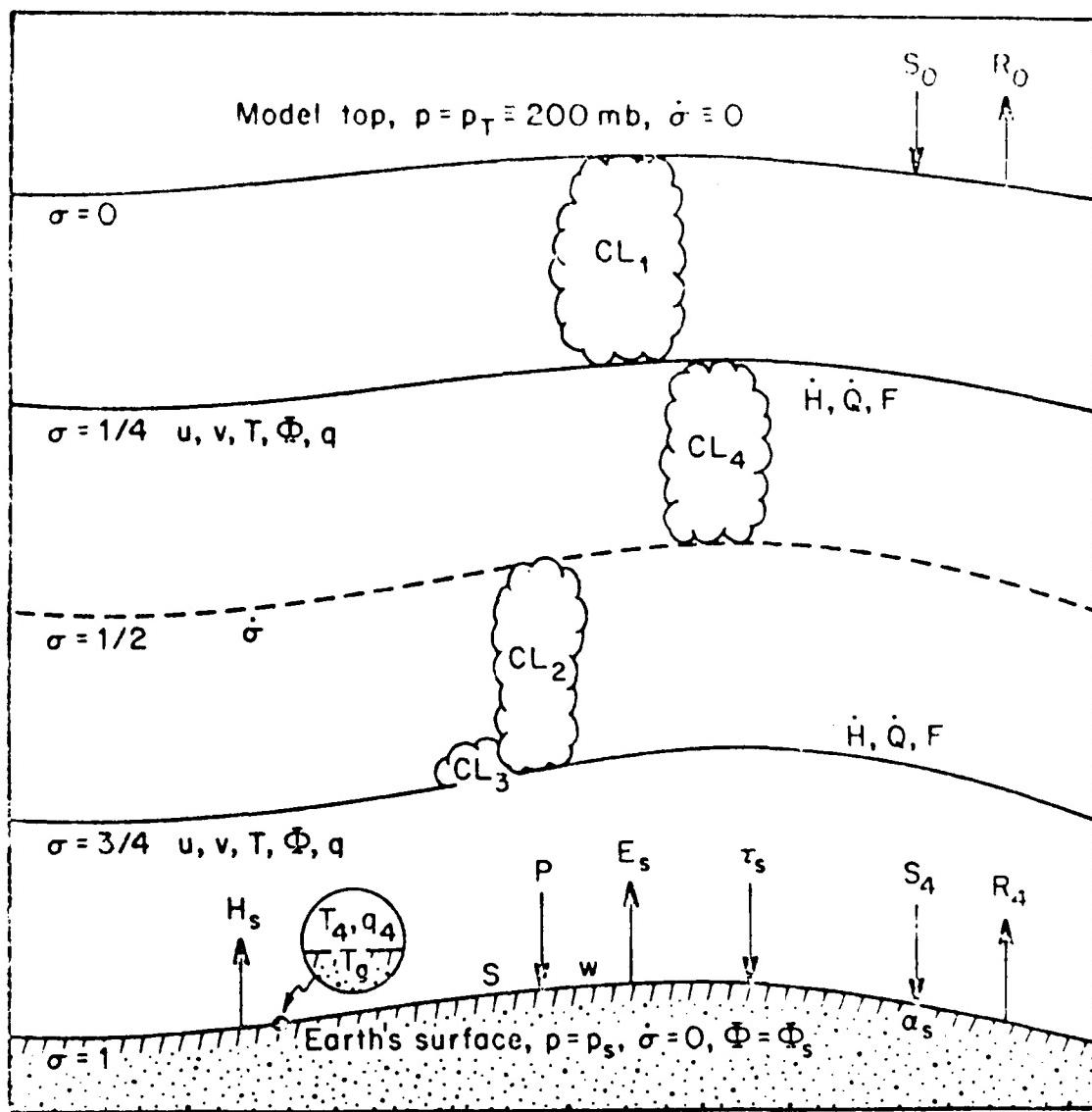
Fig. 3.1   The vertical structure and principal variables of the
OSU two-level GCM model (After Ghan et. al., 1982).
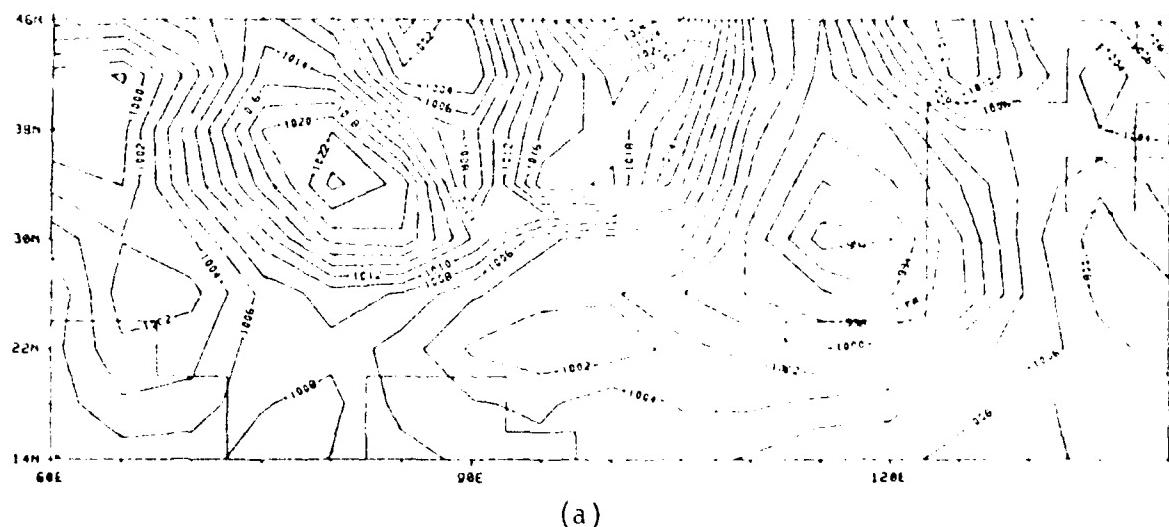
(a)
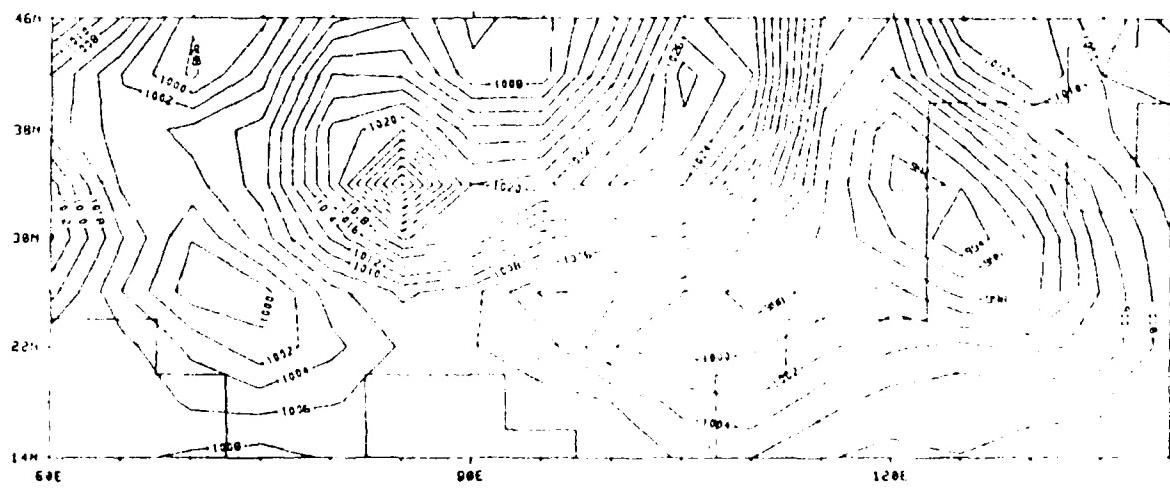
(b)

Fig. 3.2 Sea level pressure (mb) chart at 24Z for (a) April 17,
(b) April 18, (c) April 19, and (d) April 20 for WTPC.
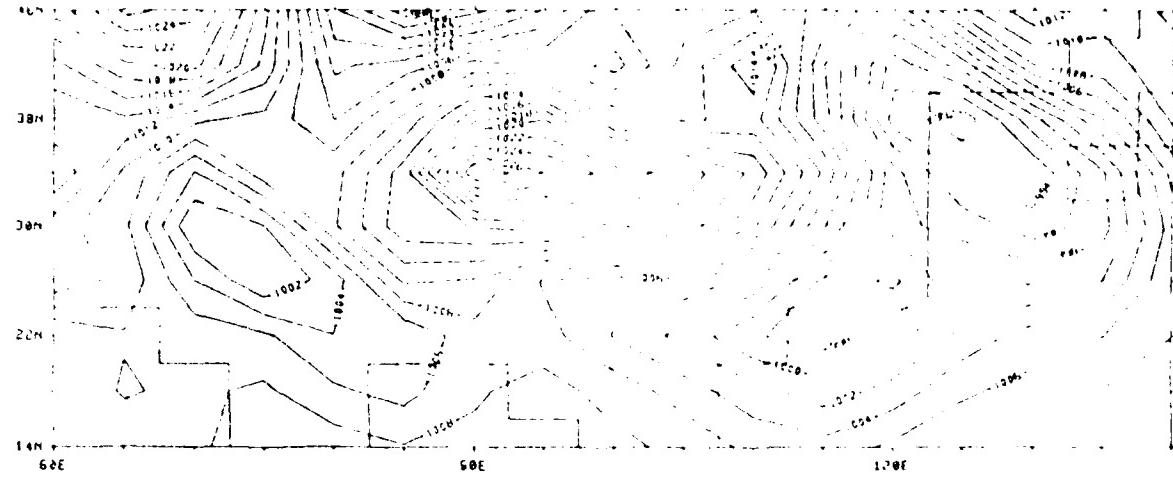
(c)
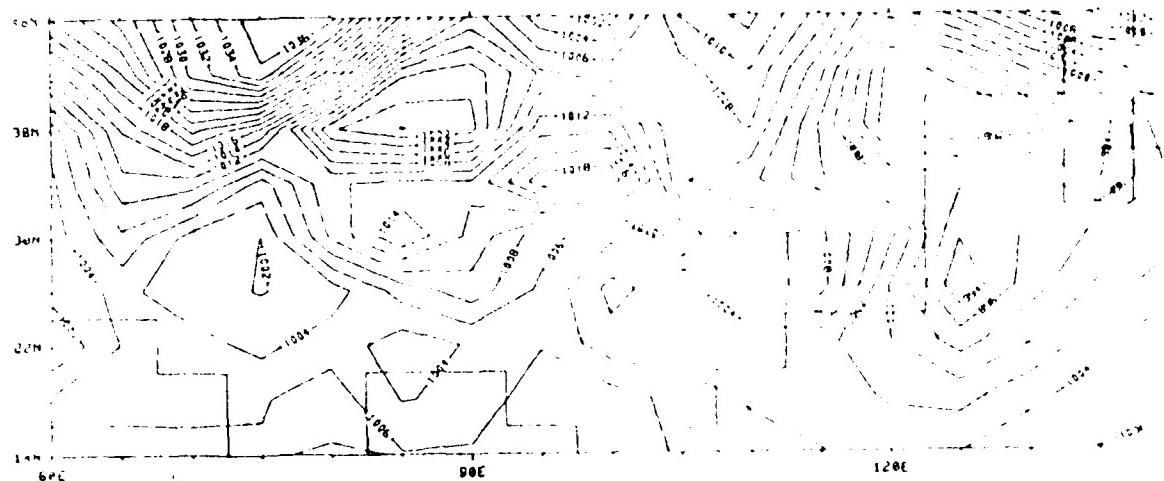
(d)
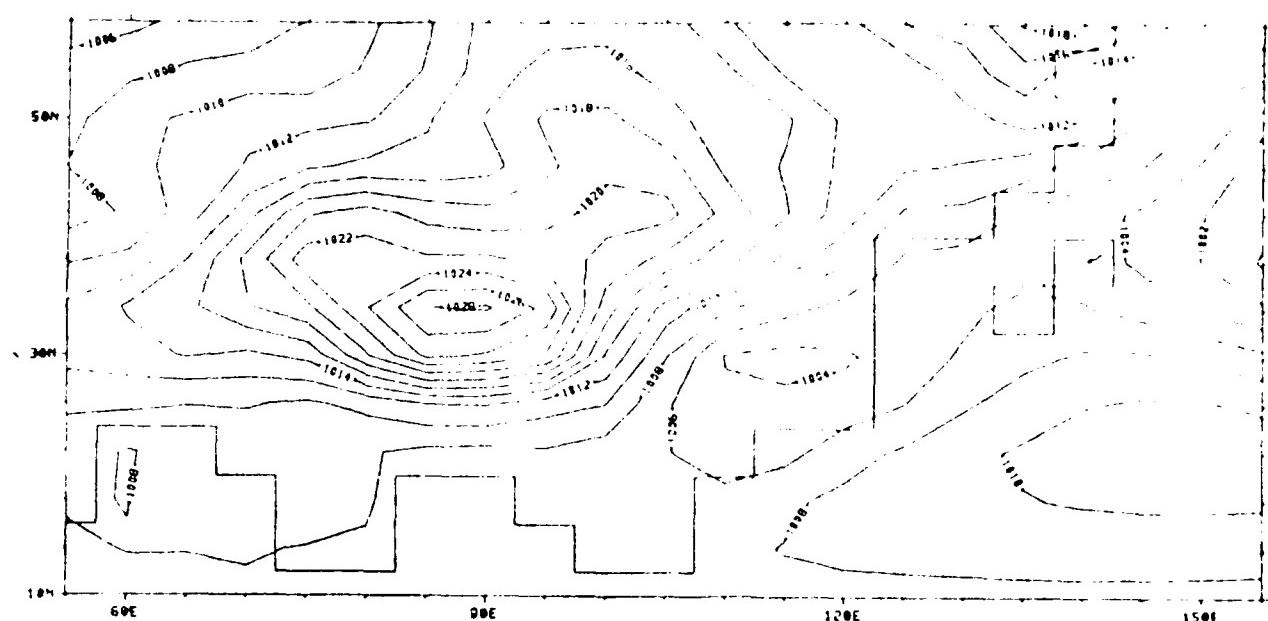
Fig. 3.3 Mean sea level pressure (mb) chart for March for WTPC.
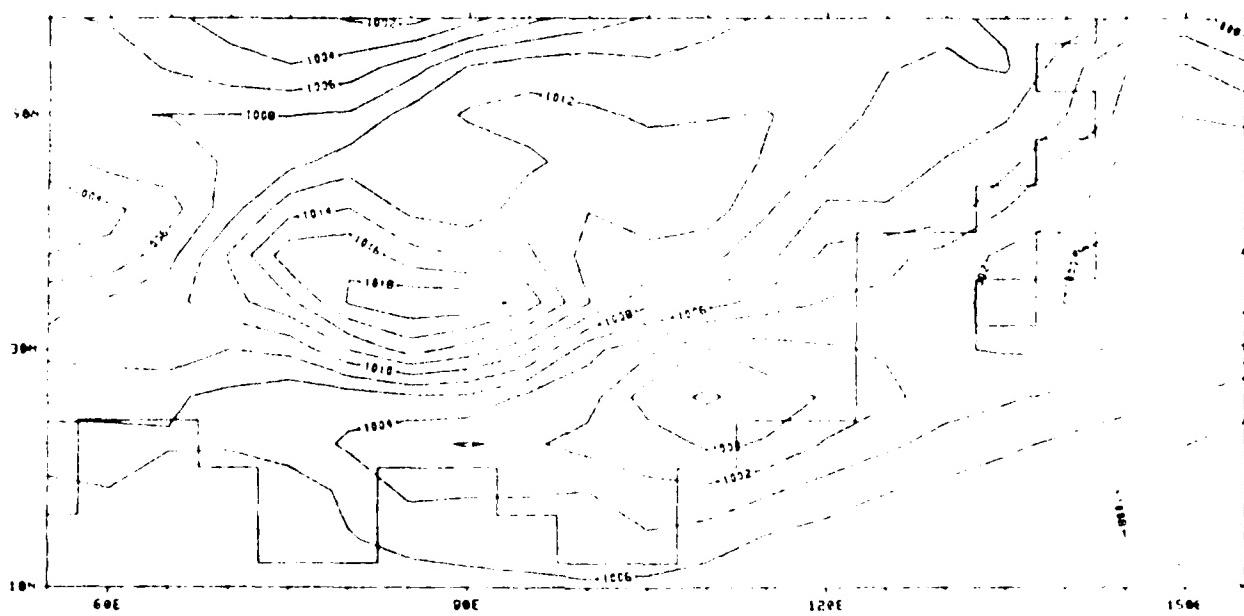
Fig. 3.4 As in Fig. 3 3. except for April.
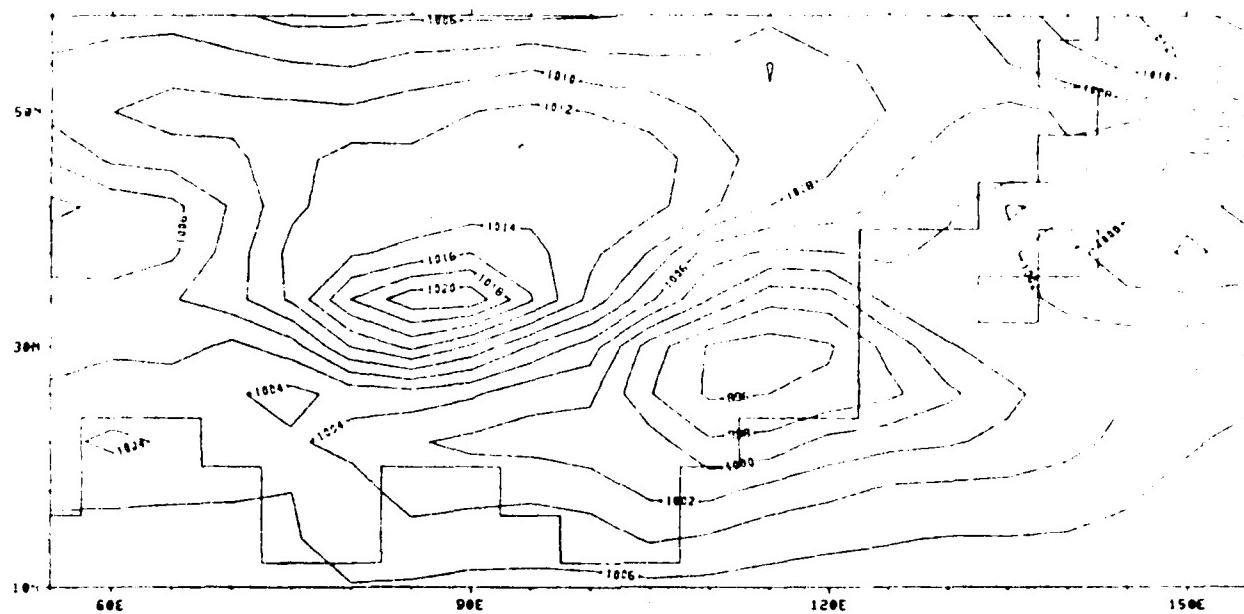
Fig. 3.5   As in Fig. 3.3, except for May.
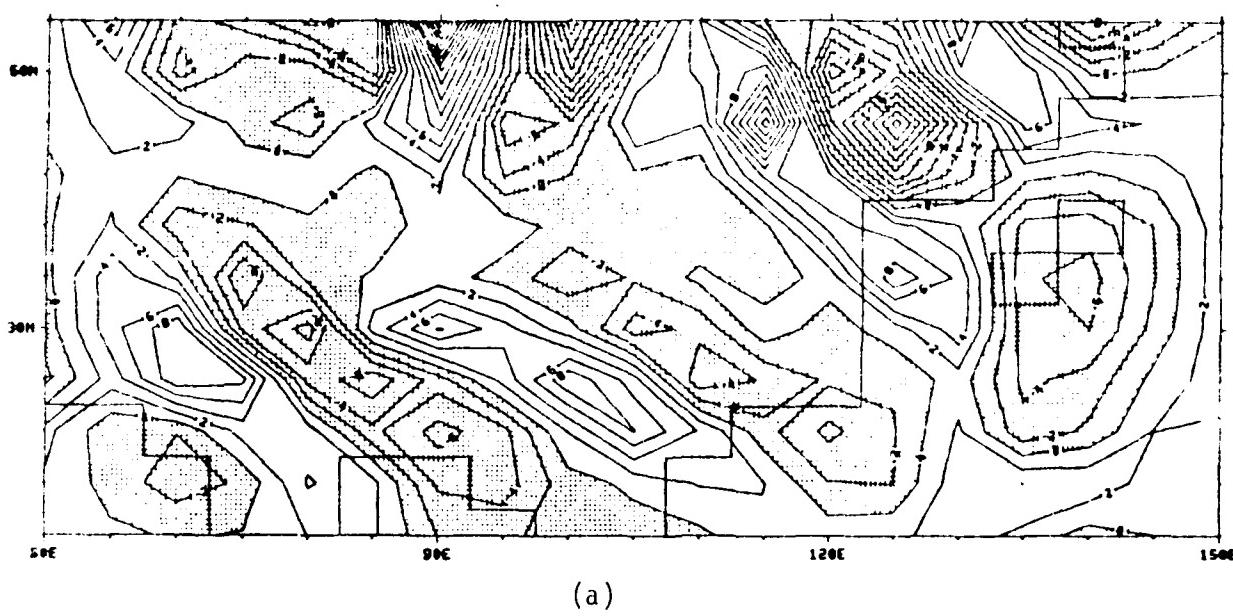
(a)
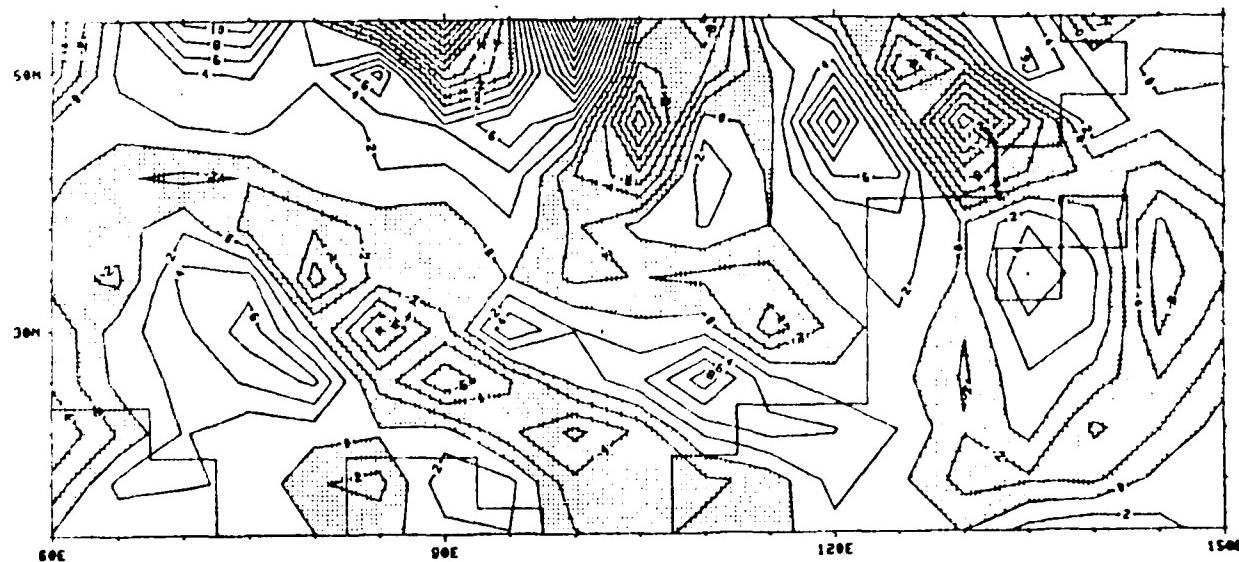
(b)

Fig. 3.6 The local time rate of change of absolute vorticity
(day^{-2}) at level 2 for the same times and condition
as in Fig. 3.2.

111
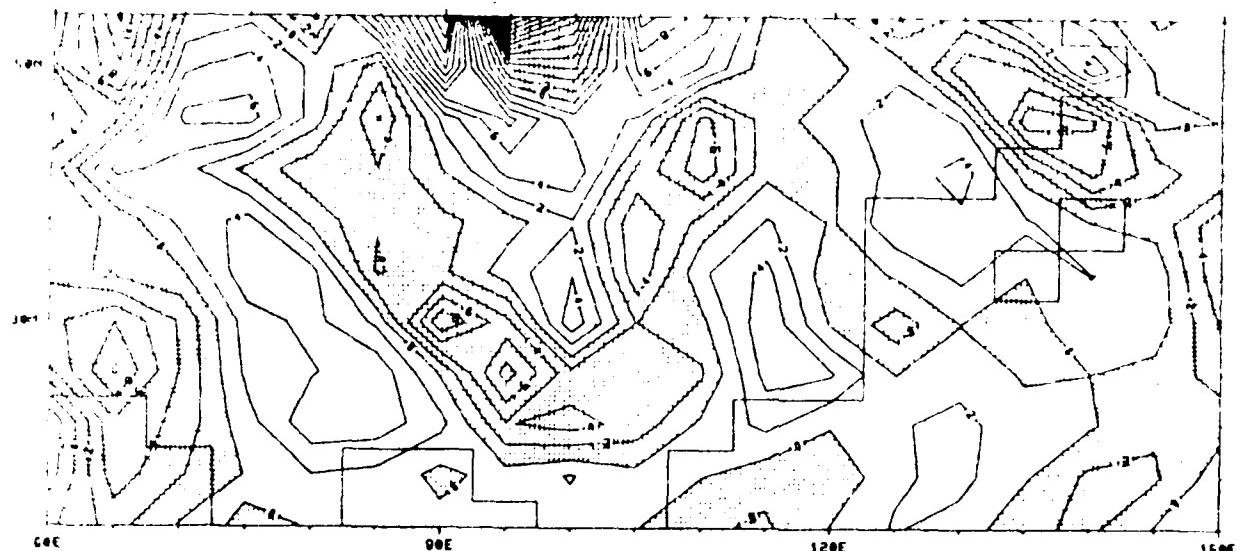
(c)
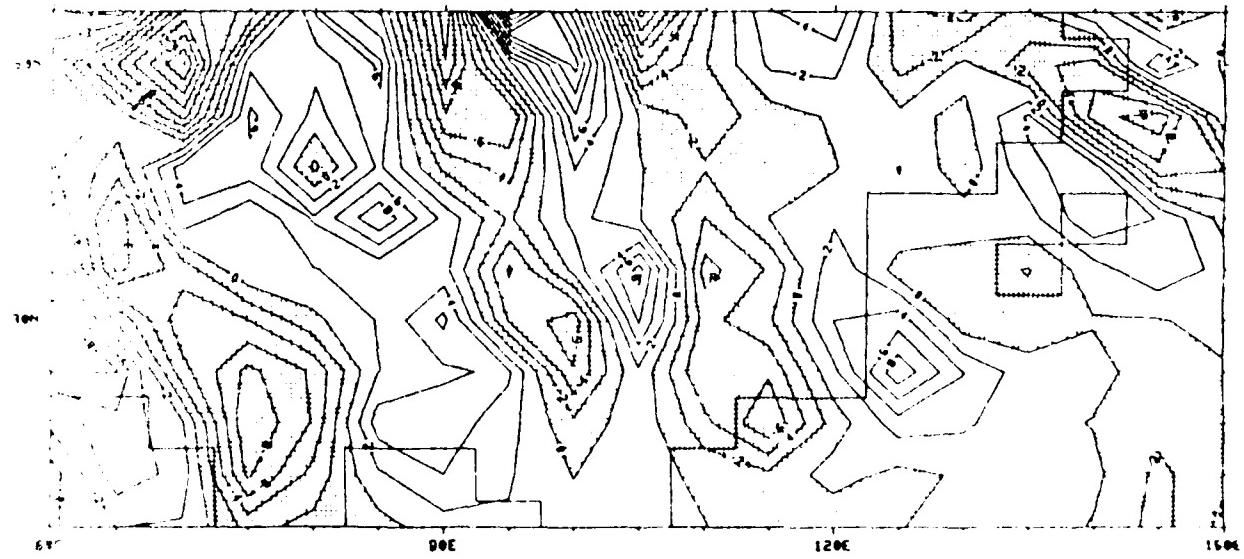
(d)
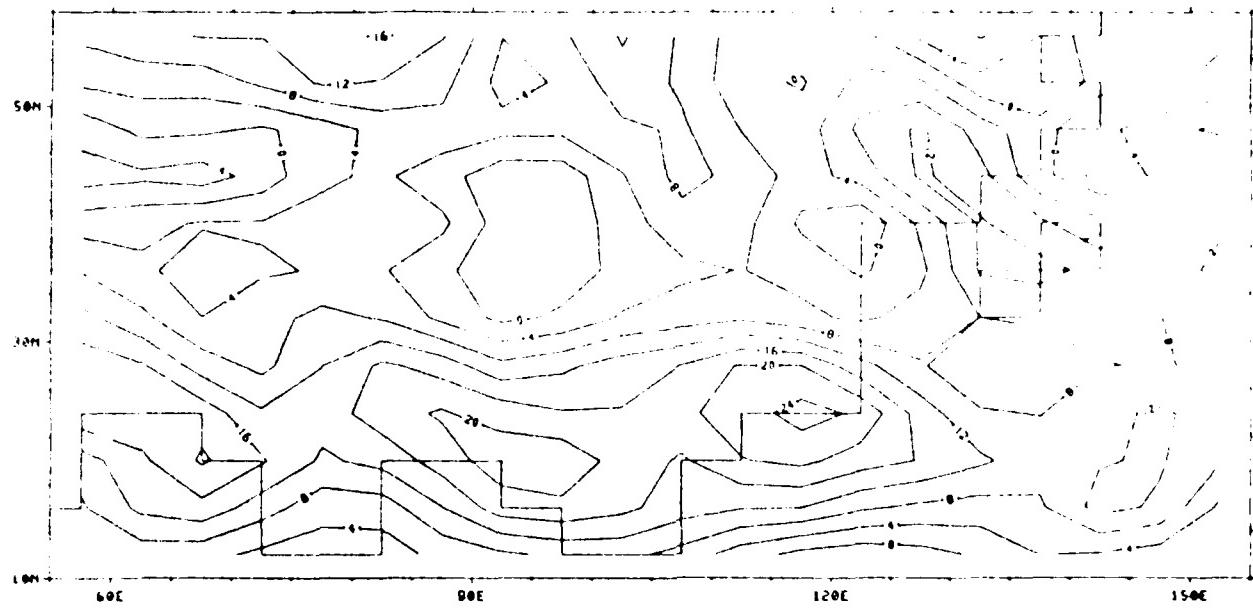
(a)
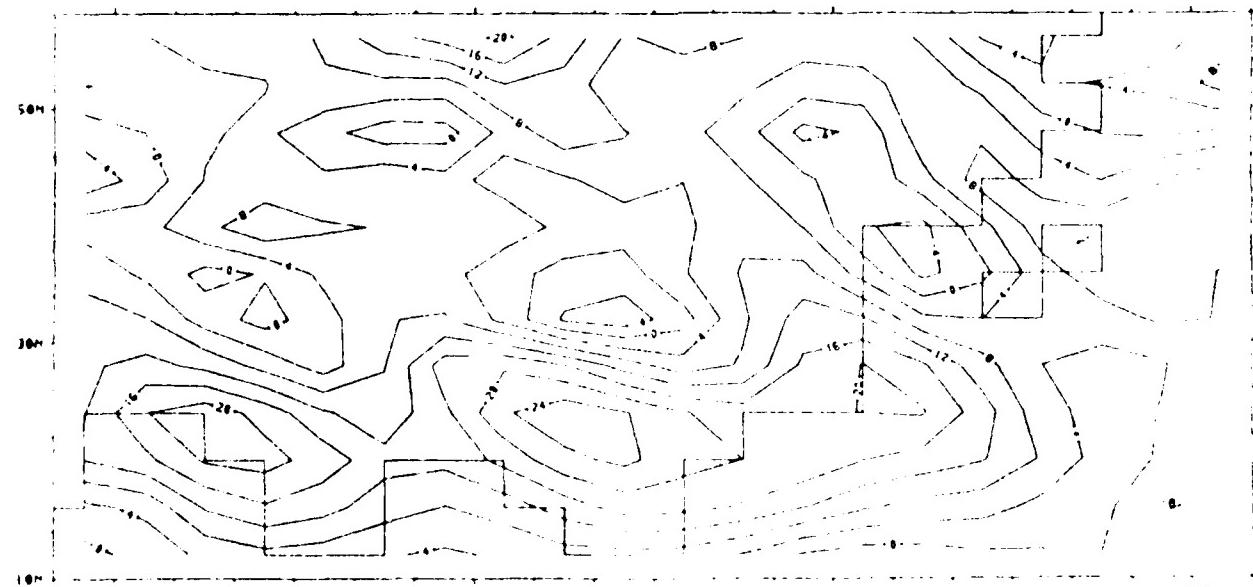
(b)

Fig. 3.7   The zonal wind component at level 3 for the same
times and condition as in Fig. 3.2.

113
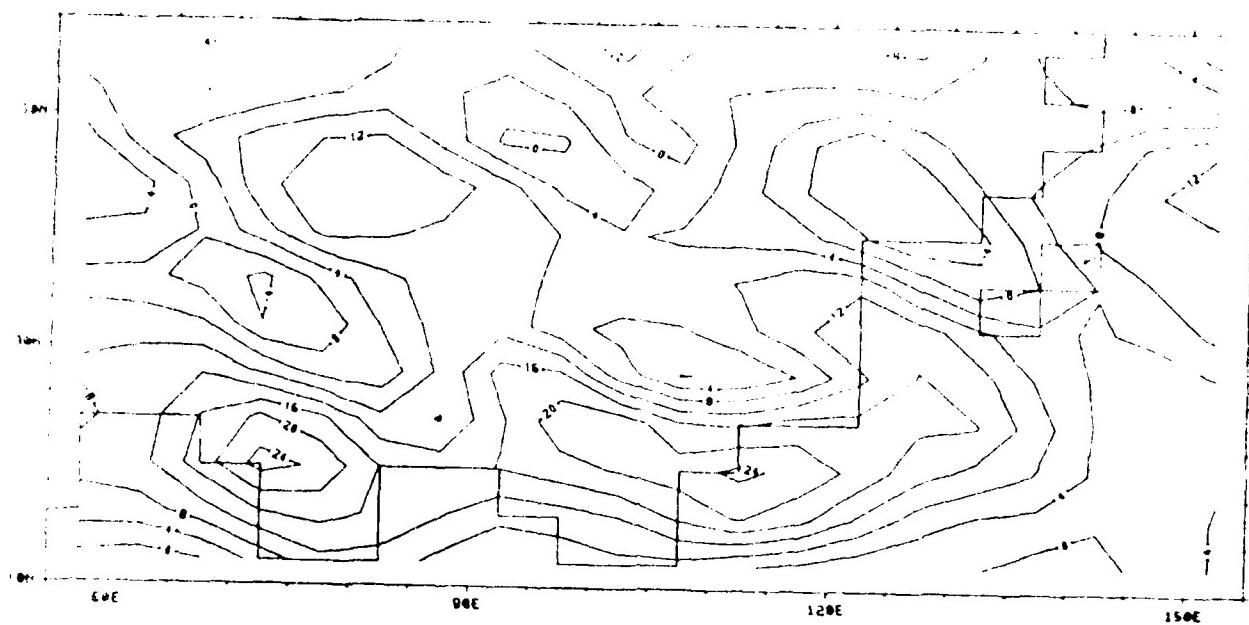
(c)
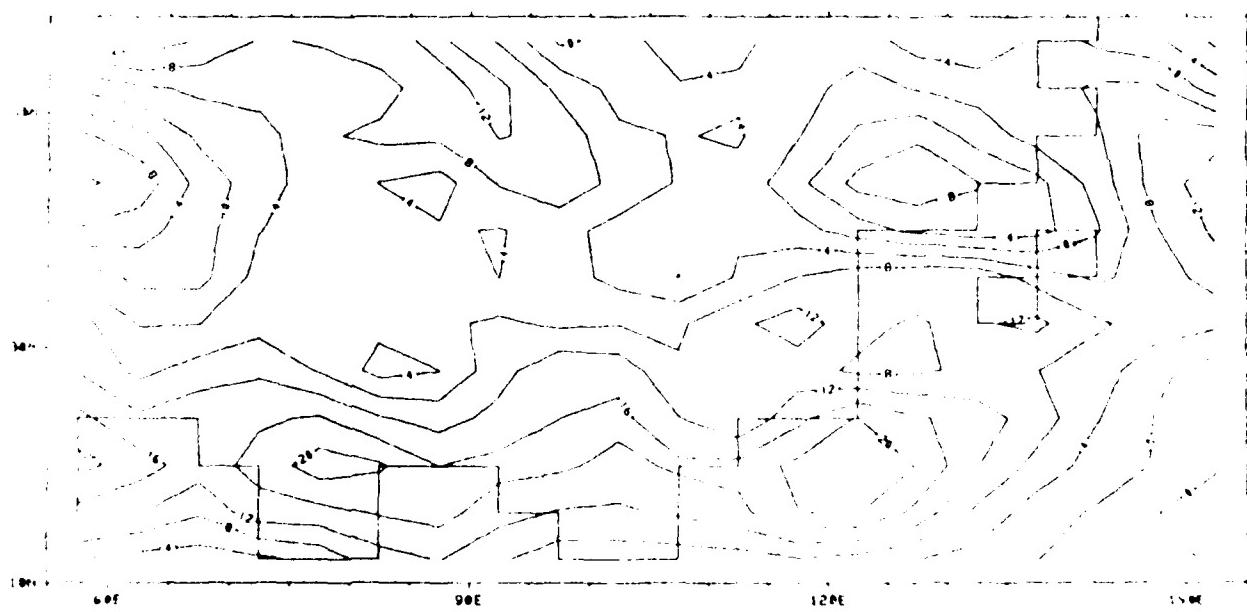
(d)
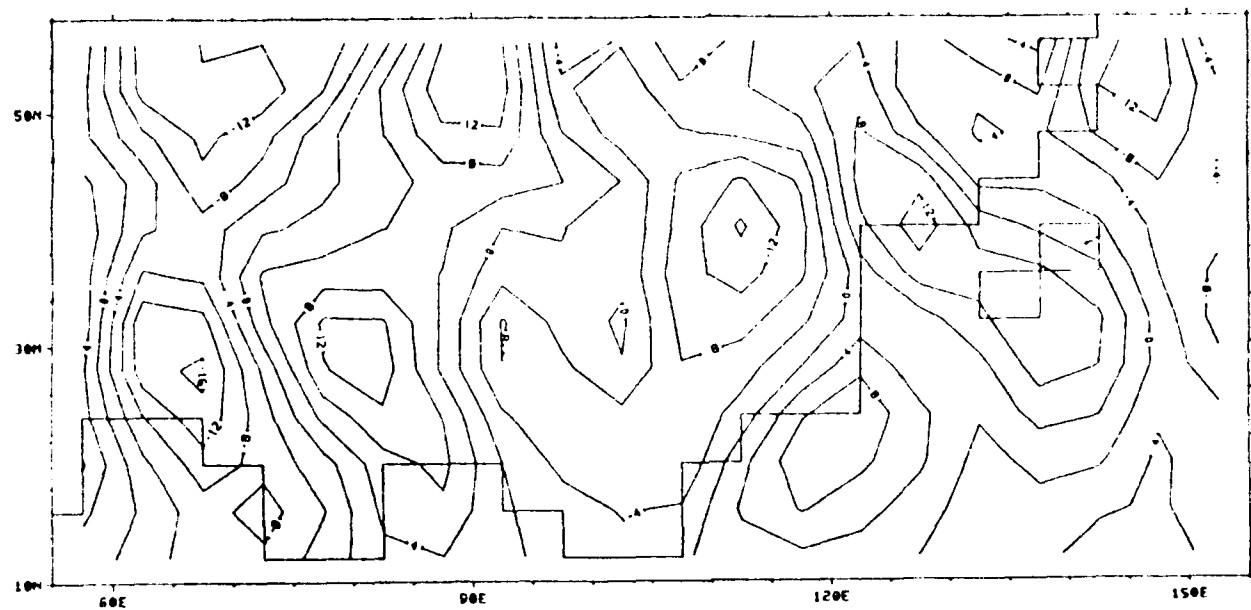
(a)
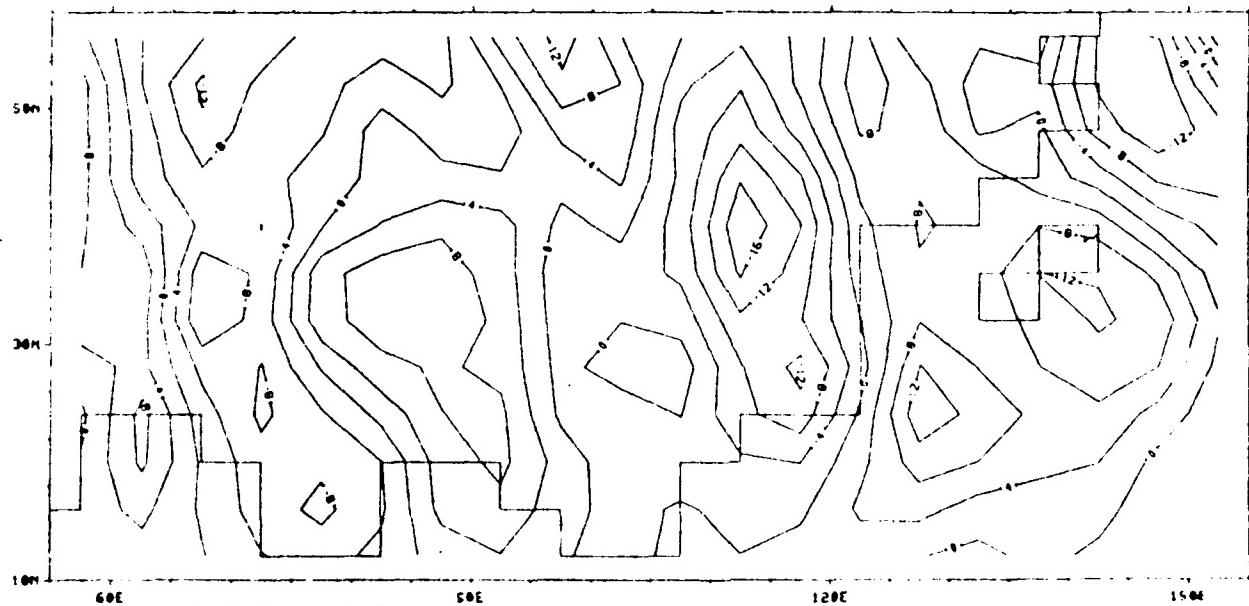
(b)

Fig. 3.8   The meridional wind (msec^{-1}) component at level 3
          for the same times and condition as in Fig. 3.?.

115

(c)

(d)

116
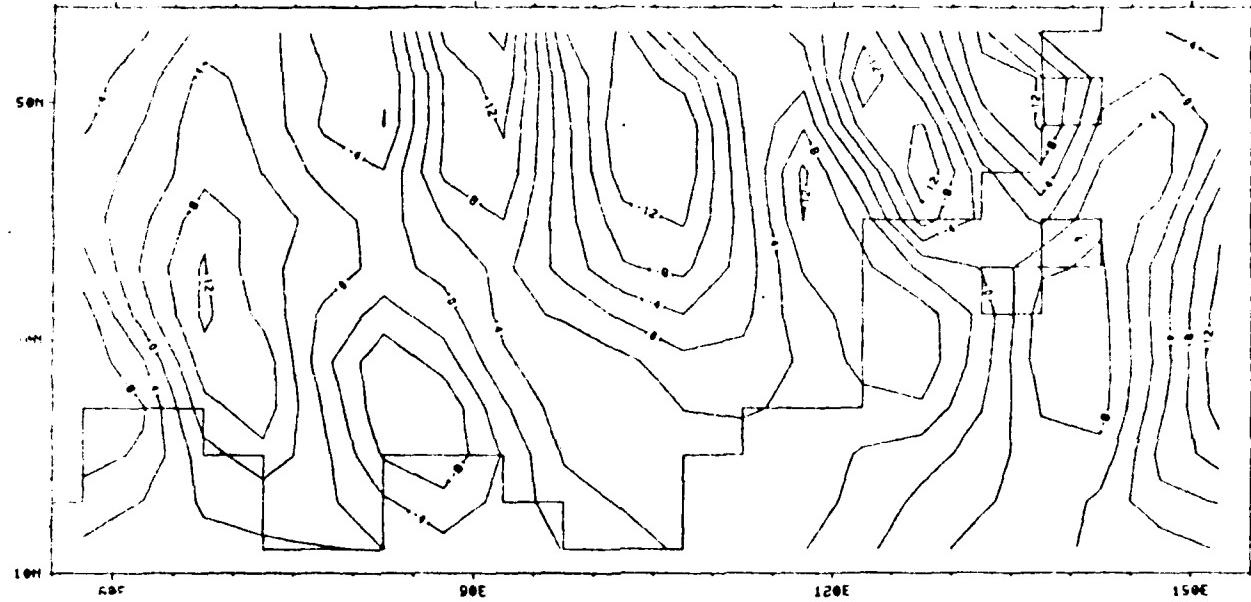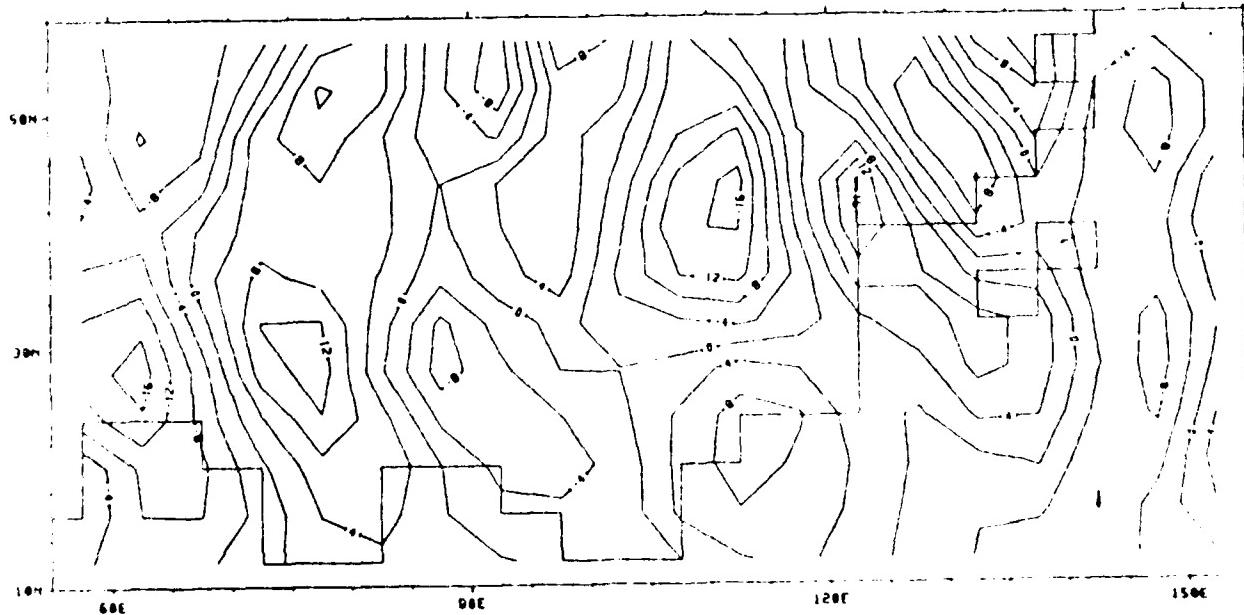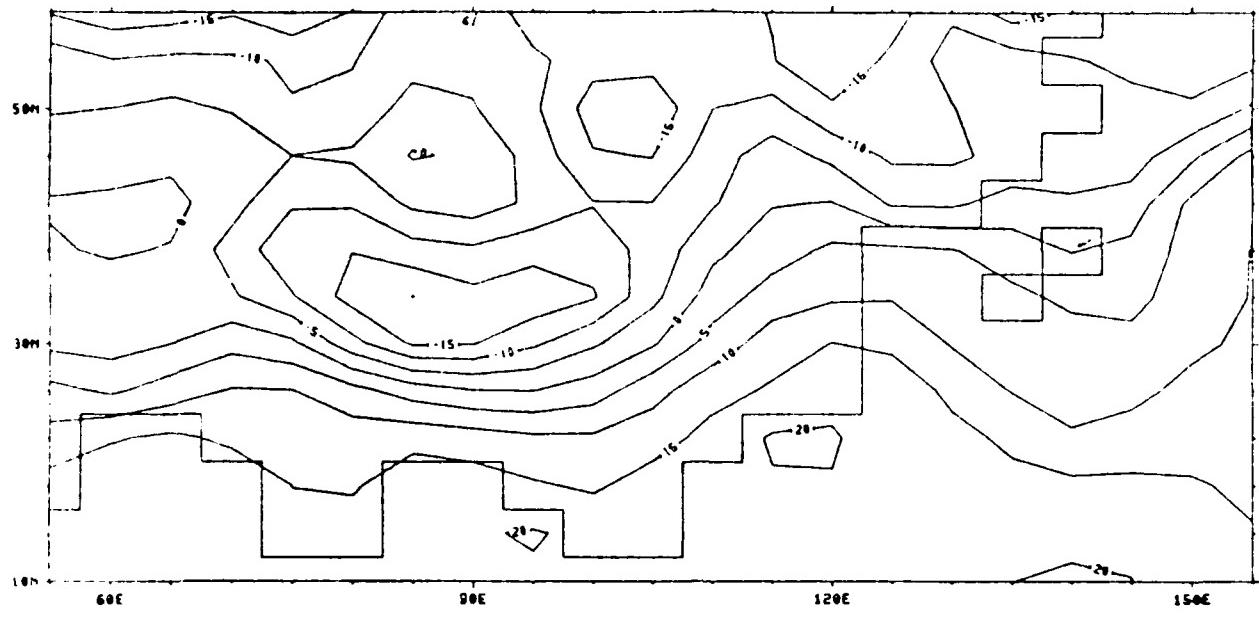
(a)
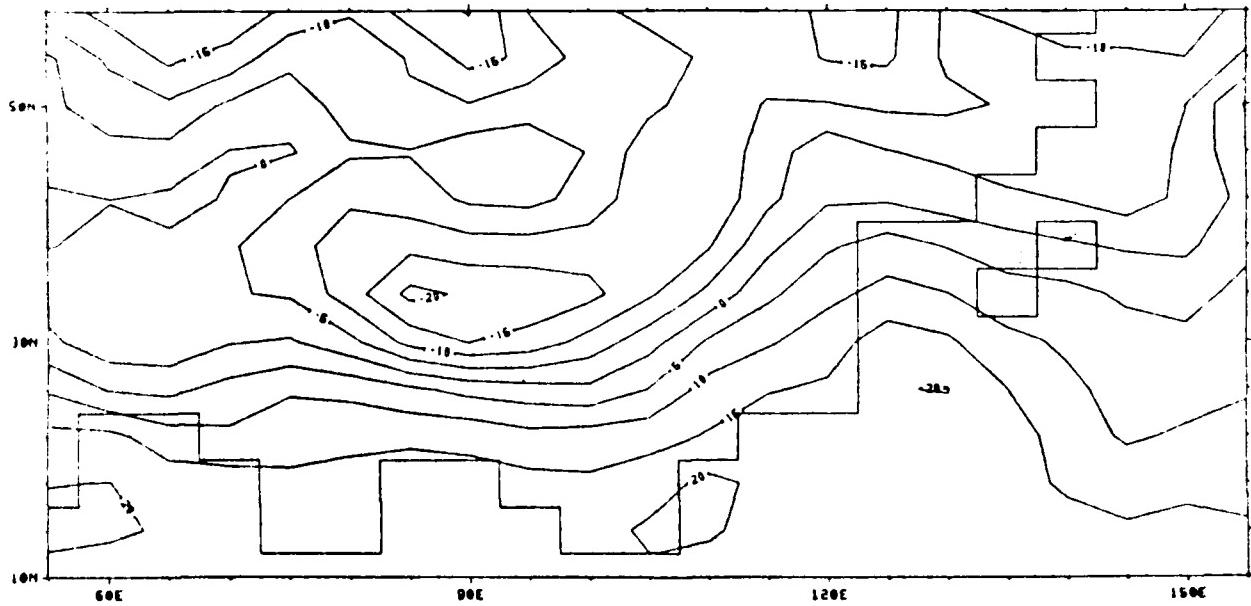
(b)

Fig. 3.9 The temperature (Deg-C) distributions at level 3
for the same times and condition as in Fig. 3.2.

117

(c)

(d)

118
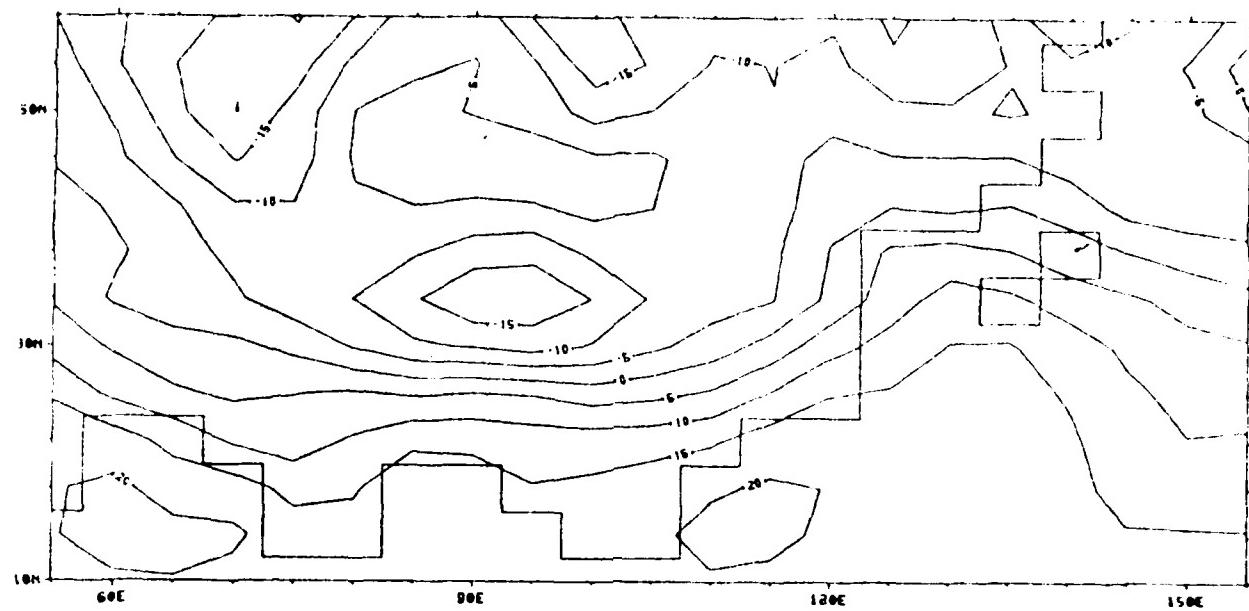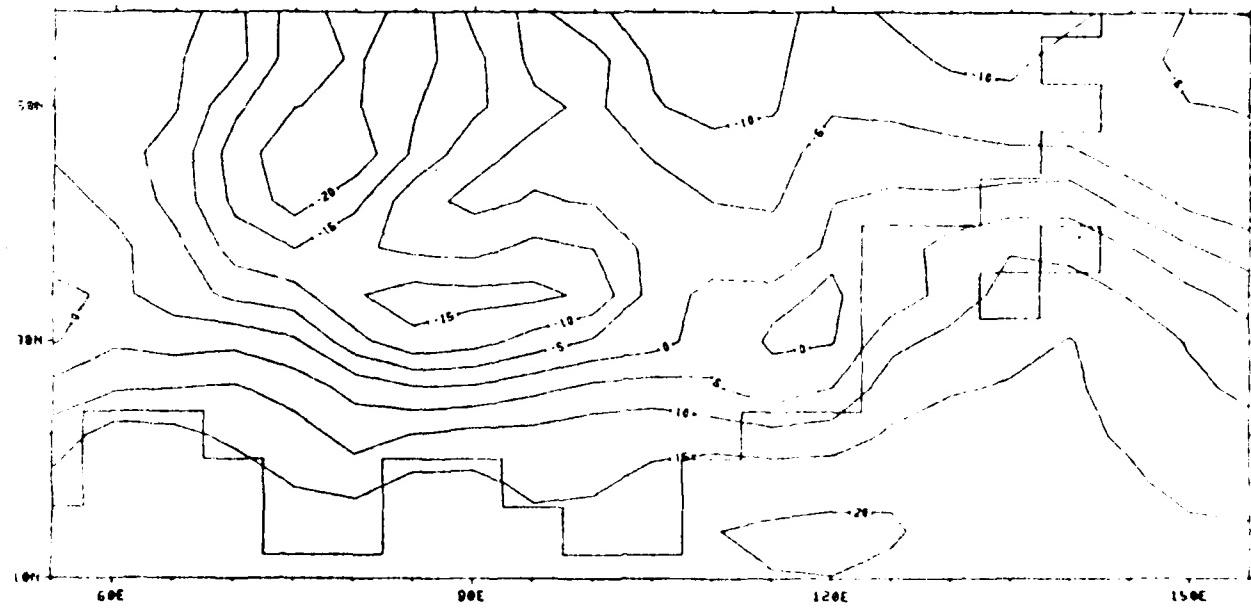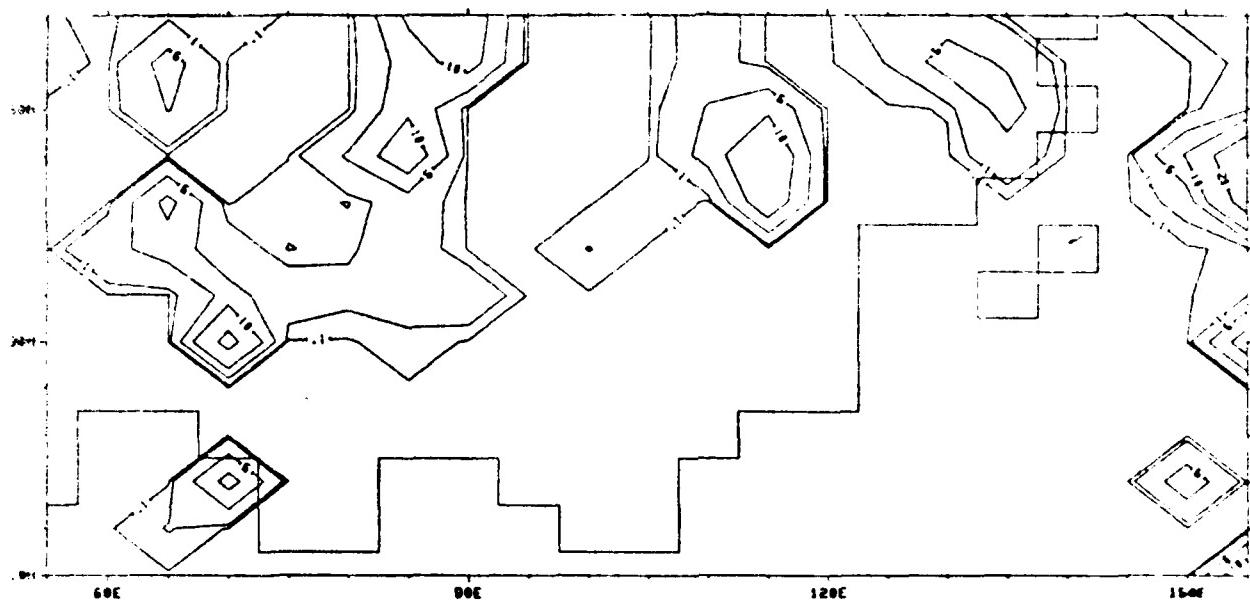
(a)
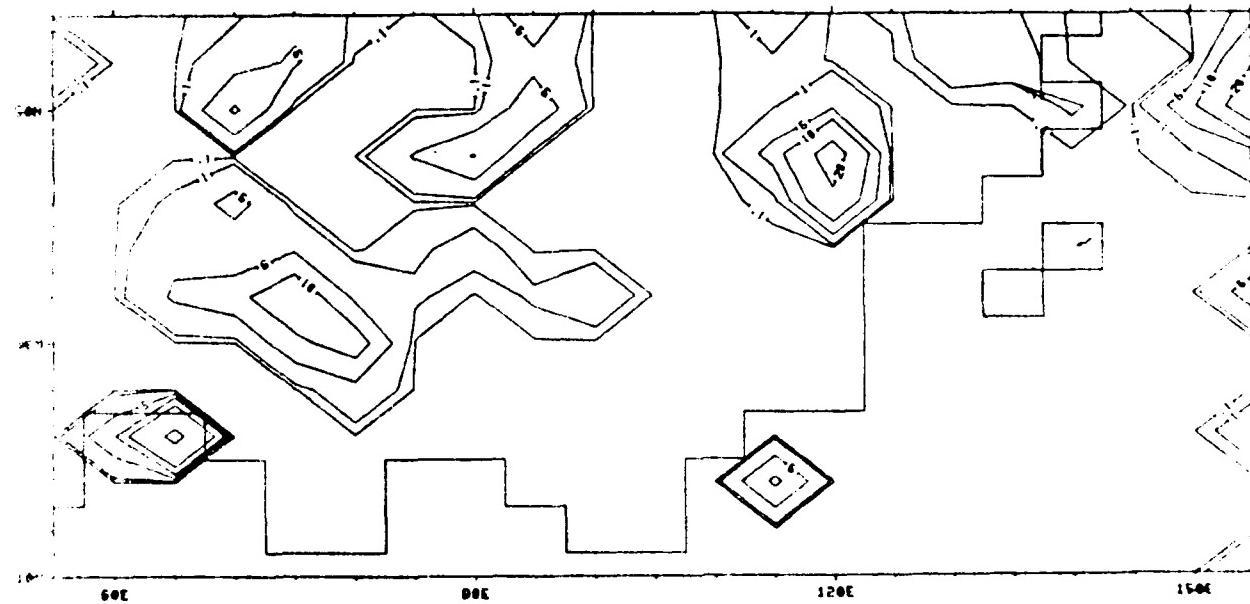
(b)

Fig. 3.10 The precipitation rate for the same times and conditions as in Fig. 3.2.

119
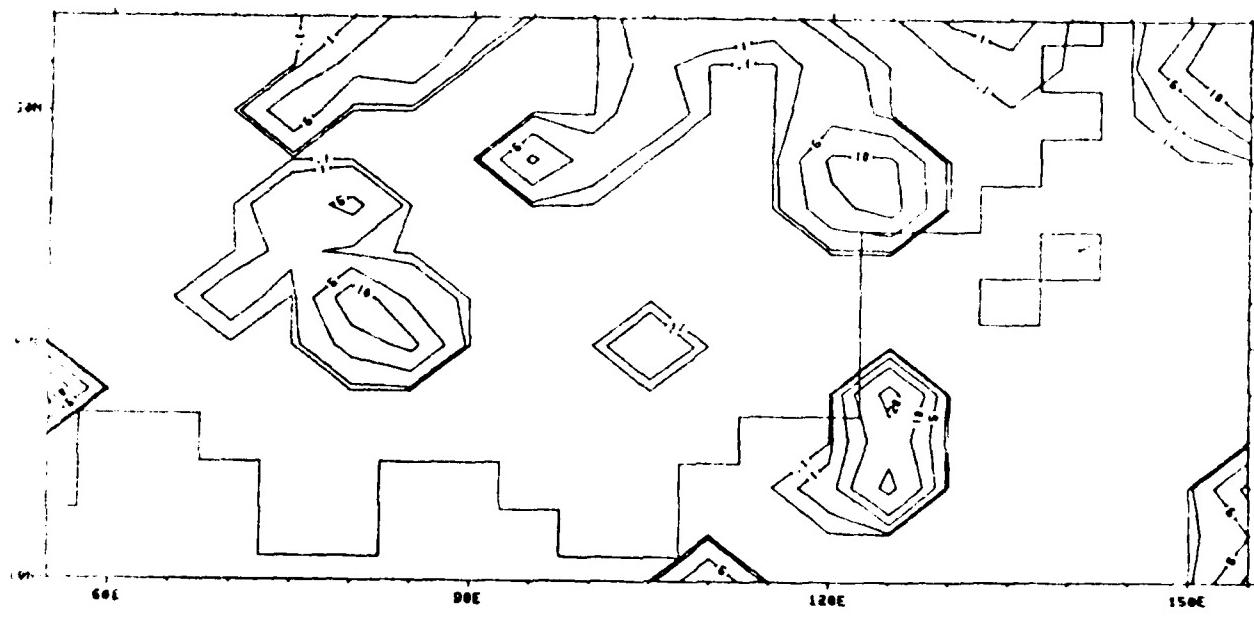
(c)
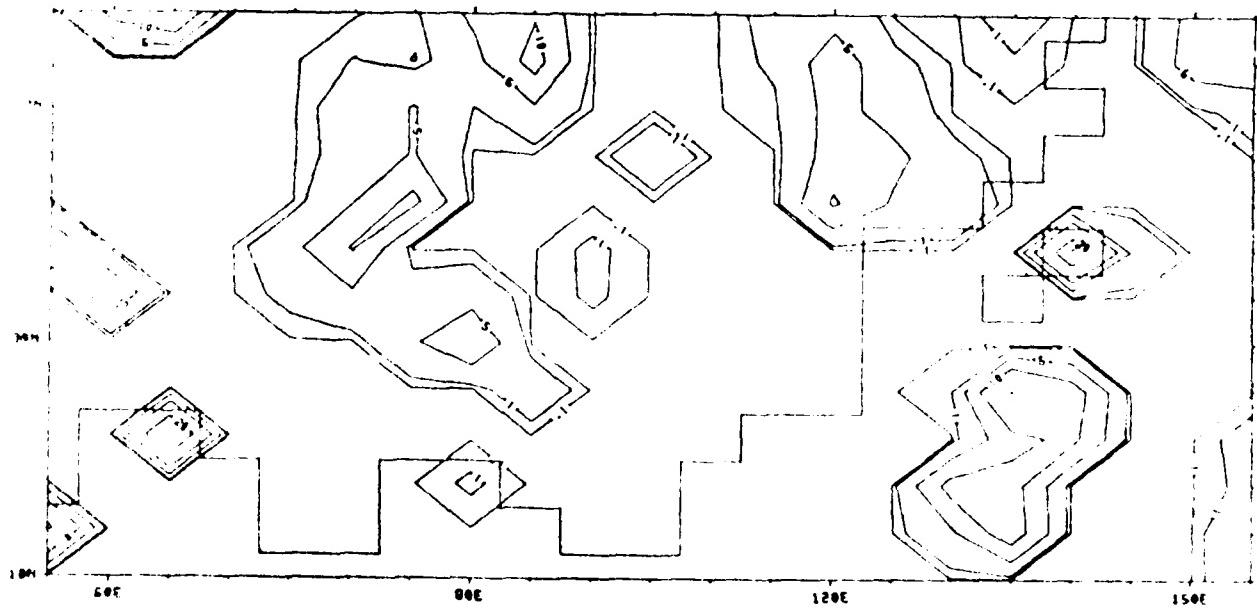
(d)
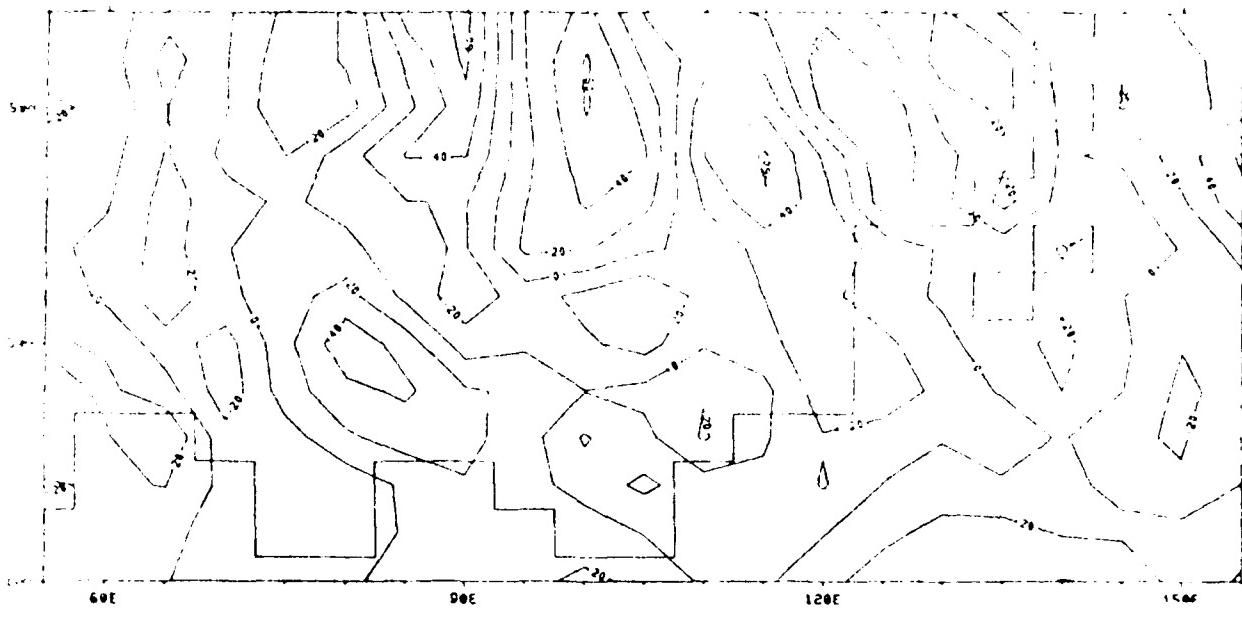
(a)
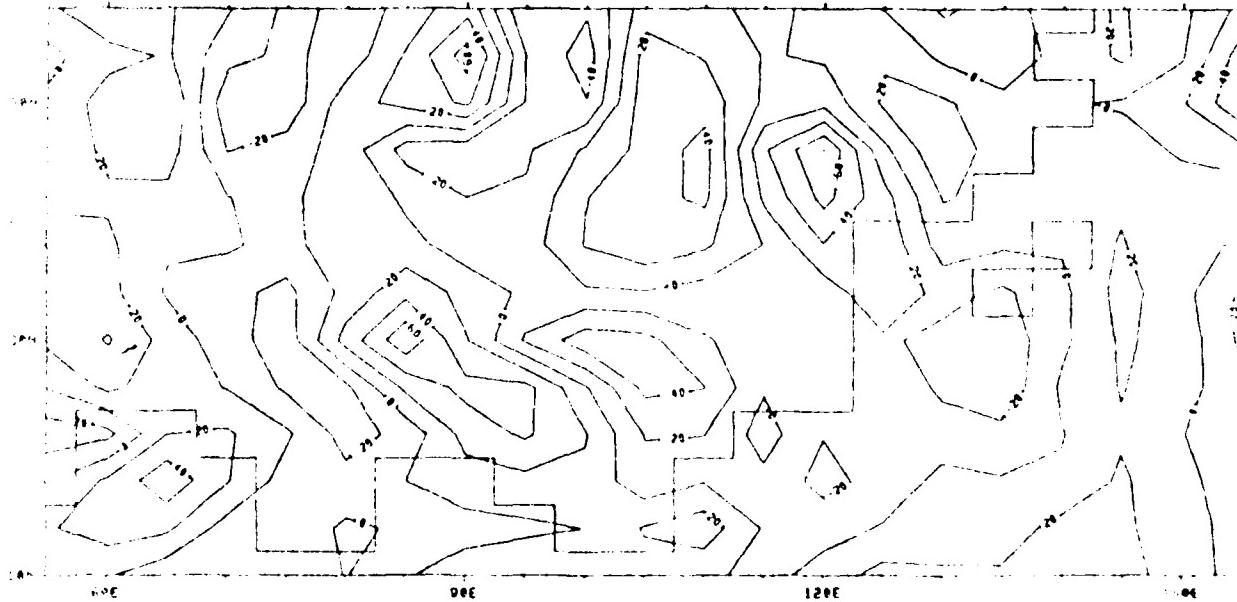
(b)

Fig. 3 11 The sigma velocity (10^{-7} sec^{-1}) at level 3 for the
same times and condition as in Fig. 3.2.

121
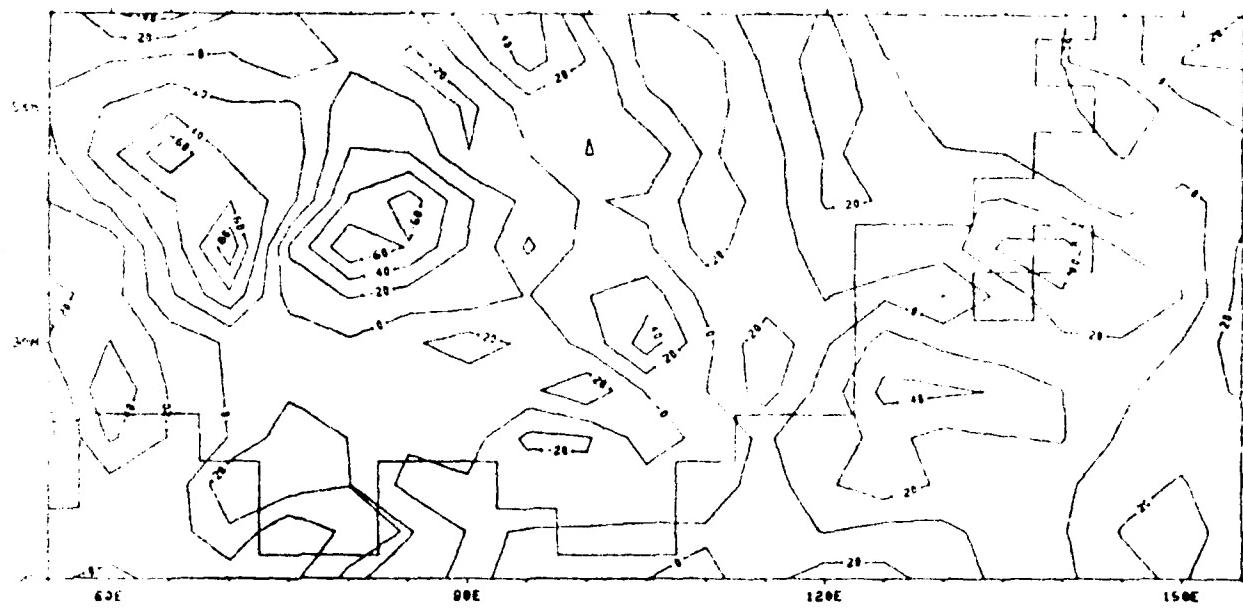
(c)
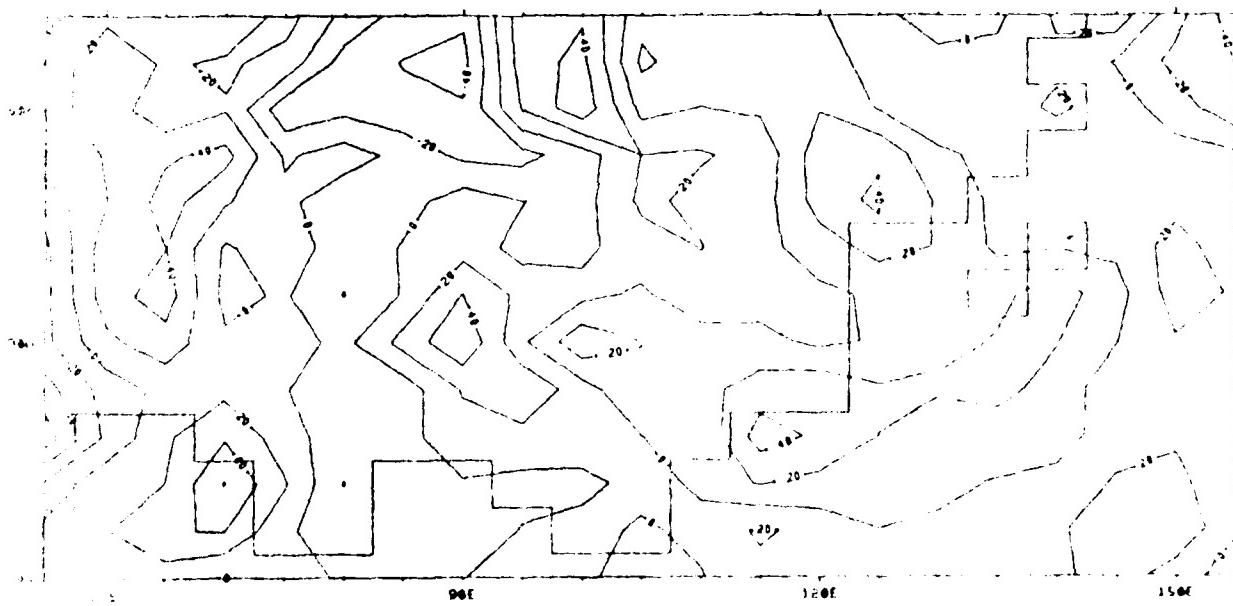
(d)
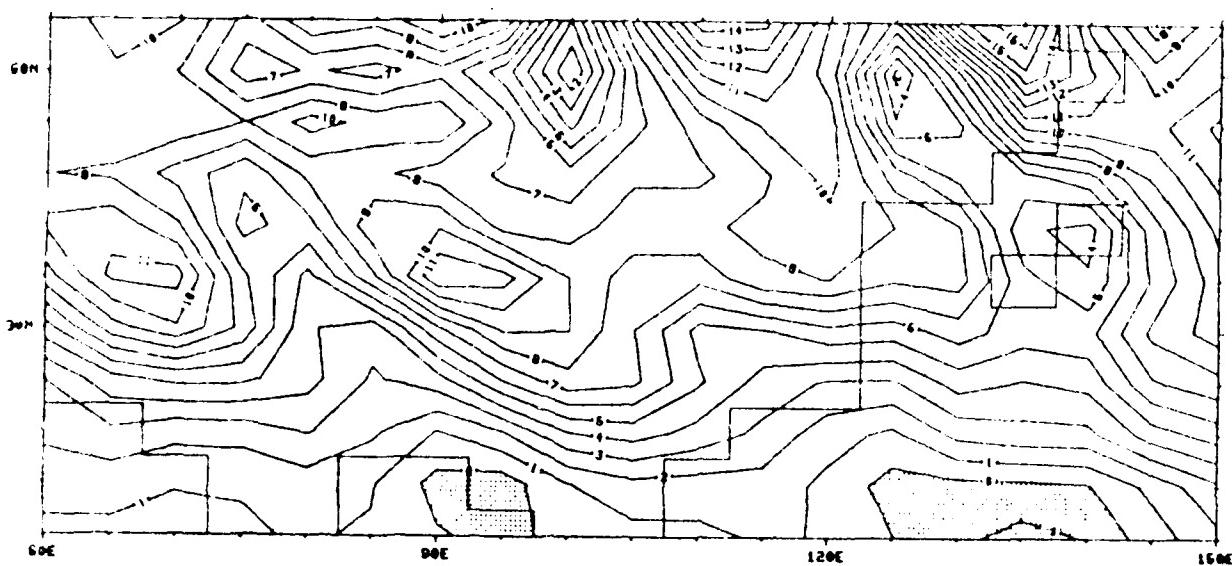
(a)
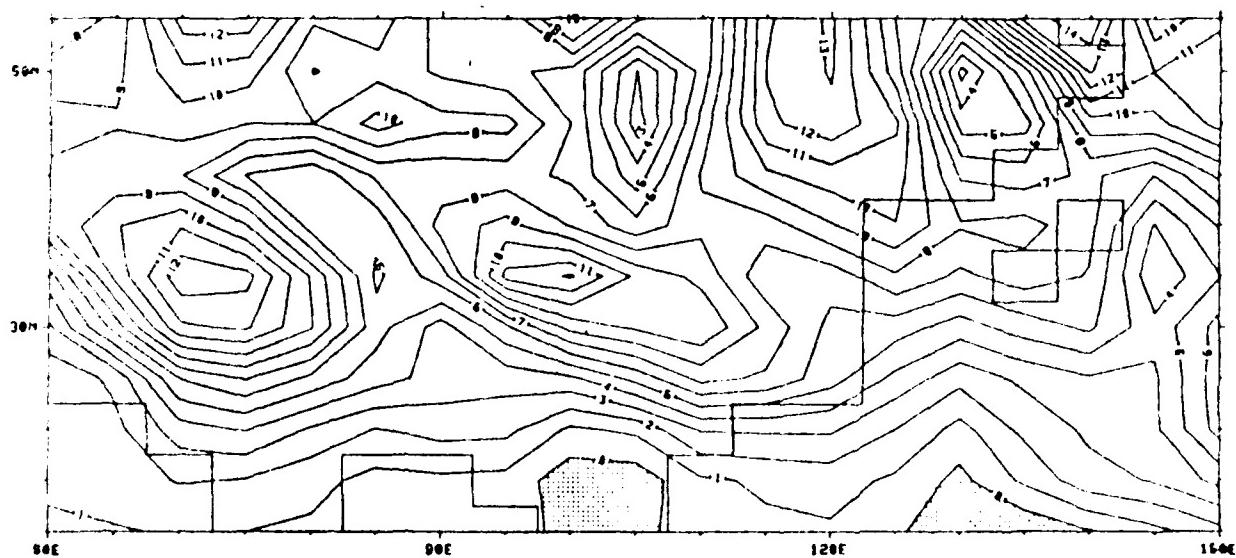
(b)

Fig. 3.12 The absolute vorticity (day^{-1}) at level 2 for the same times under condition as in Fig. 3.2.

123

(c)

(d)

124
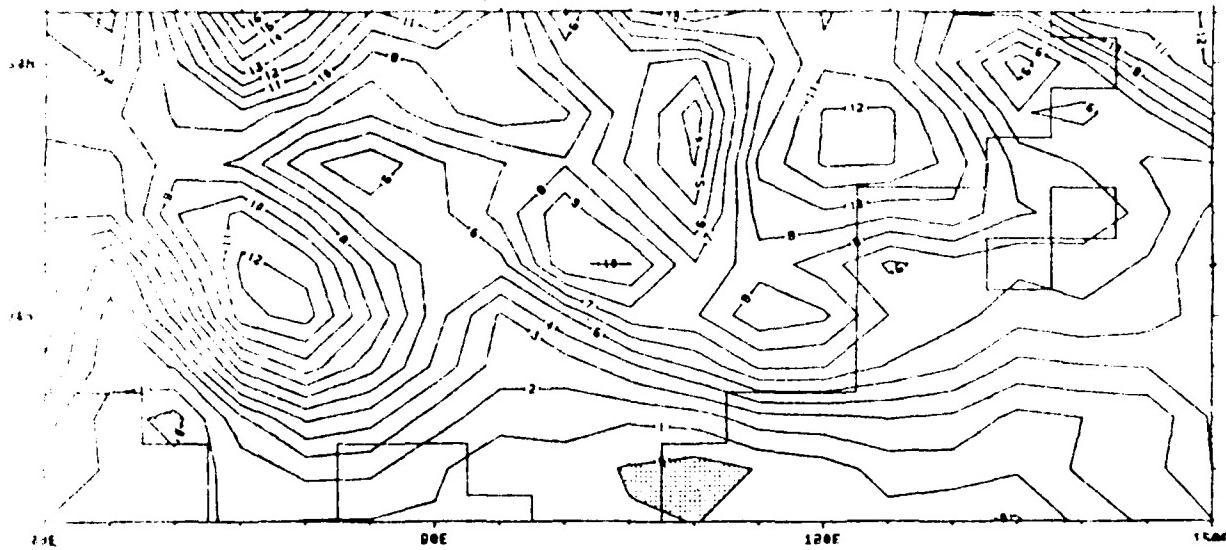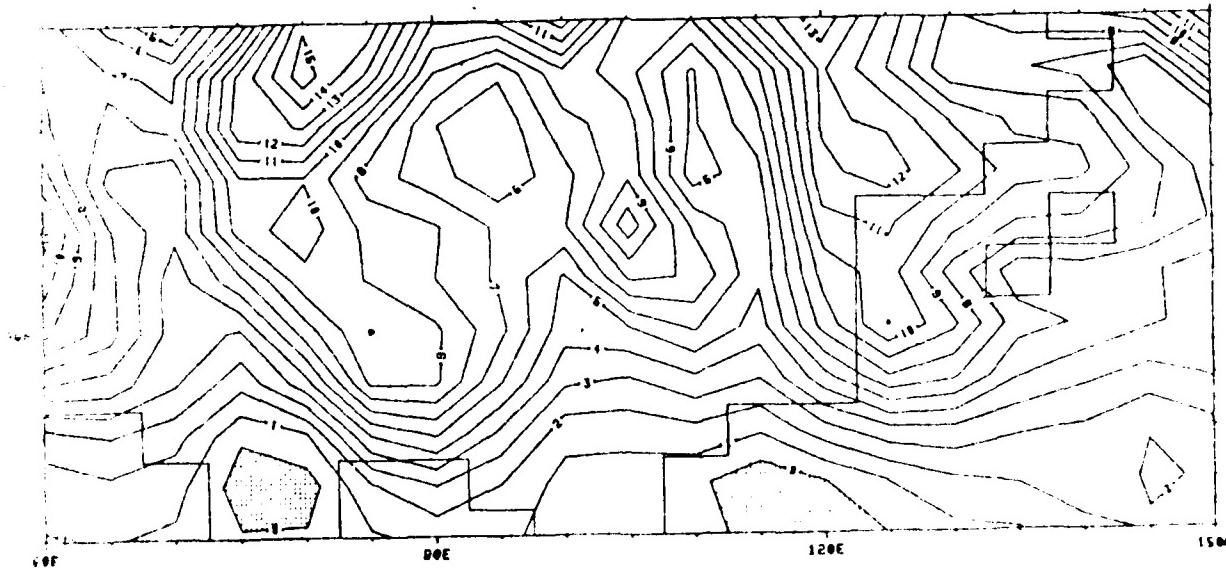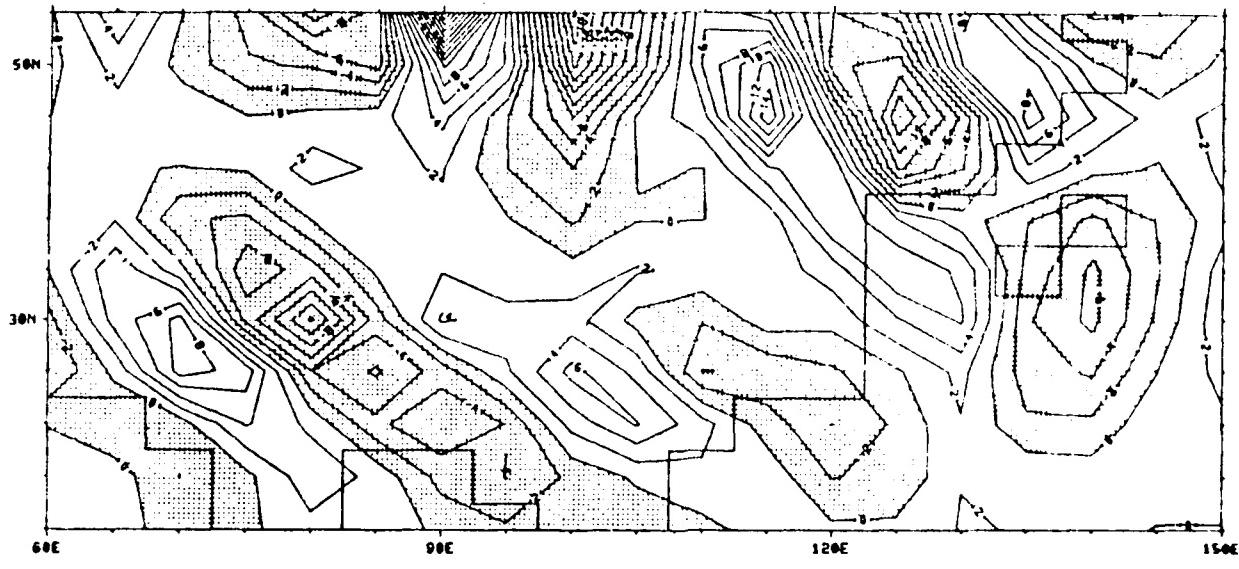
(a)
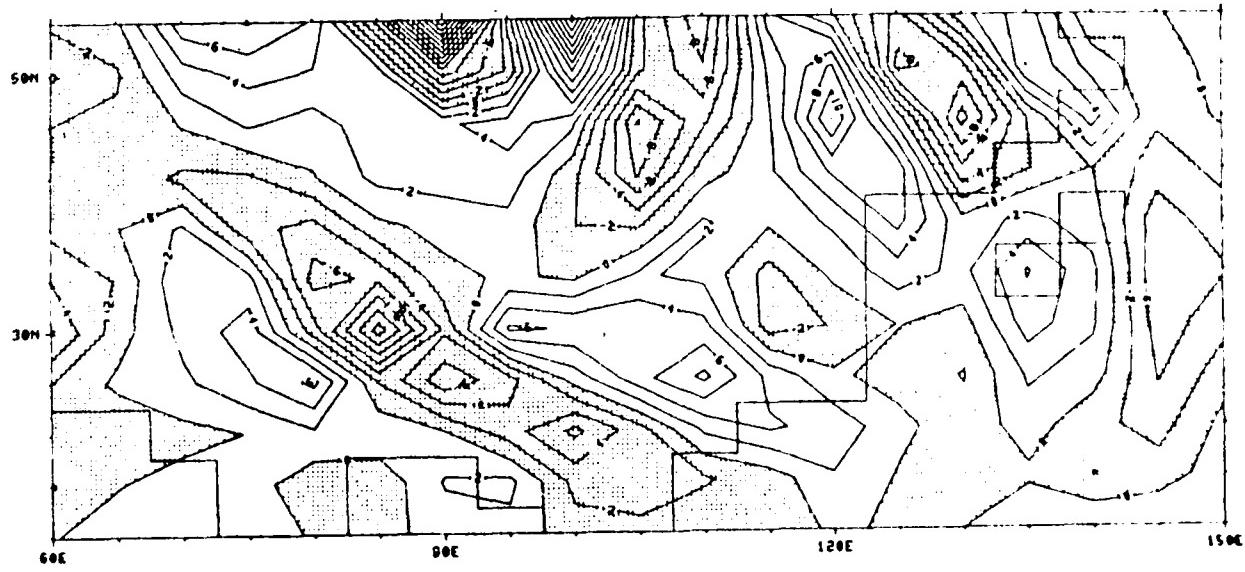
(b)

Fig. 3.13 The import of absolute vorticity (day^{-2}) at level 2
for the same times and condition as in Fig. 3.2.

125
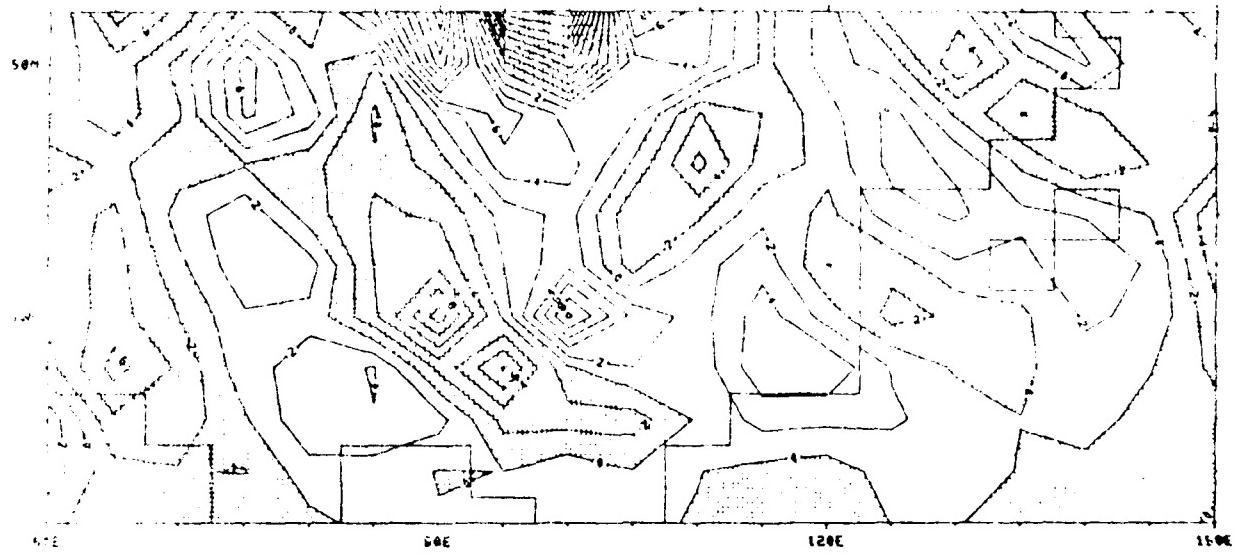
(c)
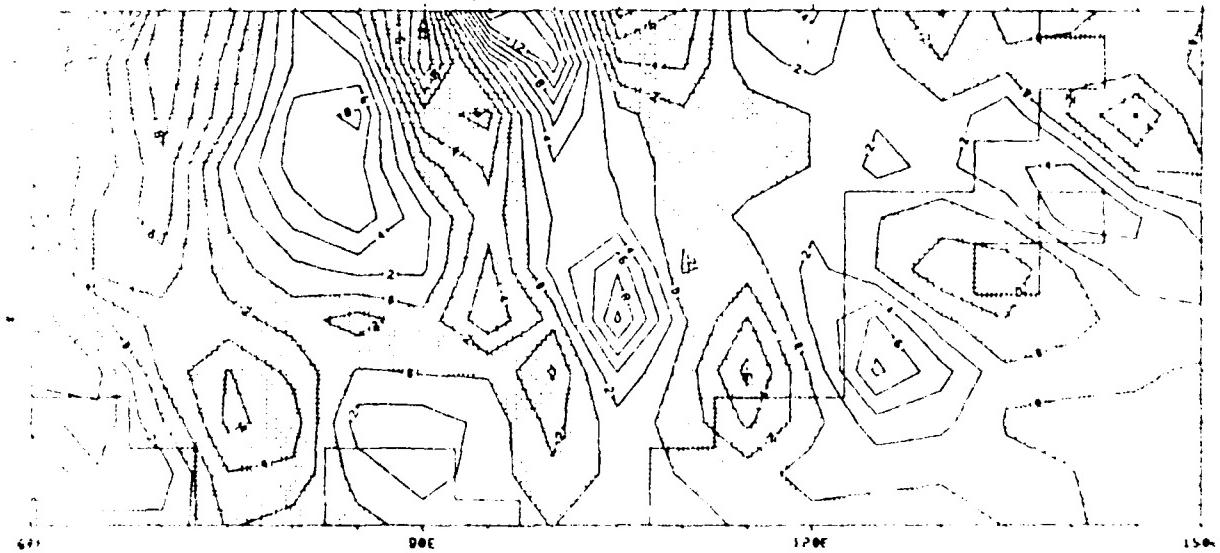
(d)
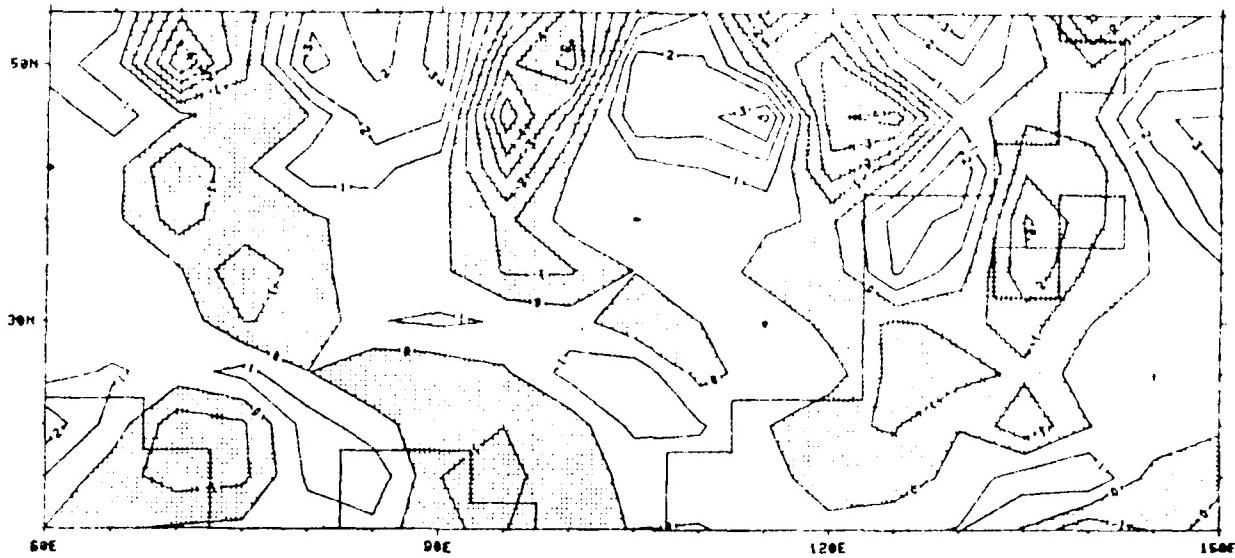
(a)
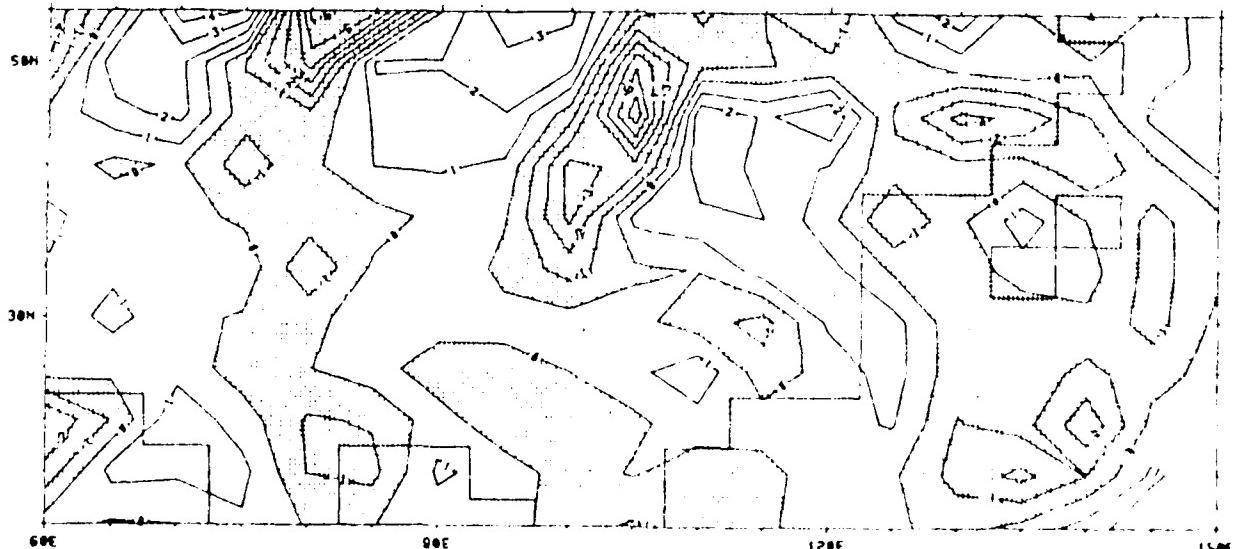
(b)

Fig. 3.14   The import of thermal vorticity (day⁻¹) at level
            2 for the same times and conditions as in Fig. 3.2.
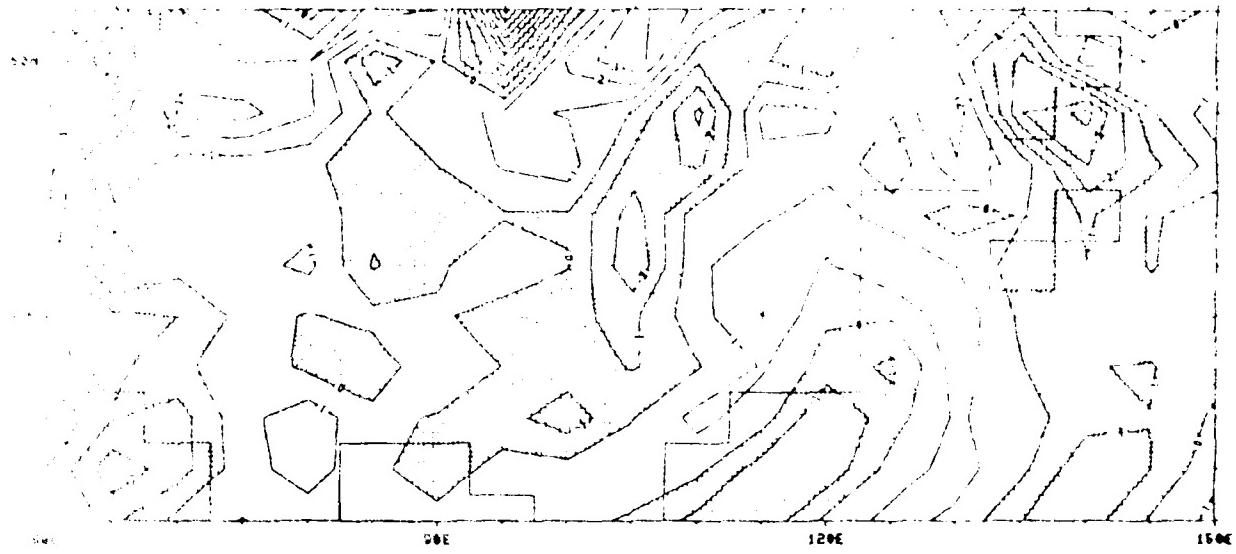
(c)
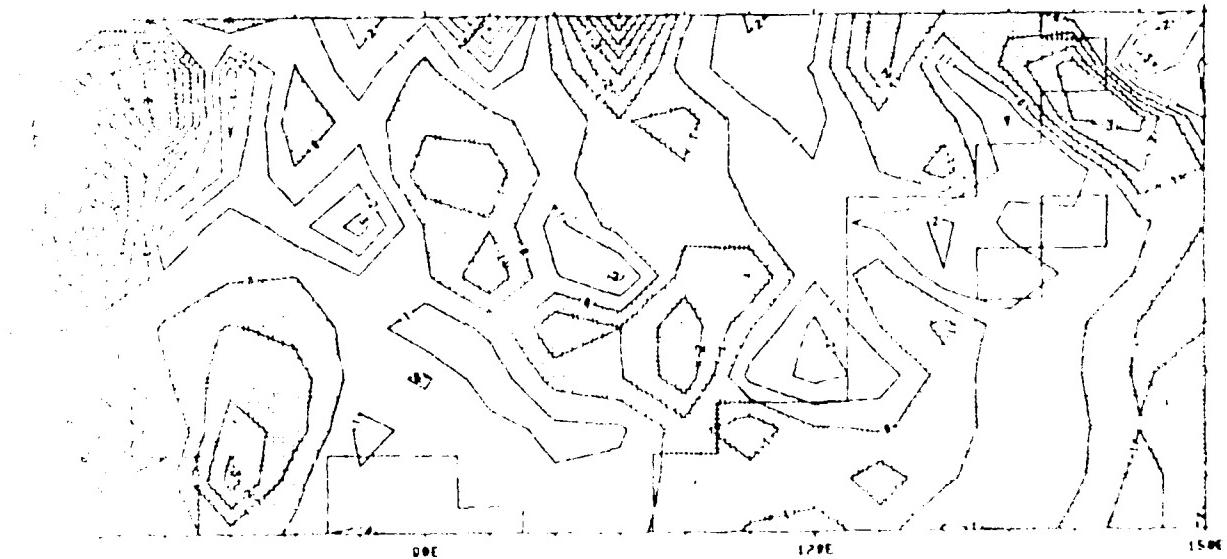
(d)
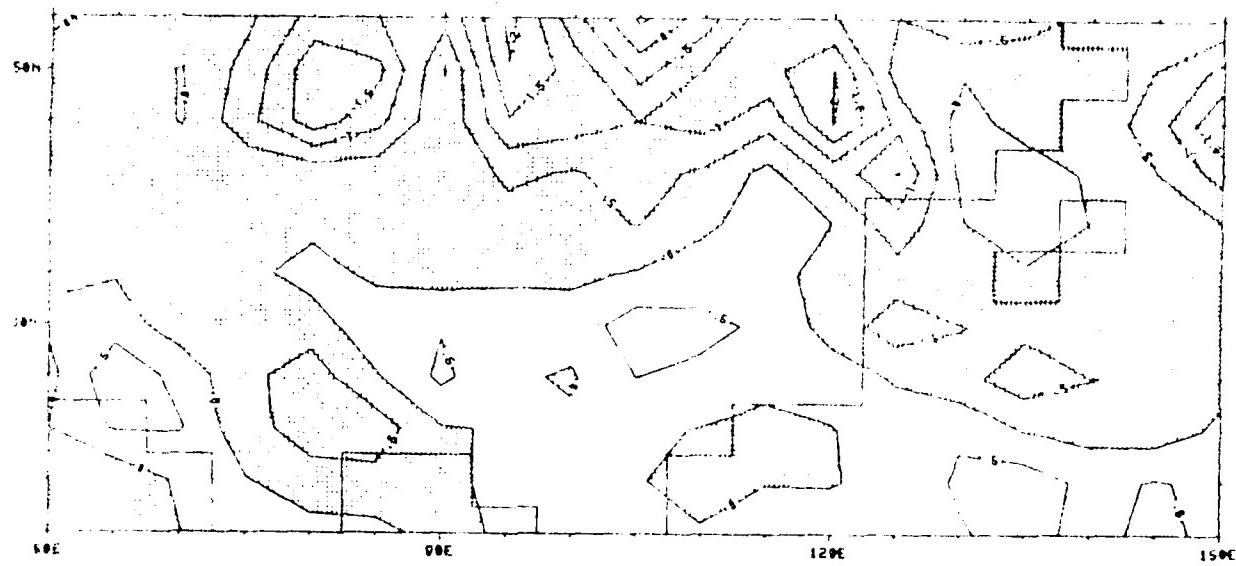
(a)
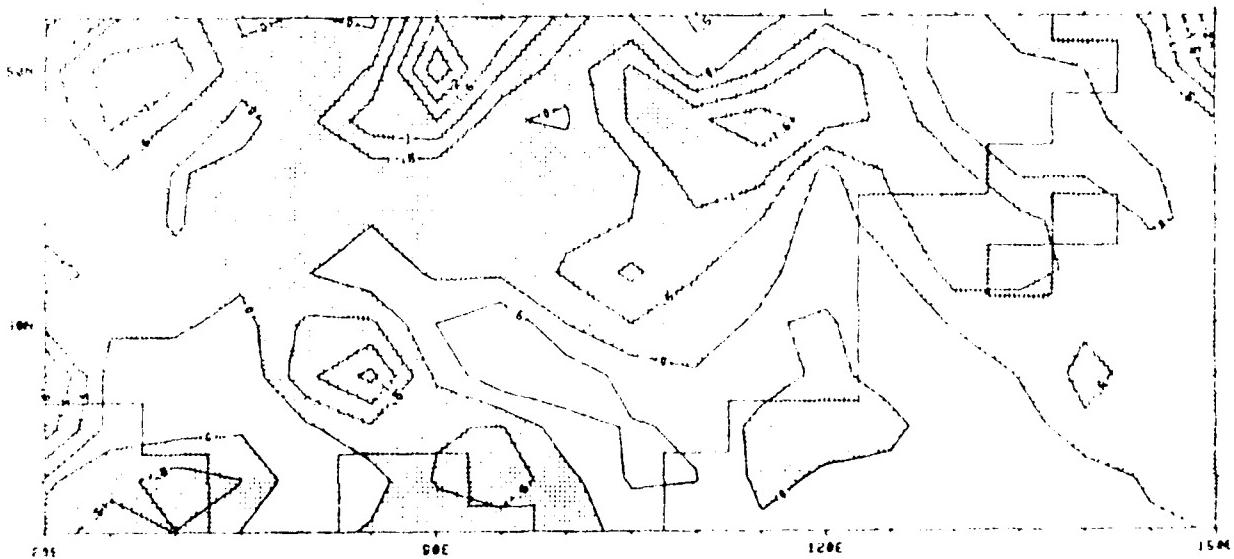
(b)

Fig. 3.15 The tilting term (day^{-2}) at level 2 for the same times and condition as in Fig. 3.2.
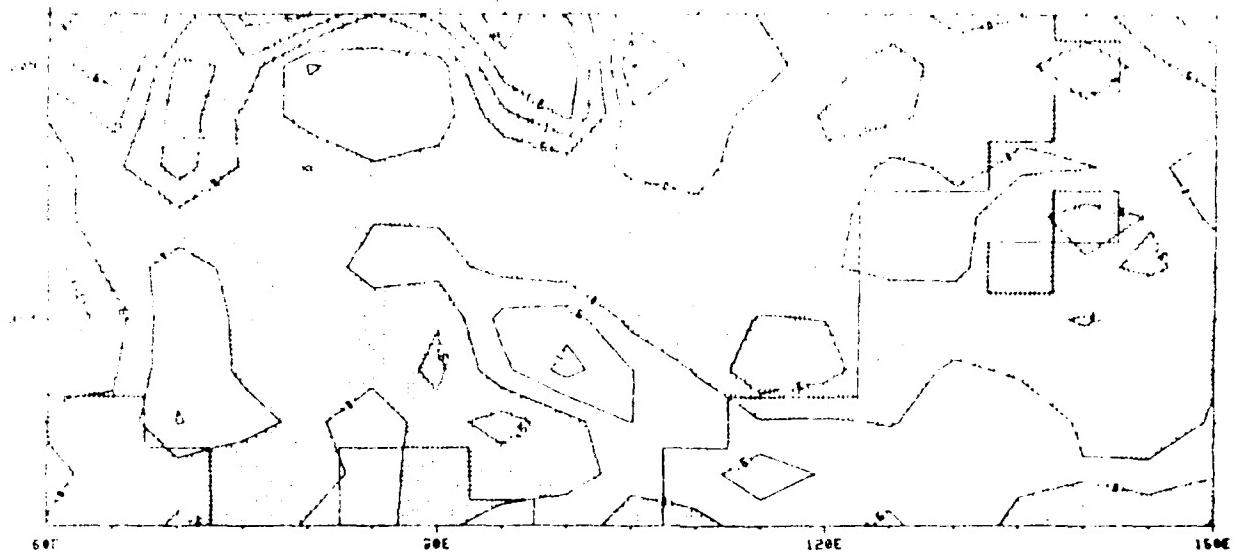
(c)
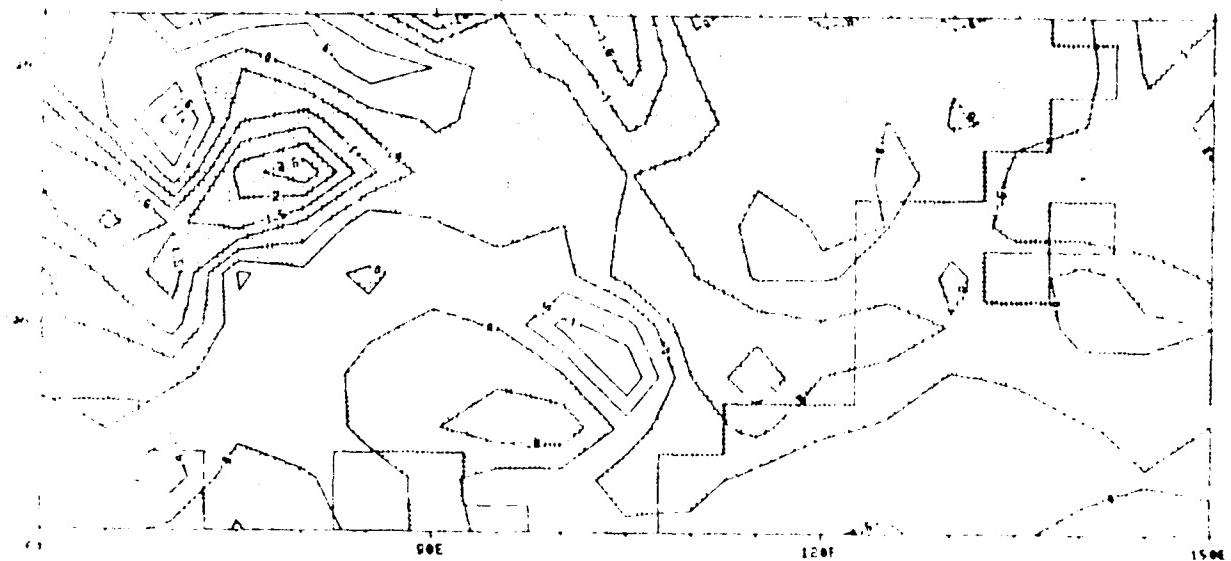
(d)
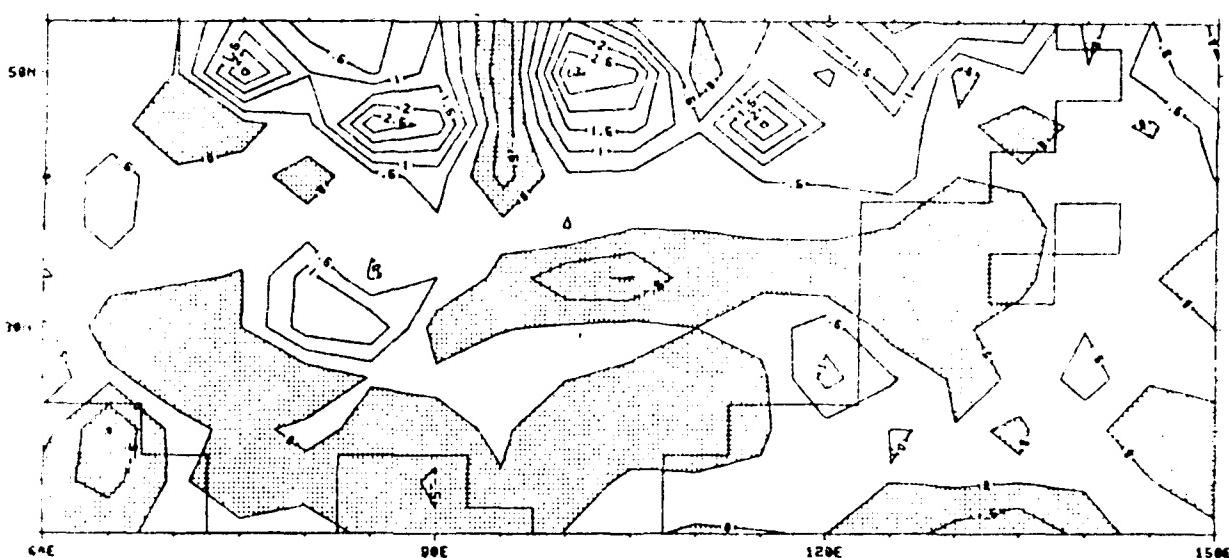
(a)
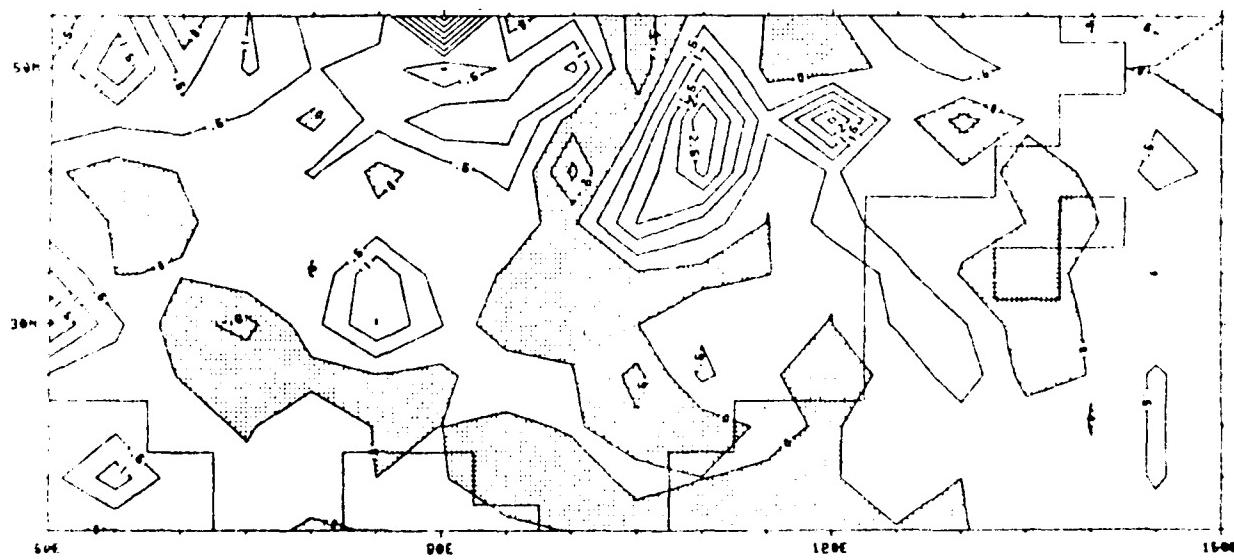
(b)

Fig. 3.16 The vertical advection of absolute vorticity
(day⁻²) at level 2 for the same times and
condition as in Fig. 3.2.
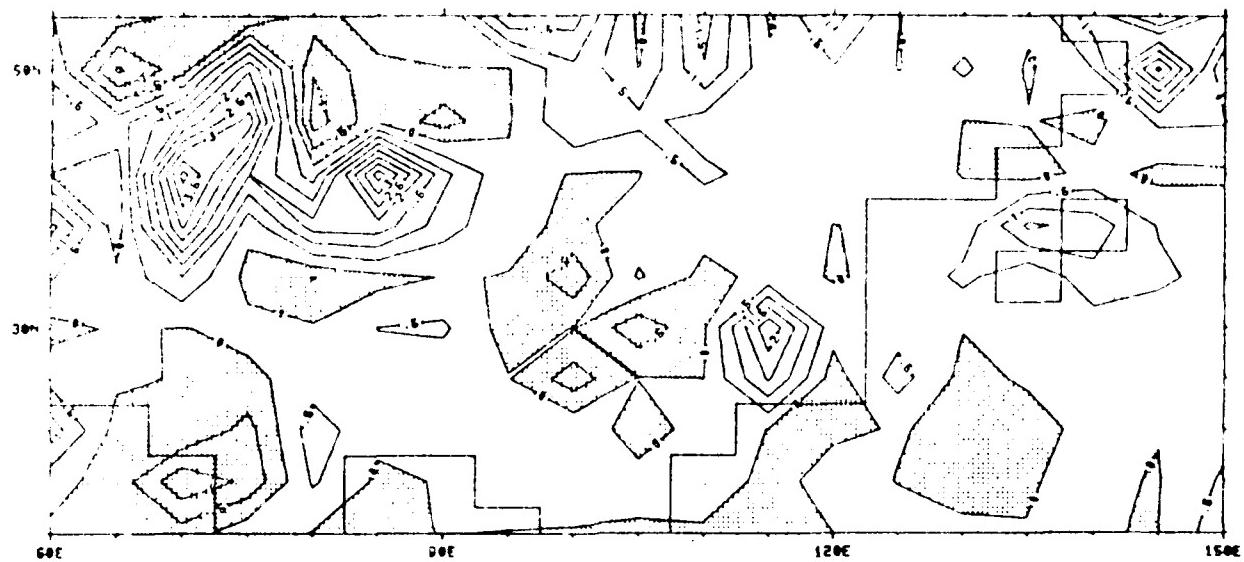
(c)
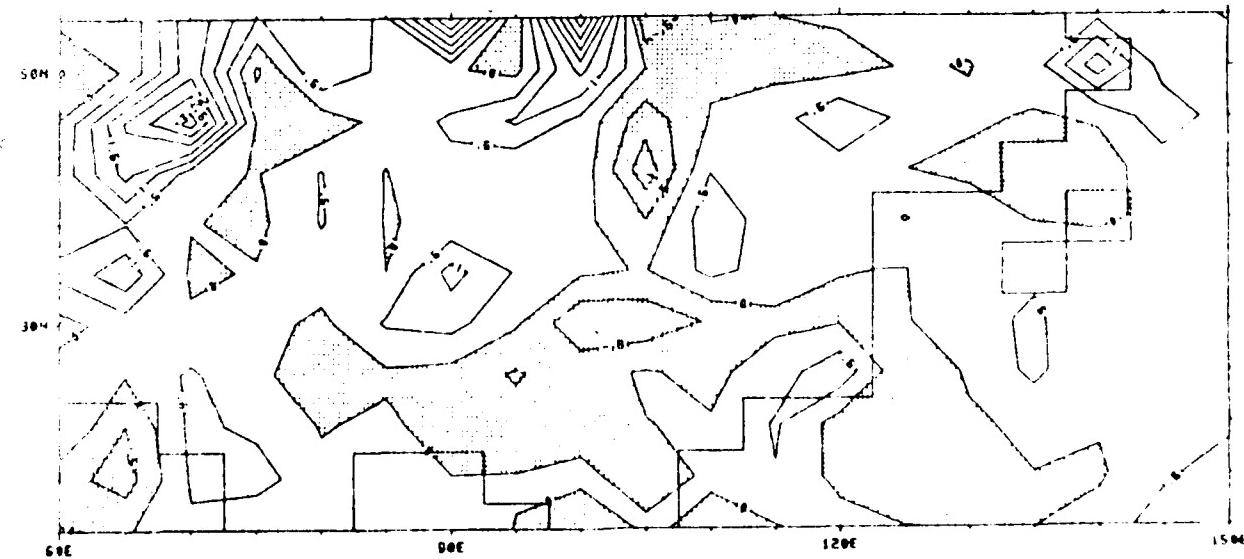
(d)
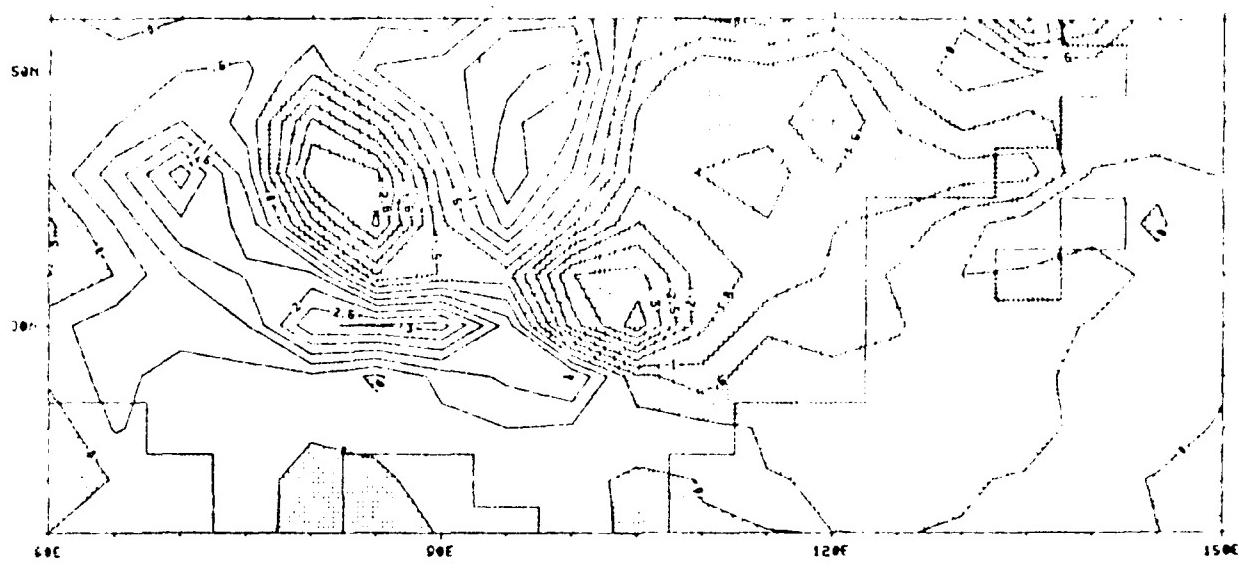
(a)
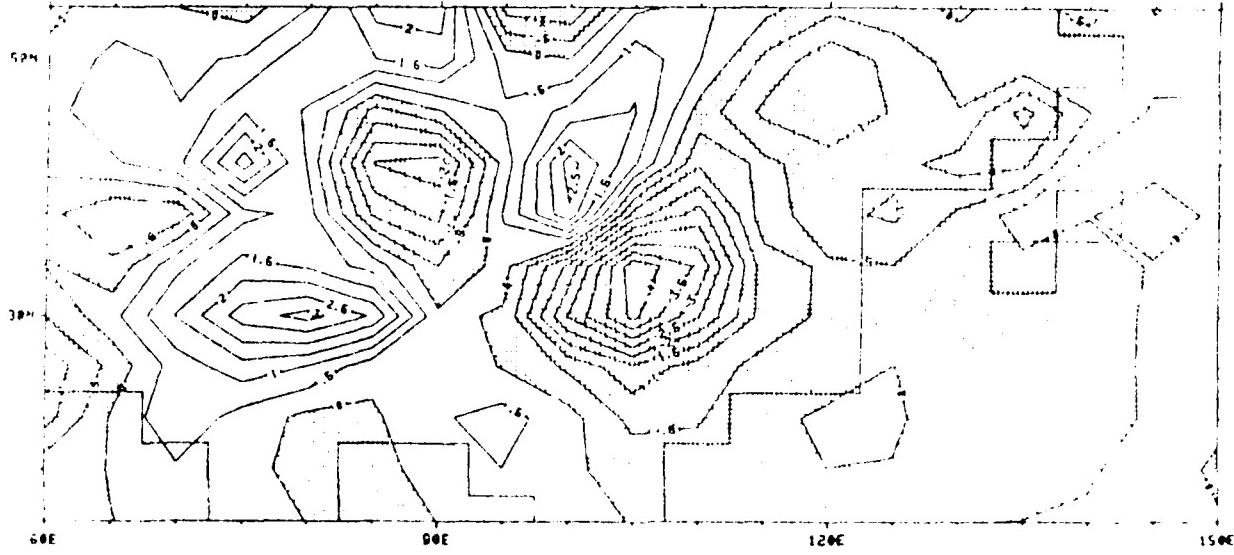
(b)

Fig. 3.17   The solenoid turn (day^{-2}) at level 2 for the same
times and condition as in Fig. 3.2.

133
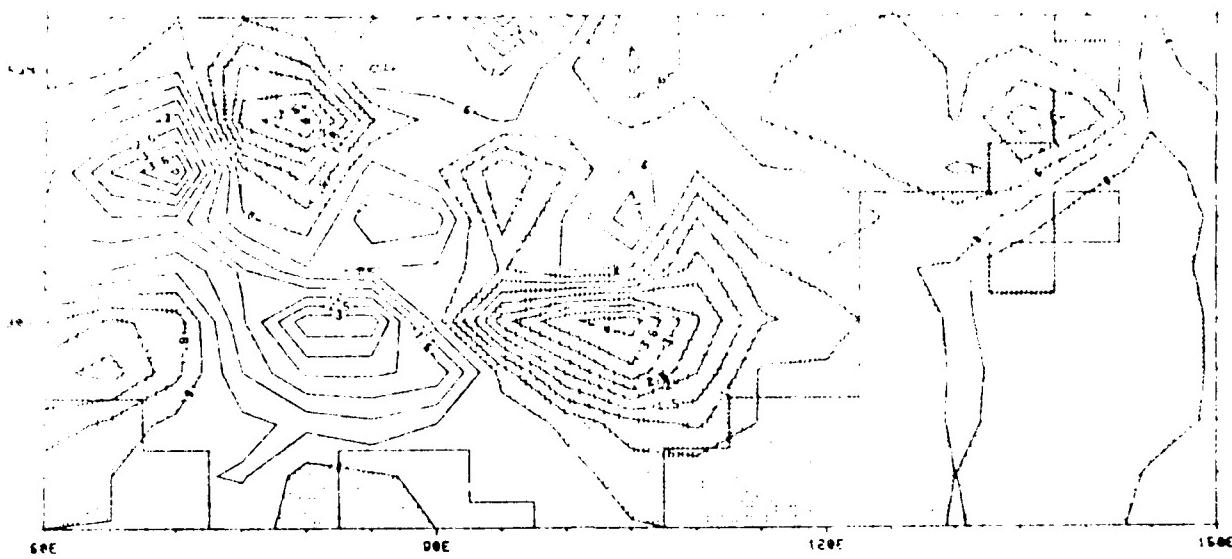
(c)
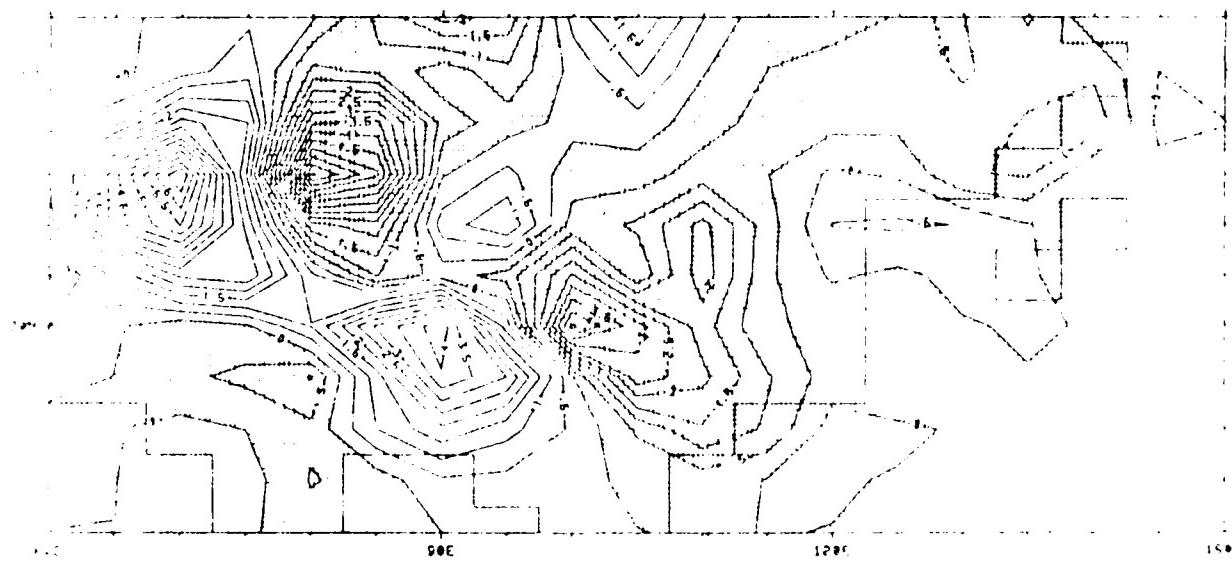
(d)
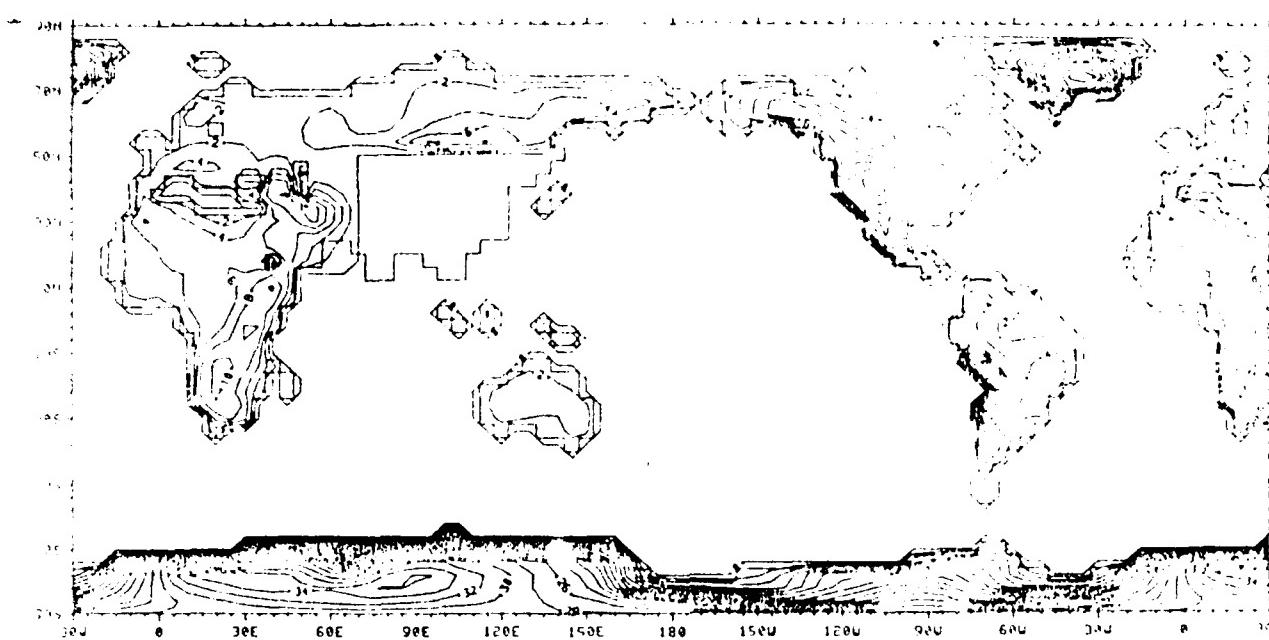
Fig. 3.18 The surface elevation $(10^2 m)$ of the earth with assumed
flat land south of $50°N$ and east of $60°E$.
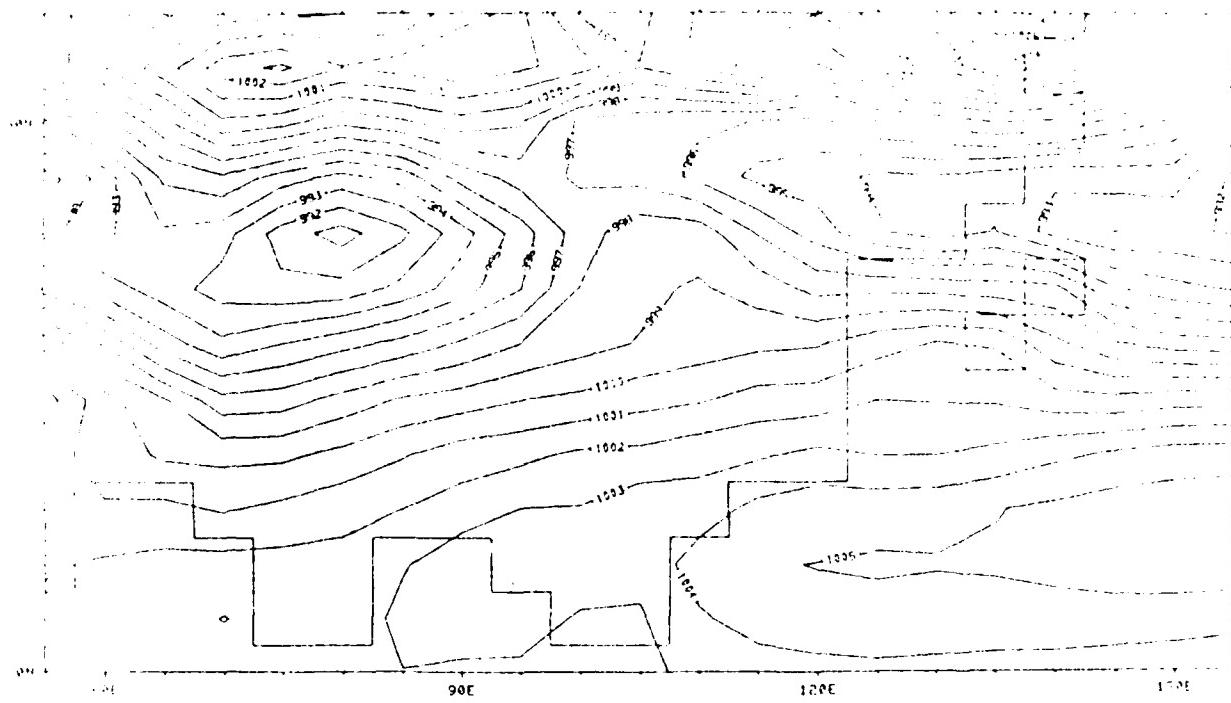
Fig. 3.19 Mean sea level pressure (mb) chart for March NTPC.
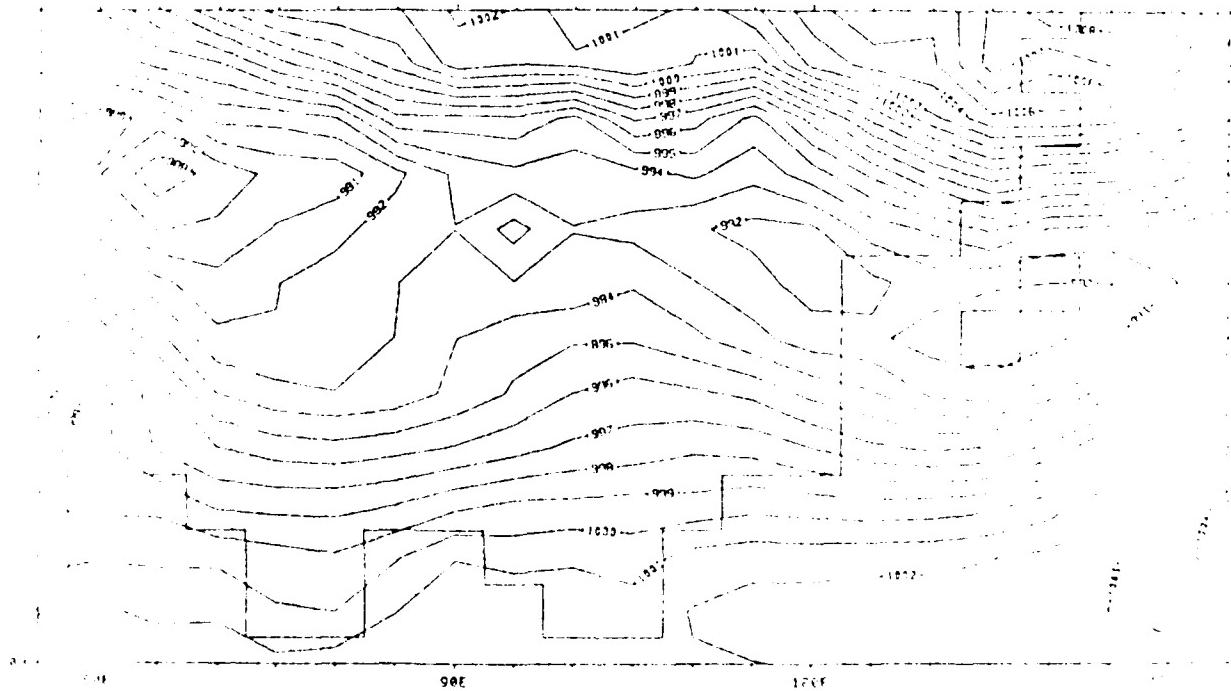
Fig. 3.20 As in Fig. 3.19, except for April.

136
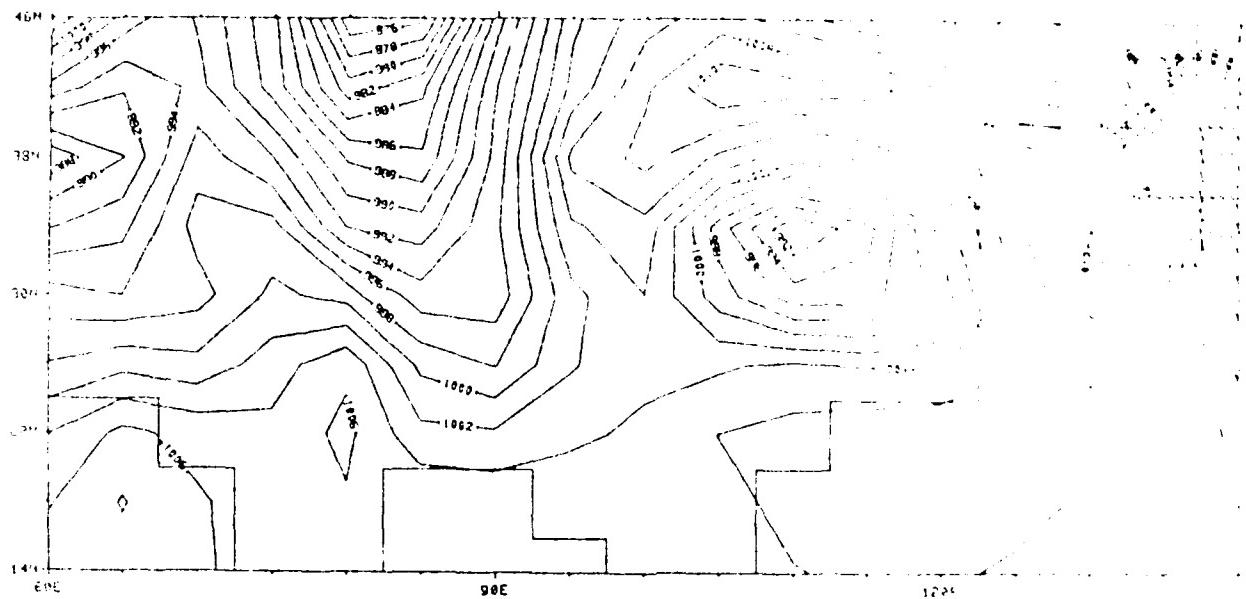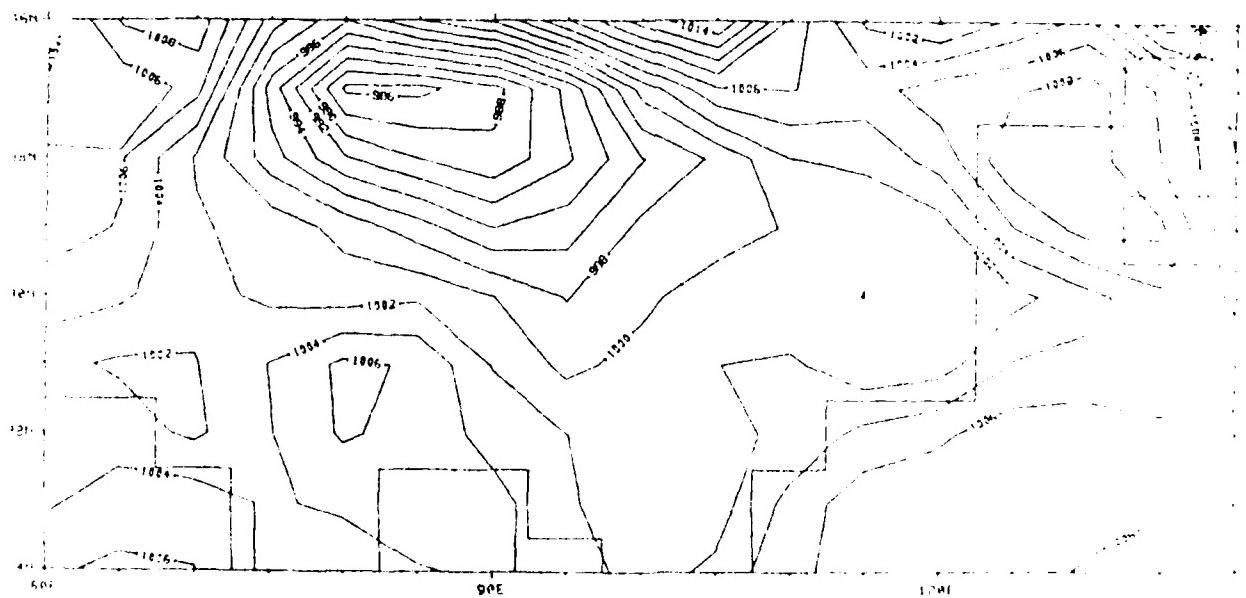
March 1

March 6

Fig. 3.21 Sea level pressure (mb) charts at 12Z calculated
in every five day intervals from March 1 to May 31
for NTPC.

137
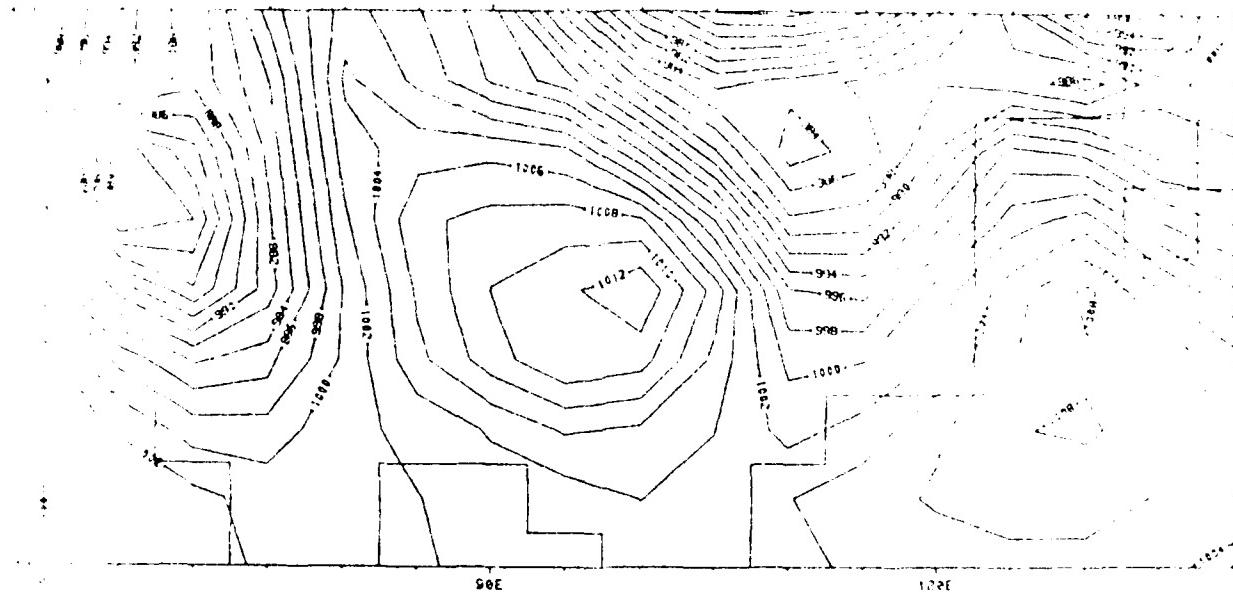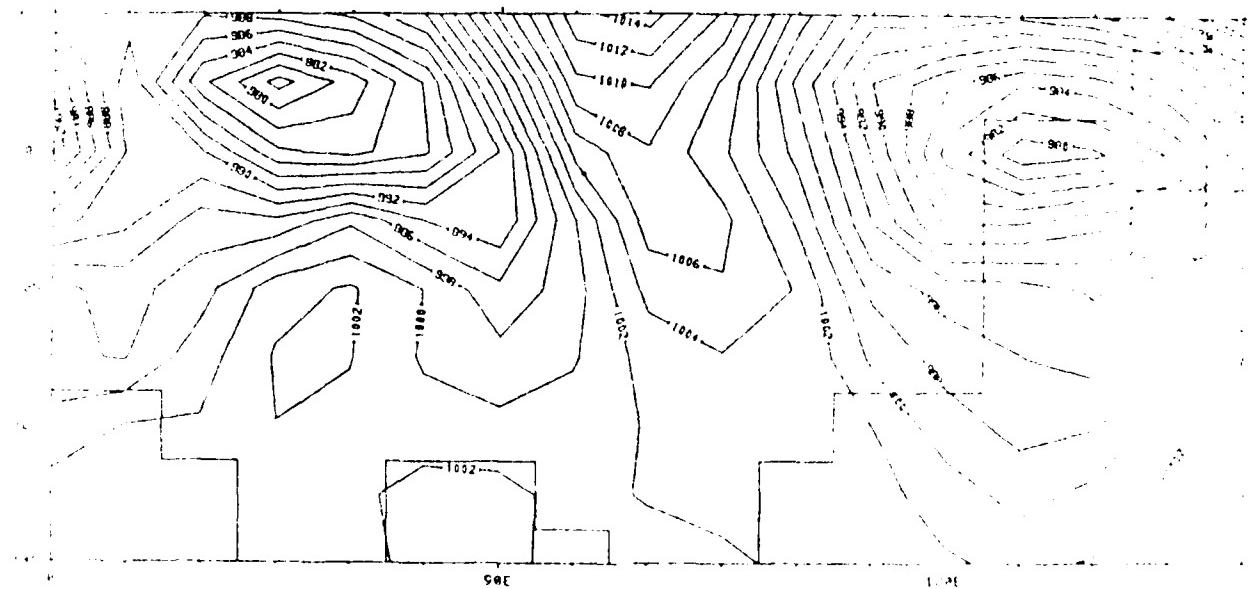
March 11

March 16

March 21
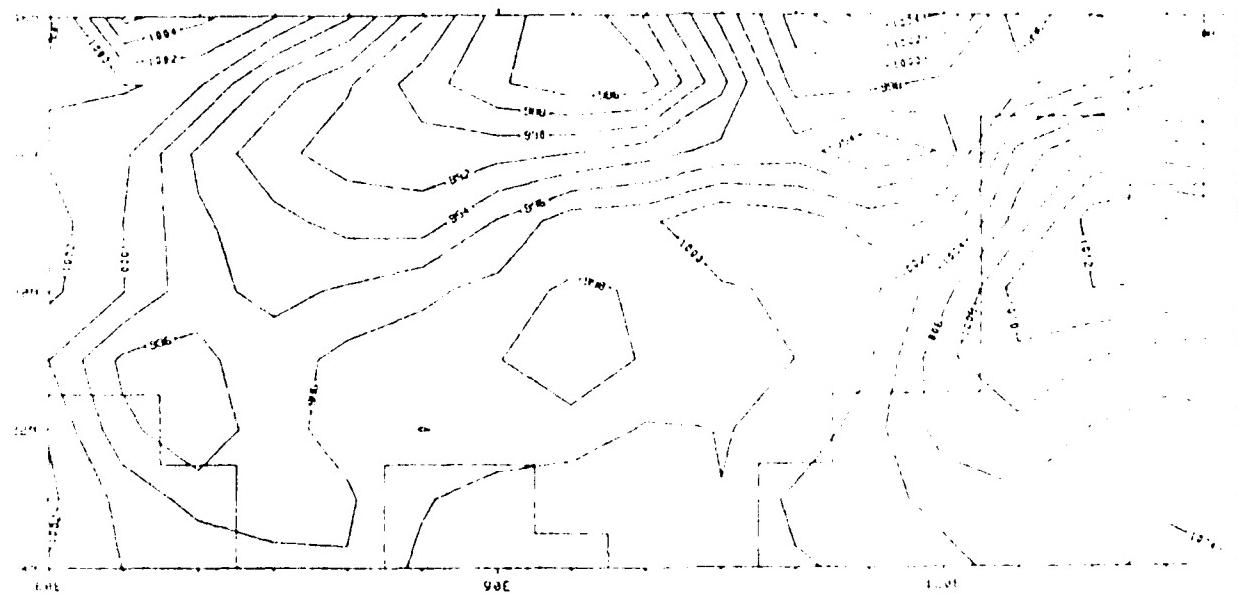
March 26
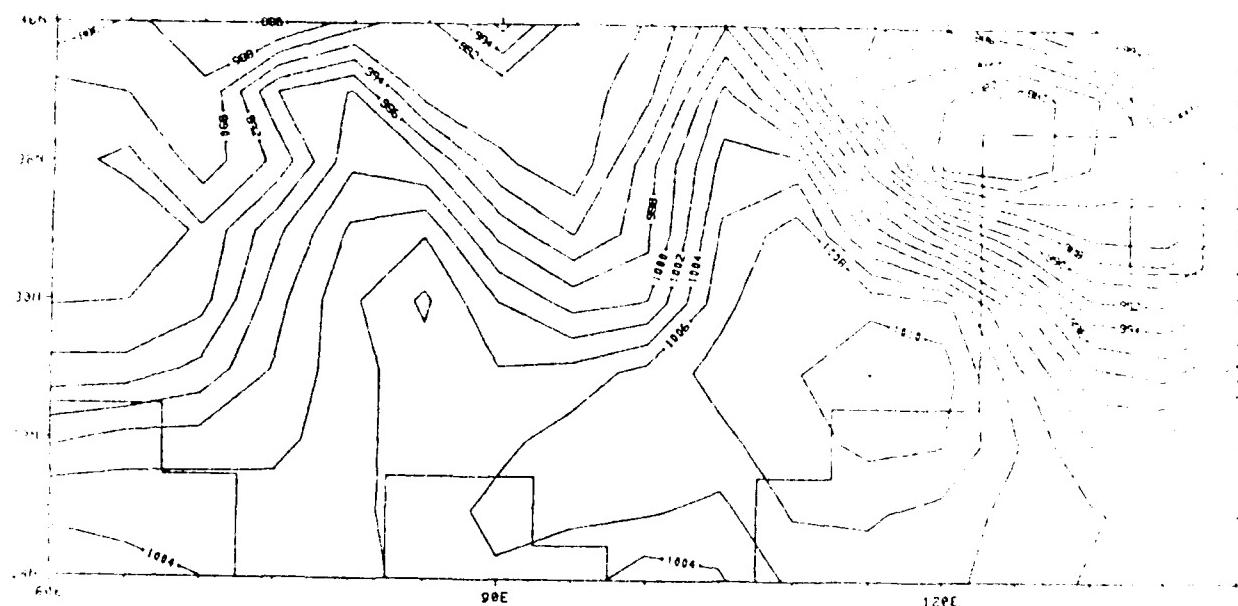
139

March 31

April 1

140

April 6

April 11

141

April 16

April 21

142

April 26

May 1

143

May 6

May 11

144

May 16

May 21

145

May 26

May 31

146
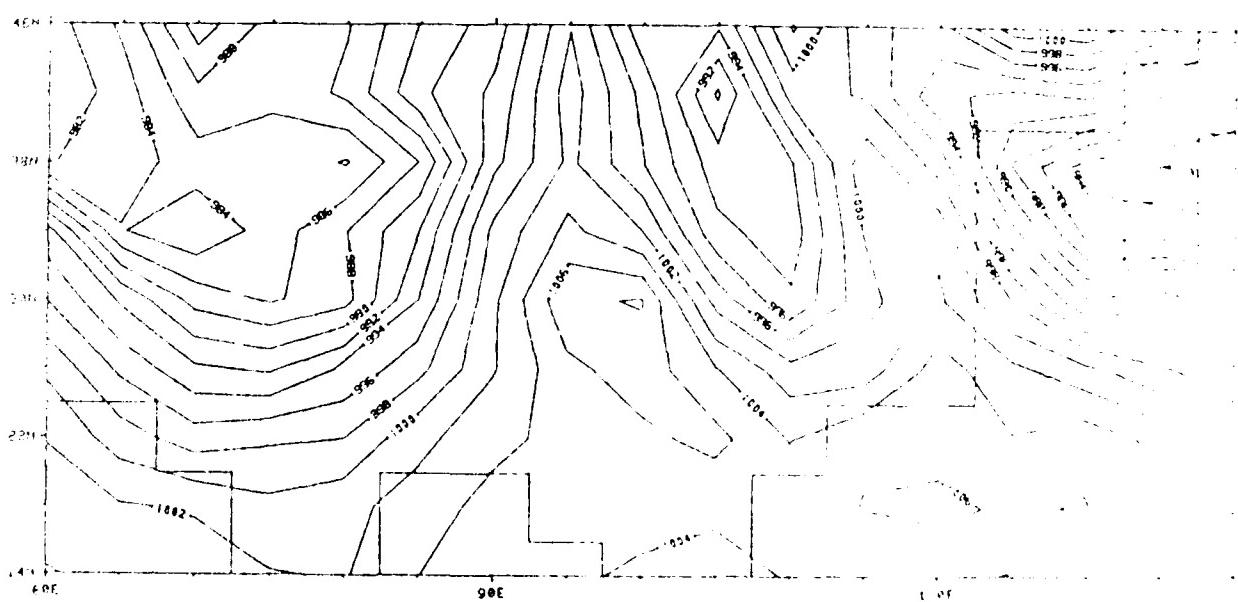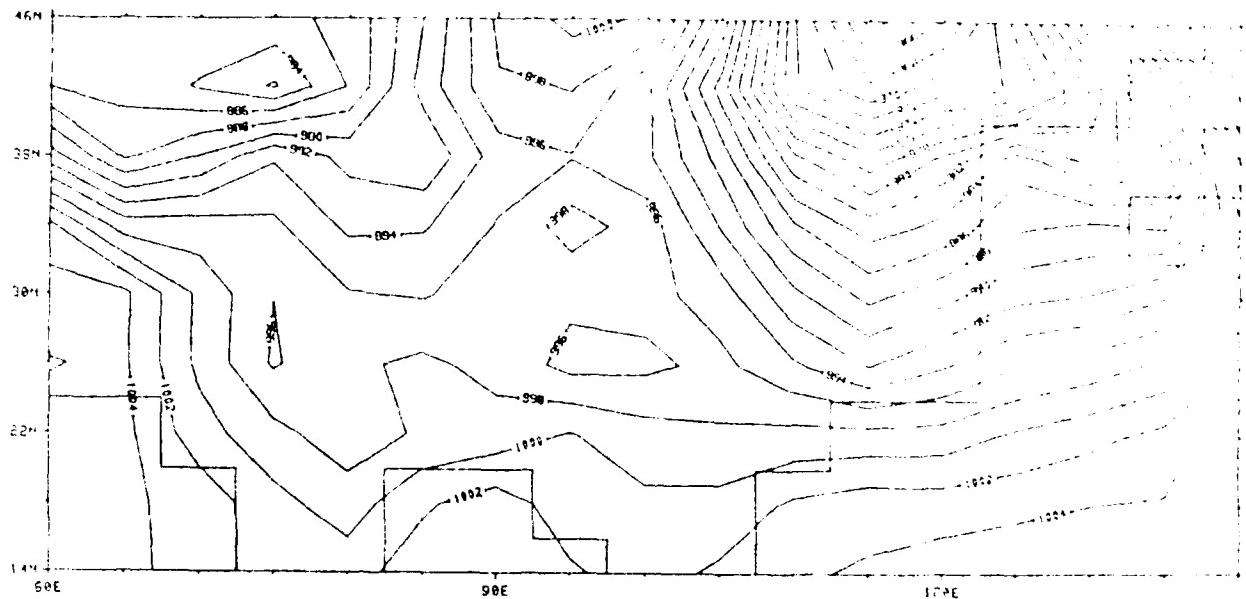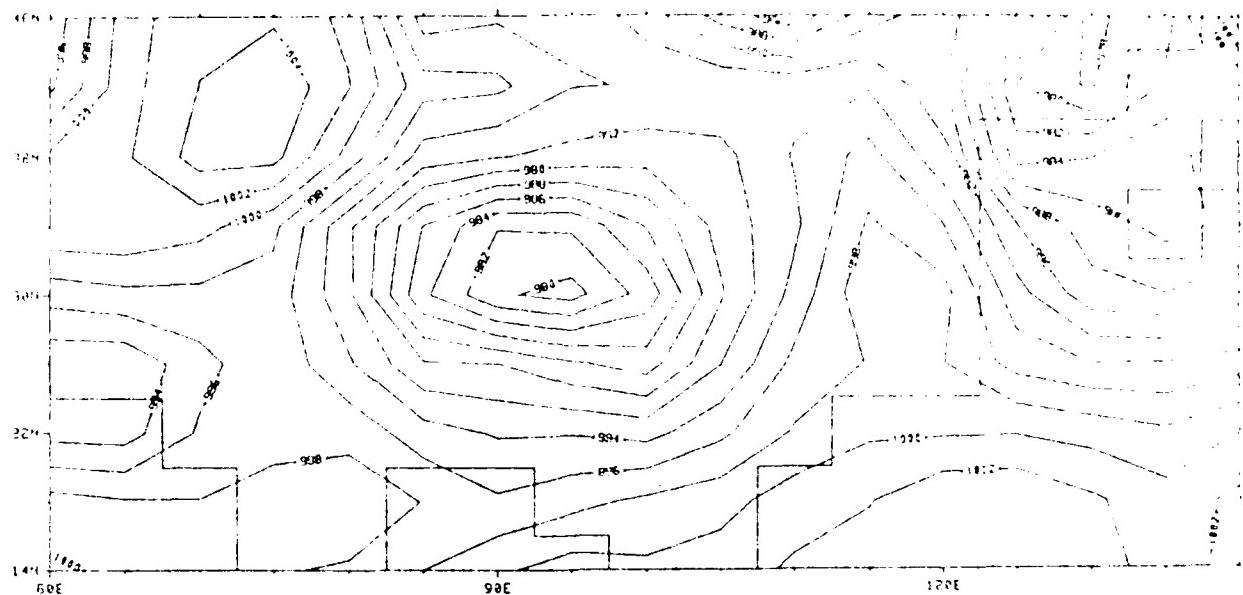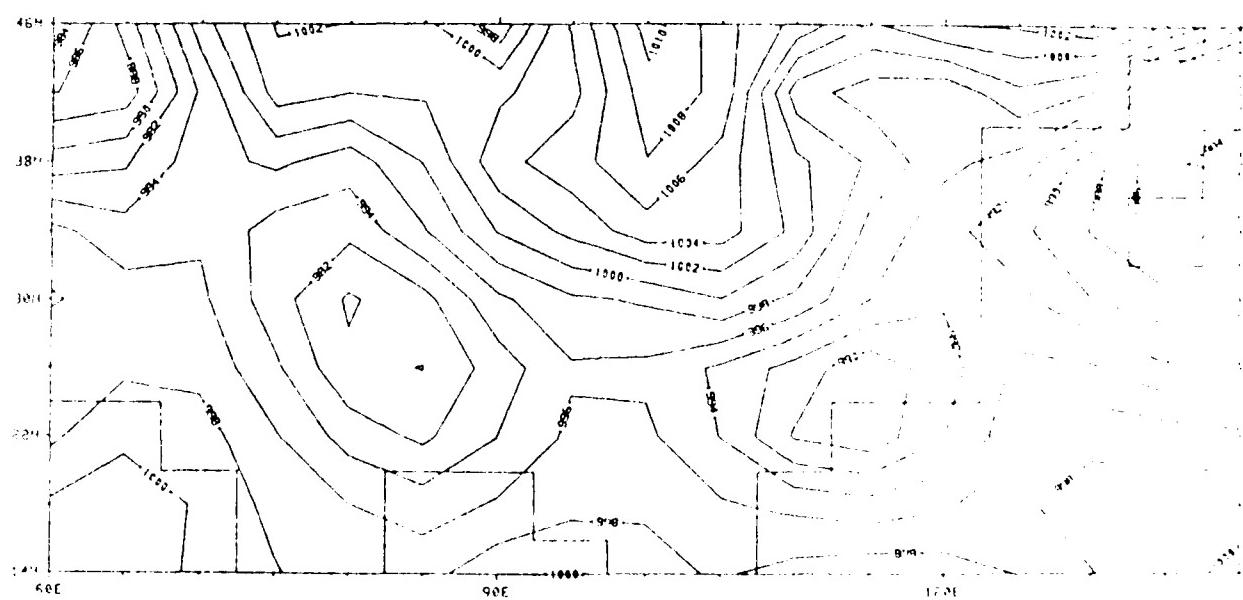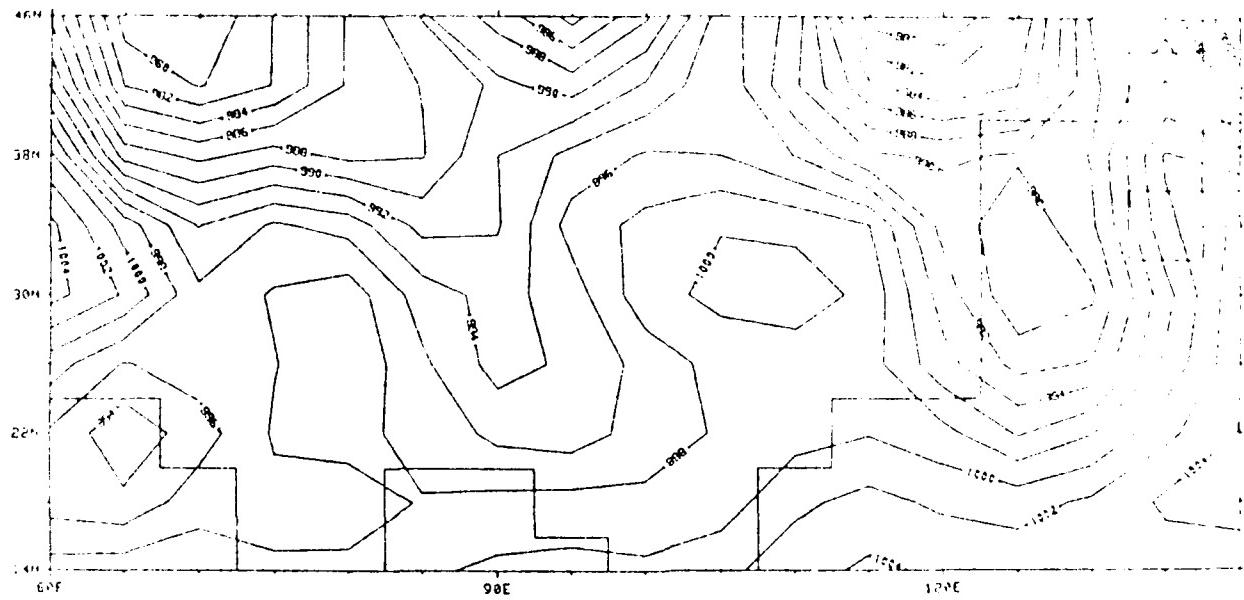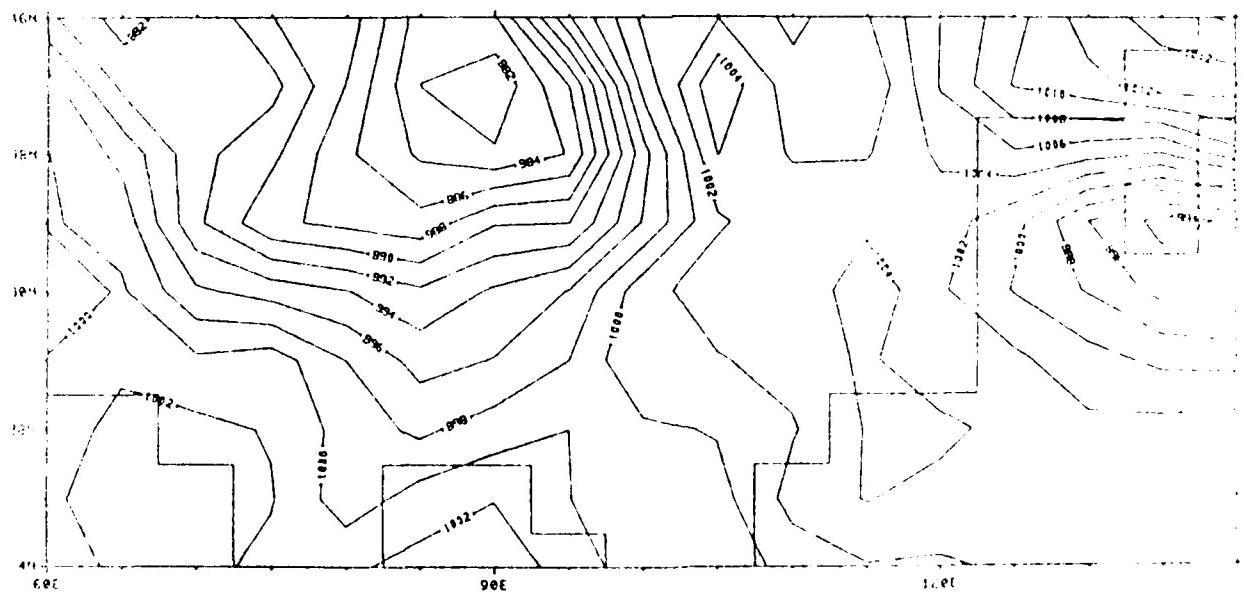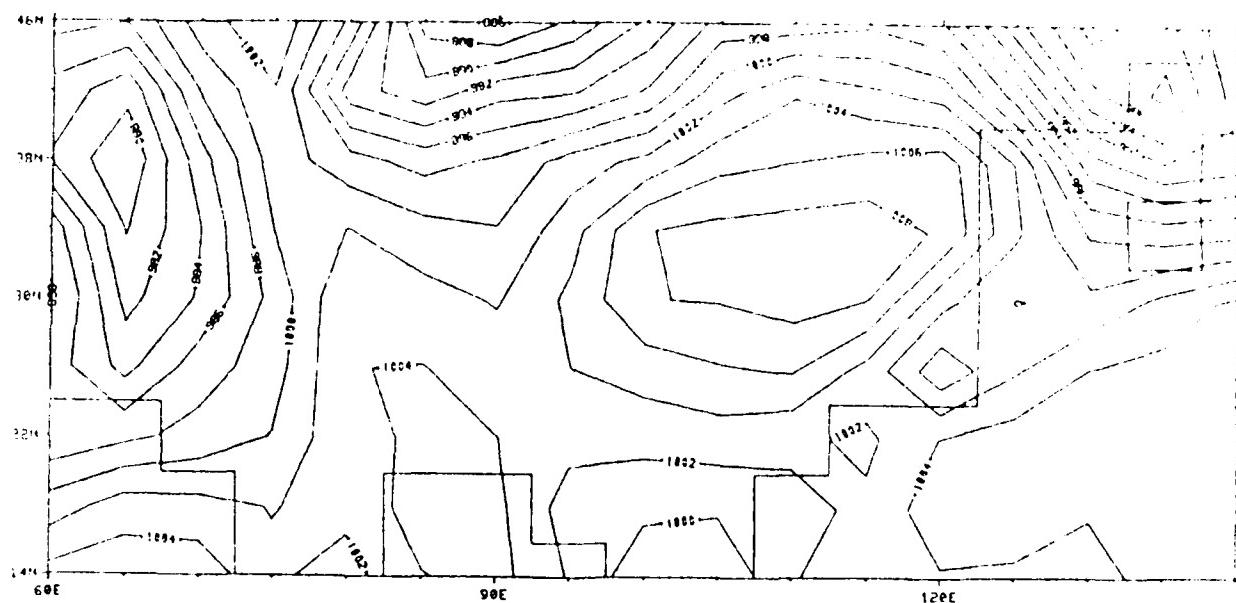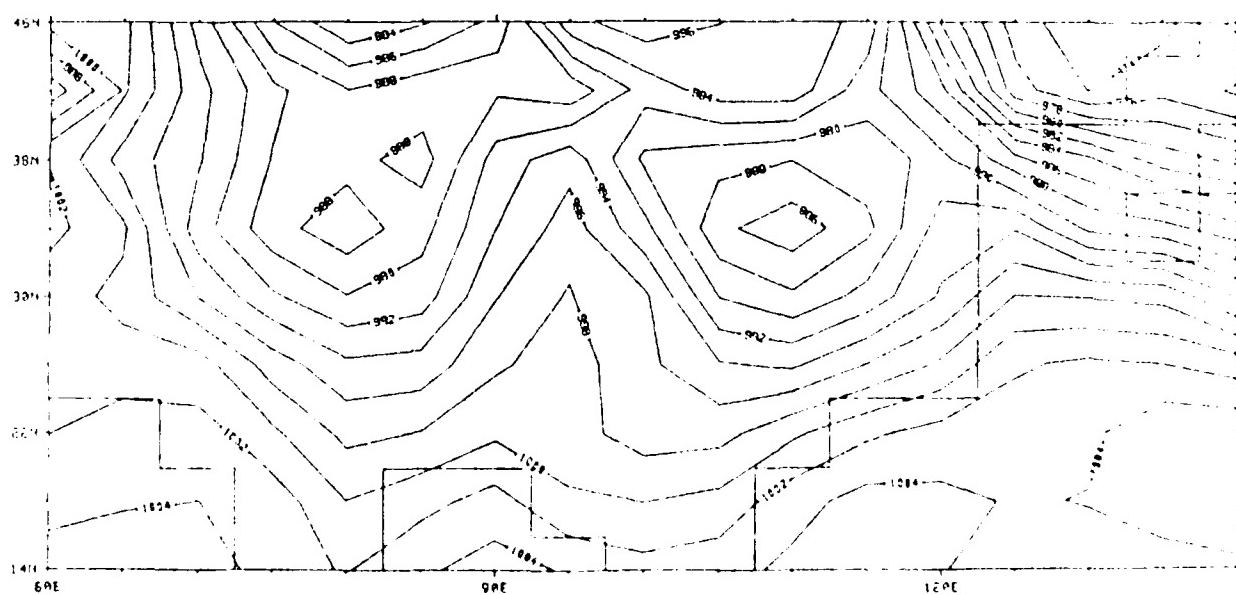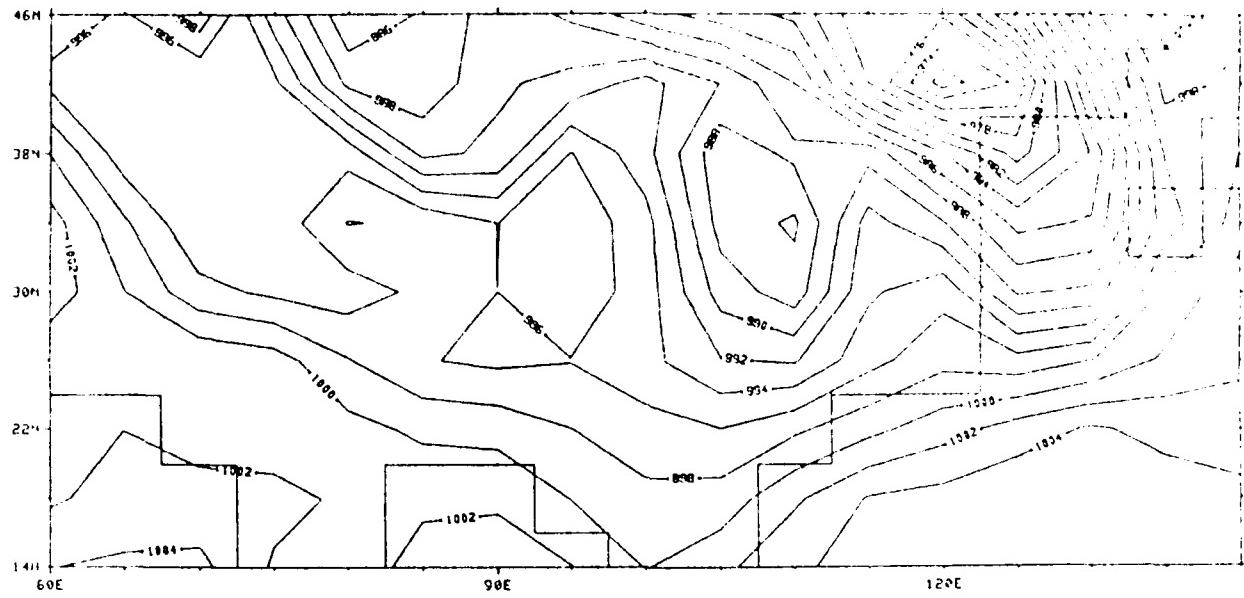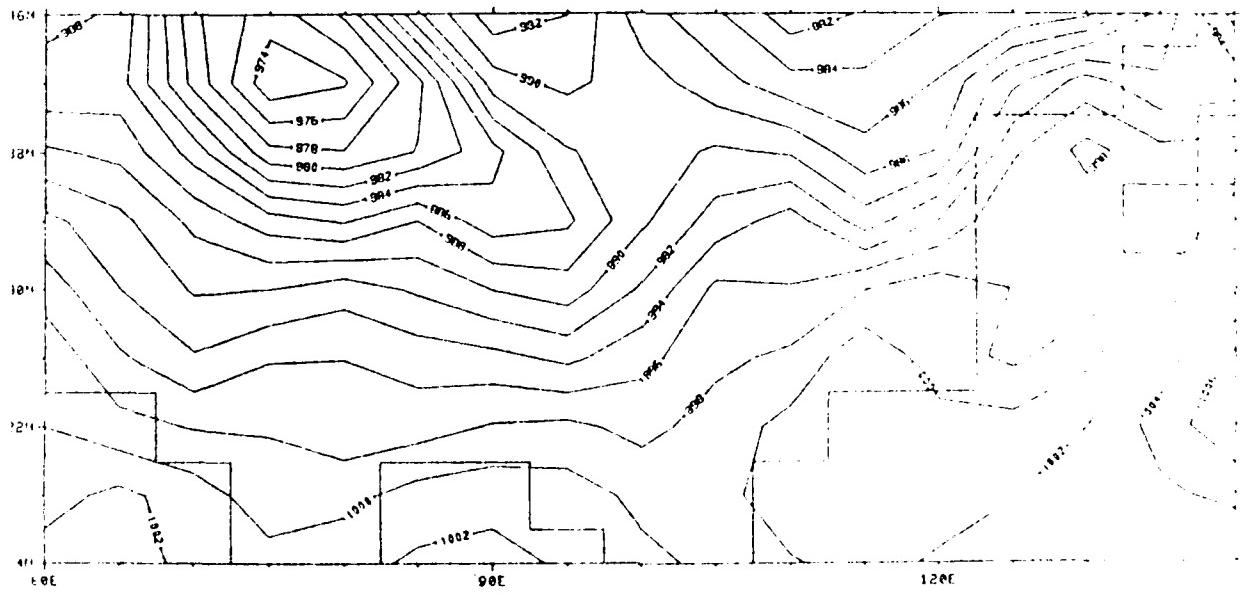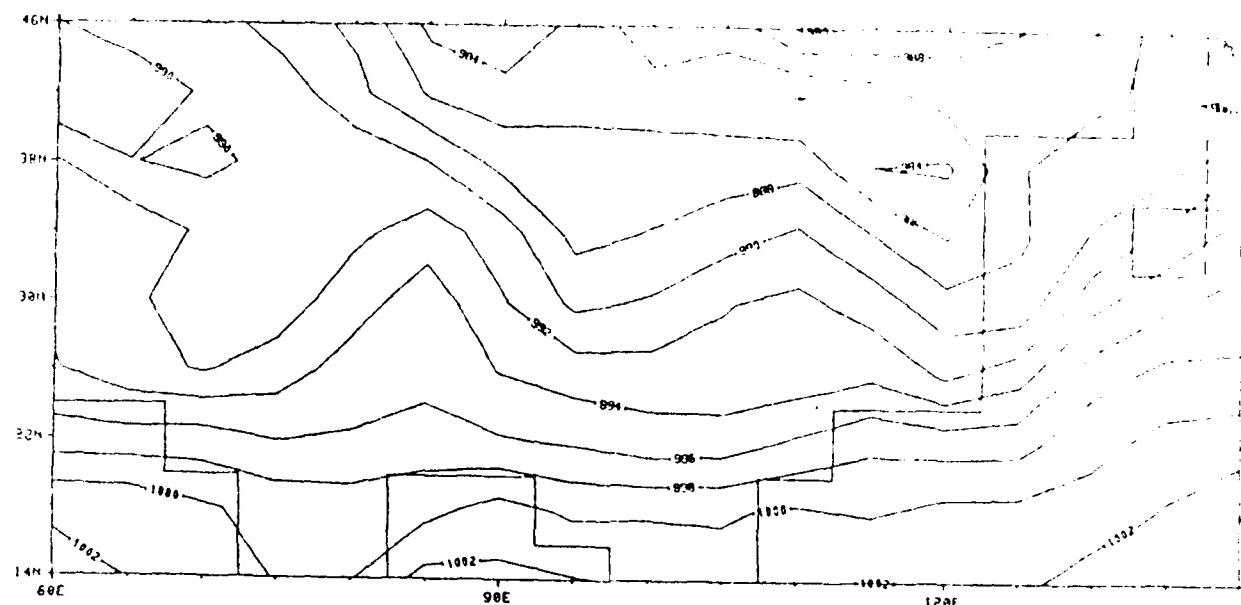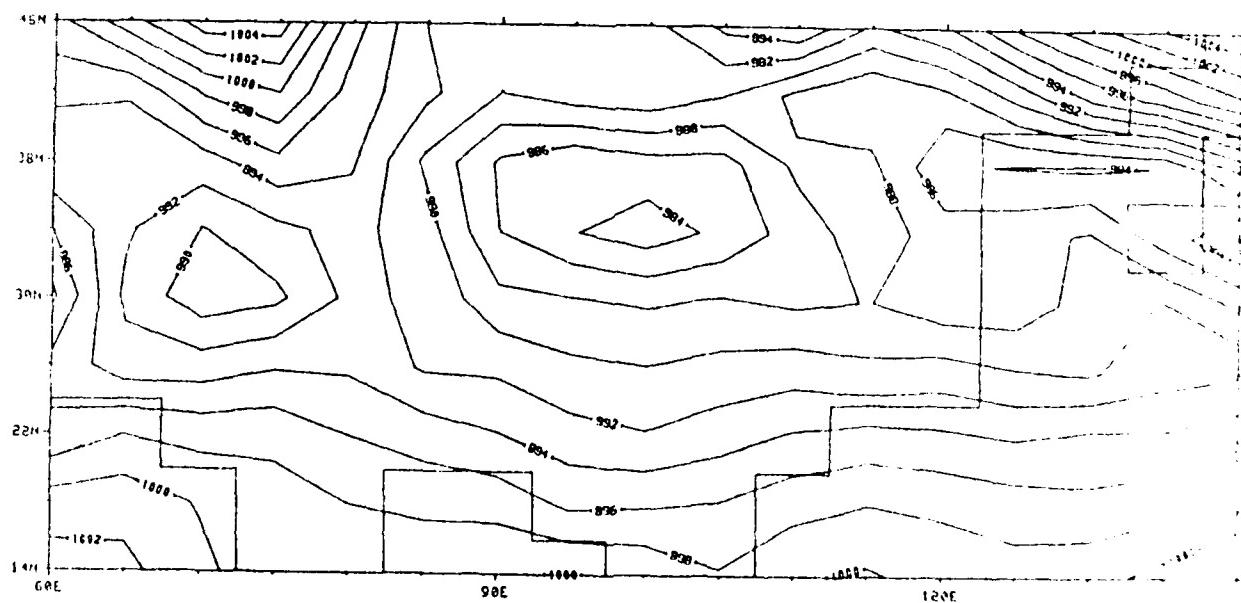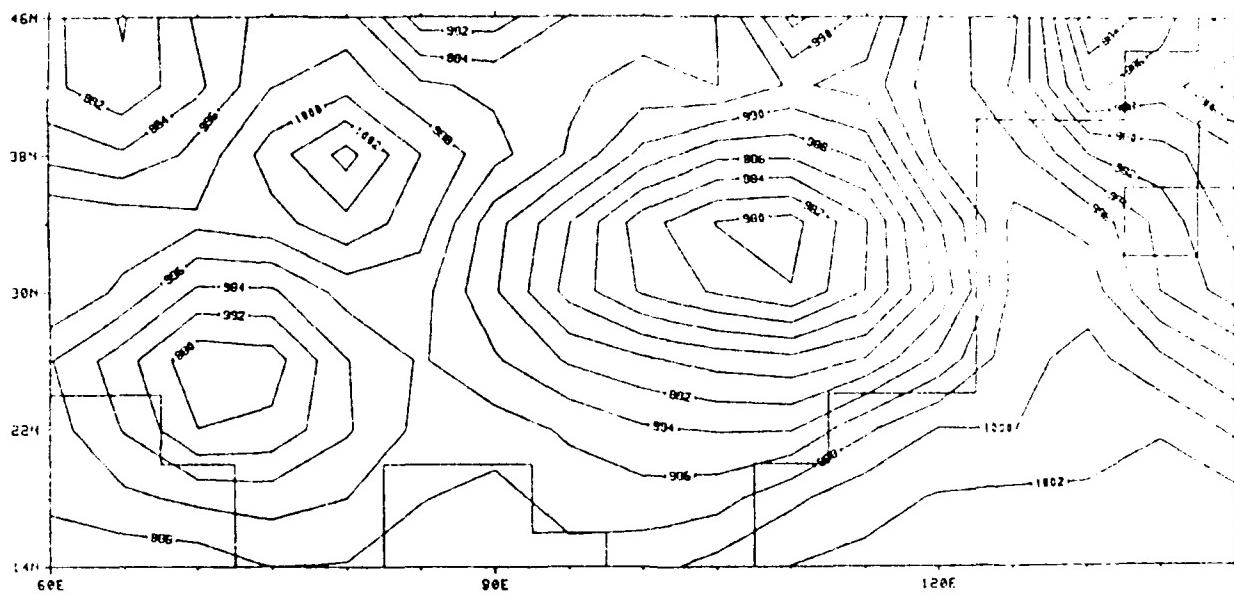
(a)
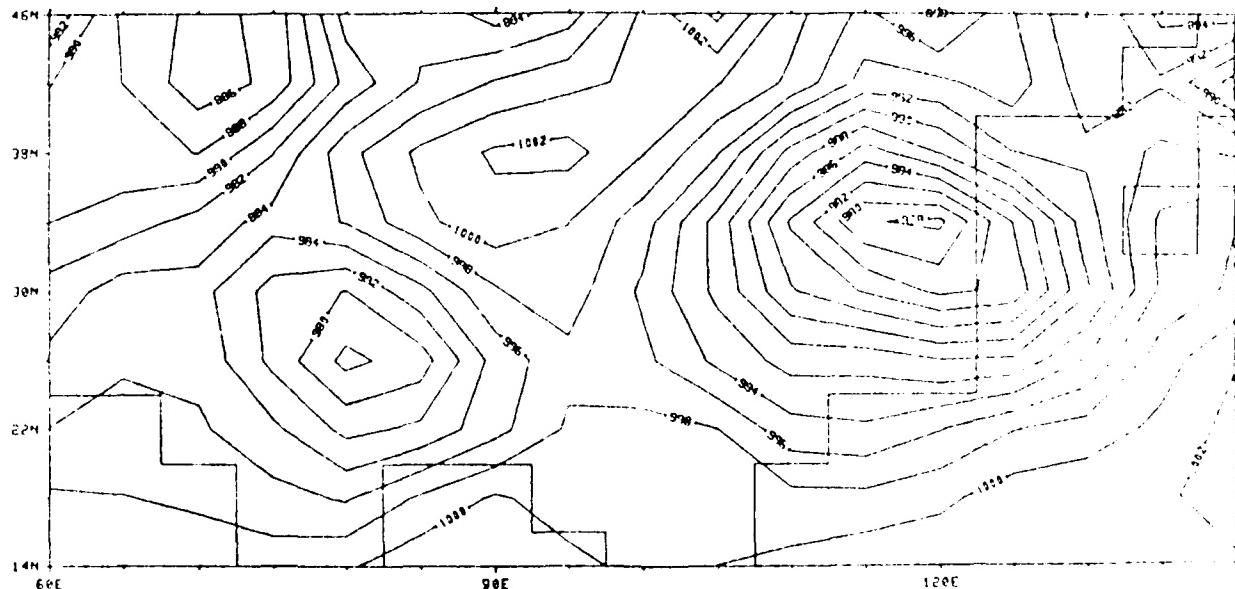
(b)

Fig. 3.22 The sea level pressure (mb) charts for the same
times as in Fig. 3.2 but No Tibetan Plateau (NTPC).

147

(c)

(d)

148
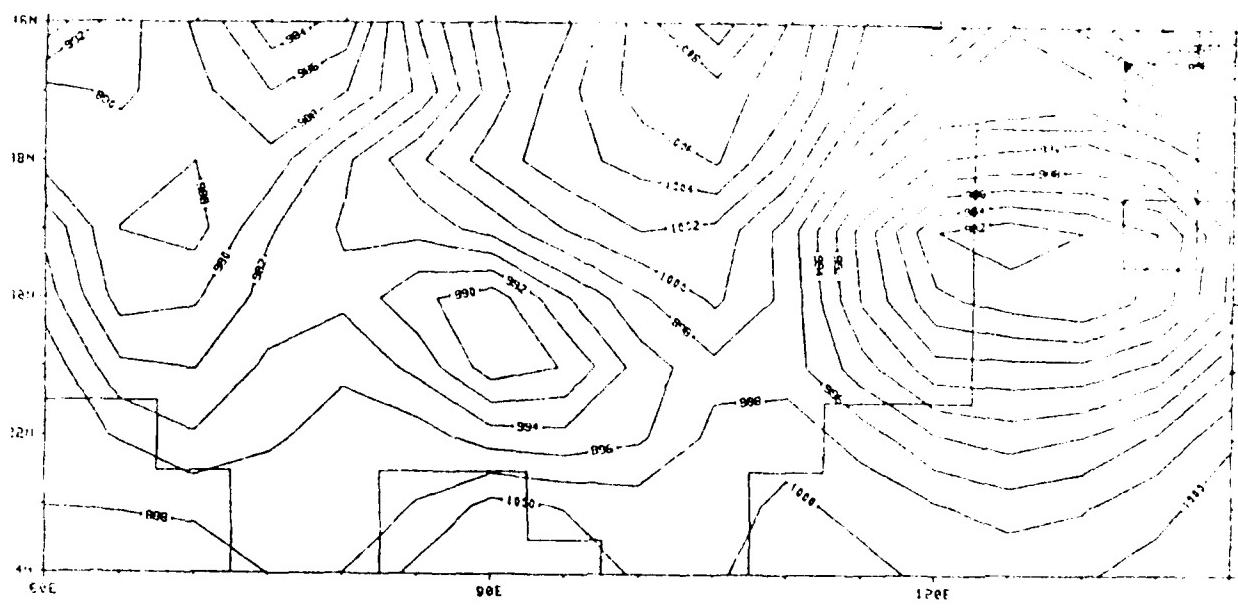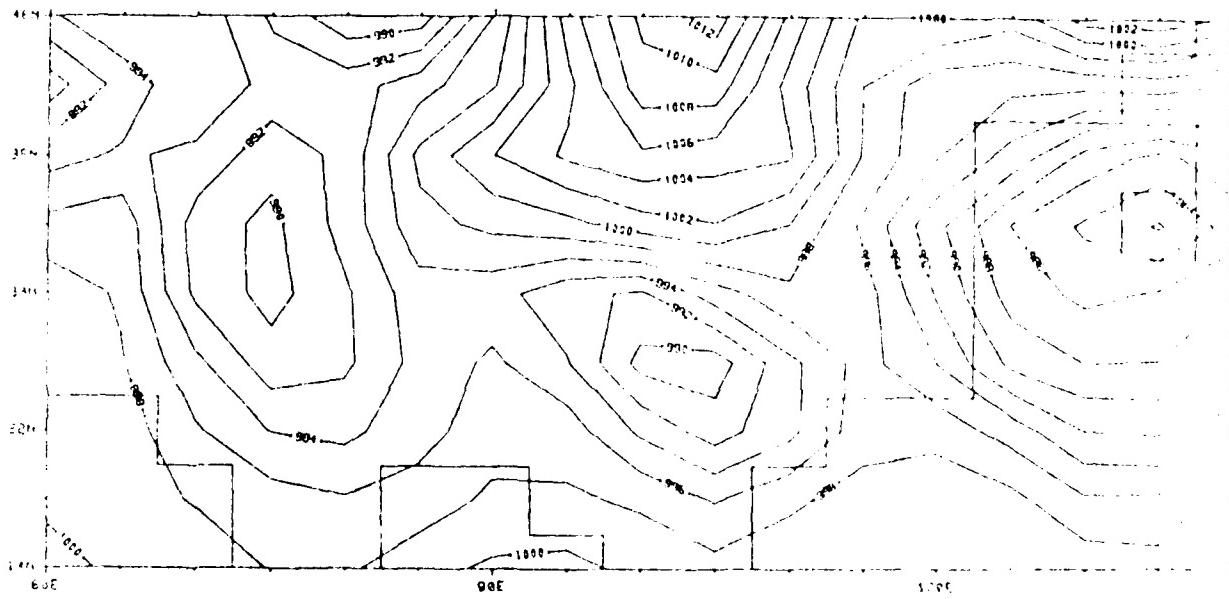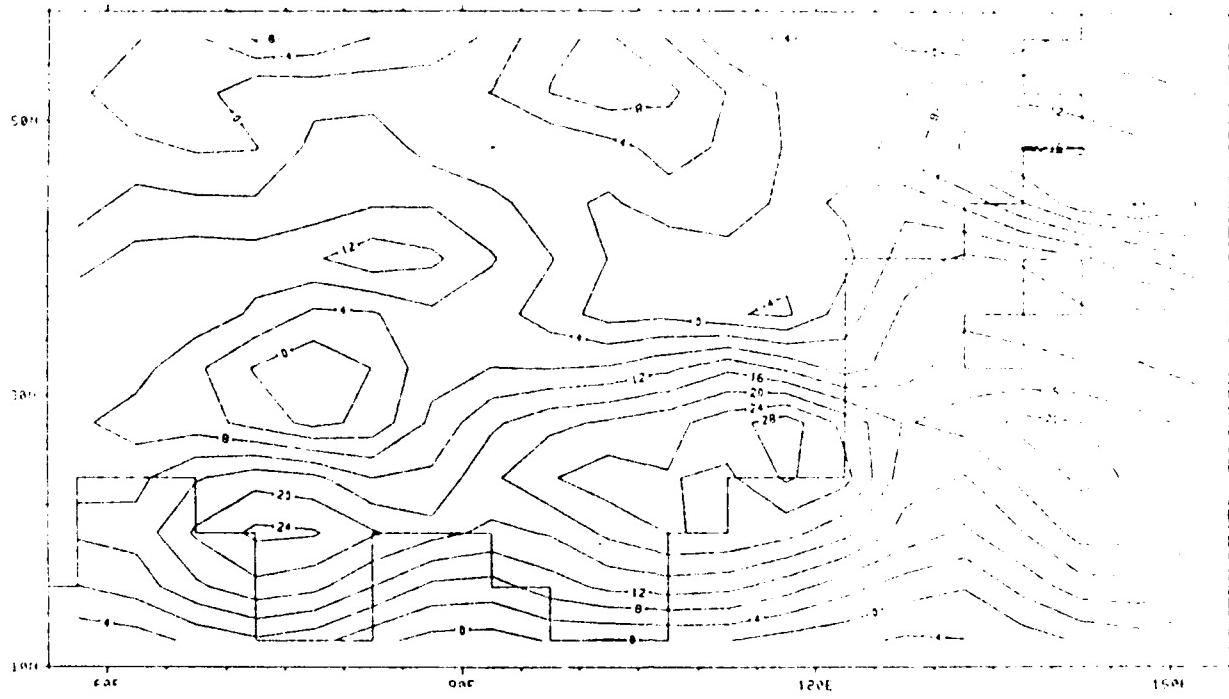
(a)
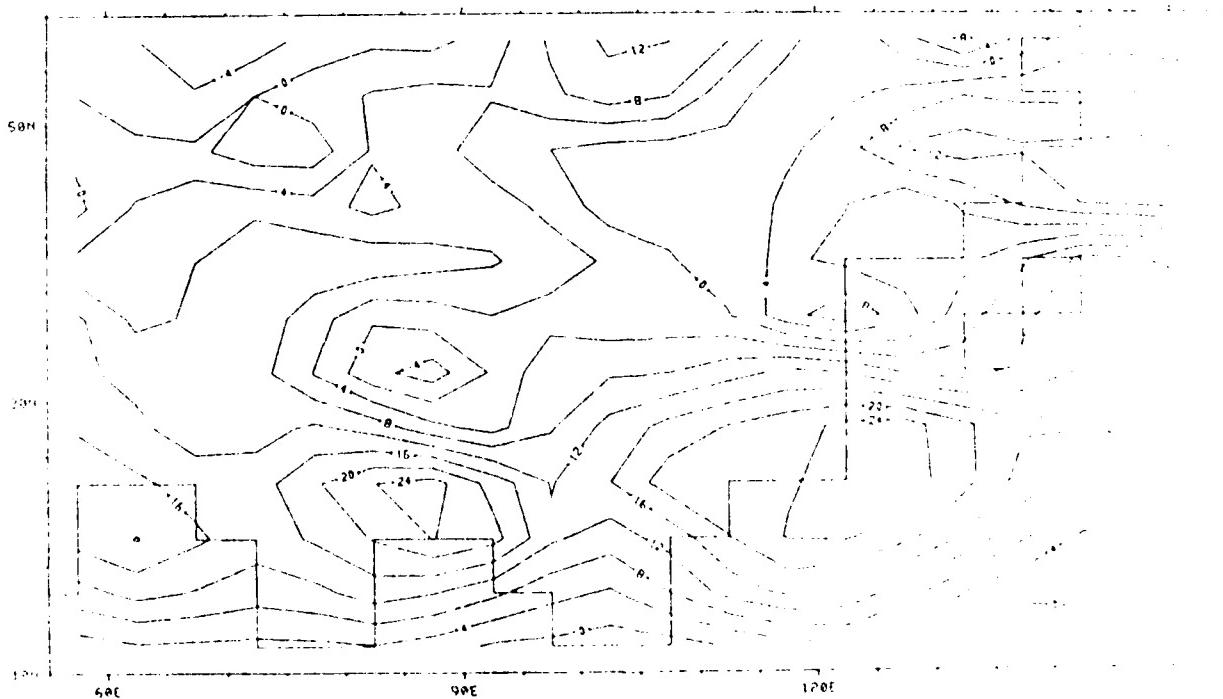
(b)

Fig. 3.23   The zonal wind (m sec^{-1}) component at level
3 for the times and condition as in fig. 3.22.

(c)

(d)

150
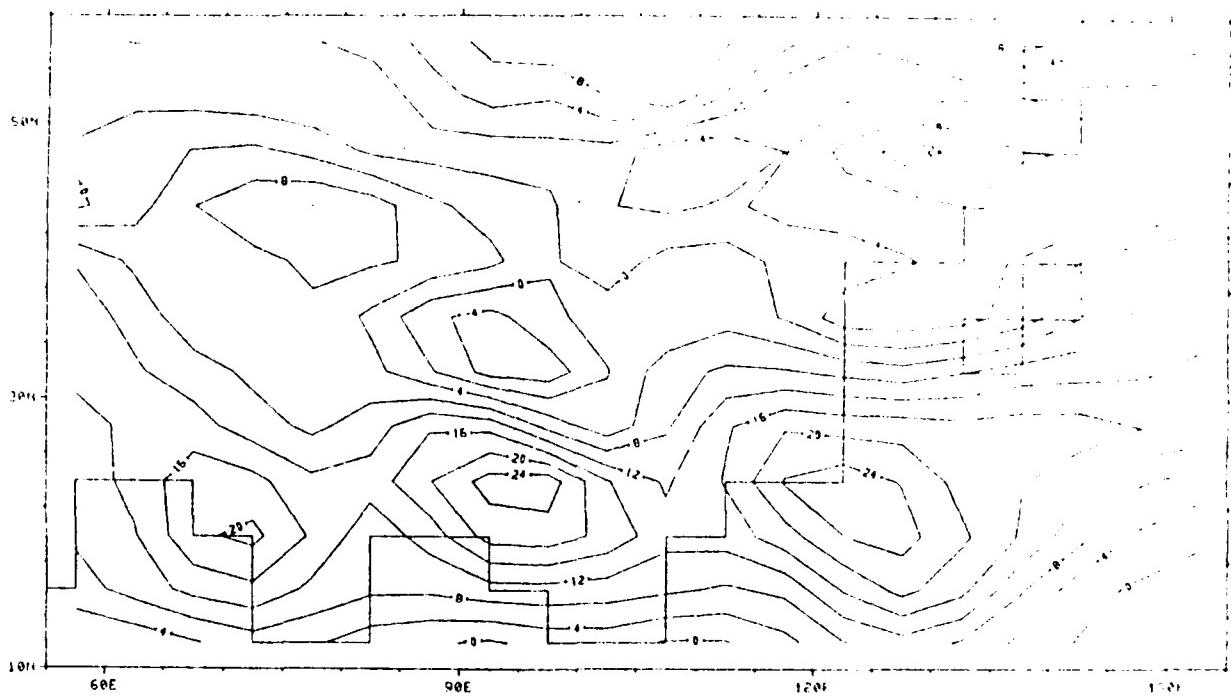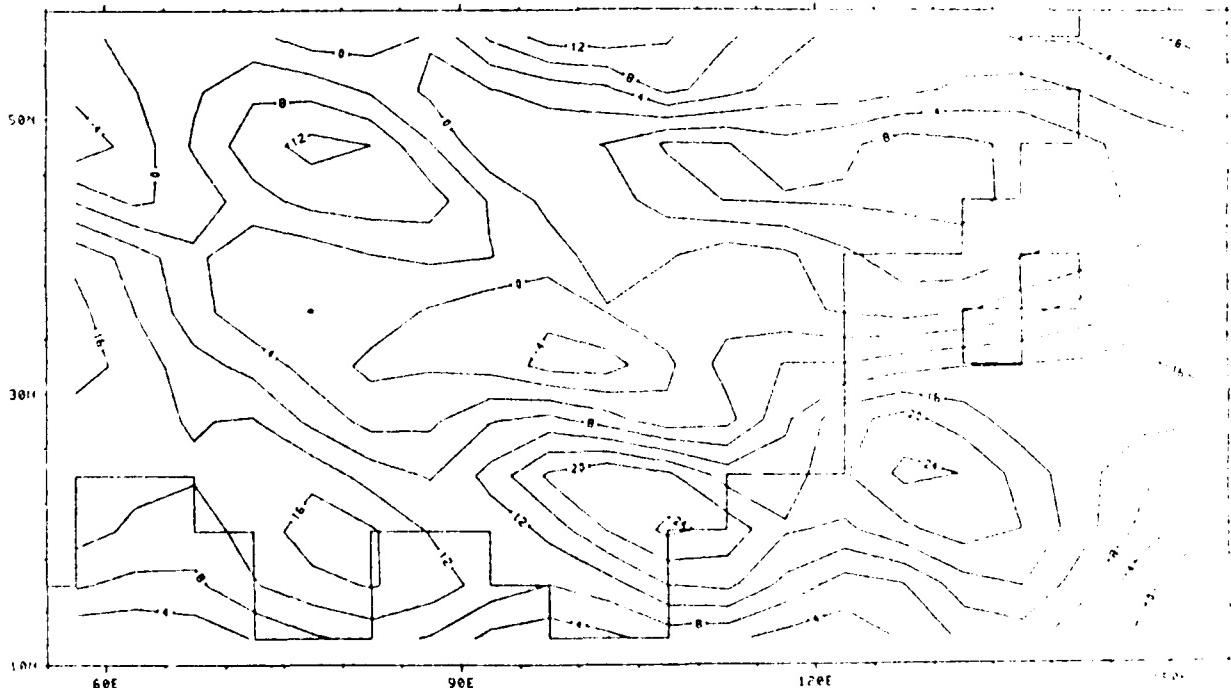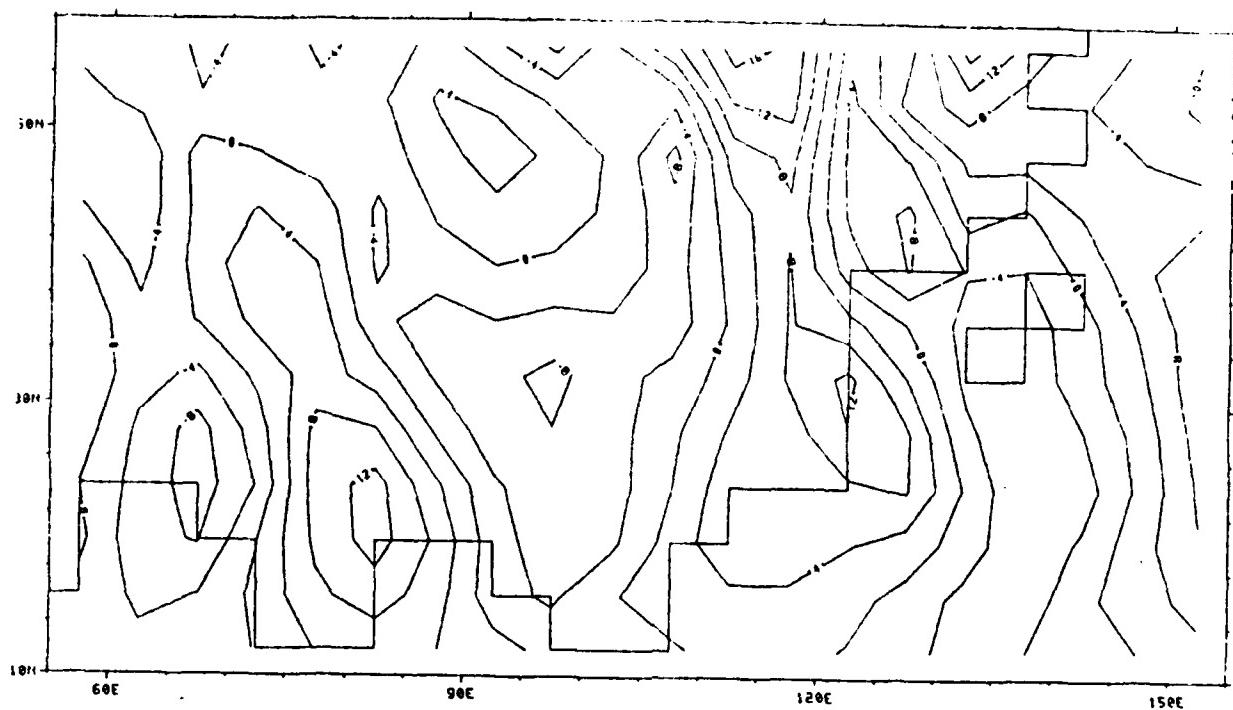
(a)
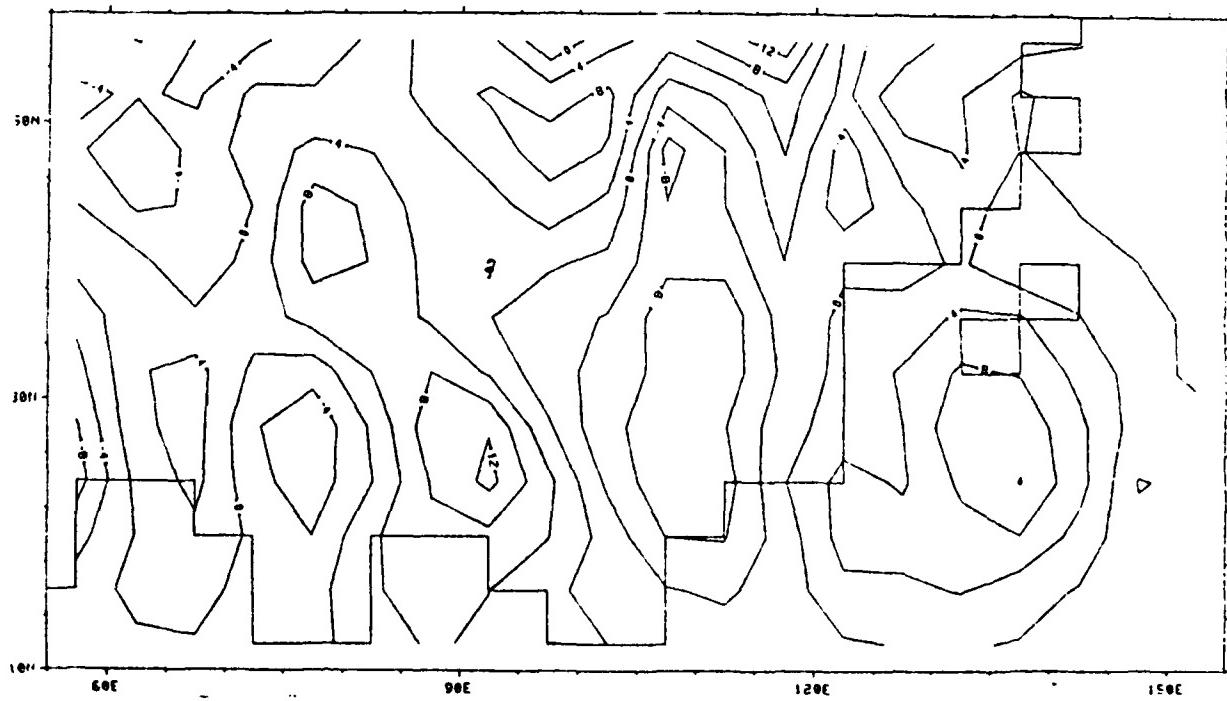
(b)

Fig. 3.24 The meridional wind (m sec^{-1}) component at level 3
for the same times and condition as in Fig. 3.22.

151
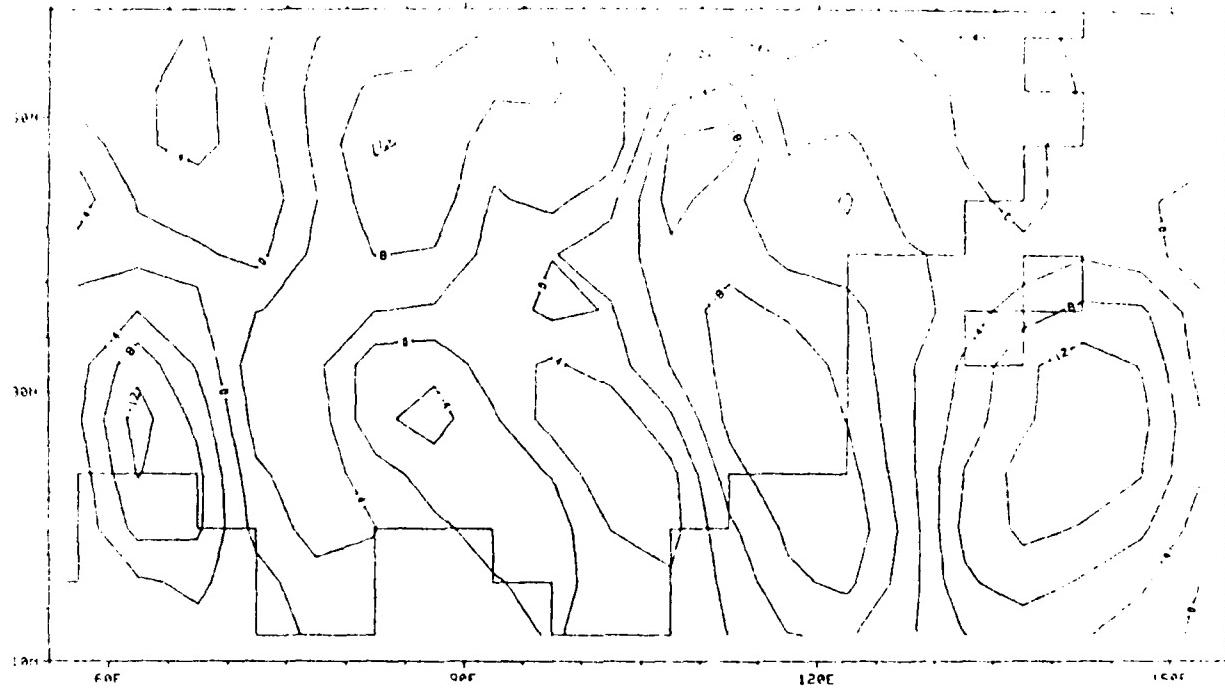
(c)
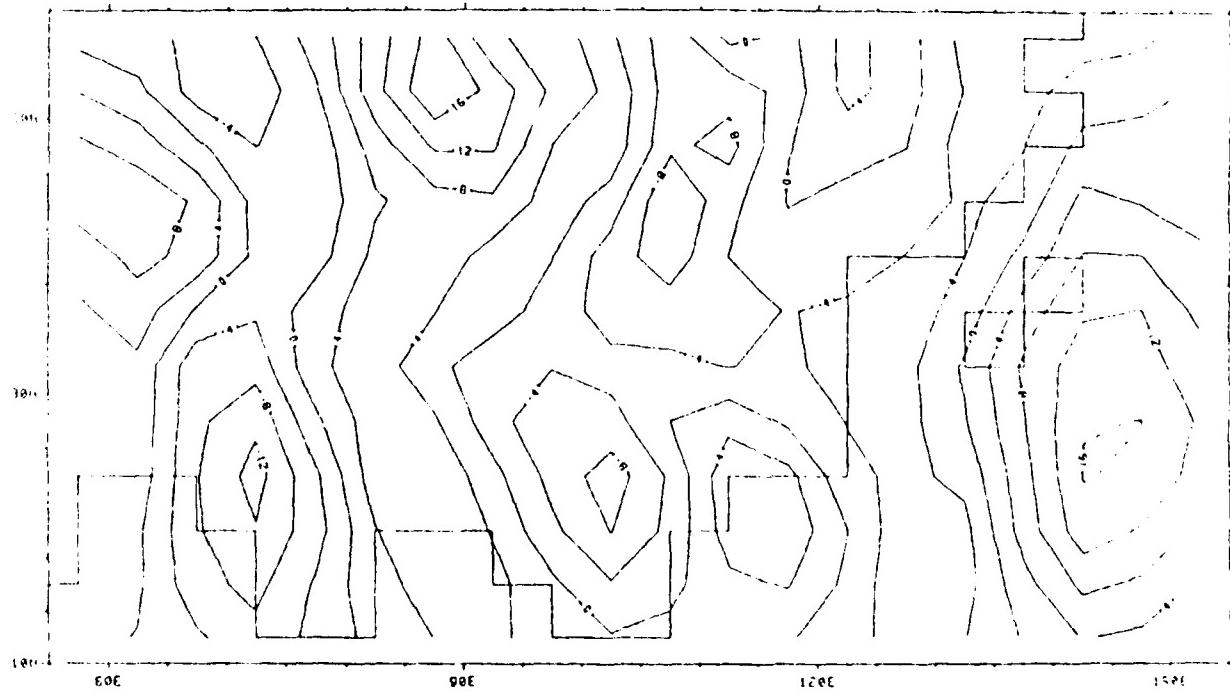
(d)
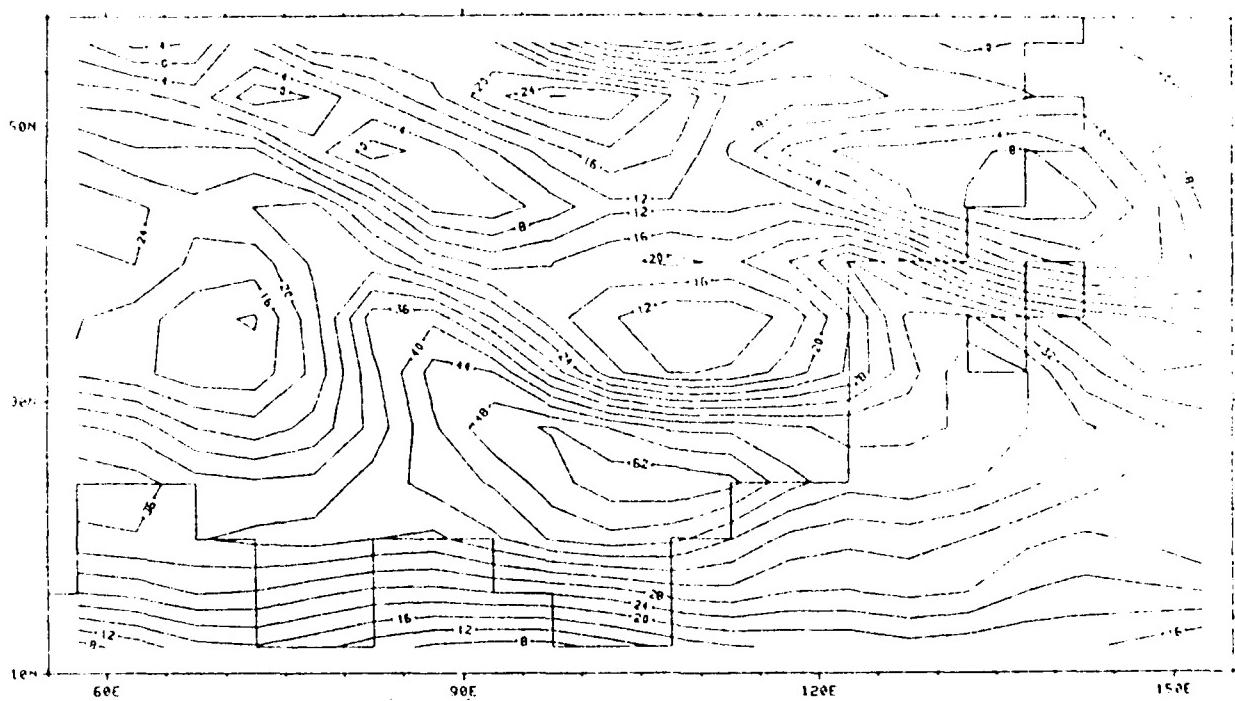
(a)
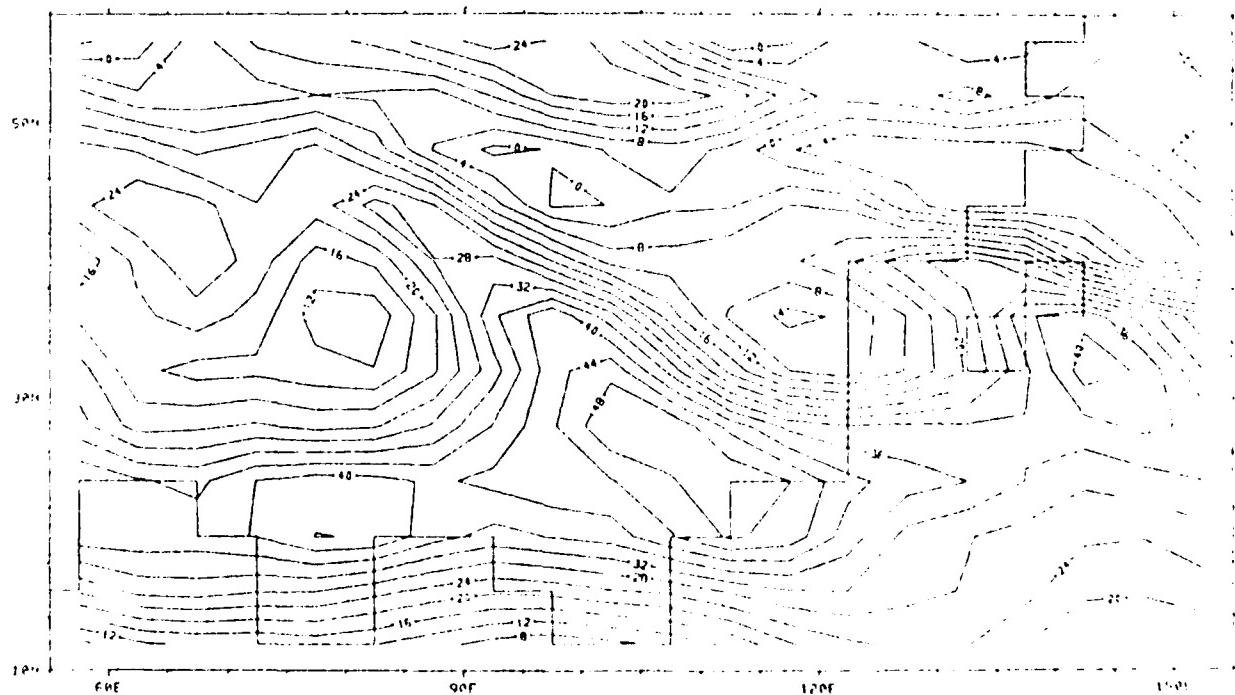
(b)

Fig. 3.25 The zonal wind (m sec^{-1}) component at level 1 for
the same times and condition as in Fig. 3.22.

(c)

(d)

154
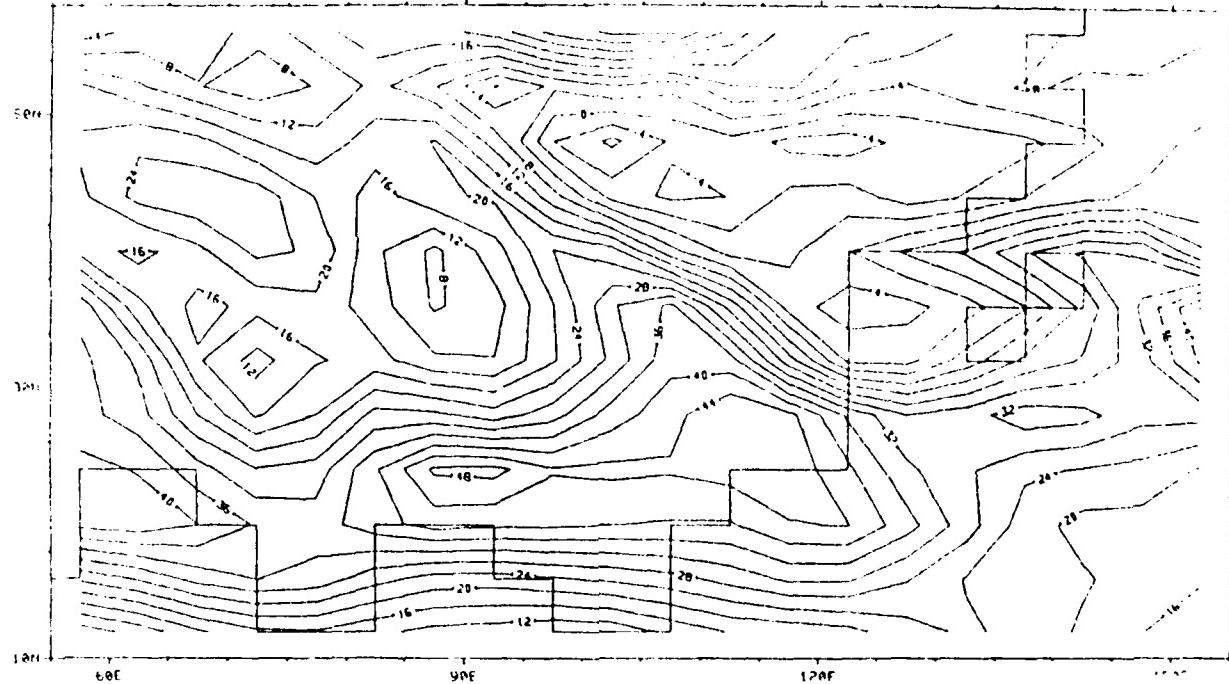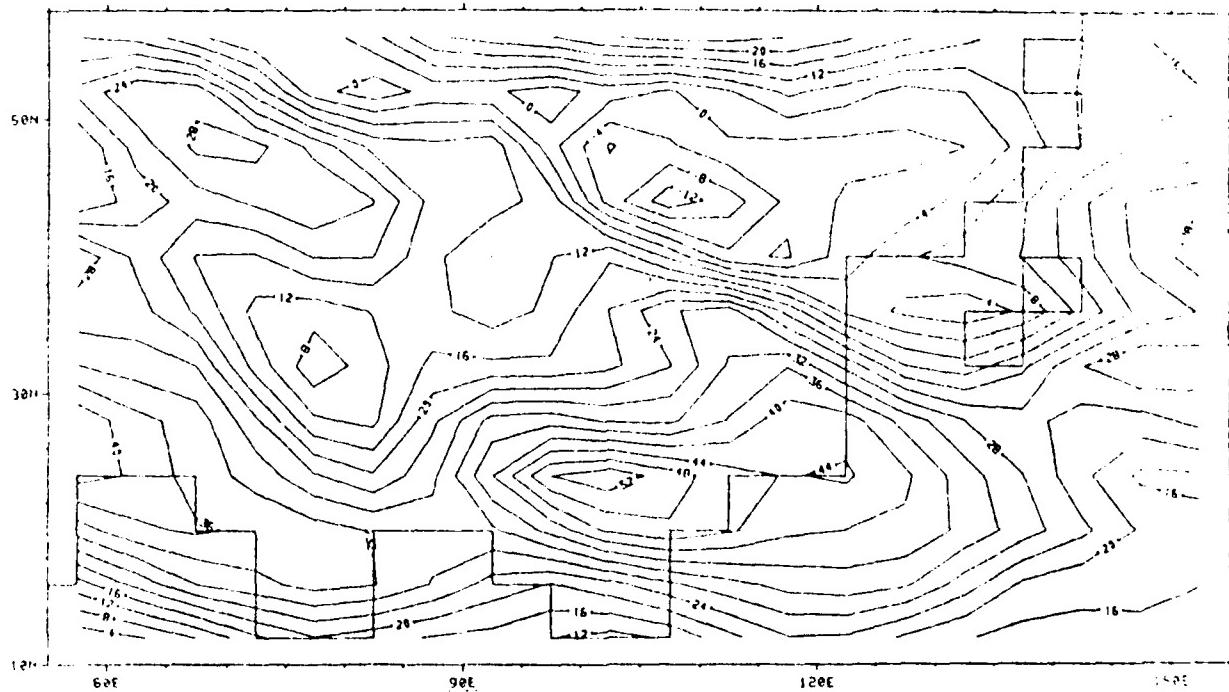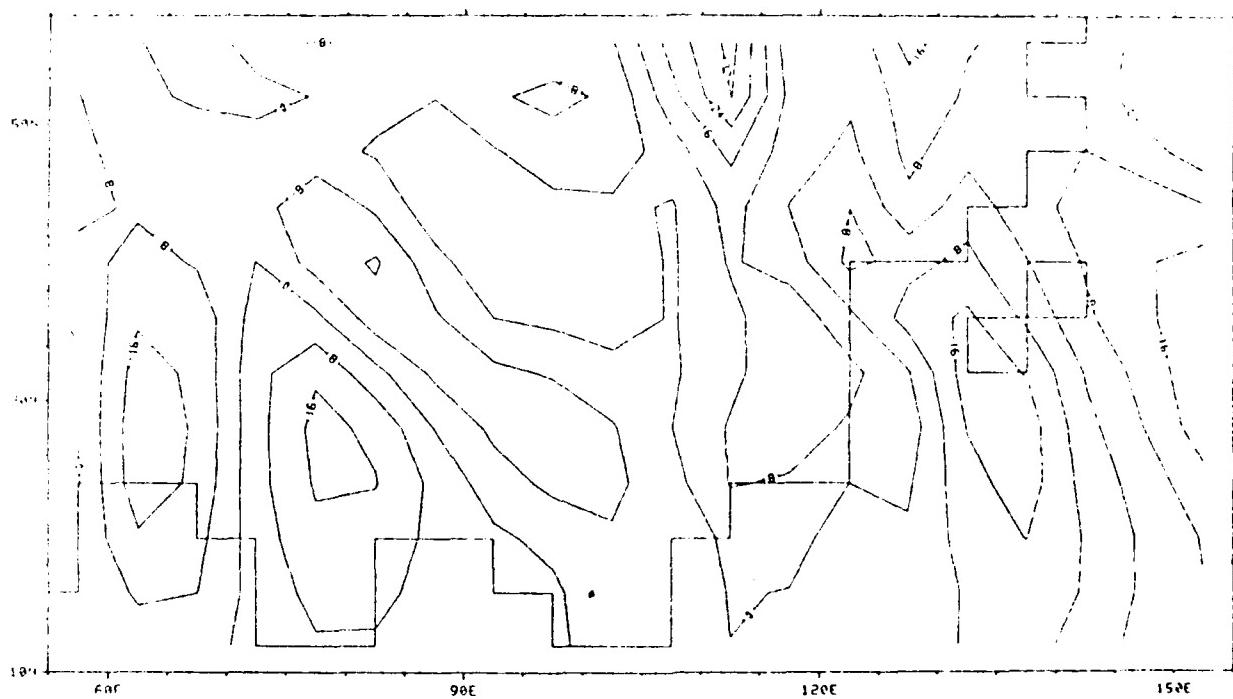
(a)
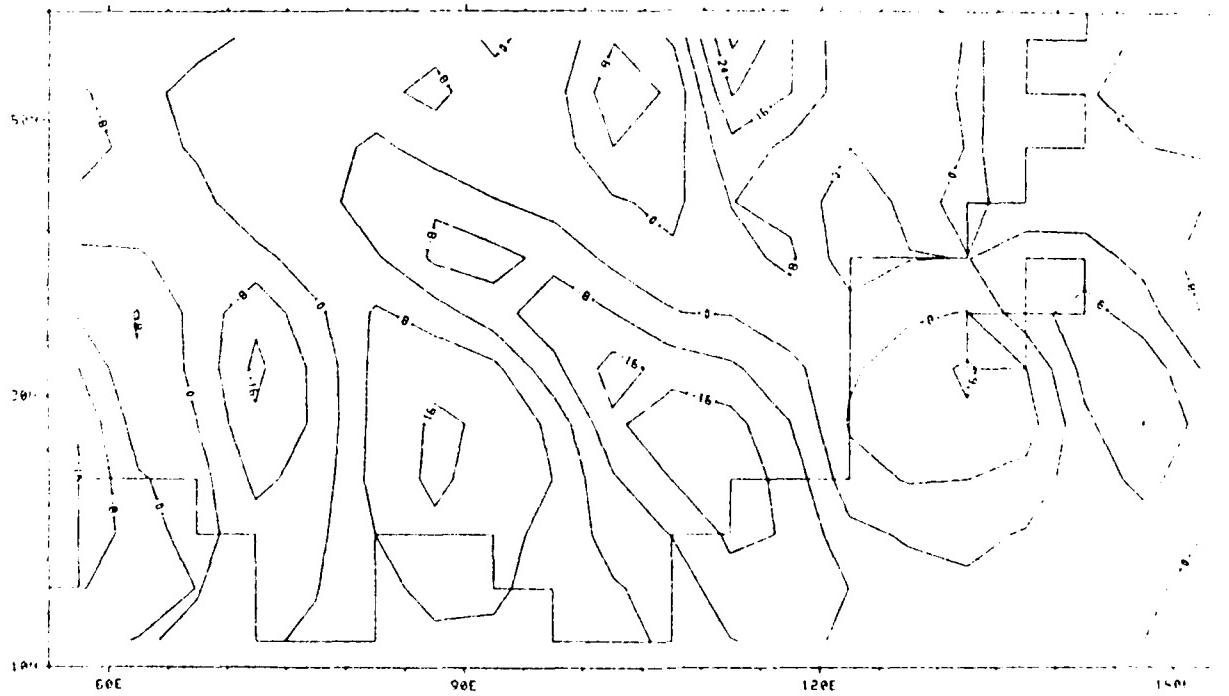
(b)

Fig. 3.26 The meridional wind (m sec^{-1}) components at level
1 for the same times and condition as in Fig. 3.22.

155
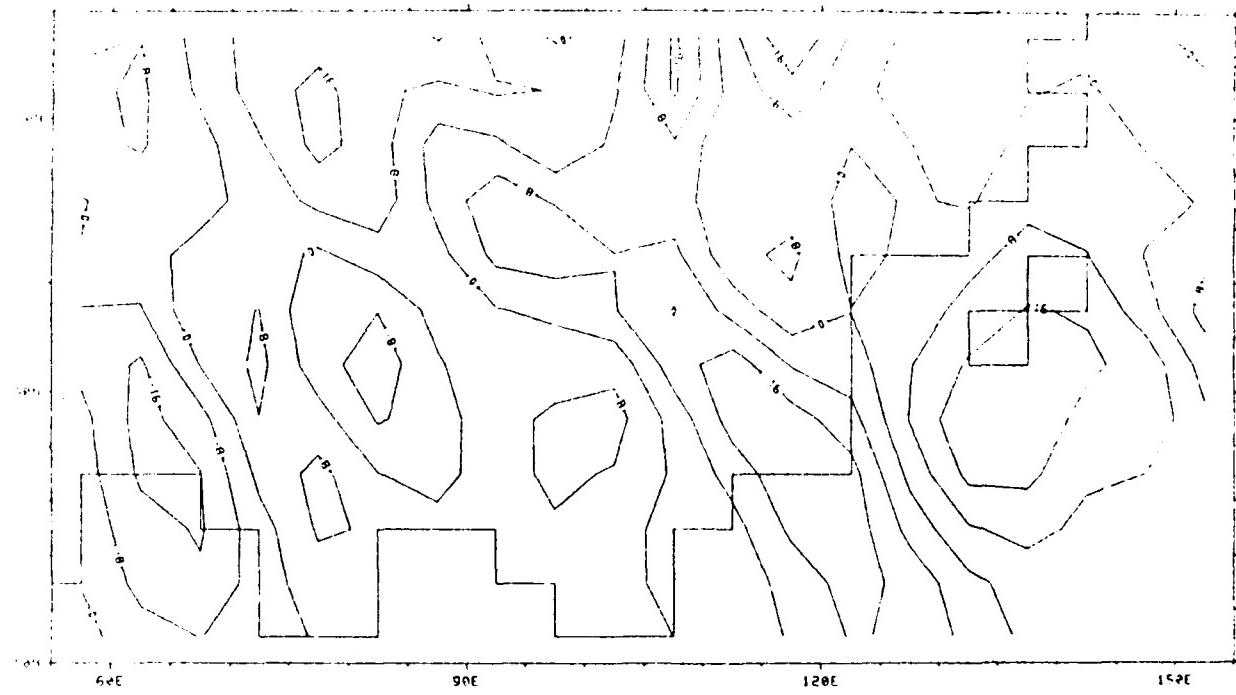
(c)
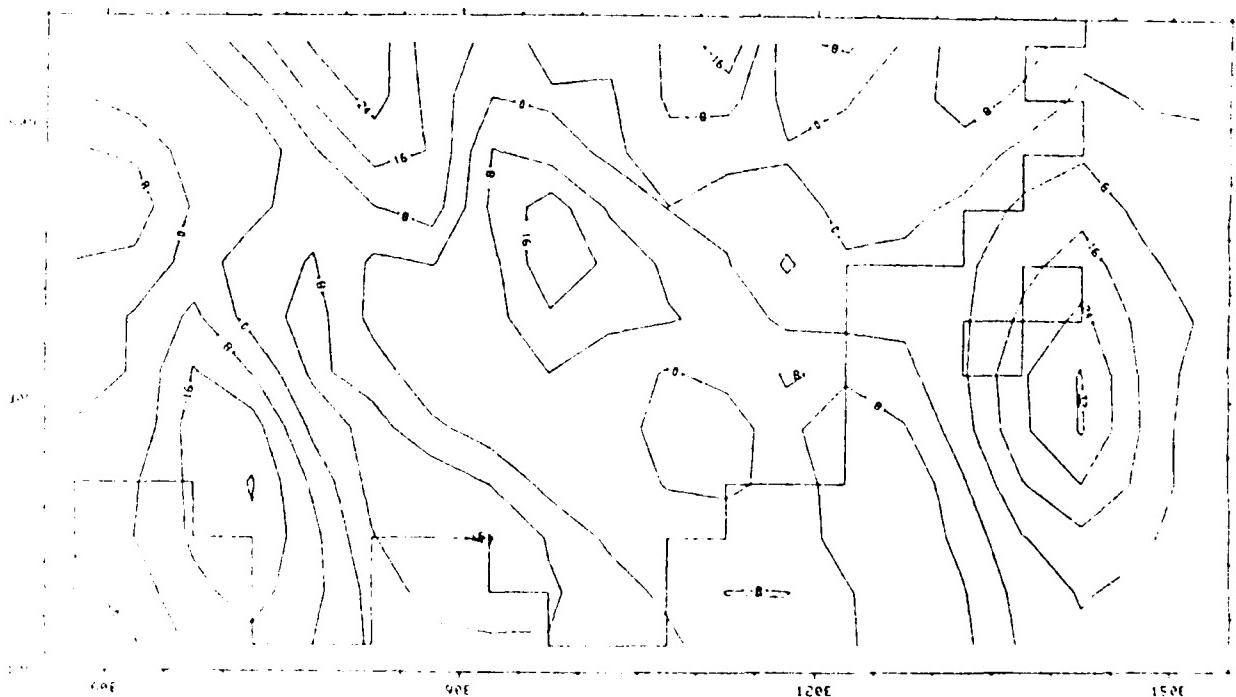
(d)
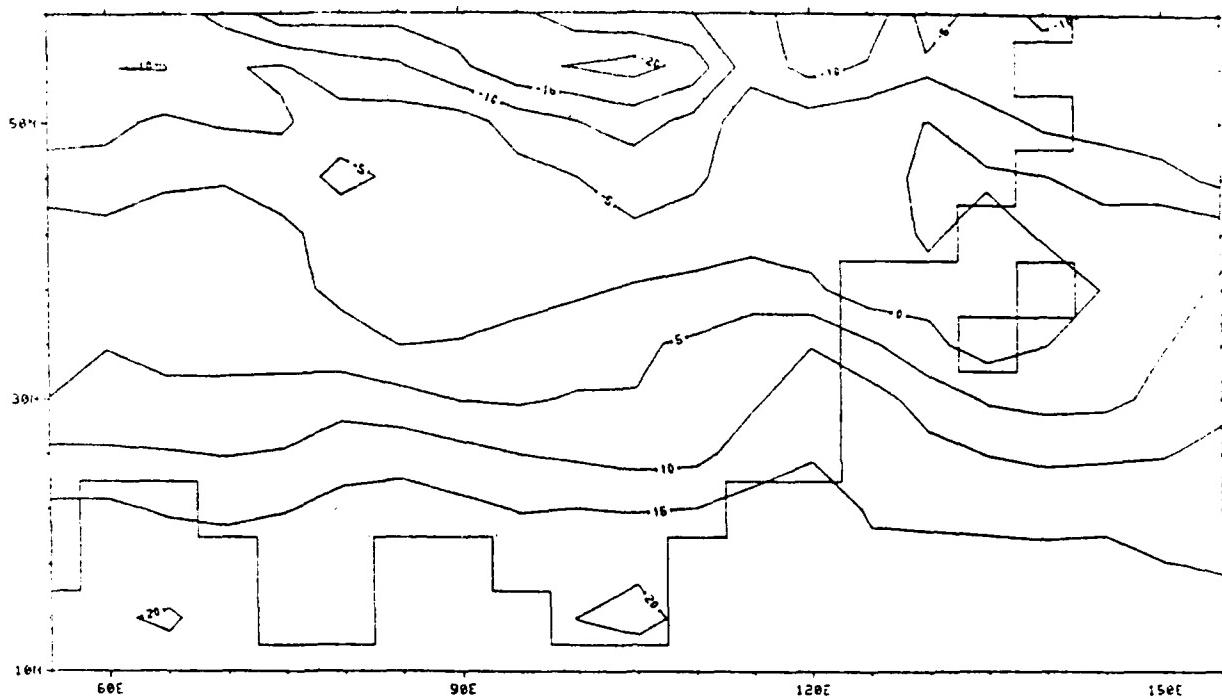
(a)
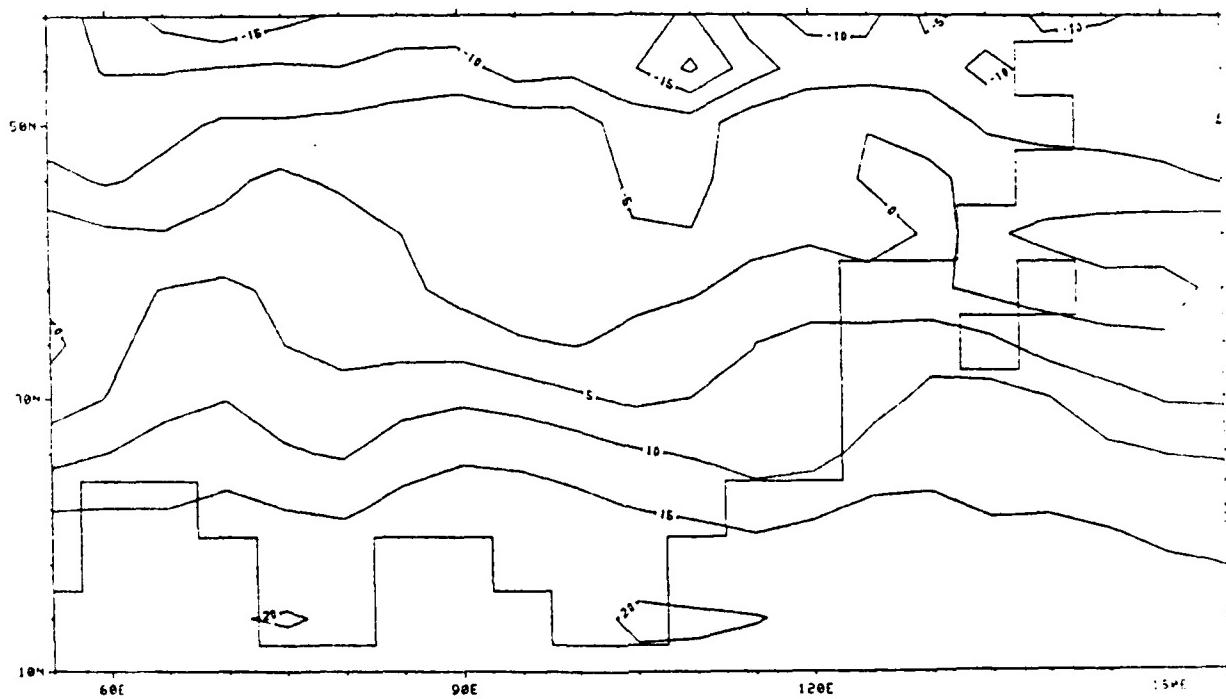
(b)

Fig. 3.27   The temperature (Deg-C) distribution at level 3
for the same times and condition as in Fig. 3.22.

157

(c)

(d)

153
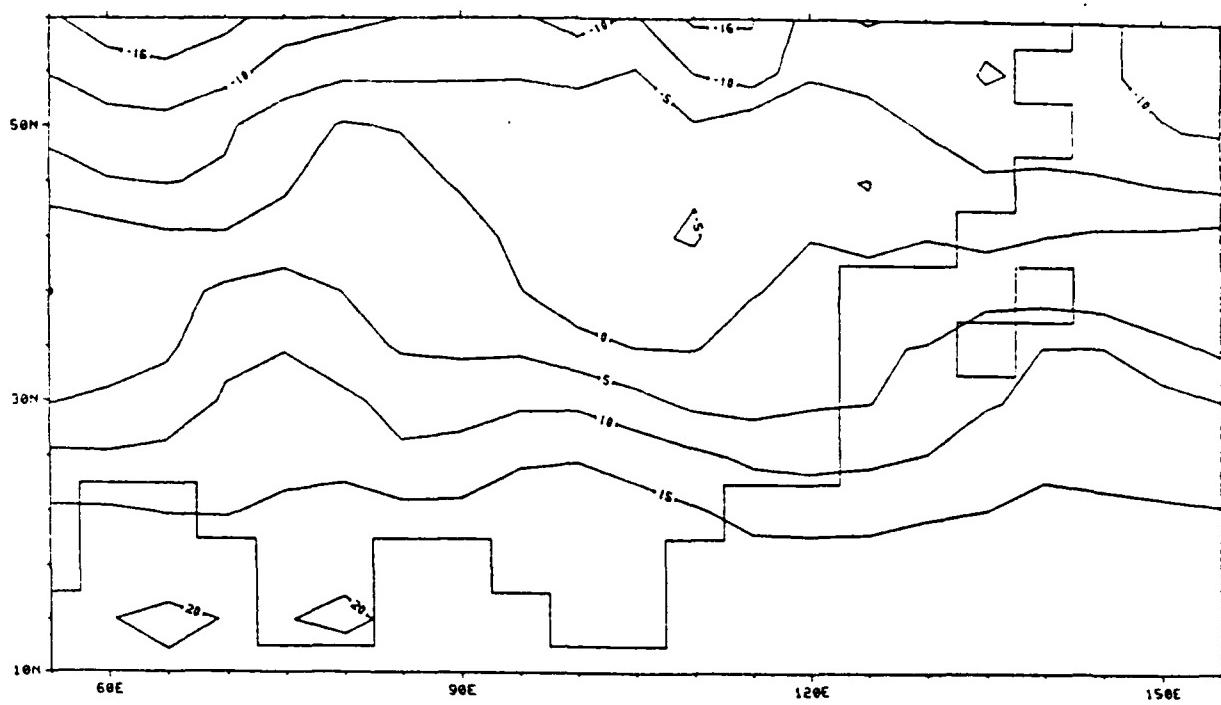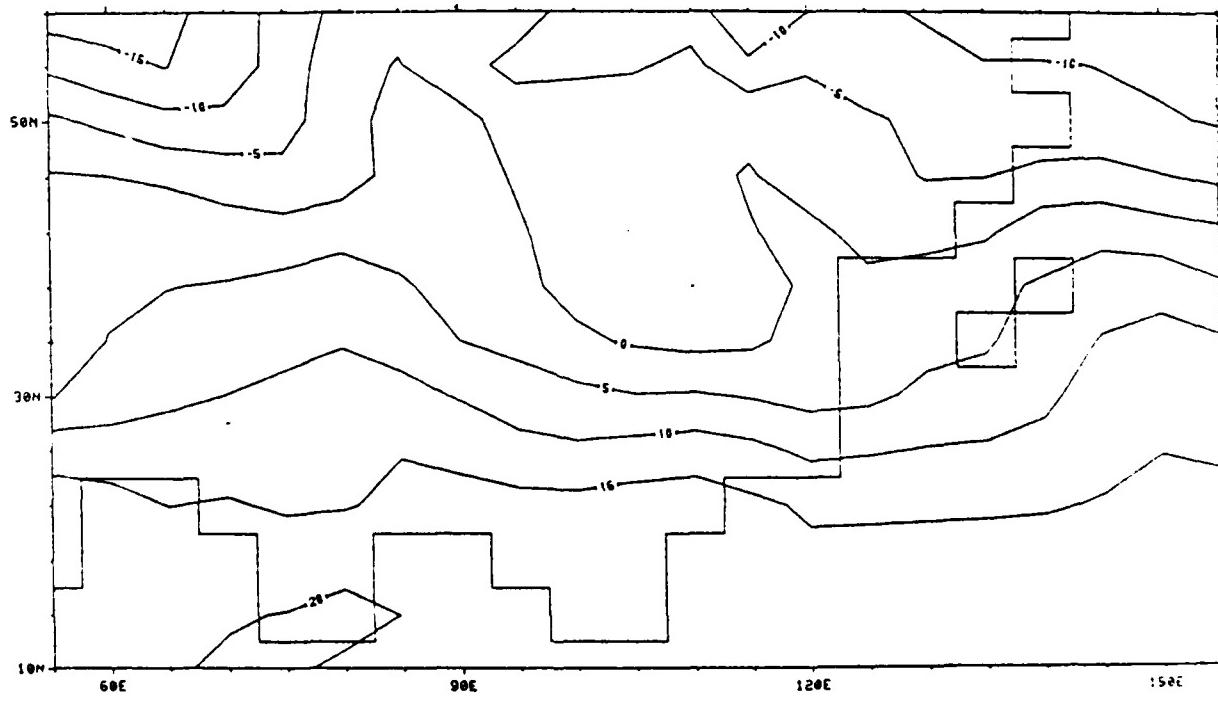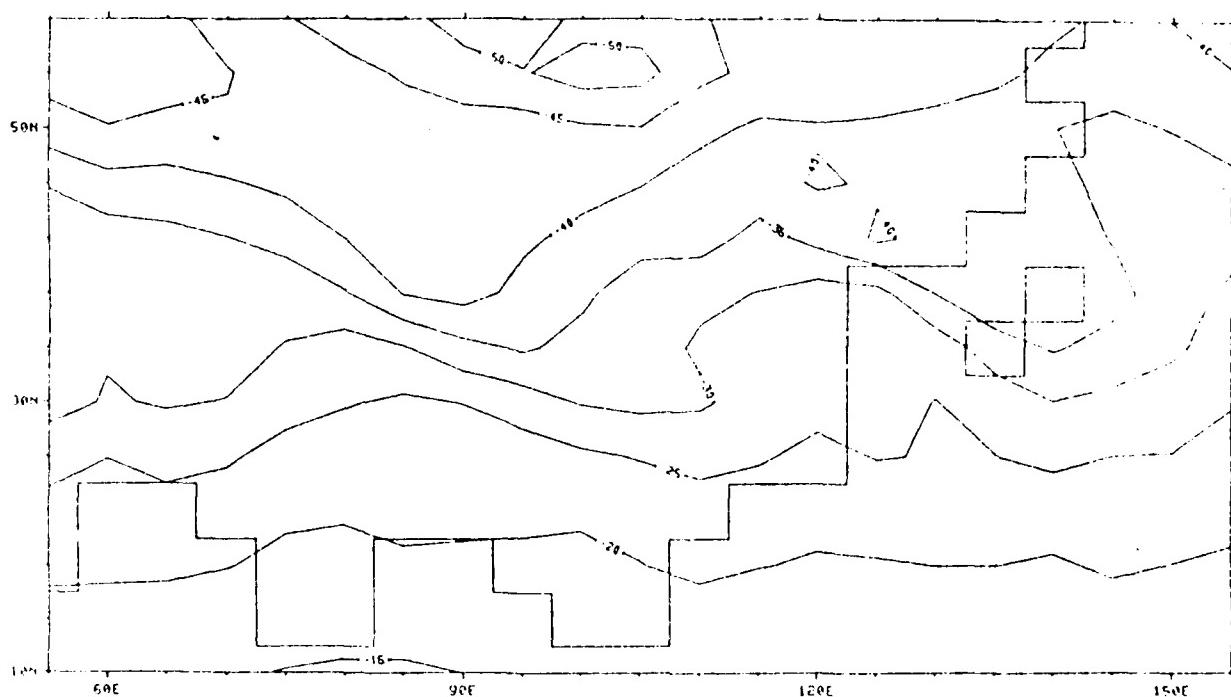
(a)
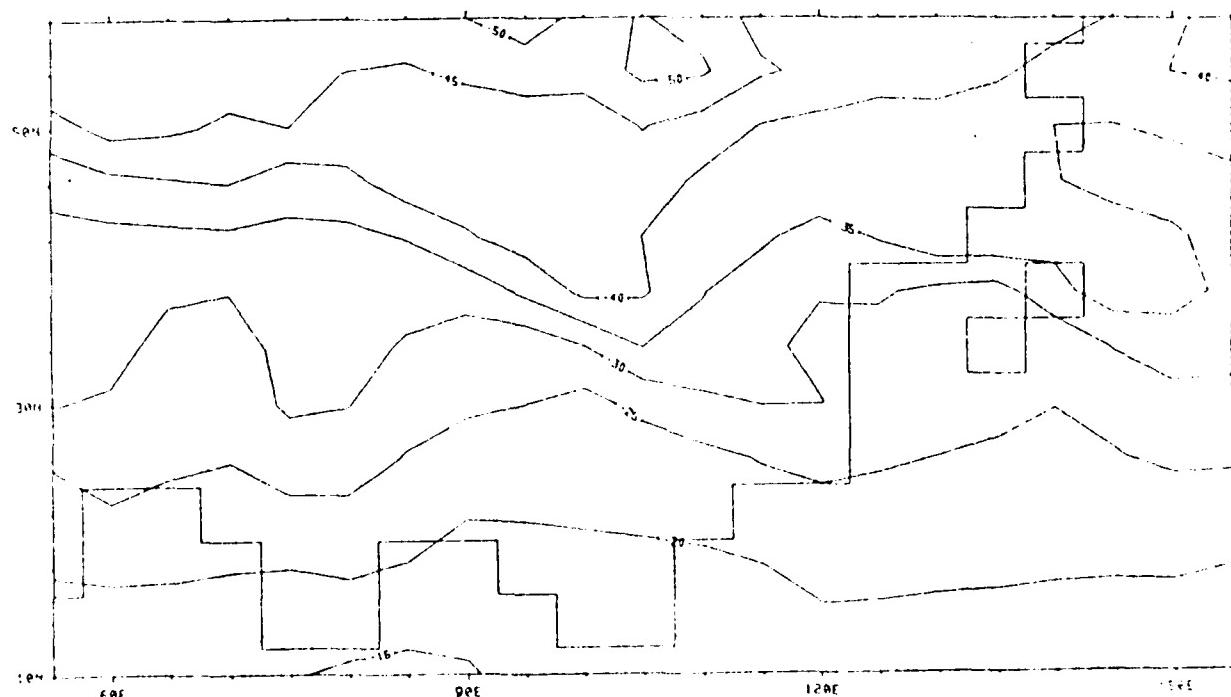
(b)

Fig. 3.28 The temperature (Deg-C) distribution at level 1
for the same times and condition as in Fig. 3.22.

159

(c)

(d)

160
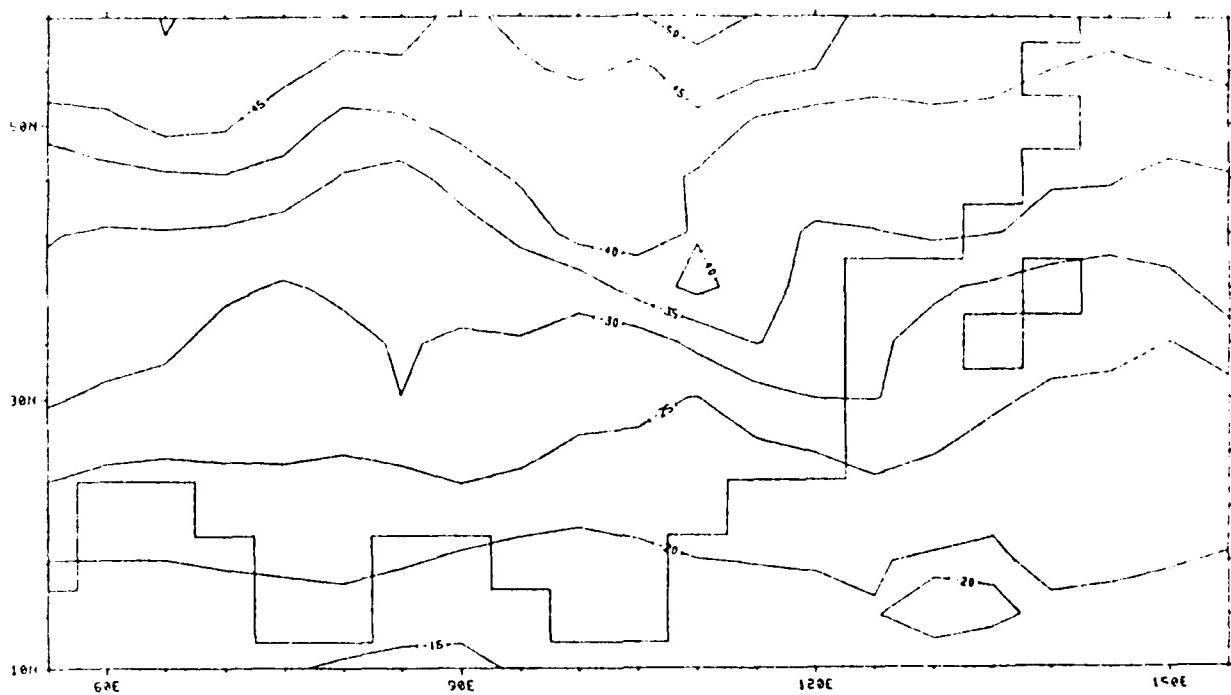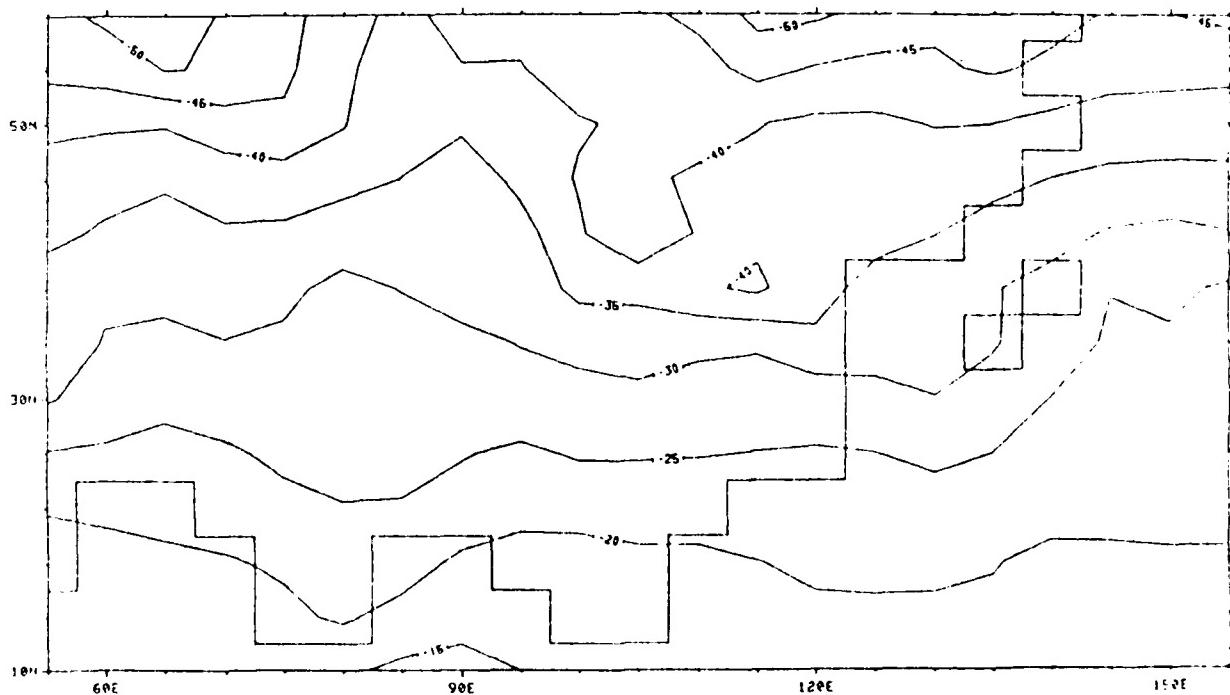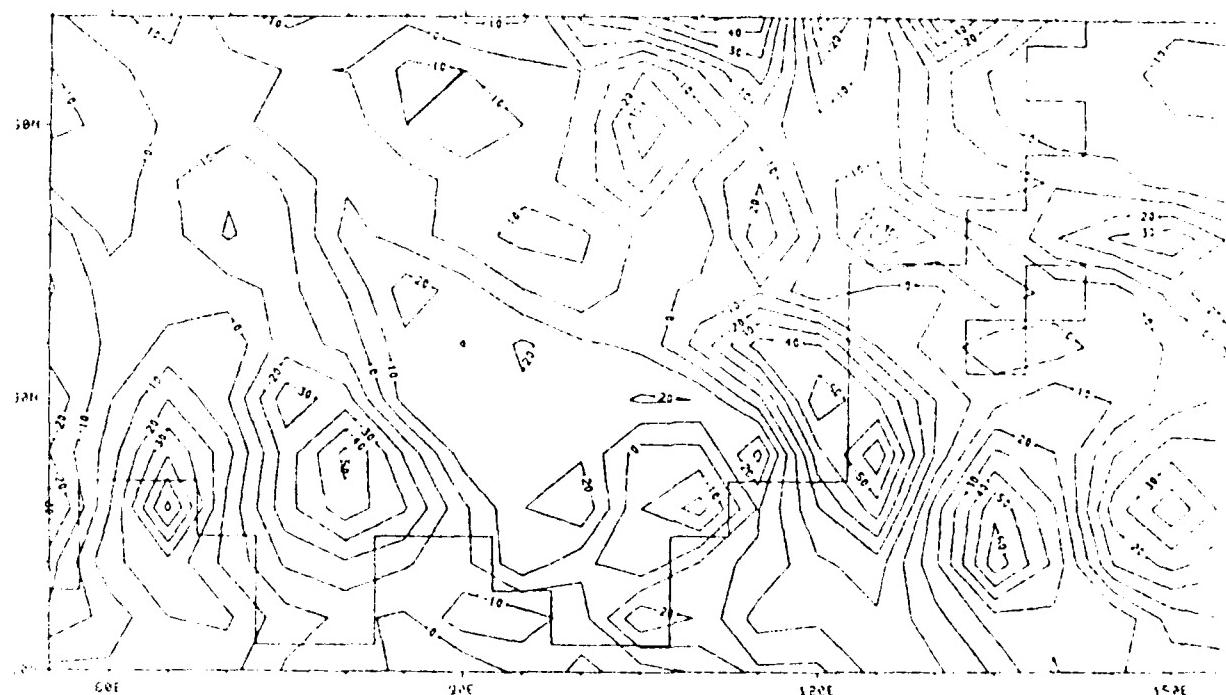
(a)
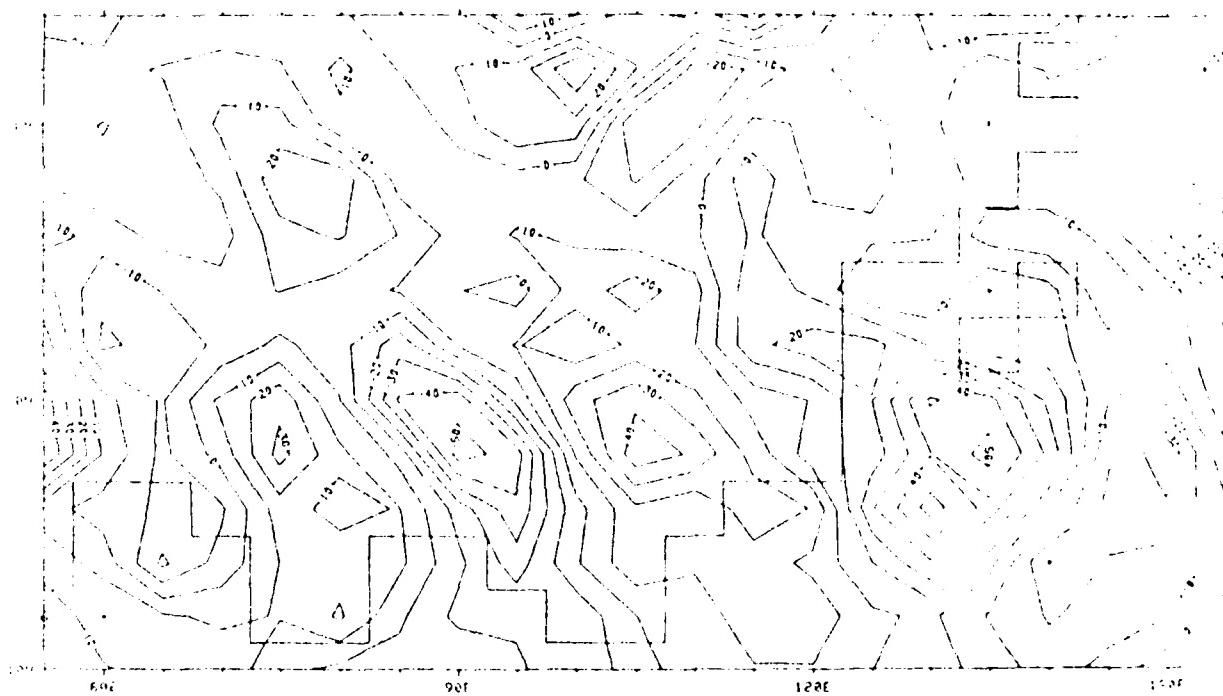
(b)

Fig. 3.29   The sigma vertical velocity (10^{-7} sec^{-1}) at level 2
for the same times and condition as in Fig. 3.22.

(c)

(d)

162
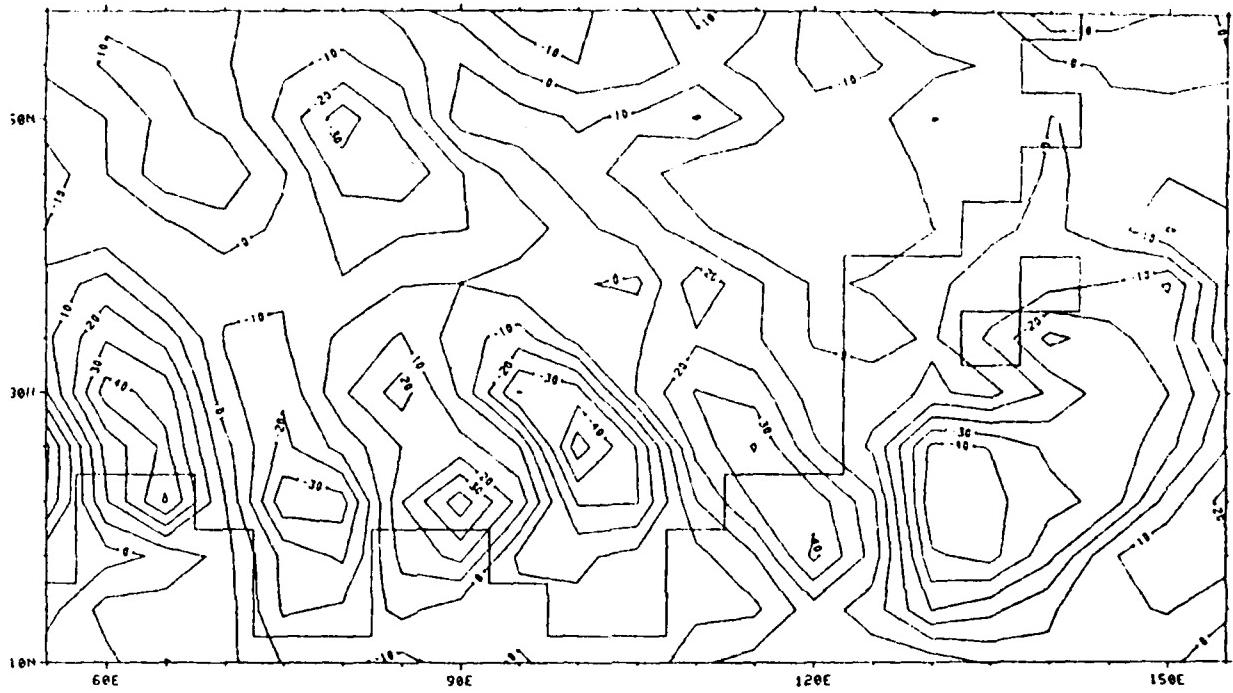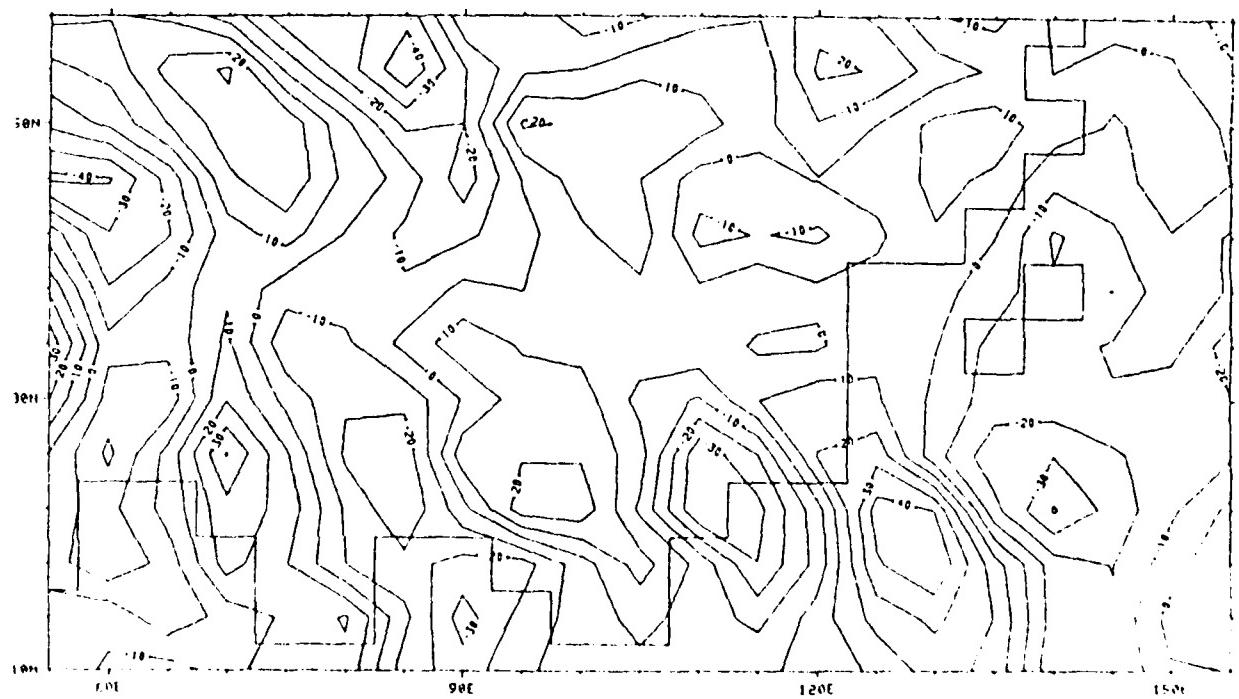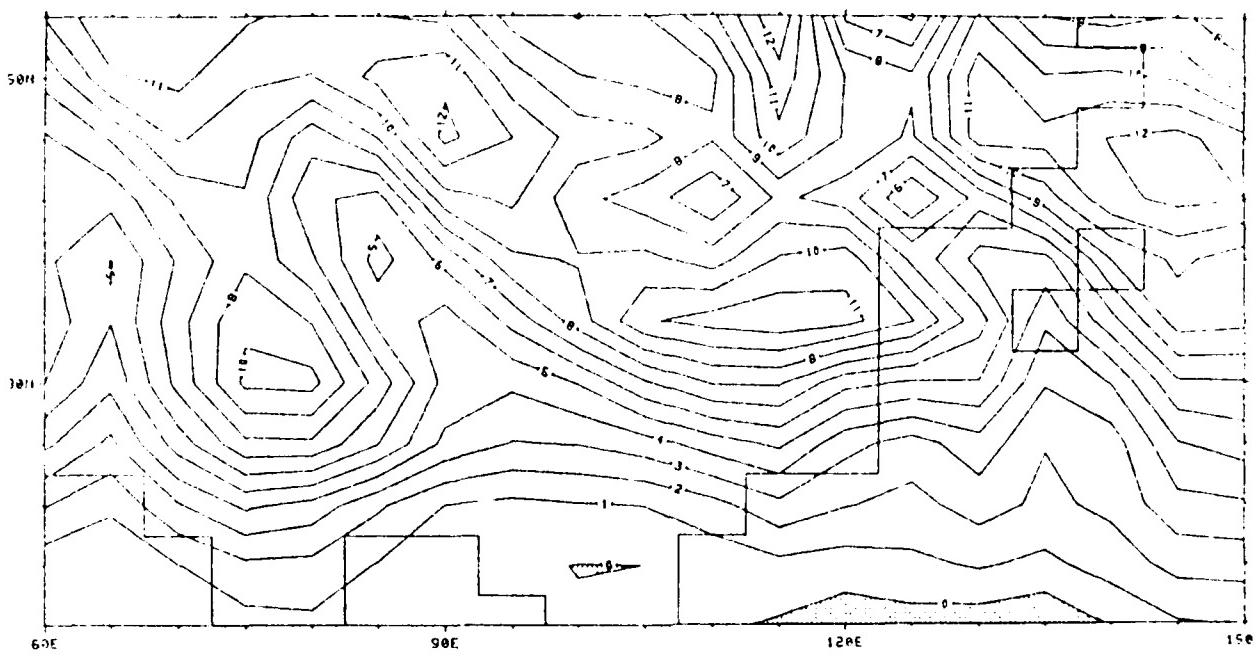
(a)
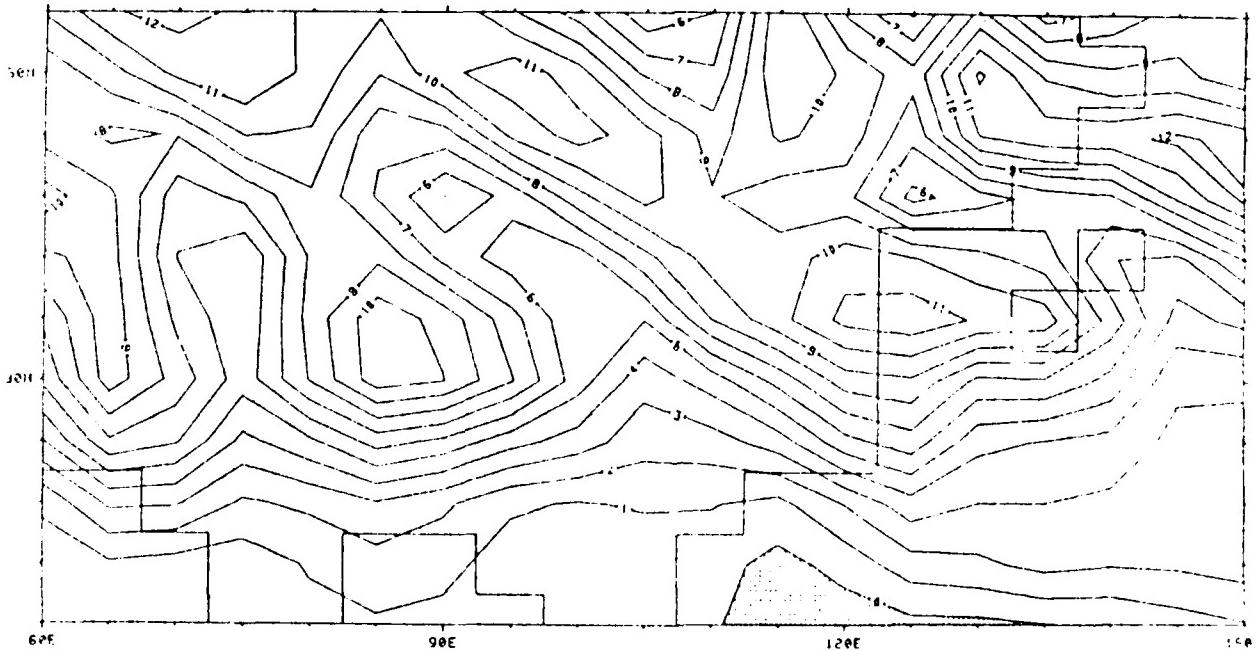
(b)

Fig. 3.30 The absolute vorticity (day^{-1}) at level 2 for
the same times and condition as in Fig. 3.22.

163

(c)

(d)

164
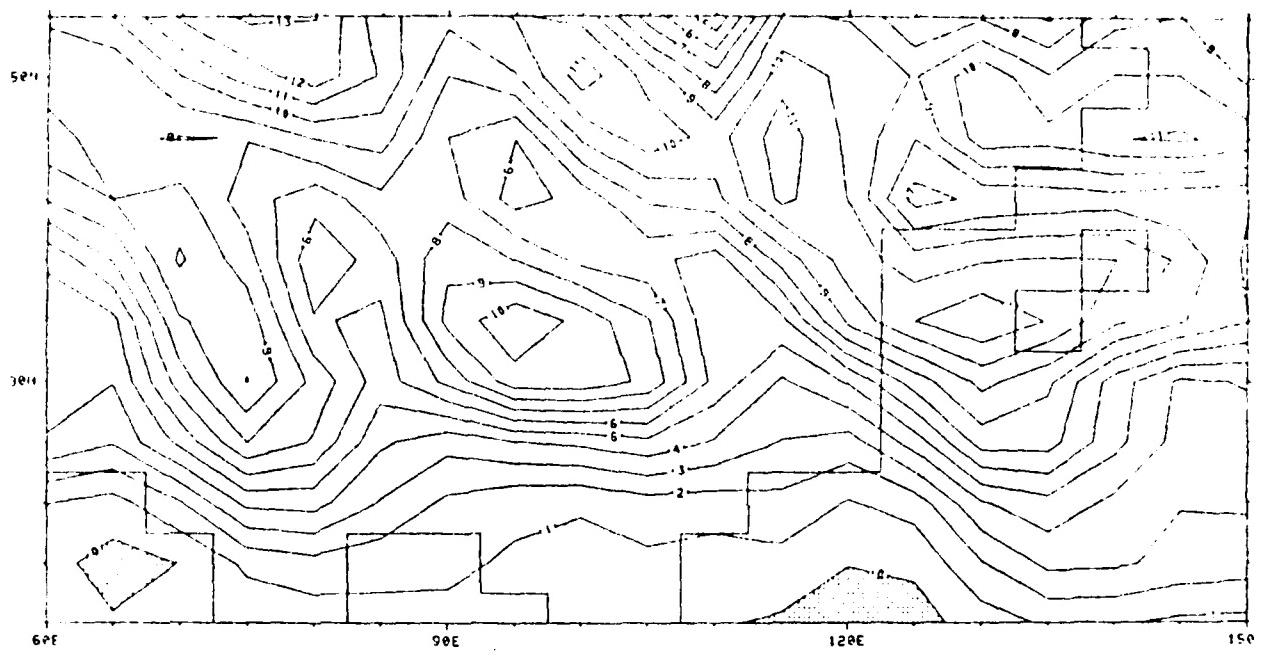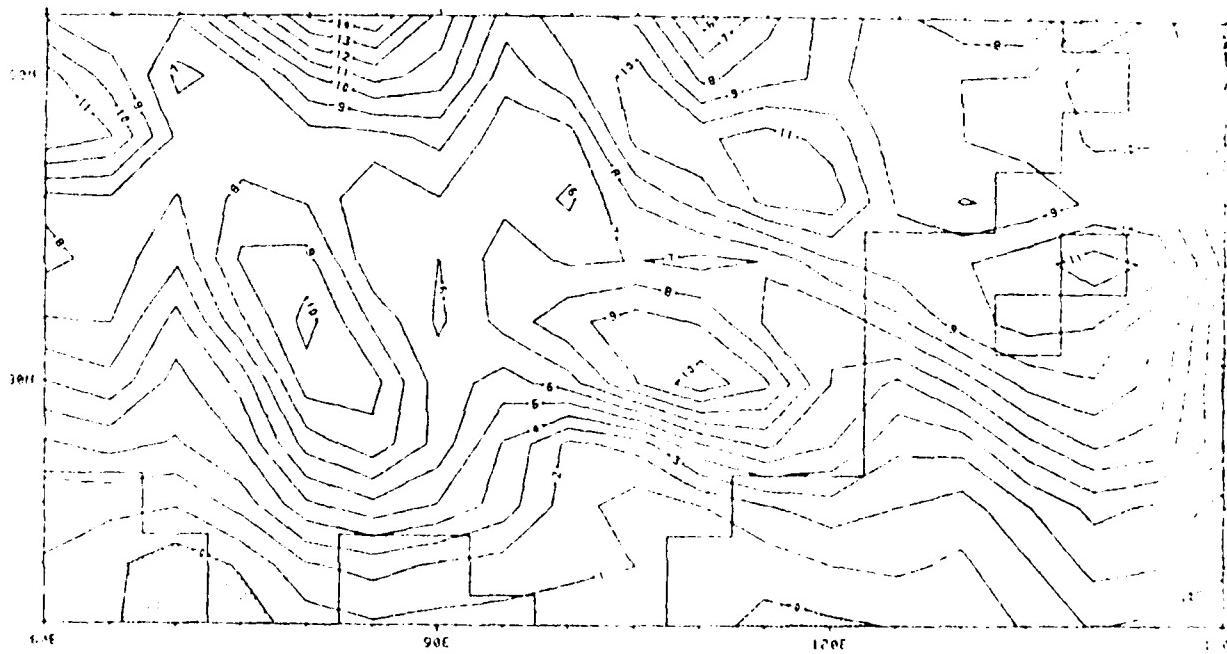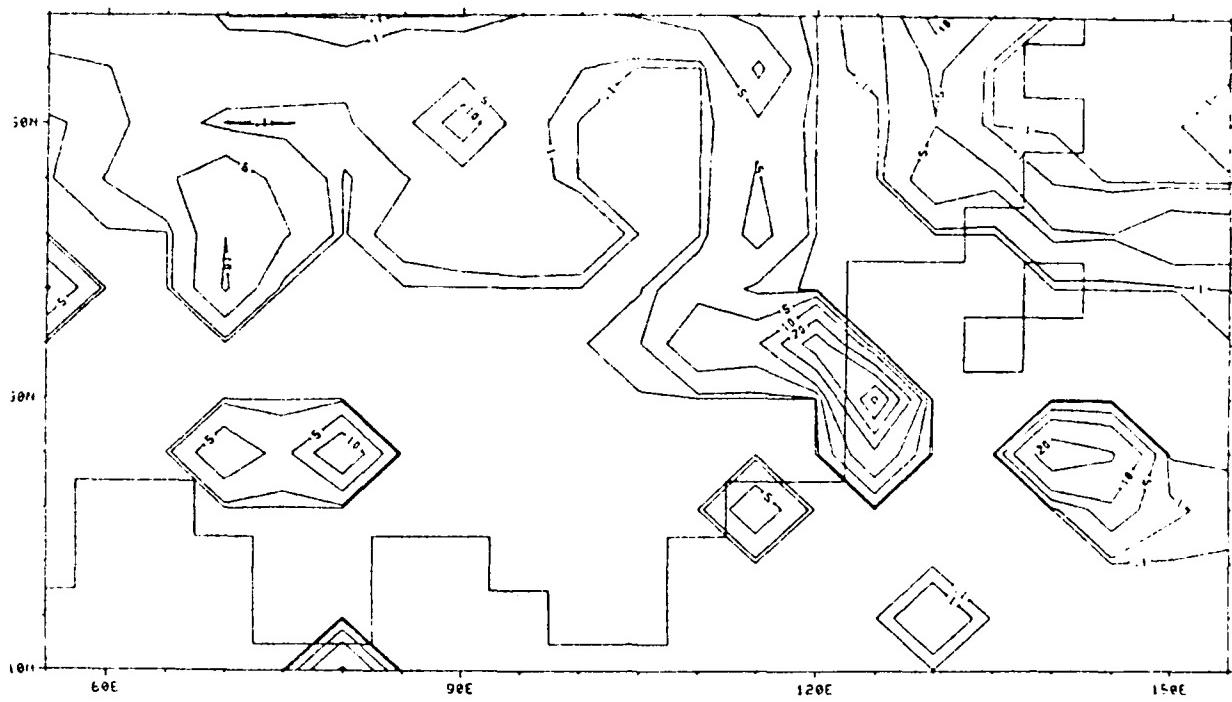
(a)
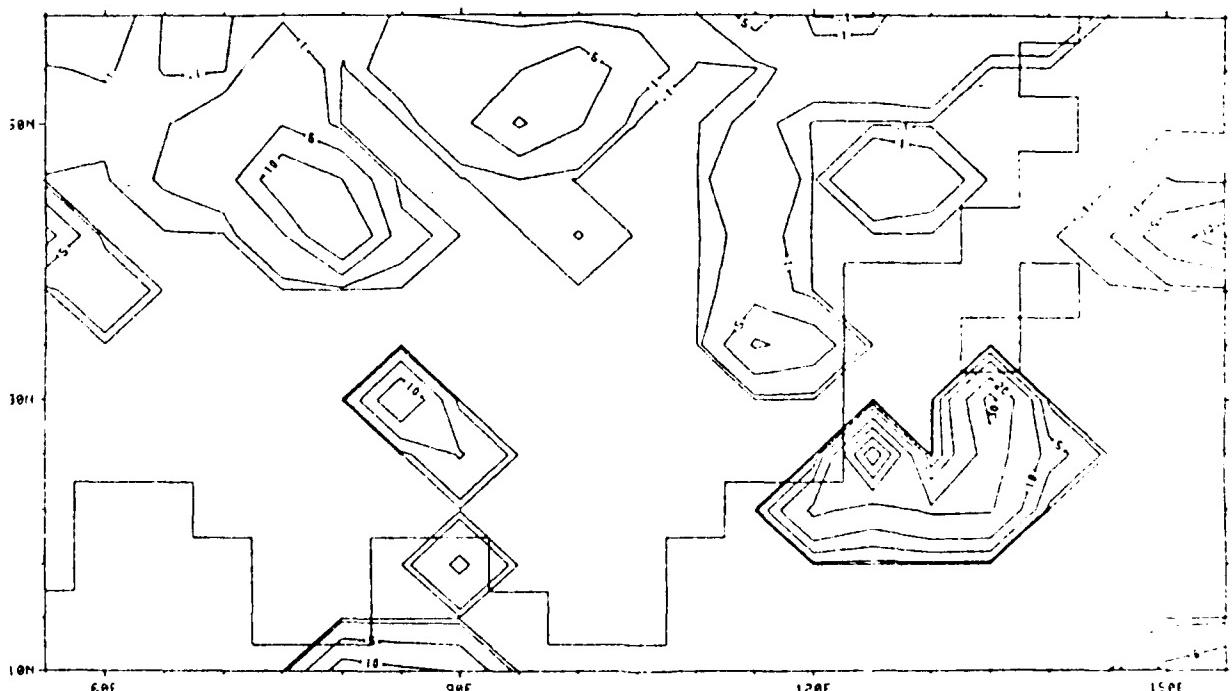
(b)

Fig. 3.31 The precipitation rate $(mm\ day^{-1})$ for the same times and condition as in Fig. 3.22.

165
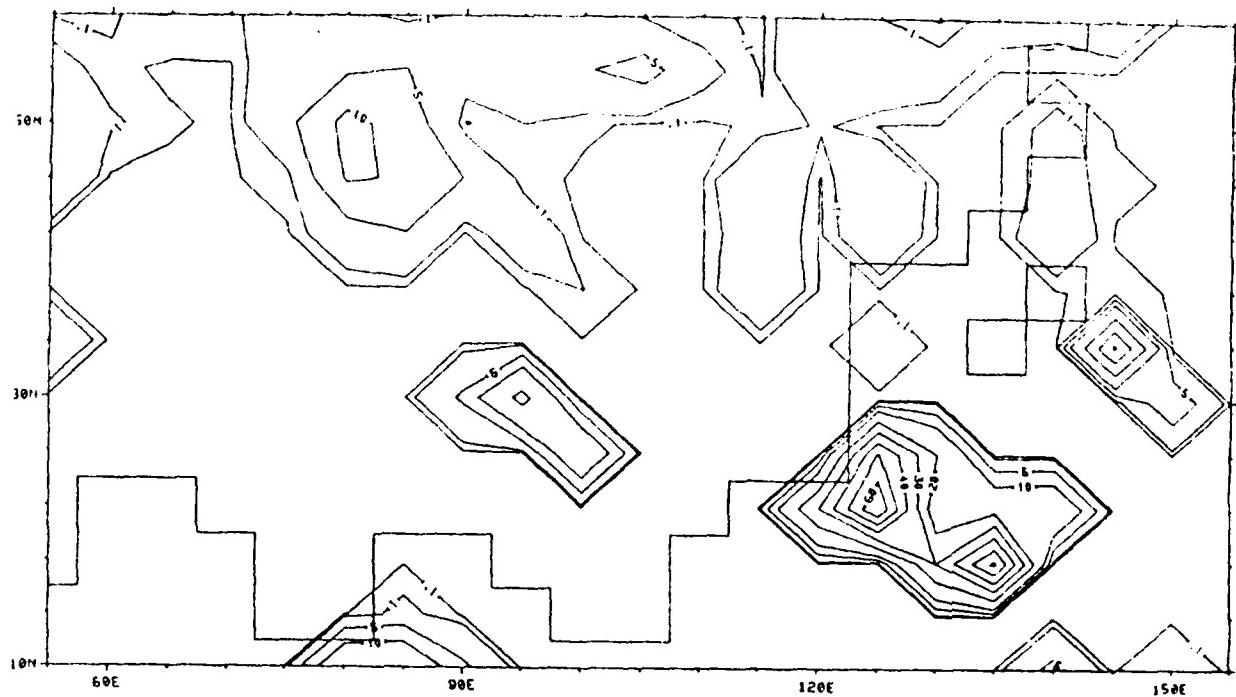
(c)
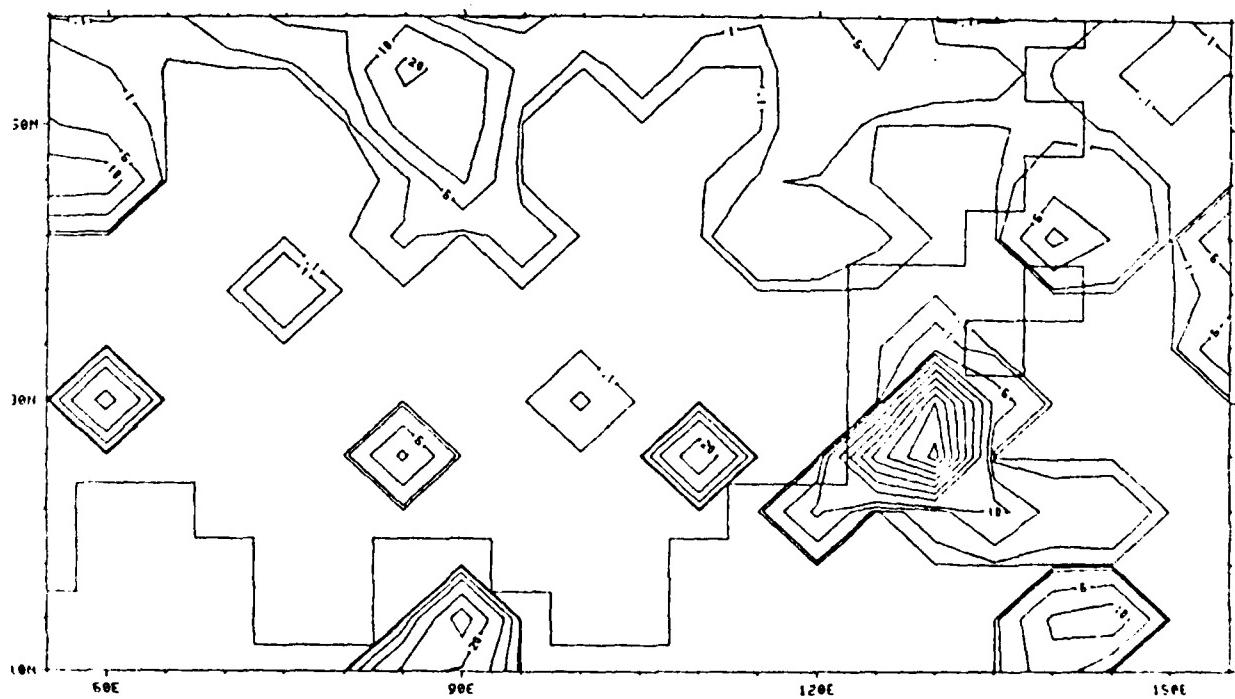
(d)
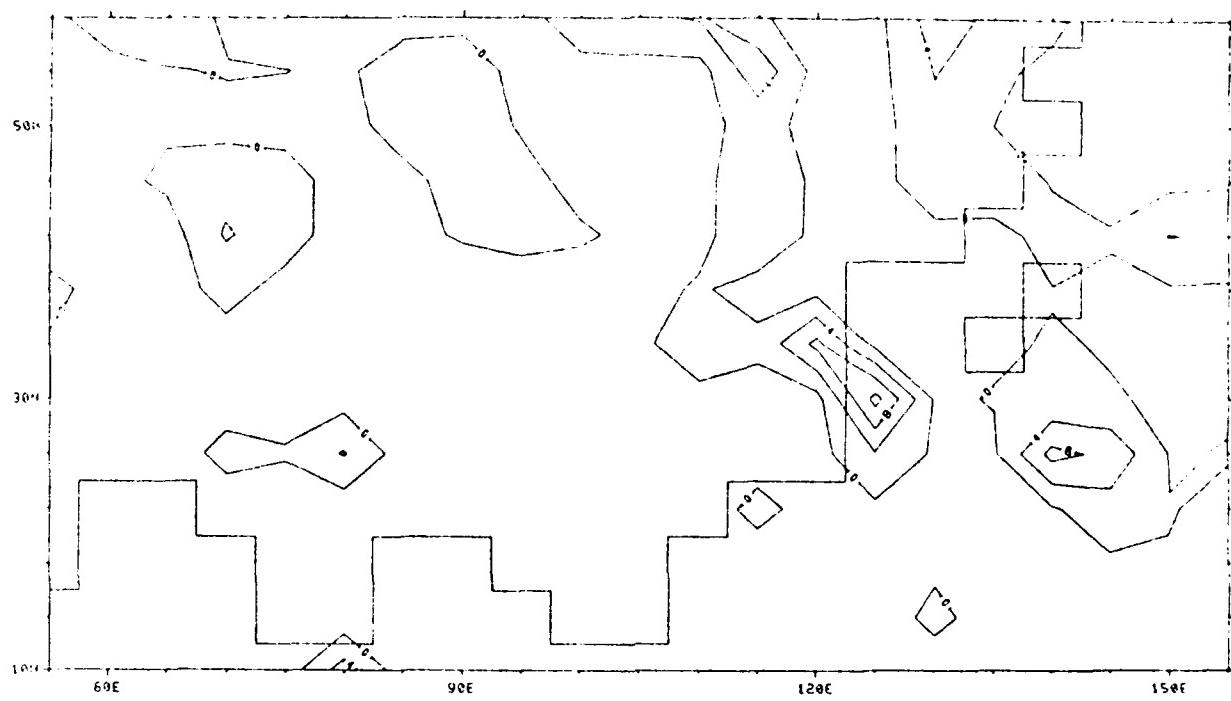
(a)
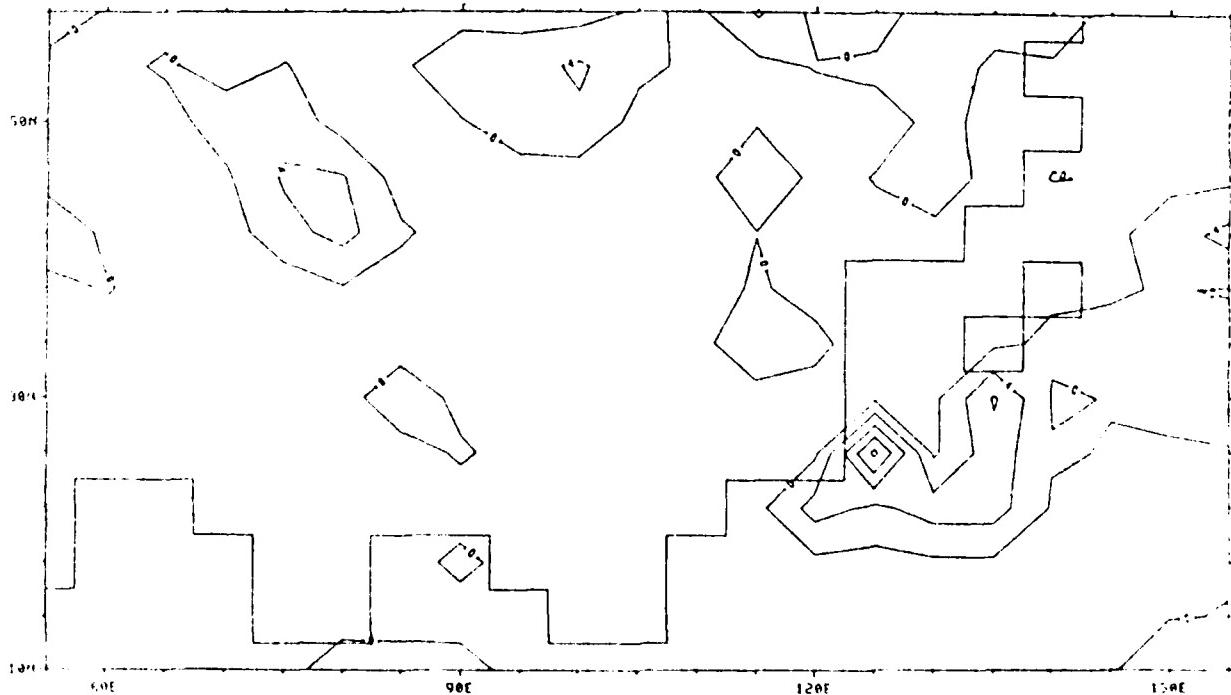
(b)

Fig. 3.32 The atmospheric heating (Deg day^{-1}) for the same time
and condition as in Fig. 3.22.

167
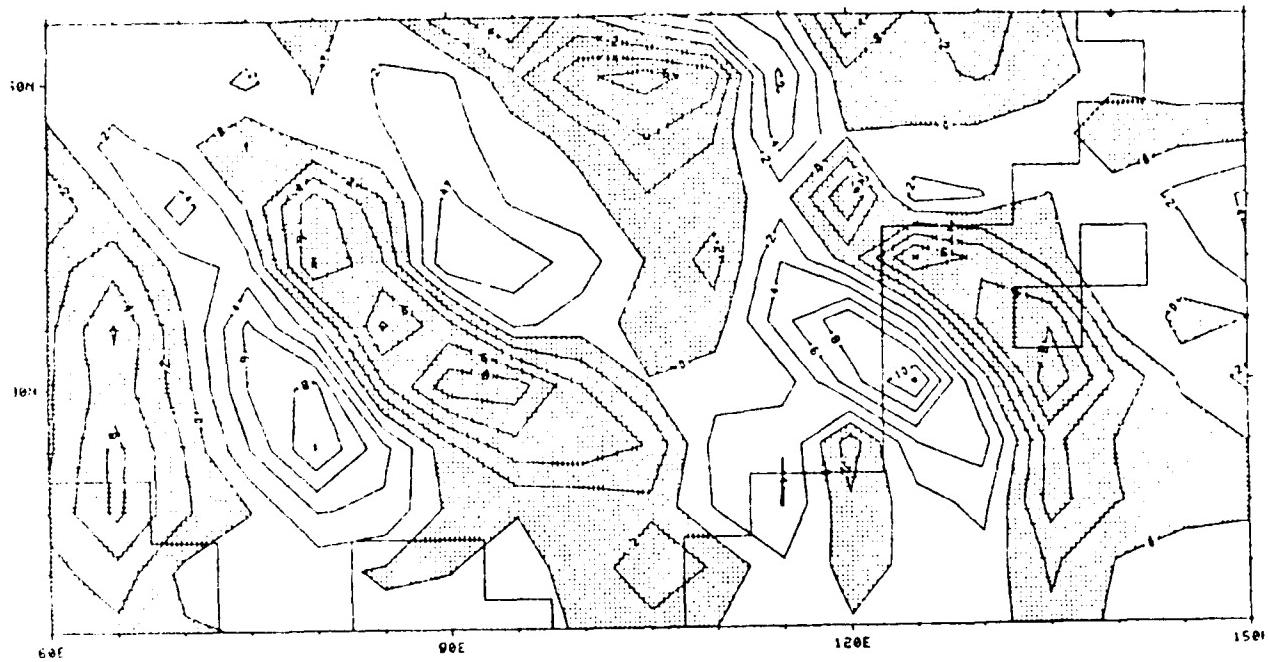
(a)
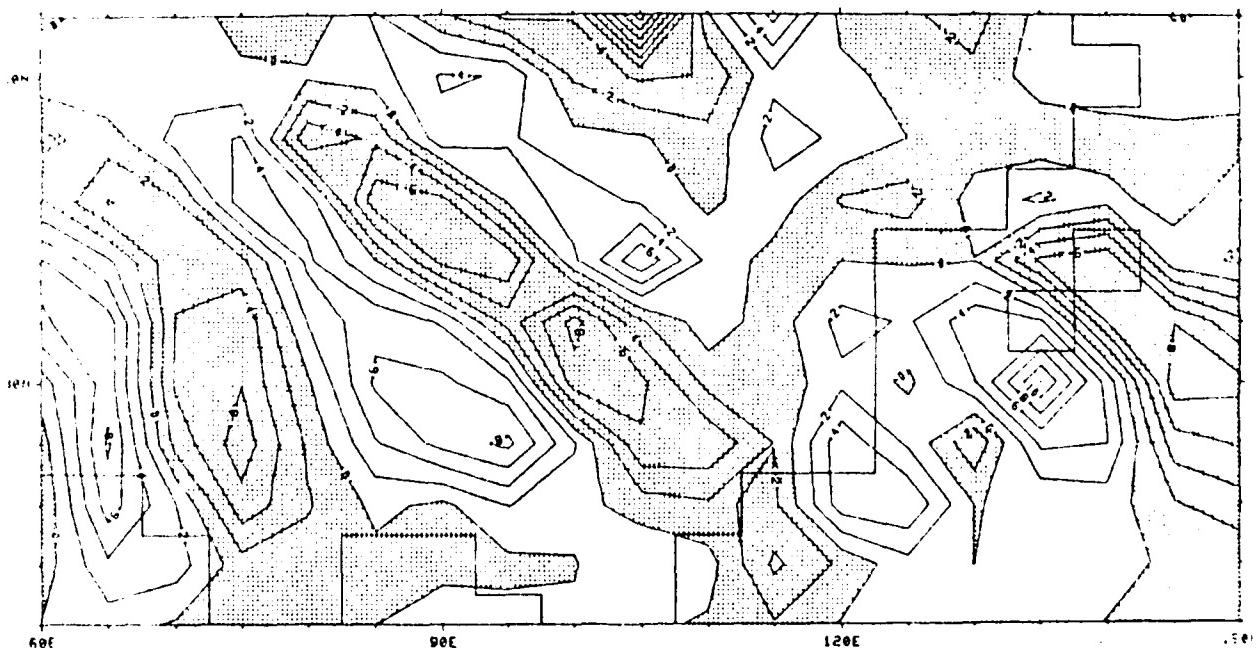
(b)

Fig. 3.33 The local time rate of change of absolute vorticity
(day $^{-1}$) for the same times and condition as in Fig. 3.22.

168

(c)

(d)

169
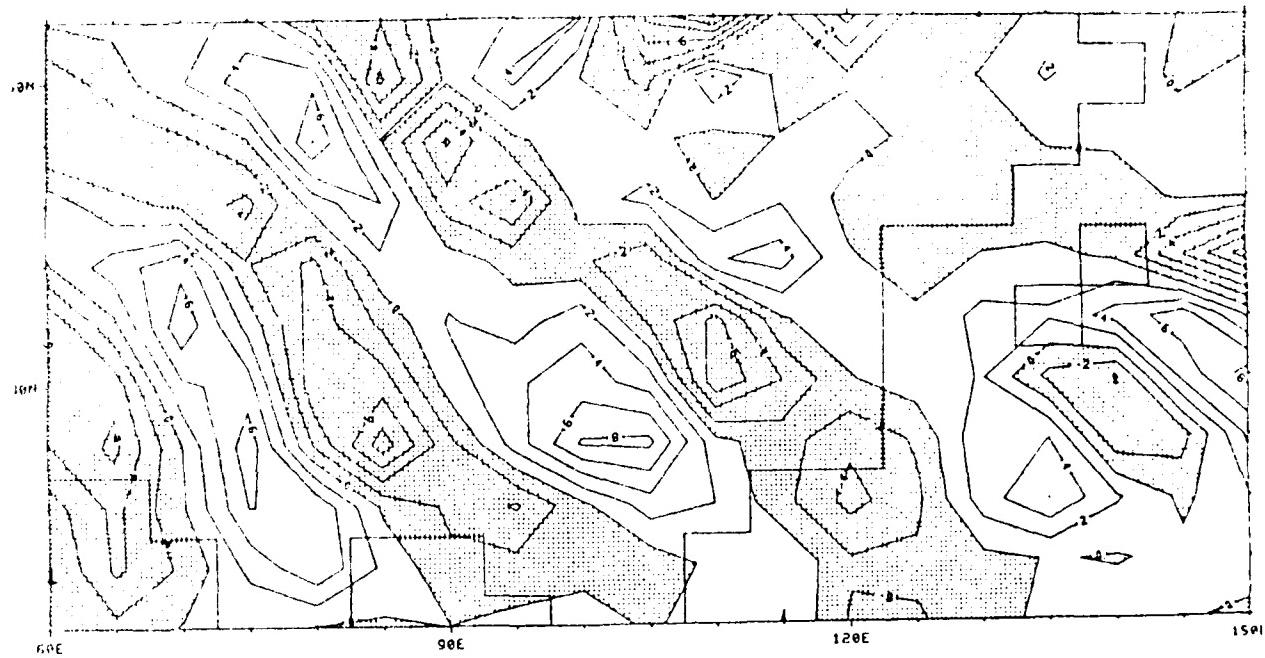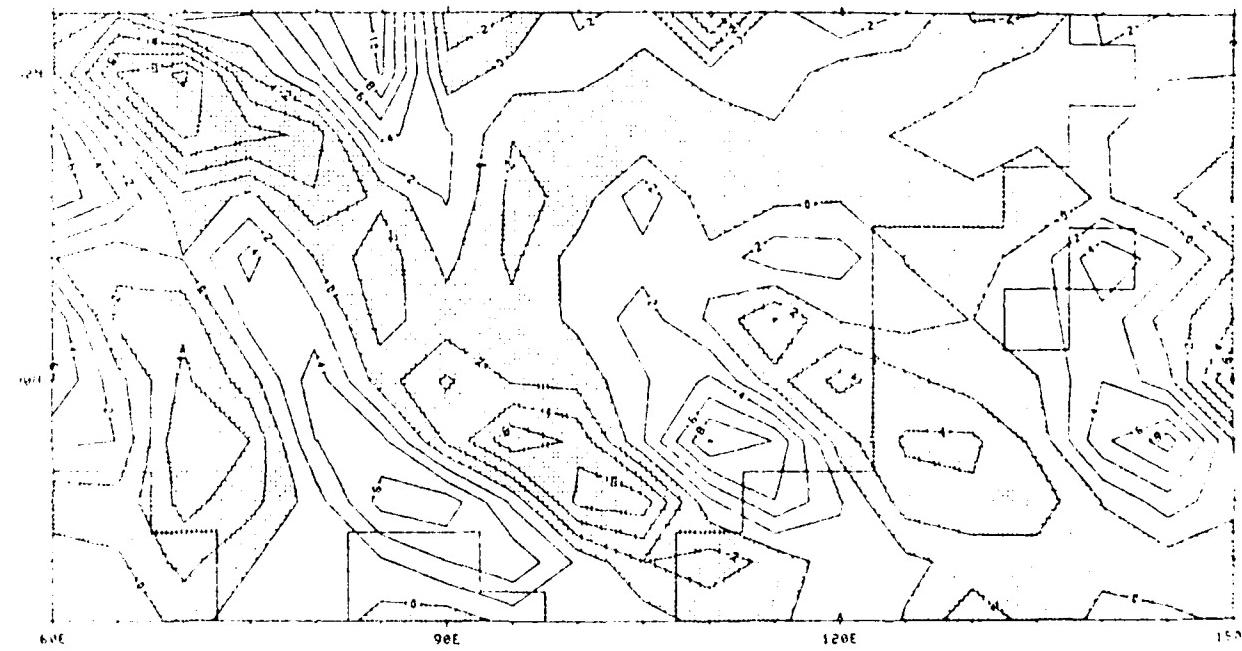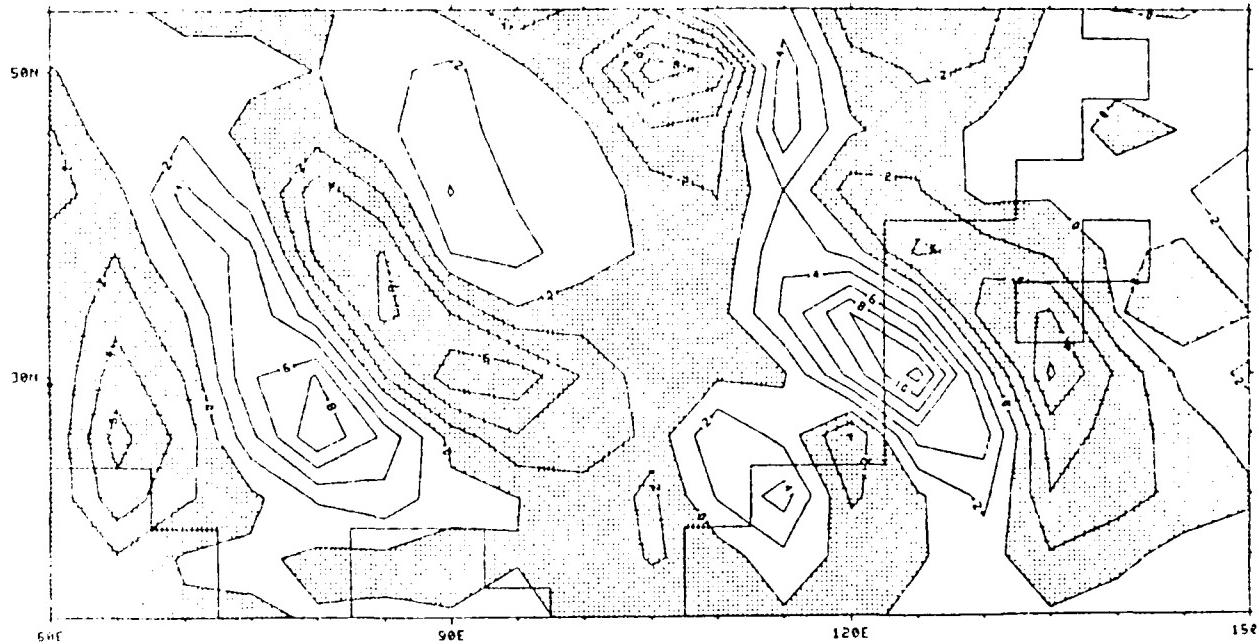
(a)
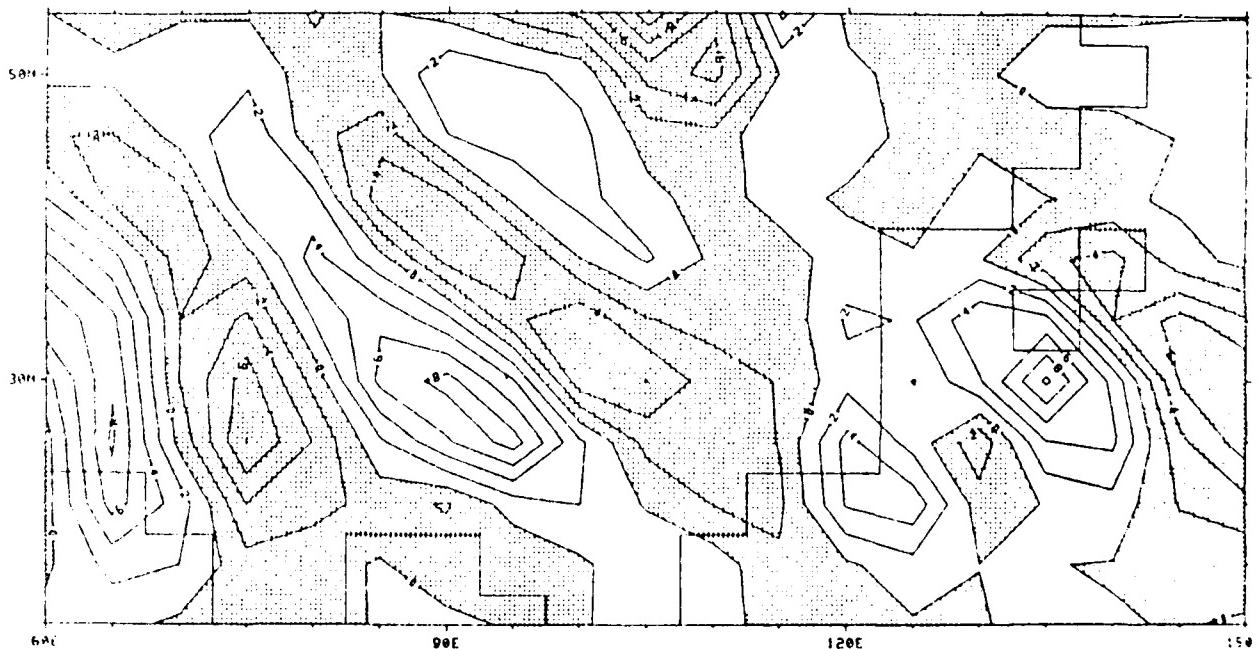
(b)

Fig. 3.34 The import of the absolute vorticity (day^{-2}) at level 2 for the same times and condition as in Fig. 3.22.

(c)

(d)

1/1
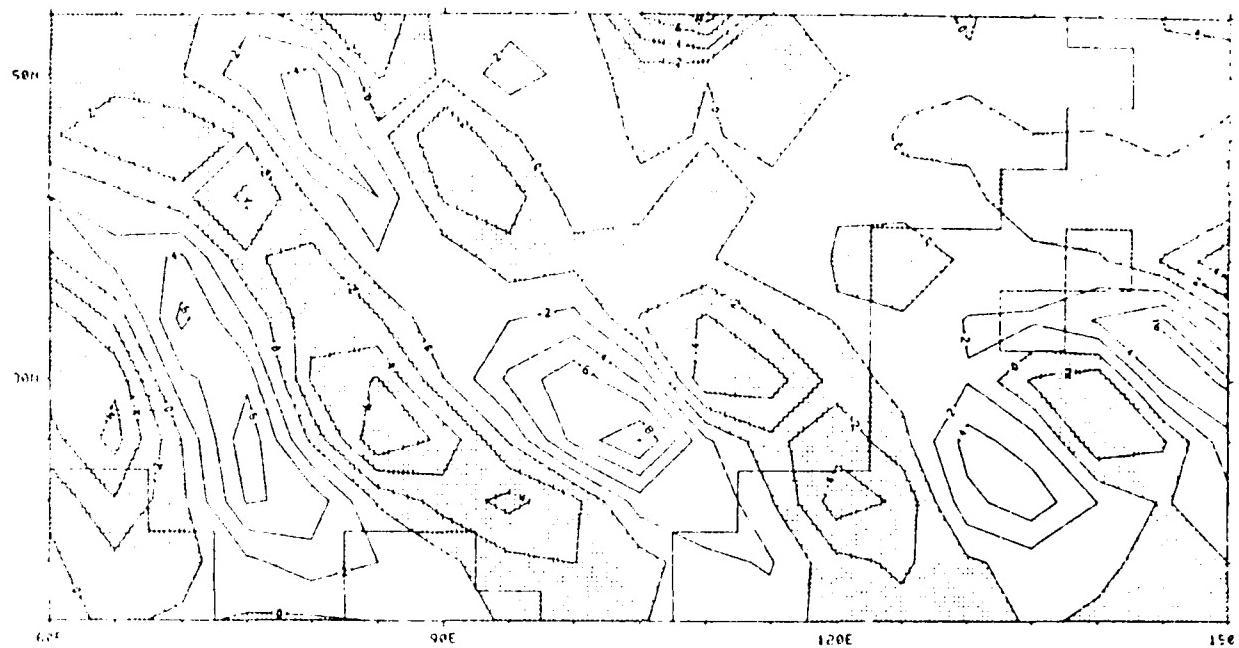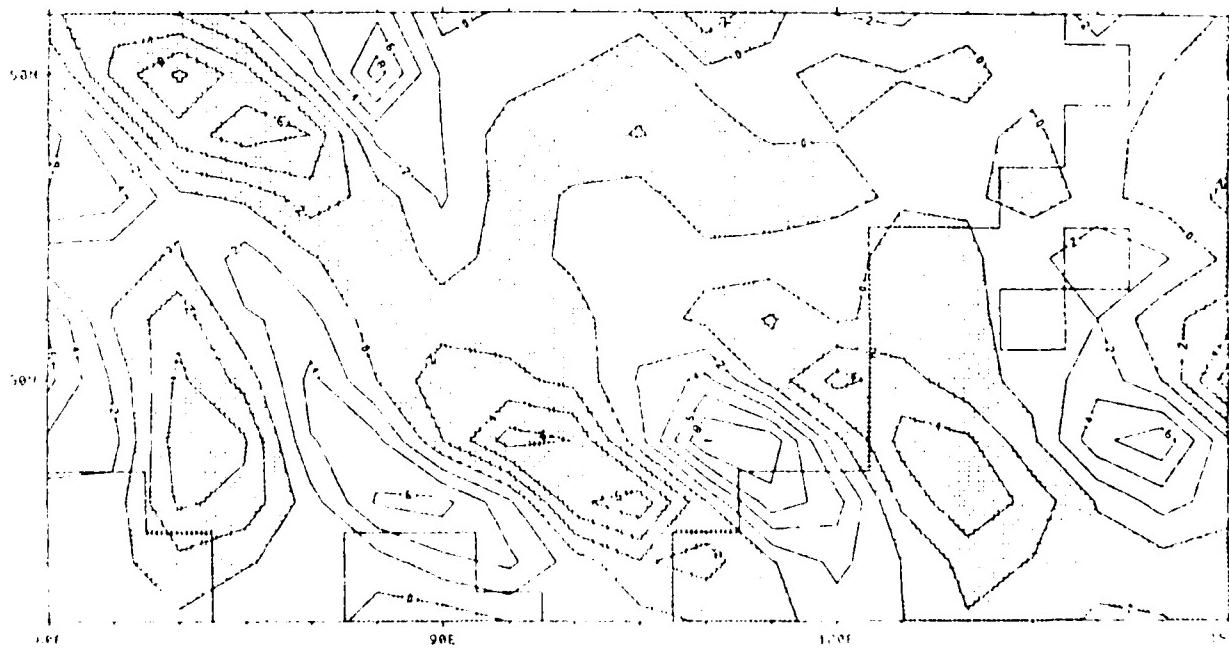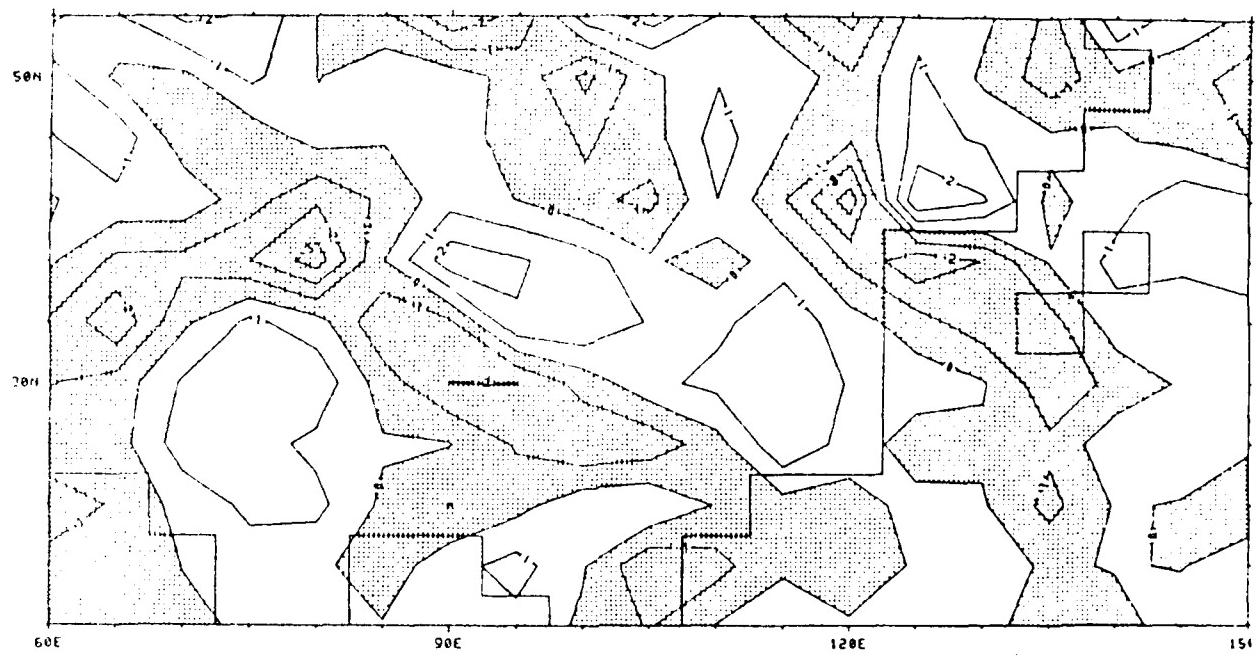
(a)
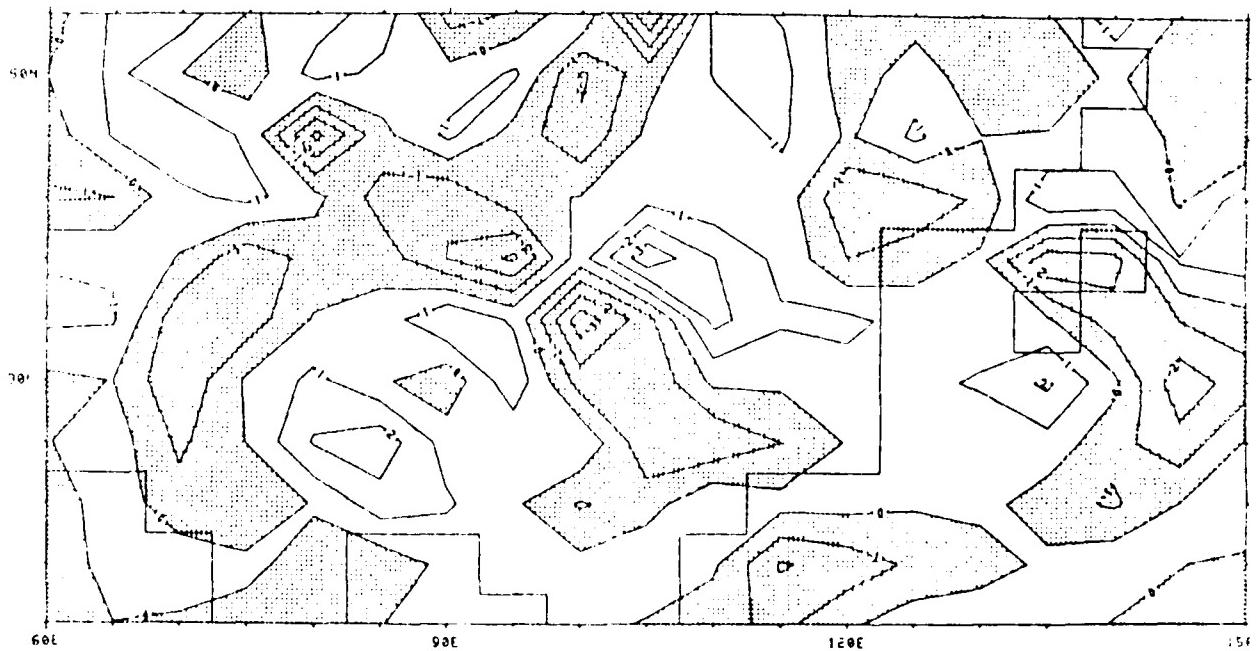
(b)

Fig. 3.35 The import of the thermal vorticity (day^{-2}) at level 2
for the same times and condition as in Fig. 3.22.

172

(c)

(d)

173
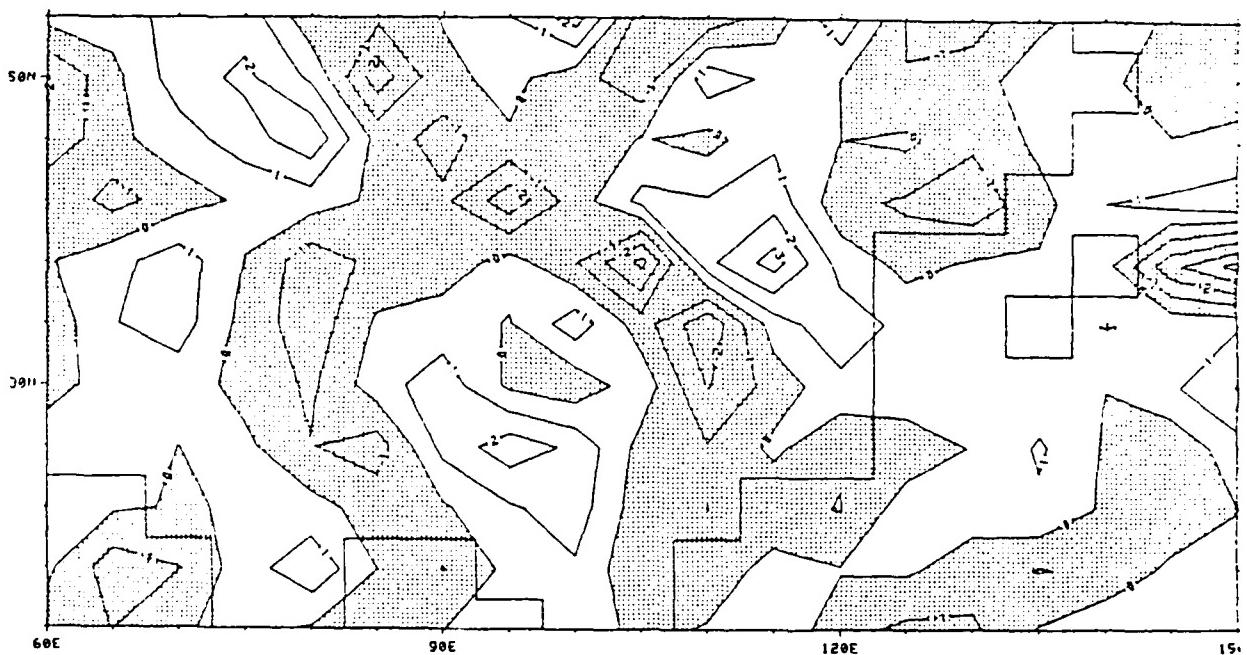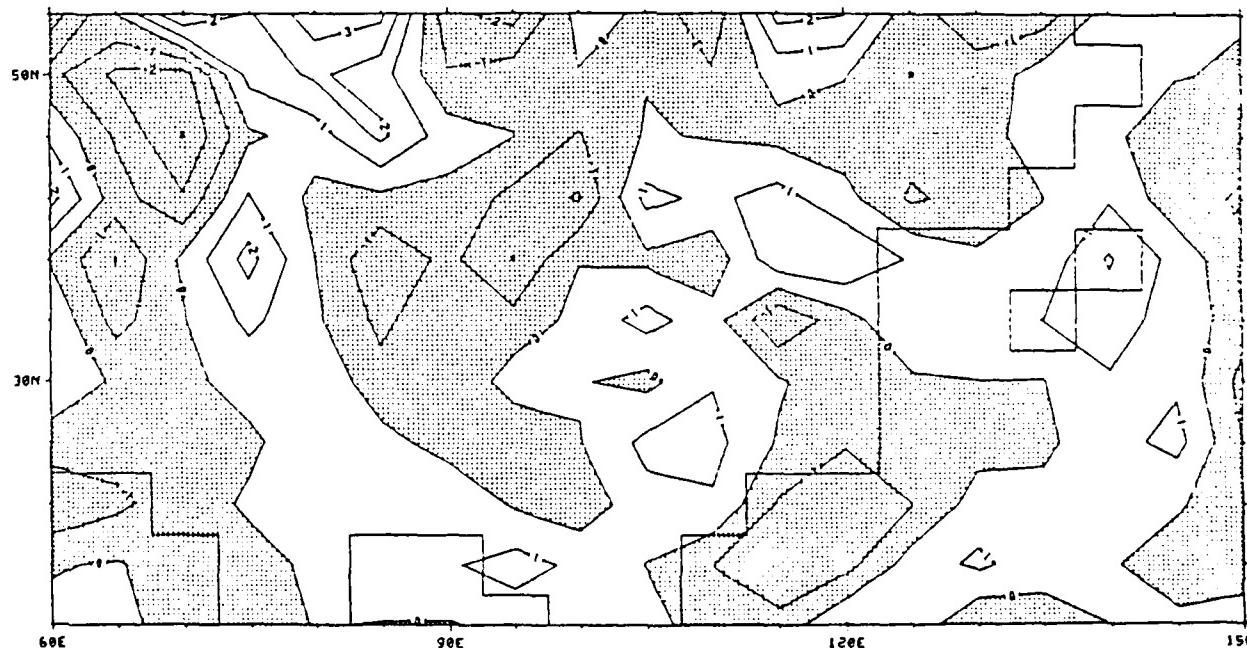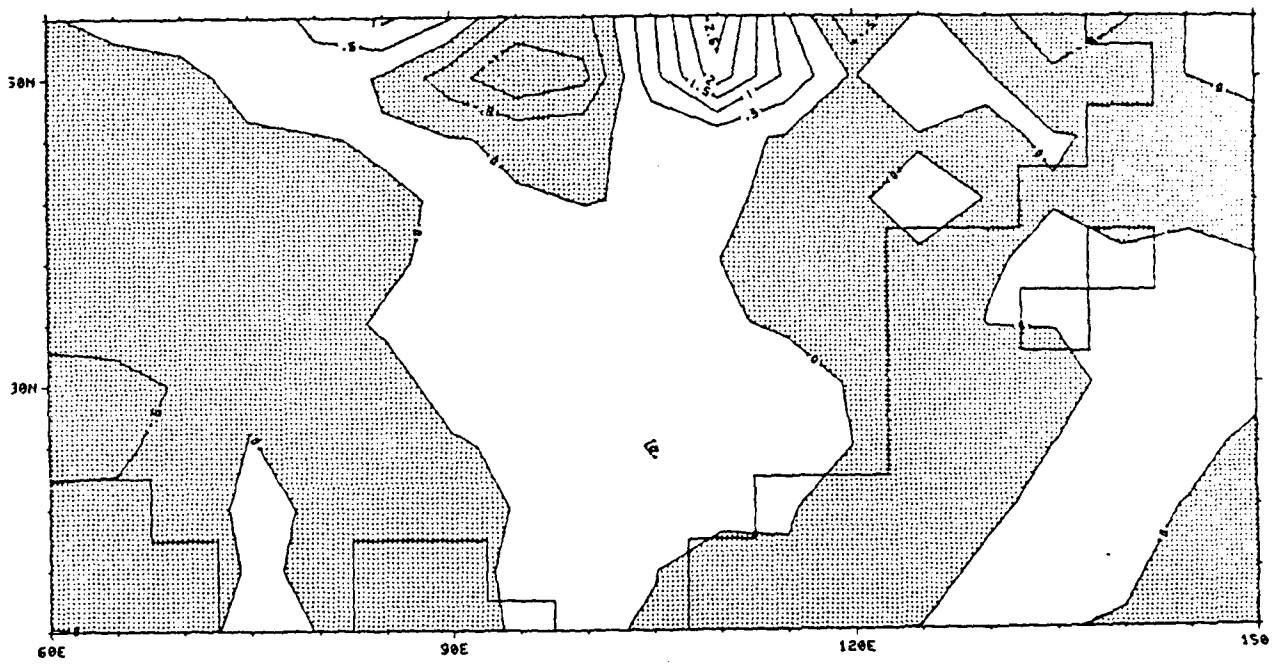
(a)

(b)

Fig. 3.36 The solenoid turn (day^{-2}) at level 2 for the same times
and condition as in Fig. 3.22.

174

(c)

(d)

175
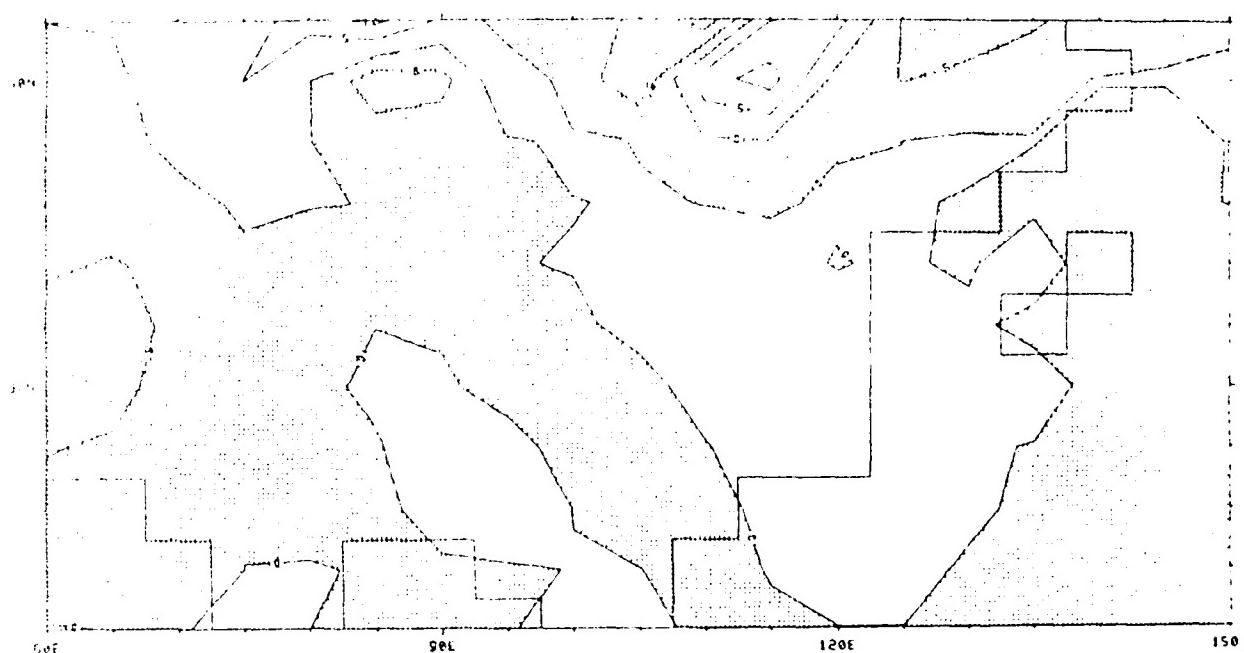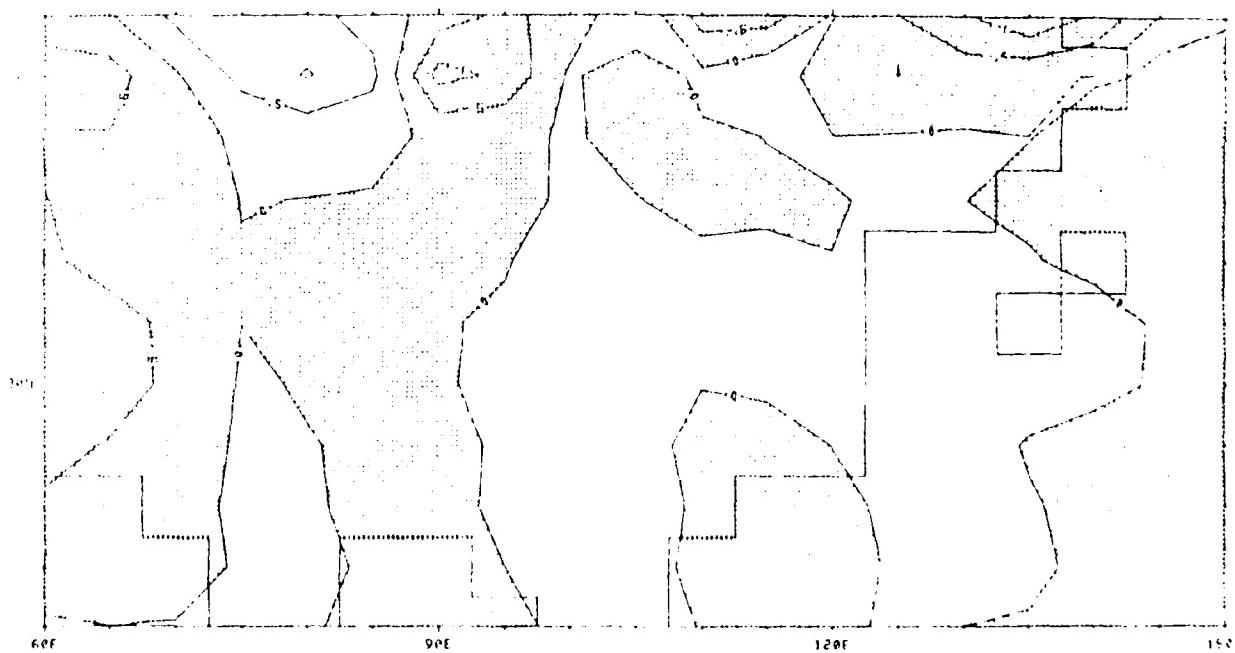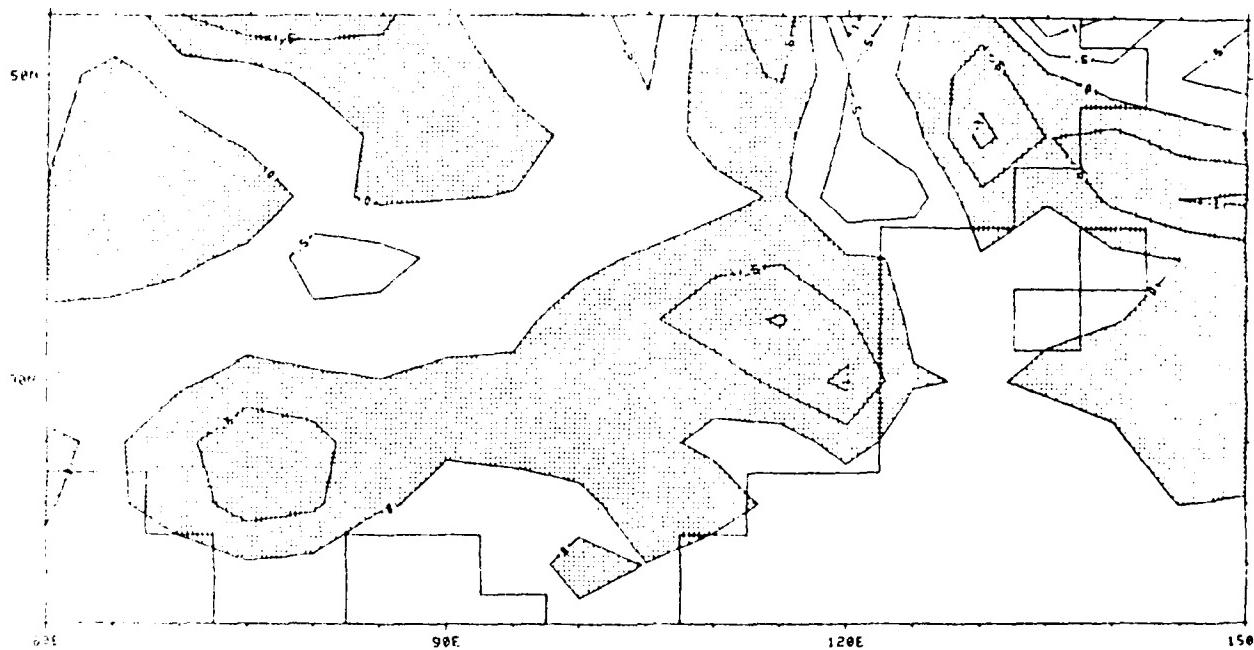
(a)
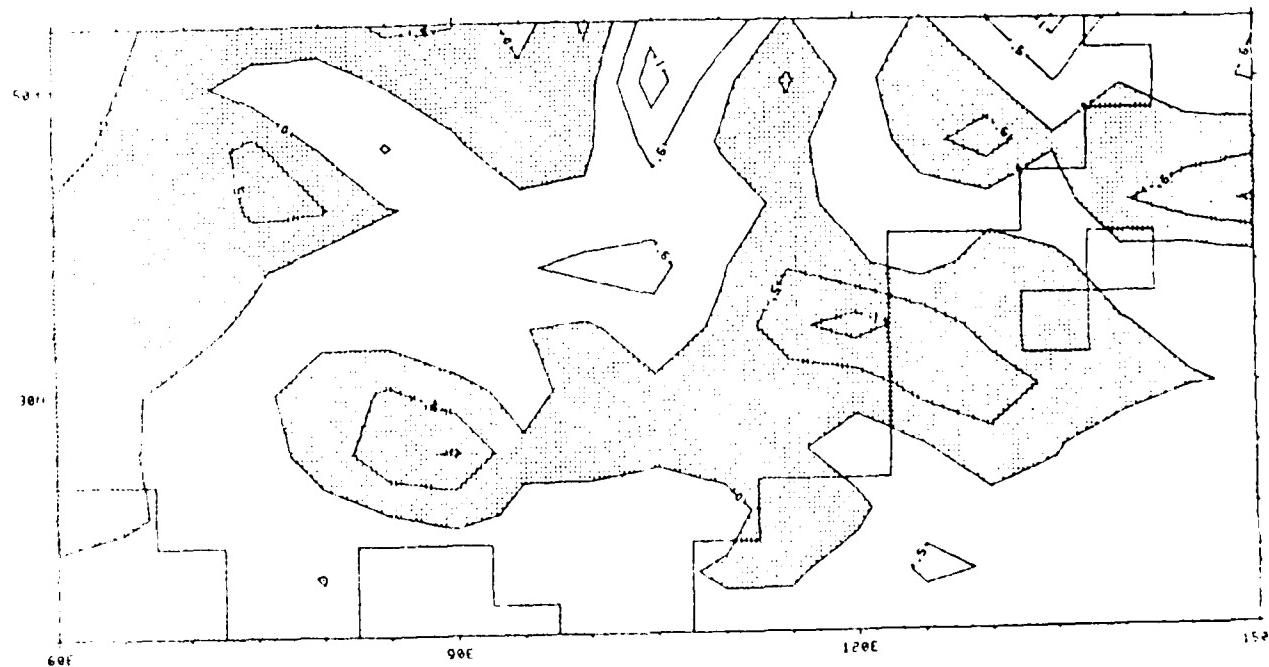
(b)

Fig. 3.37 The Newtonian friction term (day^{-2}) for the same times and condition as in Fig. 3.22.

176

(c)

(d)
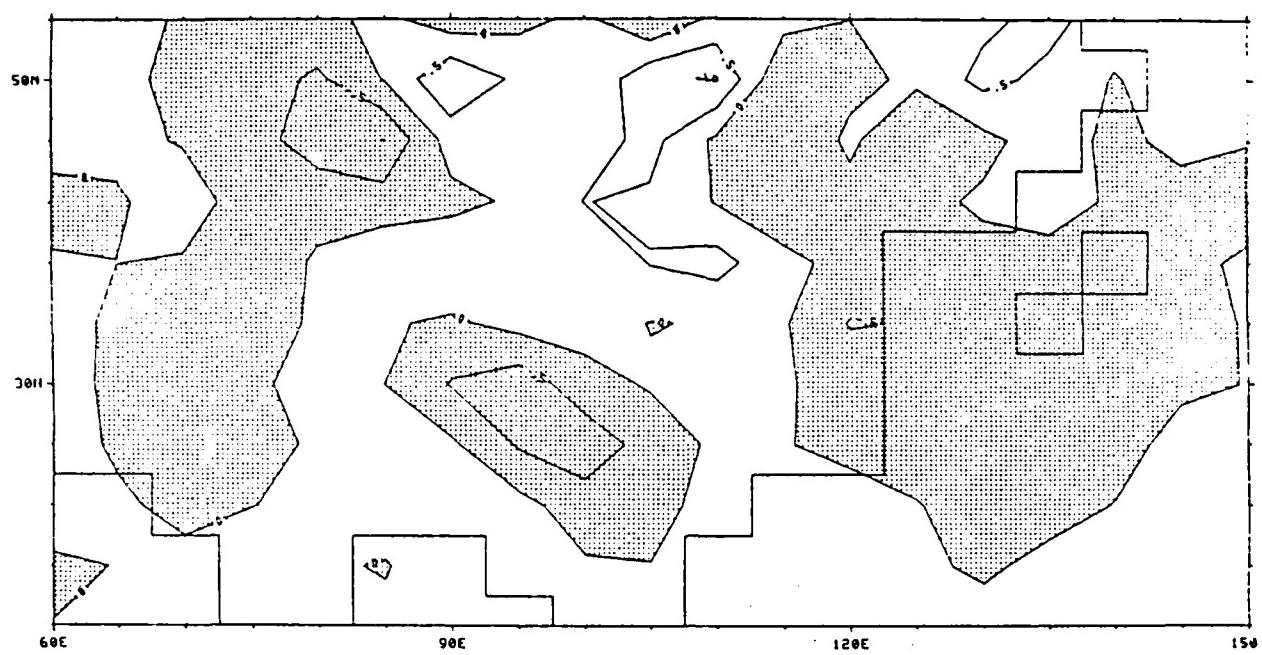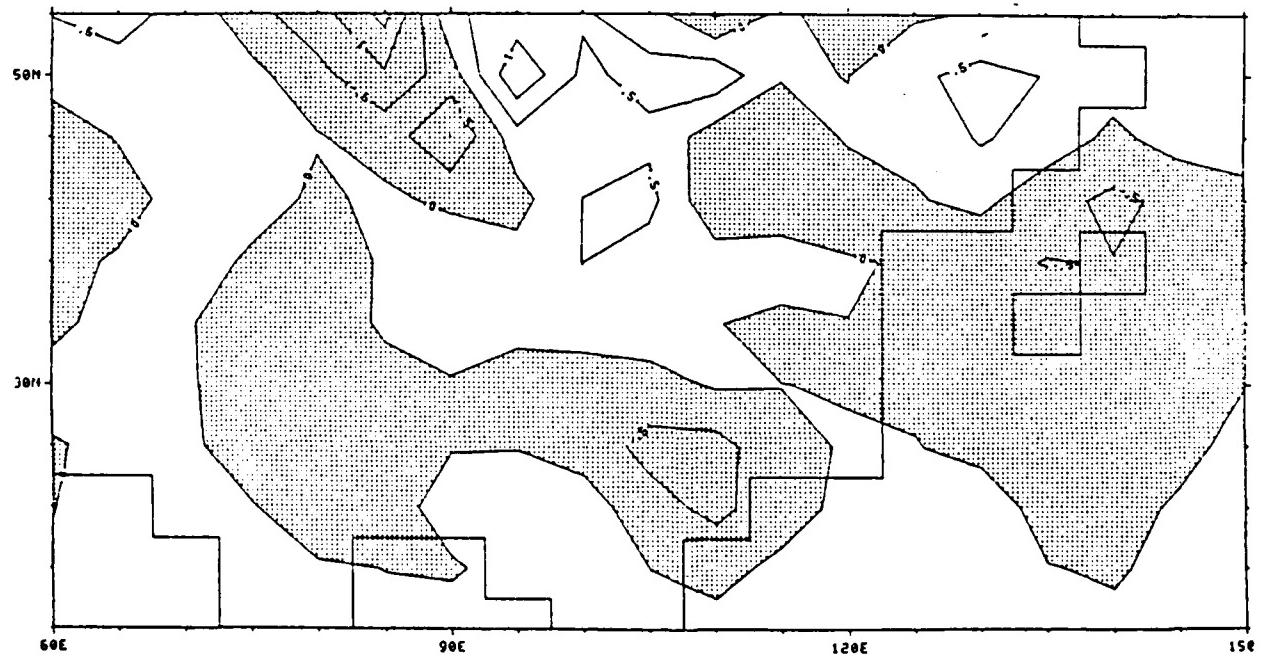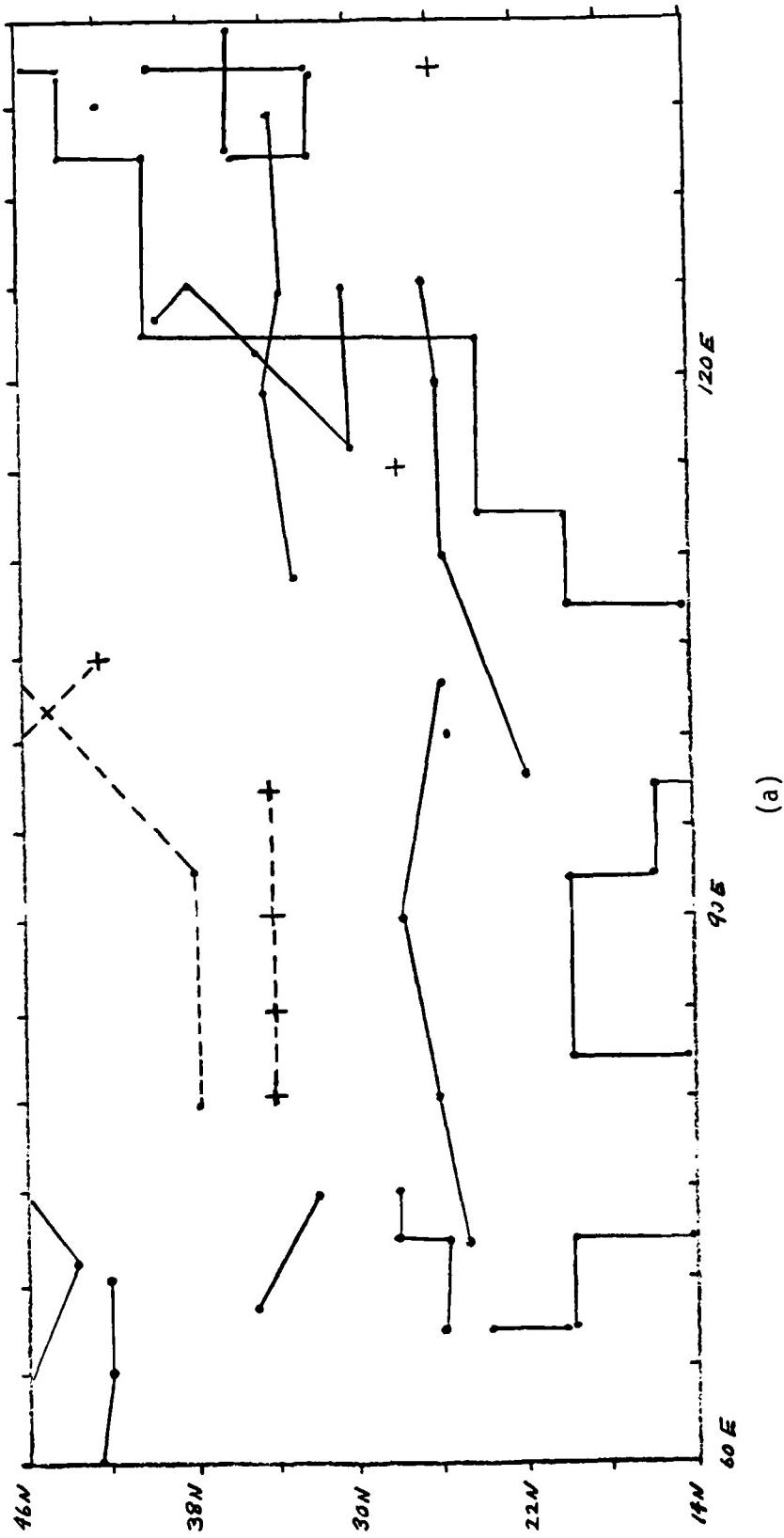
Fig. 3.38 The tracks of cyclone for both (a) WTPC and (b) NTPC.
(+--+ track for anticyclones, •——• track for cyclones)

(a)

178

(b)

END

FILMED

2–85

DTIC